ALFRED-WEGENER-INSTITUT
HELMHOLTZ-ZENTRUM FÜR POLAR- UND MEERESFORSCHUNG

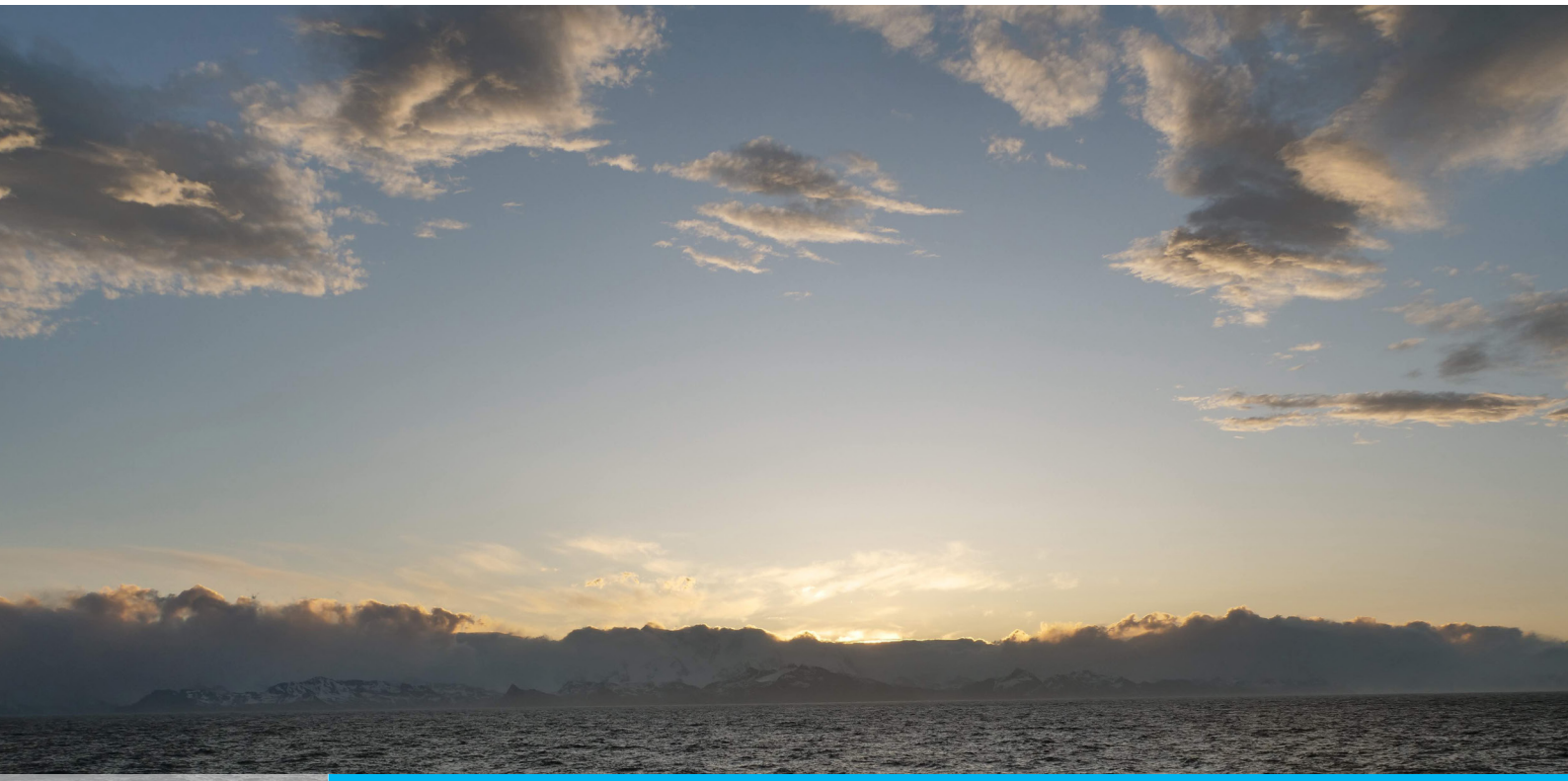

774
2023

Berichte
zur Polar- und Meeresforschung
Reports on Polar and Marine Research

The Expedition PS133/1 of the Research Vessel Polarstern to the Atlantic Ocean in 2022

Edited by
Christine Klaas
with contributions of the participants

HELMHOLTZ

Die Berichte zur Polar- und Meeresforschung werden vom Alfred-Wegener-Institut, Helmholtz-Zentrum für Polar- und Meeresforschung (AWI) in Bremerhaven, Deutschland, in Fortsetzung der vormaligen Berichte zur Polarforschung herausgegeben. Sie erscheinen in unregelmäßiger ABftolge.

Die Berichte zur Polar- und Meeresforschung enthalten Darstellungen und Ergebnisse der vom AWI selbst oder mit seiner Unterstützung durchgeführten Forschungsarbeiten in den Polargebieten und in den Meeren.

Die Publikationen umfassen Expeditionsberichte der vom AWI betriebenen Schiffe, Flugzeuge und Stationen, Forschungsergebnisse (inkl. Dissertationen) des Instituts und des Archivs für deutsche Polarforschung, sowie Abstracts und Proceedings von nationalen und internationalen Tagungen und Workshops des AWI.

Die Beiträge geben nicht notwendigerweise die Auffassung des AWI wider.

Herausgeber
Dr. Horst Bornemann

Redaktionelle Bearbeitung und Layout
Susan Amir Sawadkuhi

Alfred-Wegener-Institut
Helmholtz-Zentrum für Polar- und Meeresforschung
Am Handelshafen 12
27570 Bremerhaven
Germany

www.awi.de
www.awi.de/reports

The Reports on Polar and Marine Research are issued by the Alfred Wegener Institute, Helmholtz Centre for Polar and Marine Research (AWI) in Bremerhaven, Germany, succeeding the former Reports on Polar Research. They are published at irregular intervals.

The Reports on Polar and Marine Research contain presentations and results of research activities in polar regions and in the seas either carried out by the AWI or with its support.

Publications comprise expedition reports of the ships, aircrafts, and stations operated by the AWI, research results (incl. dissertations) of the Institute and the Archiv für deutsche Polarforschung, as well as abstracts and proceedings of national and international conferences and workshops of the AWI.

The papers contained in the Reports do not necessarily reflect the opinion of the AWI.

Editor
Dr. Horst Bornemann

Editorial editing and layout
Susan Amir Sawadkuhi

Alfred-Wegener-Institut
Helmholtz-Zentrum für Polar- und Meeresforschung
Am Handelshafen 12
27570 Bremerhaven
Germany

www.awi.de
www.awi.de/en/reports

Titel: Blick auf das wolkenverhangene Südgeorgien während PS133/1
(Foto: Christine Klaas)

Cover: View of cloud-covered South Georgia during PS133/1
(Photo: Christine Klaas)

The Expedition PS133/1 of the Research Vessel Polarstern to the Atlantic Ocean in 2022

Edited by

Christine Klaas

with contributions of the participants

Please cite or link this publication using the identifiers

https://hdl.handle.net/10013/epic.e56f5afd-f03a-478a-b163-dafb98fb3c7c
https://doi.org/10.57738/BzPM_0774_2023

ISSN 1866-3192

PS133/1

02 October 2022 – 17 November 2022

Cape Town – Punta Arenas

Chief scientist
Christine Klaas

Coordinator
Ingo Schewe

Contents

1. ÜBERBLICK UND FAHRTVERLAUF

Christine Klaas[1] [1]DE.AWI

Wissenschaftlicher Hintergrund

Das Südpolarmeer (Southern Ocean, SO) ist die größte Region der Weltmeere mit hohem Nährstoff- und niedrigem Chlorophyllgehalt (HNLC), in der die Konzentrationen von Makronährstoffen (Nitrat, Phosphat, Silikat) aufgrund der Eisenlimitierung der Phytoplankton-Produktivität hoch bleiben. Entlang der Strömung des Südlichen Antarktischen Zirkumpolarstroms (S-ACC) erstrecken sich jedoch Gebiete mit hoher Produktivität als Fahnen stromabwärts von Inseln, was auf einen starken Einfluss des Eiseneintrags von diesen Landmassen auf die Produktivität und den Kohlenstoffexport schließen lässt. Eine besonders intensive und ausgedehnte Hochproduktivitätsfahne wird von Satellitenbildern im atlantischen Sektor des SO stromabwärts von Südgeorgien angezeigt. Ein direkter Zusammenhang zwischen Südgeorgien als Eisenquelle und den Blüten im S-ACC wird jedoch aufgrund fehlender Beobachtungen und Kenntnisse der relevanten Prozesse weder in Modellsimulationen reproduziert noch durch Feldstudien belegt. Darüber hinaus zeigen die Chlorophyll-a-Saisonalität und die Chlorophyll-a-Konzentrationen auf Satellitenbildern unterschiedliche Muster mit verzögertem Auftreten der Blüte und geringerer Biomasse östlich des Georgiabeckens. Dies könnte auf Unterschiede in der Fe-Versorgung mit zunehmender Entfernung von der Insel oder auf Unterschiede bei anderen Umweltfaktoren zurückzuführen sein, die zu einer langsameren Biomasseakkumulation und einem geringeren Export führen. Schließlich sind die biogeochemischen Prozesse in der Wassersäule und ihre Auswirkungen (z.B. Kohlenstoff-, Fe- und Makronährstoffkreislauf und -export) in diesen Fahnen nur unzureichend bekannt. Unser Ziel während Island Impact war daher: i) Untersuchung der räumlichen Verteilung von Eisen und anderen Spurenmetallen, ihrer Speziation und Bioverfügbarkeit in der Wassersäule. ii) Bestimmung der Auswirkungen der Fe-Verfügbarkeit und anderer Umweltparameter (Deckschichttiefen und Stabilität über relevante Zeitskalen, andere Mikro- und Makronährstoffe und Planktoninteraktionen, einschließlich Wachstum, Sterblichkeit und Lebenszyklen der wichtigsten Phytoplankton- und Zooplanktonarten) auf Produktivität und Biogeochemie (mit Schwerpunkt auf Kohlenstoffaufnahme und -export). iii) Vergleich und Kombination der Raten biogeochemischer Prozesse und des physikalischen Transports und der Durchmischung, um die Bedeutung dieser Triebkräfte auf verschiedenen räumlichen Skalen (von der Submesoskala bis zur synoptischen Skala) in fünf Transekten, die den ACC durchqueren, beginnend bei 10°W und weiter in Richtung Südgeorgien, zu bewerten.

Während dieser Expedition wollten wir außerdem die Biologie (Mikroben- und Meiofauna) sowie die Geochemie und Schadstoffe im Tiefseegraben der Südlichen Sandwichinseln untersuchen, um einen Vergleich zwischen bathyalen, Abyssalen und hadalen Umgebungen mit unterschiedlichen Produktivitätsregimen und vertikalem Kohlenstoffexport sowie mit ähnlichen Untersuchungen im eutrophen Atacama-Graben und im oligotrophen Kermadec-Graben zu ermöglichen. Diese Studie ist in ein Netzwerk internationaler Kooperationen und Forschungsprogramme eingebettet und mit den Aktivitäten eines laufenden ERC-Advanced Grant HADES („Benthic diagenesis and microbiology of hadal trenches“; Grant-Nr. 669947) verbunden.

Die *Polarstern*-Expedition PS133/1 begann in Kapstadt am 2. Oktober 2022. Unser für den 1. Oktober 2022 geplanter Start musste aufgrund von Verzögerungen bei der Treibstofflieferung leicht verschoben werden. Am 2. Oktober um 20 Uhr war das Schiff bereit, und wir machten uns auf den Weg nach Südwesten in Richtung der Position unseres ersten Transekts, der bei 10°21,5'W und 48°38'S beginnen sollte (etwa 6 Dampftage von unserem Einschiffungshafen entfernt). Wind und Wellen nahmen nach unserem Auslaufen schnell zu, was auf die charakteristische hohe Sturmaktivität im atlantischen Sektor des Südpolarmeeres zurückzuführen war, die durch Tiefdruckgebiete von der Antarktischen Halbinsel, dem Weddellmeer und der Leeseite (Ostseite) der Anden verursacht wurde. Währenddessen hatten die Probenahmen und Messungen unterwegs bereits begonnen, und das Auspacken und Organisieren der Labore war in vollem Gange. Die Fahrt zu unserem ersten Transekt wurde jedoch am 9. Oktober unterbrochen, als wir nach Norden fuhren, um einem Sturm auszuweichen, der von Osten her auf uns zukam. Das ruhigere Wetter während dieses Umwegs, etwa 4° nördlich unserer Position, bot uns die Möglichkeit, Testausbringungen des CTD-Rosettensystems, der spurenmetallfreien CTD-Rosette und des Schleppsystems topAWI (Triaxus) durchzuführen. Am 11. Oktober fuhren wir bei zunehmendem Wind und Seegang in Richtung Süden zu unserem ersten Transekt. Aufgrund der aufgelaufenen Verspätungen und der Verkürzung unserer Expedition durch die Verlegung des Ankunftshafens von Port Stanley nach Punta Arenas, bestanden unsere Aktivitäten während des ersten Transekts aus dem Einsatz einer Unterwegs-CTD (die nach ~3h Einsatz verloren ging) und einer langen Station (unserer ersten Prozessstation, am 13.10. 22, Dauer ~36 Stunden) mit der gesamten geplanten Reihe von Einsätzen (einschließlich eines 24-stündigen Einsatzes von driftenden Sedimentfallen) und Messungen (von der Oberfläche bis zu den Tiefseesedimenten), um die Faktoren und Prozesse zu untersuchen, die zur Blütenentwicklung und zum Export im westlichsten Bereich der oben erwähnten hochproduktiven Fahne stromabwärts von Südgeorgien führen. Die Position wurde am 15. Oktober verlassen und wir fuhren nach Westen zu unserem zweiten Transekt. Aufgrund des ostwärts gerichteten Durchzugs eines neuen Tiefdruckgebiets wurde die ursprüngliche Position des Transekts (19°29'W) nach Westen auf 25°W verschoben. Der Transekt begann wie geplant mit einer Vermessung mit einem sensorbestückten, geschleppten undulierenden System (topAWI/Triaxus), dass die erste großräumige (51°S bis 54°S), hochauflösende (~1 km) Vermessung über den S-ACC von der Polarfront (PF) bis zur südlichen ACC-Front (SACCF) ermöglichte.

Am Nachmittag des 20. Oktobers wurde die erfolgreiche Vermessung mit den topAWI-Sensoren abgeschlossen. Leider führte die Bergung zu strukturellen Schäden am topAWI-System, so dass es nicht mehr eingesetzt werden konnte. Danach führten wir eine Kurzstation an der südlichen Grenze unseres Triaxus-Schnitts durch und fuhren nach Norden zu der für unsere zweite Prozessstation ausgewählten Position, die sich in einem Fleck mit hohem Chlorophyllgehalt nördlich des SACCF befand. Die Arbeiten an der ausgewählten Position der Prozessstation (ein Fleck mit hohem Chlorophyllgehalt bei 52°20'S und 25°W) verzögerten sich, da der Wind auffrischte und Ausbringung von Instrumenten verhinderte. Wir fuhren daher nach Norden (von wo aus eine frühere Rückkehr zu ruhigeren Bedingungen vorhergesagt war), um den Höhepunkt der stürmischen Verhältnisse abzuwettern und den Einsatz der Clean-CTD zu versuchen, um die latitudinalen Spurenmetallgradienten innerhalb der S-ACC zu bestimmen. Unsere zweite Prozessstation begann am Abend des 21. Oktober mit dem Einsatz eines benthischen Landers. Am 23. Oktober fuhren wir nach der Bergung unserer treibenden Fallen zur Position des benthischen Landers, um diesen zu bergen. In der Zwischenzeit wurde ein medizinischer Notfall ausgerufen. Da nach mehreren Versuchen keine Antwort von den Transpondern des Landers erhalten werden konnte, wurde die Bergung abgebrochen und wir fuhren mit Höchstgeschwindigkeit nach Westen, um unsere Patienten auf den Falklandinseln ins nächstgelegene Krankenhaus zu bringen. Nach einem schnellen und erfolgreichen Transfer unserer Patienten per Hubschrauber suchten wir Schutz im Berkley

Sound, um den Orkan abzuwettern, der sich an der Ostflanke der Anden entwickelt hatte und am 28. Oktober mit Windstärken von bis zu 66 Knoten an unserer Position vorbeizog. Als sich die Lage beruhigt hatte, fuhren wir zu unserem Untersuchungsgebiet zurück und folgten dicht den Ausläufern des Sturms in Richtung unseres letzten der ursprünglich geplanten Transekte im Georgia-Becken. Unterwegs wurden zwei kurze Stationen (30. Oktober bzw. 1. November) in subantarktischen Gewässern durchgeführt, bevor eine Unterwegs-CTD zur hochauflösenden Erfassung der physikalischen Parameter des Transekts eingesetzt wurde. Unsere letzte vollständige Prozessstation fand am 2. November statt, in dem Gebiet mit der höchsten Chlorophyll-a-Konzentration der saisonalen Blüte im Georgia-Becken. Der Transekt wurde mit CTD-Einsätzen und zwei kurzen Stationen bis zum 4. November fortgesetzt, als die zunehmenden Winde eines weiteren Tiefs, das von der Antarktischen Halbinsel kam, unsere Arbeit unterbrachen. Wir suchten Schutz vor diesem aufkommenden Sturm (mit Windstärken bis zu 11 Bft) im Windschatten von Südgeorgien. Die relativ ruhigen Bedingungen hinter der Insel boten uns die Möglichkeit, eine weitere Station auf dem Kontinentalschelf durchzuführen. Als sich die Bedingungen verbesserten, verließen wir Südgeorgien am 6. November und fuhren zu unserem letzten Untersuchungsgebiet, um die Abyssal- und Hadalsysteme entlang des Südlichen Sandwichgrabens zu untersuchen. Dort beprobten wir erfolgreich Sediment und Wassersäule an drei Stellen, darunter auch an der tiefsten Stelle (~8300 m Tiefe) des Grabens: dem Meteor Deep. Die letzte Station wurde in den frühen Morgenstunden des 10. November abgeschlossen, woraufhin wir nach Punta Arenas fuhren und den Hafen am Abend des 16. November 2022 erreichten.

SUMMARY AND ITINERARY

The Southern Ocean (SO) is the largest high nutrient low chlorophyll (HNLC) region of the world's oceans, where macronutrient (nitrate, phosphate, silicate) concentrations remain high, due to iron limitation of phytoplankton productivity. However, along the flow of the Southern Antarctic Circumpolar Current (S-ACC), areas of high productivity extend as plumes downstream of Islands suggesting strong influence of iron input from these land masses on productivity and carbon export. A particularly intense and extensive high productivity plume is indicated by satellite imagery in the Atlantic sector of the SO downstream of South Georgia. A direct linkage between South Georgia as an iron source and blooms in the S-ACC is, however, not reproduced in model simulations or supported by field studies; due to the lack of observations and knowledge of relevant processes. Further, chlorophyll *a* seasonality and concentrations from satellite imagery shows different patterns with delayed bloom occurrence and lower biomass eastward of, and away from, the Georgia Basin. This could be due to differences in Fe supply with increasing distance from the island or differences in other environmental drivers leading to slower biomass accumulation and lower export. Finally, water column biogeochemical processes and impacts (such as carbon, Fe and macronutrient cycling and export) in these plumes are poorly known. Our purpose during Island Impact was, therefore: i) To investigate the spatial distribution of iron and other trace metals, their speciation and bioavailability in the water column. ii) To determine the impact of Fe availability and other environmental parameters (mixed layer depths and their stability over relevant time scales, other micro and macronutrients, and plankton interactions including growth, mortality and life cycles of key phytoplankton and zooplankton species or assemblages) on productivity and biogeochemistry (with a focus on carbon uptake and export). iii) to compare and combine rates of biogeochemical processes and physical transport and mixing to assess the importance of these drivers at different spatial scales (sub-mesoscale to synoptic) in five transects crossing the ACC starting downstream of South Georgia at 10°W and progressing towards the island.

During this expedition, we further aimed to study the biology (microbial and meiofauna) and geochemistry and pollutants in the hadal trench of the South Sandwich Islands, for comparison between bathyal, abyssal and hadal environments experiencing different regimes of productivity and vertical carbon export, as well as between similar investigations conducted in the eutrophic Atacama Trench and oligotrophic Kermadec Trench region. This later study is embedded in a network of international collaborations and research programs and linked to the activities of an ongoing ERC-Advanced Grant HADES ("Benthic diagenesis and microbiology of hadal trenches"; Grant-Nr. 669947).

Polarstern expedition Leg PS133/1 started from Cape Town on 2 October 2022. Our departure planned for 1 October 2022 had to be slightly postponed due to delays in fuel delivery. On 2 October, 8 PM, the ship was ready and we started making our way to the southwest towards the position of our first transect starting at 10°21.5'W and 48°38'S (about 6 days steaming distance from our port of embarkment). Winds and waves picked up quickly after our departure, affected by the characteristic high storm activity in the Atlantic sector of the Southern Ocean due to low pressure systems originating in the Antarctic Peninsula, Weddell Sea as well as in the leeward (eastern side) of the Andes. All the while, underway sampling and measurements had started, and unpacking and organizing the labs was in full swing. Steaming to our first transect, was, however, cut short on 9 October when we headed North to avoid a storm heading our way

from the east. The calmer weather during this detour, about 4° latitude North of our position, afforded us the possibility to do test deployments and sensors of the CTD-rosette system, the trace-metal clean CTD rosette and the undulating towed system topAWI/Triaxus. On the 11 October, with increasing wind and sea state, we headed South towards our first transect. Due to the accumulated delays and the shortening of our leg by the shift in port of arrival from Port Stanley to Punta Arenas, our activities during the first transect consisted of the deployment of an underway CTD (lost after ~3 h deployment) and one long station (our first process station, starting the 13.10.22, duration ~36 hours) with the whole planned suite of deployments (including a 24 h drifting sediment traps deployment) and measurements (from the surface to the deep-sea sediments) to study the factors and processes leading to bloom development and export in the westernmost extend of the aforementioned high productivity plume downstream of South Georgia. The position was left on the 15 October and we headed west to our second transect. Due to the eastward bound passage of a new low-pressure system, the original position of the transect (19°29'W) was shifted to the west at 25°W. The transect started as planned with a survey using the sensor laden towed undulating system (topAWI/Triaxus) resulting in the first large-scale (51°S to 54°S) high-resolution (~1 km) survey across the S-ACC from the Polar Front (PF) to the Southern ACC Front (SACCF). In the afternoon of 20 October, after successfully finishing the underway survey (unfortunately resulting in structural damage to the topAWI system during recovery), we carried out a short station at the southern limit of our survey and headed North to the position selected for our second process station, located in a high chlorophyll patch North of the SACCF. Work at the chosen process station position (a high chlorophyll patch at 52°20'S and 25°W) was delayed as winds picked up preventing our deployments. We, therefore, headed North (where an earlier return to quieter conditions was predicted) to weather the peak of the gale force winds and to attempt a trace-metal clean CTD deployment in order to determine latitudinal trace metal gradients within the S-ACC. Our second process station started in the evening of 21 October with the deployment of a benthic lander and drifting sediment traps. On 23 October, after recovery of our drifting traps, we headed to the benthic lander position for recovery. In the meantime, a medical emergency was declared; since, after several attempts, no response from the lander's transponders could be detected, its recovery was interrupted and we headed west at maximum speed to deliver our patients in the Falkland Islands. After a quick and successful transfer of our patients via helicopter, we took shelter in Berkley Sound to weather the hurricane-force storm from a low that developed in the eastern flank of the Andes and passed our position on 28 October with winds up to 66 kn. As conditions quieten down, we left to our study area following closely on the tail of the storm heading towards our last of the originally planned transect in the Georgia Basin. Underway, two short stations were carried out (30 October and 1 November, respectively) in subantarctic waters before deploying an underway CTD for high resolution physical parameter coverage of the transect. Our last full process station was carried out on 2 November, in the area with highest chlorophyll a concentration of the Georgia Basin. The transect was continued with underway CTD deployments and two short stations until November 4, when increasing winds from another low originating in the Antarctic Peninsula interrupted our work. We sought shelter from this oncoming storm (with winds reaching 11 Bft) in the lee of South Georgia. The relative calm conditions behind the Island afforded us the possibility to carry out another station in the continental shelf. As conditions improved, we left South Georgia on 6 November and headed towards our last study area to investigate the abyssal and hadal systems along the South Sandwich Trench. There we successfully sampled sediment and water column at three positions, including the deepest (~8,300 m depth) location in the trench: the Meteor Deep. The last station was completed in the early hours of 10 November, whereupon we headed back to Punta Arenas, reaching port in the evening of 16 November 2022.

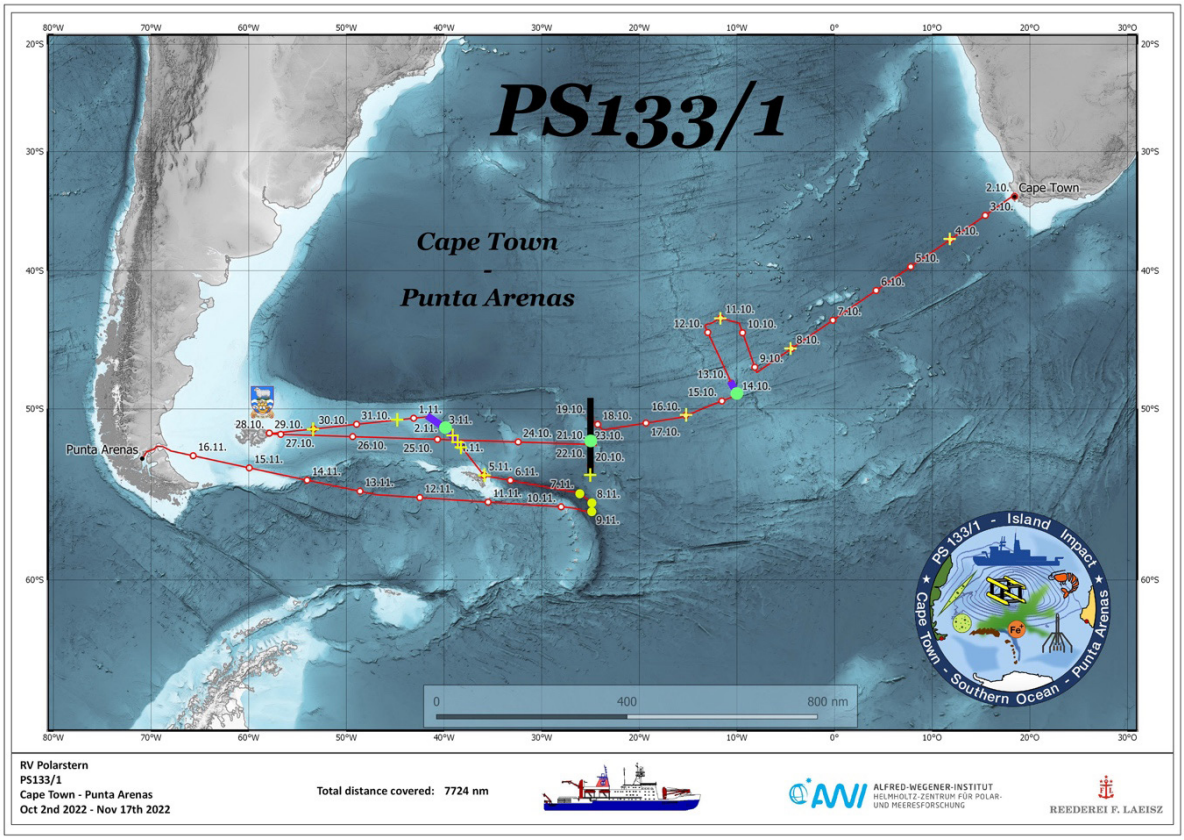

Abb. 1.1: Übersicht über den Fahrtverlauf (rote Linie) und die Stationsarbeit während PS133/1: Grüne Punkte zeigen die Position der Prozessstationen, gelbe Punkte die Abyssal- und Hadal-Stationen, gelbe Kreuze die anderen kürzeren Stationen (einschließlich CTD-Rosetten-Tests zu Beginn der Fahrt). Lila unterlegte Bereiche zeigen die Lage der Unterwegs-CTD Messungen während der Fahrt, schwarz schattierte Bereiche zeigen die Ausdehnung der topAWI/Triaxus-Messungen. Siehe https://doi.pangaea.de/10.1594/PANGAEA.957236 für eine Darstellung des Master tracks in Verbindung mit der Stationsliste für PS133/1

Fig. 1.1: Overview of the cruise track (red line) and station work during PS133/1: Green dots show the position of the process stations, yellow dots the abyssal and hadal stations, yellow crosses the other shorter stations (including the CTD-rosette tests at the beginning of the cruise). Purple shaded areas indicate the location of the underway CTD surveys, black shaded areas shows the extent of the topAWI/Triaxus survey at 25°W. See https://doi.pangaea.de/10.1594/PANGAEA.957236 to display the master track in conjunction with the station list for PS133/1

2. WEATHER CONDITIONS DURING PS133/1

Sonja Stoeckle[1], Frank Otte[1] [1]DE.DWD

On Sunday, 2 October 2022 at 8 pm ship time *Polarstern* left the port of Cape Town sailing towards the Southwest. A high-pressure ridge stretching from the southern Atlantic across South Africa dominated the weather conditions during departure. At first the sky was almost clear with calm winds about 3 Bft from southerly directions and temperature at 16°C. On Monday night, *Polarstern* crossed the cold front of a severe storm far south of South Africa. It was overcast and rained a bit. Further, a westerly air flow with 5 to 6 Bft dominated between the high-pressure ridge and the stormy low in the South. On Wednesday, 5 October 2022 another cold front swung through along the cruise track. The wind speed increased to 7 Bft, 8 Bft later. Also, the significant wave height and the swell increased to 5 m. At the rear of the cold front the temperature dropped from 14°C to 8°C. In the further course, a high over the South Atlantic temporarily extended southwards, which slowly weakened the pressure gradient. By Friday, 7 October 2022, the wind had decreased to 3 Bft and the sea had also calmed down. On Saturday, 8 October 2022, a swell of 3 meters from the southwest prevailed with a sunny 4 to 8 degrees.

On Sunday 9 October 2022 heavy seas were expected on the original course. To avoid this, the direction of travel was changed to the north-west. *Polarstern* was sailing north-west along the edge of the storm, which was initially north of the Falkland Islands and then moved south-east. During the night of Monday, 10 October 2022, peak winds of 9 Bft from the north-west were reached. The significant sea increased to 5 m. In the further course, a high over the South Atlantic and a low air pressure over the Southern Ocean prevailed a strong westerly wind in between. The wind was mostly blowing with 6 to 7 Bft. The significant wave height was at 3 to 4 m. The wind temporarily increased to 8 Bft. The sea matured completely. On Wednesday, 12 October 2002, a high-pressure ridge spread from the South Atlantic towards the Weddell Sea. The current between the Weddell Sea and the Gough Forties steepened to the southwest. In combination with the mature swell from west and the wind sea from south-southwest, there was a temporary cross sea of 5 m with single waves of around 7 m. Further on, the high-pressure ridge shifted eastwards, calming the sea temporarily to 2 to 3 m. Winds from northerly directions of 5 to 7 Bft prevailed. As early as Thursday, 13 October 2022, a low developed on the Antarctic Peninsula with an elongated low-pressure trough that extended northward to about 40° S.

A secondary depression developed at the low-pressure trough, which deepened considerably. The wind increased rapidly up to 8 to 9 Bft from the north-west as the secondary low was approaching. There were also stormy gusts. In the further course, an extensive low-pressure complex over the Southern Ocean and a high over the South Atlantic were preserved. Due to the persistent stormy winds, the sea rocked up to a significant wave height of 7 to 8 m with individual waves reaching an amplitude of 10 to 12 m on Sunday 16 October 2022. This was the highest sea state observed on the voyage. With temperatures between 0 and 4 degrees, snow and rain alternated. In the days that followed, the pressure constellation remained similar, with strong to stormy winds from West, mostly at 6 to 7 Bft. The significant wave height was at least at 4 m during this period. Small structures were repeatedly embedded in the westerly current, causing wind and waves to temporarily increase again to up to 9 Bft and a significant wave height of 6 m.

A medical emergency was declared on Sunday, 23 October 2022, causing the route to be changed and *Polarstern* set off for the Falkland Islands as quickly as possible. During the transit, the strong westerly current continued to prevail at 6 to 7 Bft with a significant wave height of 3 m. On Tuesday, 25 October 2022, it rained mainly sometimes with drizzle and correspondingly limited visibility. During the night of Wednesday, 26 October 2022 a high pressure temporarily spread from the north. The wind shifted to the north as a result, but continued to blow strongly. The clouds cleared up and it became temporarily cloud-free. On the night of Thursday, 27 October 2022, a cold front crossed *Polarstern* from the west. It was raining heavily. A moist base layer has formed at the rear edge of the cold front as a result of the heavy rain. An extensive foggy area developed, which only moved eastwards in the morning hours. The swell steadily decreased as we headed west and on Thursday, 27 October 2022 was still 1.5 m off the east coast of the Falkland Islands. Temperatures rose from 1°C to 9°C.

A hurricane forced low developed east of the Andes on Thursday, 27 October 2022 with a strong westerly current. The center of the storm shifted eastward and passed just south of *Polarstern* across the Falkland Islands on Friday, 28 October 2022. *Polarstern* recorded a pressure drop from 998.6 hPa by 40.2 hPa to 958.4 hPa within about 36 hours. *Polarstern* was situated in Berkley Sound to weather the violent storm. The highest wind speeds with peaks of 12 Bft (approx. 66 kt) occurred on Friday around 16 UTC. The hurricane force winds created a wind sea of 1.5 m in the bay. As the low progressed, the center of the storm shifted east-southeast at a speed of 25 kt and widened at the same time. As of Sunday, the area affected by the storm covered a spatial extent from the ice shelf edge to 40°S. On Monday, 31 October 2022 the hurricane low began to fill up slowly. Simultaneously, a high east of Argentina extended east-southeast along 50°S. In doing so, *Polarstern* entered the area of influence of the high-pressure area. As a result, wind and waves decreased. Winds from westerly directions of 5 to 7 Bft prevailed, the significant sea was 3 to 4 m. With temperatures between 2 and 5 degrees, the degree of cloud cover gradually increased, so especially on Friday night when light to moderate rain fell. On the backside of the warm front, partly foggy views developed.

On Tuesday, 1 November 2022, a warm front lay over the cruising area. It was raining with moderate visibility. The wind was blowing from the southwest at 6 to 7 Bft, the significant wave height was 3 m with a swell from the southwest. On the back of the front the influence of a high centered on the Rio Grande threshold increased. The cloud cleared and there was no precipitation. On Friday, 4 November 2022, a strong low-pressure system developed just east of the Antarctic Peninsula. It rapidly deepened and moved to the South Sandwich Islands by Saturday 5 November 2022. A stormy, sometimes hurricane-like west current built up between the low and the high above the South Atlantic. In order to avoid this weather, *Polarstern* sailed to the leeward area of South Georgia to weather the weather. Local wind systems with gusty westerly winds of between 7 and 10 Bft were created by the overflow of the mountain ranges on South Georgia. In the afternoon, *Polarstern* was in the lee with wind speeds between 1 and 3 Bft. During the night the clouds completely cleared. The waves at the station had a significant wave height of 2 to 3 m.

The high above the Rio Grande Sill shifted over the Argentine Basin and intensified through Sunday 6 November 2022. Simultaneously, the high generated a ridge into the Weddell Sea that gradually shifted eastward on Monday 7 November 2022. Mild and humid air was advected into the research area. There was broken to overcast clouds. First, a bit of snow fell, later the precipitation transitioned into drizzle. At temperatures around 0 degrees, it was partly freezing. During these days, the wind was blowing from a westerly direction at 5 to 7 Bft, the wave height reached 3 m. On Wednesday, 9 November 2022, a strong low moved eastward from the Antarctic Peninsula and shifted its center south of the research area across the Southern Ocean. As a result, the westerly current temporarily increased to 8 Bft.

In the night of Thursday, 10 November 2022, *Polarstern* left the last research station and made its way to Punta Arenas. The transit in the direction of Punta Arenas was initially characterized by a secondary low, which moved eastwards from the Falkland Islands into the sailing area and crossed *Polarstern* on Friday, 11 November 2022. The temperatures dropped to -1°C during snowfall, otherwise the temperature on the ground was 2°C. The wind was blowing from a westerly direction at 5 to 7 Bft, with snow showers gusting at 8 Bft. The significant wave height remained at 3 to 4 m. The further voyage was characterized by a high-pressure edge situation with the main center over the South Atlantic. On Sunday, 13 November 2022, *Polarstern* entered the high-pressure ridge that stretched east from the Falkland Islands into the Weddell Sea. On the reverse side, the wind turned to northerly directions and very humid air originating from the Argentine Basin was brought in. As a result, an extensive area of sea fog reached *Polarstern*. With winds of around 5 Bft from a northerly direction, it was foggy and there was little drizzle at times. It was not until Tuesday,15 November 2022, that *Polarstern* entered an air mass that had dried up in the southern Andes due to foehn effects. The fog dissolved or was pushed eastwards and it became almost cloud-free. On Wednesday, 16 November 2022, the Andean foehn collapsed and high air pressure spread from the north. As a result of the pressure wave, the wind in the shipping area increased rapidly. Then the wind temporarily blew from the west at 8 to 9 Bft. During the course of the day, winds of around 6 Bft prevailed and the wind direction veered to the north-west again. On the night of Thursday, 17 November 2022, *Polarstern* reached the Strait of Magellan. The weather up to the arrival in Punta Arenas was cloudy with changing winds from northeast to west with 5 to 8 Bft. Very gusty wind conditions awaited us in the port. With temperatures between 10 and 13 degrees, there were occasional light rain showers.

3. PHYSICAL OCEANOGRAPHY

Wilken-Jon von Appen[1], Jens Hölemann[1], Hauke Becker[1], Ryan Mole[1], Annika Oetjens[1], Anna Hölemann[2]
not on board: Lilian Dove[3], Sophie Clayton[4], Alexander Haumann[5]

[1]DE.AWI
[2]DE.Uni_Hamburg
[3]US.Caltech
[4]US.ODU
[5]US.Princeton

Grant-No. AWI_PS133/1_02

Objectives

The Antarctic Circumpolar Current features many strong fronts that suppress the exchange of tracers across the fronts. Therefore, tracers (such as for example iron from South Georgia) injected between two fronts remain between those two fronts to first order. Hence it is important to understand second order mesoscale and submesoscale processes such as instabilities and eddies that facilitate cross-frontal exchange and thereby the injection of iron into parts of the ocean that might otherwise be micro-nutrient limited. Synoptic sections, especially at high spatial resolution, are an important tool to study these processes. Due to the remoteness and harshness of the environment, there is a dearth of such observations in the Atlantic sector of the ACC. We aimed to change that. In addition to analysis inherently based on these observations, they are also an important constraint on model simulations of the region.

Work at sea

We collected 29 CTD profiles, towed the topAWI/Triaxus along one long transect, and towed the underway CTD along another long transect and deployed 12 drifters (Fig. 3.1).

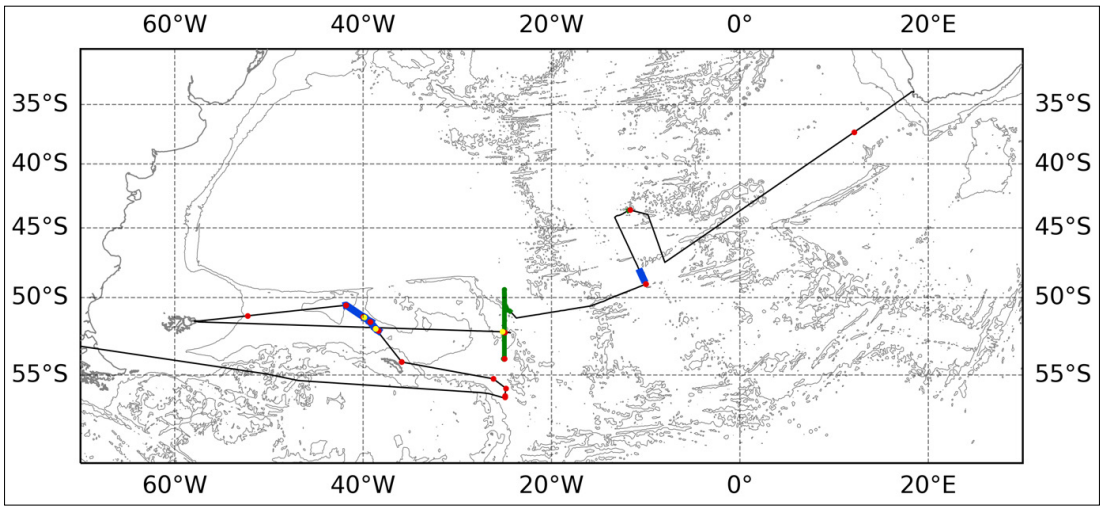

Fig. 3.1: Cruise track (black) with locations of CTD stations (red), topAWI/Triaxus tows (green), underway CTD tows (blue), and drifter deployment locations (yellow). The coastlines are shown in grey as well as the 2,000 m and 4,000 m isobaths.

CTD

Hydrographic measurements during PS133/1 were conducted using two CTD systems: CTD-OZE and a clean CTD ("CTD-Clean"). The sensors and rosette of CTD-OZE were provided by the physical oceanography group from DE.AWI ("CTD-OZE"). The sensors and rosette of the CTD-Clean were provided by the ecological chemistry group from DE.AWI ("CTD-Clean") and through the use of titanium and plastic in place of steel, it allows the sampling of trace metals, in particular iron. In the following, we describe the technical setup of the CTD rosettes, followed by a description of the general procedure of performing CTD casts during the cruise. We then present further information on the actual deployments, including a description of initial test casts and an overview of technical issues throughout the cruise. Please note the summarizing Table for all casts (Table 3.1).

The standard sensor configuration of the CTD-OZE system throughout the cruise consisted of two temperature sensors, two conductivity cells, a pressure sensor, two oxygen sensors, two fluorescence sensors, a transmissometer, and a photosynthetically active radiation (PAR) sensor, see Table 3.1 for more details. After the first three casts (conf1), the oxygen sensors were exchanged (conf2). Then, additionally the main bottle including the pressure sensor was exchanged (conf3) and used for one cast with an outdated calibration file. Finally, the updated calibration file (conf4) was used for the remaining eight casts of the cruise.

Tab. 3.1: Sensor configurations for the CTD-OZE system used during PS133/1

	SN	**Calibration Date**	**Channel**	**Description**
CTD				SBE 911plus
Temperature (primary)	1373	2019-10-11	F0	SBE3plus
Conductivity (primary)	1198	2019-09-17	F1	SBE4c
Pressure	0321	2017-11-14	F2	SBE9, substituted by SN 0287 with calibration date 1992-11-20 for conf3 and with calibration date 2017-11-14 for conf4
Temperature	2929	2019-09-13	F3	SBE3plus
Conductivity	1199	2019-09-17	F4	SBE4c
Oxygen (primary)	2292	2022-02-09	V0	SBE43, substituted by SN 4303 with calibration date 2022-08-06 for conf2-conf4
Oxygen	3654	2022-02-09	V1	SBE43, substituted by SN 4305 with calibration date 2022-08-16 for conf2-conf4
Altimeter	51533	--	V2	Teledyne Benthos PSA916
Fluorescence	7239	2021-12-09	V3	WETLabs ECO CDOM Fluorometer
Fluorescence	1346	2016-01-15	V4	WETLabs ECO Chlorophyll Fluorometer
Beam Transmission	0814	2011-10-24	V5	WETLabs C-Star
Photosynthetically Active Radiation (PAR)	2197	2021-11-30	V6	SEA-BIRD PAR-LOG
Lowered Acoustic Doppler Current Profiler (L-ADCP)	206f-6241	--	--	WorkHorse Broadband ADCP Version 50.40
Nitrate	1318	--	V7	Power only

Two Acoustic Doppler Current Profilers were attached to the rosette as well; more information can be found in the respective subsection below.

Furthermore, there was a Sea-Bird SUNA nitrate sensor (SN 1318) on the rosette. As this sensor has a depth rating of 2,000 m, it was only attached during 6 casts shallower than that. The device was programmed to start sampling - and record the data internally - as soon as power is supplied. Power was supplied by the SBE911, so that data acquisition started when the CTD is turned on. The nitrate measurements were not processed by the finalization of this report, so that no preliminary results are available here.

Also, an Underwater Vision Profiler (UVP) was attached to the rosette (see also Chapter 13). The UVP started automatically when it is lowered below 20 m and stopped recording when heaved above 30 m. Therefore, the usual procedure for a CTD deployment was as follows: lowering the rosette to 22 m, waiting for up to two minutes for the UVP and the CTD pump to turn on, heaving back to the surface. Then the downcast started by lowering the rosette with 0.5 m/s for the first 150 m and then increasing the speed to 1 m/s. For maximum depths close to the sea floor, at approximately 100 m above the depth obtained from the ship's system the lowering speed got reduced to 0.5 m/s, with a further reduction closer to the bottom, especially when the altimeter did not show a meaningful signal. When the altimeter worked, full-depth casts were stopped 10 m above ground.

The standard sensor configuration of the CTD-Clean system throughout the cruise consisted of two temperature sensors, two conductivity cells, a pressure sensor, one oxygen sensor, one fluorescence sensor, a transmissometer, and a photosynthetically active radiation (PAR) sensor, see Table. 3.2 for more details. For the last CTD-Clean cast, which went down to 7,000 m, all sensors except for the pressure, temperature, and conductivity sensors were removed to avoid possible damage due to the large pressure.

Tab. 3.2: Sensor configurations for the CTD-Clean system used during PS133/1

	SN	**Calibration Date**	**Channel**	**Description**
CTD				SBE 911plus
Temperature (primary)	6519	2022-07-19	F0	SBE3plus
Conductivity (primary)	4964	2022-06-28	F1	SBE4c
Pressure	1431	2020-11-19	F2	SBE9
Temperature	6491	2022-07-19	F3	SBE3plus
Conductivity	4982	2022-06-28	F4	SBE4c
Oxygen (primary)	4047	2020-10-30	V0	SBE43
Empty	--	--	V1	--
Fluorescence	6450	2020-08-12	V2	WETLabs ECO Chlorophyll Fluorometer
Beam Transmission	2064	2020-11-20	V3	WETLabs C-Star
Altimeter	74480	2020-03-06	V4	Valeport VA500
Empty	--	--	V5	--
Photosynthetically Active Radiation (PAR)	2067	2020-11-11	V6	SEA-BIRD PAR-LOG
Empty	--	--	V7	--

For water sampling the CTD-OZE Niskin bottles were fired on the upcast after waiting for 45 s at each target depth for both sampling the 'true' ambient water mass and also allowing for lagging sensors to adjust. These water samples are partly used for calibrating the salinity and oxygen observations. Results from the on-board salinometer are presented in the subsequent section. When there was a communication issue with the bottle firing unit no samples were used (see Table. 3.3).

The CTD-Clean, equipped with Ocean Test Equipment (OTE) bottles, was having problems with closing all bottles for the whole duration of the cruise but the number of successfully closed bottles increased during the cruise. For the CTD-OZE there were problems with the termination causing issues for the oxygen sensors (replaced) and the CTD-bottle (replaced). The altimeter is showed noise signals during the whole cast but at roughly 60-80 m above ground a signal could usually be detected.

For some stations the station and cast numbers differ from the logged names from the ship's system. This was not corrected for in the file names and header information. A list of the respective file names and correct station numbers is provided in Table. 3.4.

Tab. 3.3: Meta-data of all CTD stations from PS133/1. The station names refer to the file numbers and headers of the CTD data. A few stations were logged differently in the ship's system (see also Table. 3.4).

Station	Date Time at depth [UTC]	Lat [°N]	Lon [°E]	CTD depth [m]	Description	Comments
001_01	2022-10-04 09:30	-37.3572	12.1187	2000	Test station CTD-OZE	
clean_2_ Test1	2022-10-08 10:05	-45.8084	-4.2974	50	Test station CTD-Clean	Not all bottles closing properly
clean_2_ Test2	2022-10-08 13:48	-45.9368	-4.5557	1000	Test station CTD-Clean	
test	2022-10-11 13:41	-43.6300	-11.6650	52	CTD-Clean	No usable CTD data, communication error
003_03	2022-10-13 21:33	-49.0647	-9.9920	3208	CTD-OZE	No Altimeter signal, got to ~50 m above ground
003_15	2022-10-14 13:28	-49.0579	-9.9790	300	CTD-Clean	Communication error, had to abort during upcast and turn off deck unit
003_20	2022-10-14 21:30	-49.0748	-9.9883	2500	CTD-Clean	Still problems with bottle closing, termination needs to be redone
005_01	2022-10-20 17:34	-53.9999	-24.9968	1000	CTD-Clean	
005_02	2022-10-20 20:32	-54.0010	-24.9937	4650	CTD-OZE	No connection to rosette, error message at 2,300 m, pump switching on and off, oxygen sensors deviate greatly, cast terminated

Station	Date Time at depth [UTC]	Lat [°N]	Lon [°E]	CTD depth [m]	Description	Comments
006_03	2022-10-22 02:01	-52.3305	-24.9912	1000	CTD-Clean	Winch problem, first 30 m slow, then everything back to normal
006_04	2022-10-22 04:36	-52.3314	-24.9788	4312	CTD-OZE (new oxygen sensors)	Again no connection to bottle carousel, continue cast, altimeter works fine, bottles not all closed
006_14	2022-10-22 14:40	-52.3291	-24.9560	1000	CTD-Clean	
007_01_ conf3_0287	2022-10-30 18:52	-51.2316	-52.2356	2047	CTD-OZE (new CTD SN: 0287)	Problems with config file, now config3, no UVP
008_03	2022-11-01 18:56	-50.5191	-41.7963	1667	CTD-OZE	now config4
008_05	2022-11-01 20:45	-50.5191	-41.7940	1000	CTD-Clean	
009_03	2022-11-02 16:21	-51.2877	-40.0026	3732	CTD-OZE	
009_06	2022-11-02 20:38	-51.2881	-40.0019	3732	CTD-Clean	
009_16	2022-11-03 06:51	-51.2892	-39.9982	300	CTD-Clean	
010_03	2022-11-04 03:58	-51.6361	-39.2451	1000	CTD-OZE	
010_05	2022-11-04 05:02	-51.6360	-39.2443	300	CTD-Clean	
011_01	2022-11-04 13:54	-52.0602	-38.6931	1000	CTD-Clean	
012_01	2022-11-04 17:19	-52.2139	-38.3681	1000	CTD-Clean	Cable in path of transmissometer
014_12	2022-11-05 23:12	-54.1951	-35.9075	230	CTD_Clean	
014_04	2022-11-05 16:09	-54.1940	-35.9103	228	CTD-OZE	
015_03	2022-11-07 17:28	-55.2153	-26.1630	1000	CTD-OZE	Probably bubble problem in sensor pair 1 (sal, oxy) in upper ~40 m
016_03	2022-11-08 16:18	-55.8028	-24.8393	1000	CTD-OZE	
017_03	2022-11-09 09:30	-56.2430	-24.9395	4000	CTD-OZE	MUC cast right before this cast, slight repositioning of ship during cast, strong currents so reduced speed on downcast to keep cable stable, at times ship drifting at 0.5-1 m/s

Station	Date Time at depth [UTC]	Lat [°N]	Lon [°E]	CTD depth [m]	Description	Comments
017_07	2022-11-09 19:36	-56.2894	-24.9462	7000	CTD-Clean	Only Tem 1/2, Con 1/2, Pres, and bottle firing unit attached, ship drifting
017_08	2022-11-09 22:43	-56.3347	-24.9219	99	CTD-OZE	Last CTD

Tab. 3.4: Overview of stations that need to be renamed for matching the ActionLog of the ship

Station number in CTD protocols and header	Station number as logged by the ship
001_01 (OZE)	0_Underway_28
clean_2_Test1	No Dship entry
clean_2_Test2	No Dship entry
test (clean)	001_01
007_01_conf3_0287	007_01
012_01	013_01

Salinity measurements

We obtained high precision salinity measurements with an Optimare Precision Salinometer (OPS, SN 006) for potential recalibration of the conductivity sensors. An overview of all taken samples as well as the results from the salinometers can be found in Table. 3.5. The samples were taken from the Niskin bottles of both CTDs (CTD-OZE and CTD-Clean). Before taking the actual sample, the bottles and rubber lids were rinsed 3 times. Then the bottles were closed, sealed (crimped) with an aluminium cap, and stored.

We measured the water samples in three batches of 16, 16 and 7 bottles, respectively, that is, 39 samples in total (31 CTD-OZE, 8 CTD-Clean). The day before each session, the salinity bottles were heated in a water bath to approximately 30°C, and then left to cool down for about 20 h. The pressure within the bottles was released with an injection needle directly after the warm bath. Before using the OPS, the samples were shaken thoroughly for overcoming any stratification in the bottle. During sampling by the OPS, the opening of the bottles was sealed with parafilm to inhibit evaporation. The metal inlet tube of the OPS was cleaned with a Kim-wipe between samples.

Salinity measurements started with the standardization of the OPS using standard seawater. The respective bottle was sealed with the original cap and regularly sampled at the end of each session again. Each salinity measurement of a water sample from the Niskin bottles is calculated from the average of three individual OPS measurements that are allowed to differ by less than 0.0005 PSU. The salinity values measured by the two sensors of the CTD (Sal00 and Sal11) are calculated from the mean of 49 data scans recorded at the time of closing the Niskin bottle.

The first evaluation of the results shows that at some stations the salinities measured with the sensors were lower by up to 0.0108 PSU than the salinities measured with the OPS. This relatively high deviation occurred mainly on the first day of measurements. On the two following days of measurements, the deviation became smaller (Fig. 3.2). Both CTD sensors showed the same temporal trend. After the first measurement day (8.11.2022), a cleaning of the OPS

was performed by the laboratory electrician, because no standardization was possible on the planned next measurement day. Therefore, we suspect that the high deviations were primarily due to problems with the salinometer and not due to a change in the CTD sensors over time. However, a more detailed error analysis will only be possible after the expedition.

Tab. 3.5: All salinity values (PSU) calculated with the salinometer and the conductivity sensors of the two CTDs (CTD-OZE and CTD-Clean).

Expedition	Station	Pressure	date/measure	Salinity OPS	Salinity CTD Sal00	Difference Sal00-OPS	Salinity CTD-Sal11	Difference Sal11-OPS
CTD-OZE								
PS133/1	003_03	3048.572	08.11.2022	34.6921	34.6846	-0.0075	34.6838	-0.0083
PS133/1	003_03	3049.572	08.11.2022	34.6929	34.6846	-0.0083	34.6846	-0.0083
PS133/1	003_03	2026.834	08.11.2022	34.7293	34.7221	-0.0072	34.7218	-0.0075
PS133/1	003_03	2026.834	08.11.2022	34.7291	34.7221	-0.0070	34.7218	-0.0073
PS133/1	006_04	3050.643	08.11.2022	34.6747	34.6687	-0.0060	34.6676	-0.0071
PS133/1	006_04	2029.584	08.11.2022	34.6937	34.6858	-0.0079	34.6852	-0.0085
PS133/1	006_04	2029.584	08.11.2022	34.6938	34.6858	-0.0080	34.6852	-0.0086
PS133/1	006_04	3050.643	08.11.2022	34.6749	34.6687	-0.0062	34.6676	-0.0073
PS133/1	007_01	2027.714	08.11.2022	34.7175	34.7085	-0.0090	34.7072	-0.0103
PS133/1	007_01	2027.714	08.11.2022	34.7176	34.7085	-0.0091	34.7072	-0.0104
PS133/1	007_01	1925.889	08.11.2022	34.7121	34.7036	-0.0085	34.7023	-0.0098
PS133/1	007_01	1925.889	08.11.2022	34.7130	34.7036	-0.0094	34.7023	-0.0107
PS133/1	008_03	1520.366	08.11.2022	34.7179	34.7085	-0.0094	34.7071	-0.0108
PS133/1	008_03	1520.366	08.11.2022	34.7179	34.7085	-0.0094	34.7071	-0.0108
PS133/1	008_03	1265.04	12.11.2022	34.6973	34.6908	-0.0065	34.6896	-0.0077
PS133/1	008_03	1265.04	12.11.2022	34.6969	34.6908	-0.0061	34.6896	-0.0073
PS133/1	009_03	2029.706	12.11.2022	34.6921	34.6867	-0.0054	34.6854	-0.0067
PS133/1	009_03	2029.706	12.11.2022	34.6920	34.6867	-0.0053	34.6854	-0.0066
PS133/1	009_03	1010.752	12.11.2022	34.7034	34.6978	-0.0056	34.6966	-0.0068
PS133/1	009_03	1010.752	12.11.2022	34.7033	34.6978	-0.0055	34.6966	-0.0067
PS133/1	010_3	1011.341	12.11.2022	34.7017	34.6949	-0.0068	34.6932	-0.0085
PS133/1	015_3	909.864	12.11.2022	34.6885	34.6821	-0.0064	34.6801	-0.0084
PS133/1	015_3	909.864	12.11.2022	34.6888	34.6821	-0.0067	34.6801	-0.0087
PS133/1	015_3	556.33	12.11.2022	34.6902	34.6840	-0.0062	34.6824	-0.0078
PS133/1	015_3	556.33	13.11.2022	34.6868	34.6840	-0.0028	34.6824	-0.0044
PS133/1	016_3	1011.019	13.11.2022	34.7052	34.7027	-0.0025	34.7008	-0.0044
PS133/1	016_3	1011.019	13.11.2022	34.7044	34.7027	-0.0017	34.7008	-0.0036
PS133/1	017_3	4075.941	13.11.2022	34.6480	34.6473	-0.0007	34.6448	-0.0032
PS133/1	017_3	4075.941	13.11.2022	34.6497	34.6473	-0.0024	34.6448	-0.0049
PS133/1	017_3	2029.902	13.11.2022	34.6765	34.6725	-0.0040	34.6711	-0.0054
PS133/1	017_3	2029.902	13.11.2022	34.6764	34.6725	-0.0039	34.6711	-0.0053
CTD-Clean								
PS133/1	005_1	1009.225	08.11.2022	34.6847	34.6741	-0.0106	34.6763	-0.0084
PS133/1	005_1	1009.225	08.11.2022	34.6846	34.6741	-0.0105	34.6763	-0.0083
PS133/1	006_3	1013.338	12.11.2022	34.7062	34.6986	-0.0076	34.7004	-0.0058

Expedition	Station	Pressure	date/measure	Salinity OPS	Salinity CTD Sal00	Difference Sal00-OPS	Salinity CTD-Sal11	Difference Sal11-OPS
PS133/1	006_3	1013.338	12.11.2022	34.7063	34.6986	-0.0077	34.7004	-0.0059
PS133/1	009_6	1010.709	12.11.2022	34.7015	34.6936	-0.0079	34.6958	-0.0057
PS133/1	009_6	1010.709	12.11.2022	34.7014	34.6936	-0.0078	34.6958	-0.0056
PS133/1	009_6	2026.339	12.11.2022	34.6917	34.6847	-0.0070	34.6871	-0.0046
PS133/1	009_6	2026.339	12.11.2022	34.6970	34.6847	-0.0123	34.6871	-0.0099

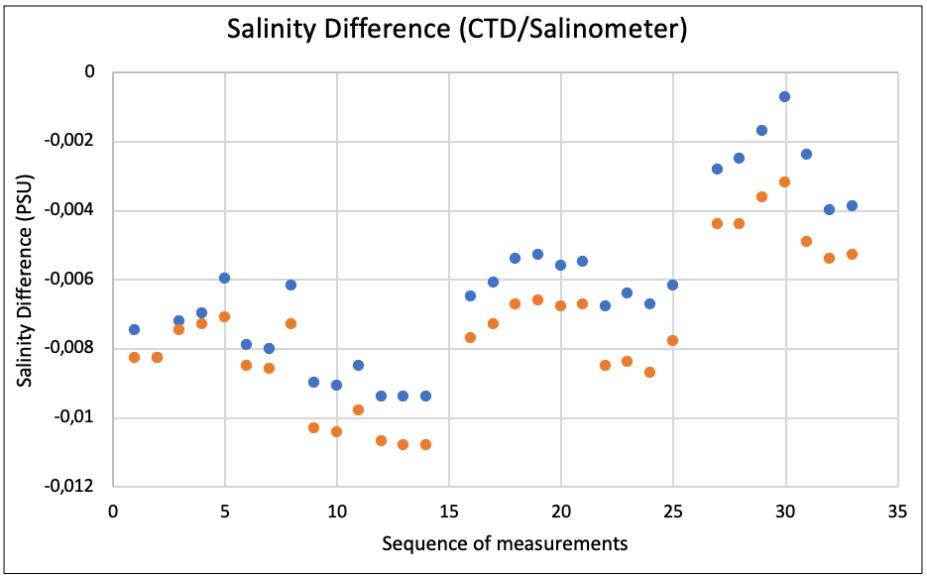

Fig. 3.2: Plot of the differences in salinity measured with the OPS salinometer and the CTD-OZE sensors: The X-axis shows the time sequence of the measurements. The blue dots show the results from the CTD sensor Sal00. The red dots show the results from the CTD sensor Sal11. Measurement days 2 and 3 started with measurement 16 and measurement 27, respectively.

$\delta^{18}O$

We collected 91 water samples for for $\delta^{18}O$ measurements in 30 mL plastic bottles from the CTD-OZE system following deployment at 10 stations (Table 3.6). In general, samples were taken from several layers within the upper 1,000 m and then at a reduced vertical resolution below 1,000 m where applicable. Additionally, we targeted specific water layers and took samples from both the temperature and salinity subsurface maxima and minima whenever available; this strategy was designed to target the Antarctic Intermediate Water and North-Atlantic Deep Water layers (salinity minimum and maximum) as well as the local winter water and surface subduction layers (temperature minimum and maximum).

The $\delta^{18}O$ samples will be analyzed in the AWI Potsdam mass spectrometry lab. It was originally planned to take approximately 190 water samples for $\delta^{18}O$ testing, however, the difficult conditions during the cruise and the consequent reduced number of CTD stations prevented this from happening. The scientific outcome of the resulting $\delta^{18}O$ sampling is unclear at this point, however the historical coverage of $\delta^{18}O$ sampling in the area is very sparse. Our sampling adds significantly to this record as the samples are the first retrieved for $\delta^{18}O$ testing in many of these locations.

Tab. 3.6: Overview of the $\delta^{18}O$ sampling. Time and location for the respective stations are provided in Table 3.3 and are omitted here; (bot) indicates samples taken 10 m above the seafloor.

Station PS133/1_	Niskin bottle	Depth [m]	$\delta^{18}O$ Bottle ID
003_03	1	3000	#001
003_03	4	1500	#002
003_03	3	2000	#003
003_03	4	1500	#004
003_03	5	1000	#005
003_03	9	500	#006
003_03	11	300	#007
003_03	20	20	#008
006_04	1	4313 (bot)	#009
006_04	3	2000	#010
006_04	4	1500	#011
006_04	4	1500	#012
007_01	1	2000	#013
007_01	2	1900	#014
007_01	2	1900	#015
007_01	6	1000	#016
007_01	7	800	#017
007_01	8	700	#018
007_01	10	500	#019
007_01	12	300	#020
007_01	14	200	#021
007_01	17	100	#022
008_03	1	1500	#023
008_03	1	1500	#024
008_03	2	1250	#025
008_03	2	1250	#026
008_03	8	500	#027
008_03	10	300	#028
008_03	12	200	#029
008_03	16	90	#030
008_03	20	40	#031
008_03	22	30	#032
009_03	1	3675 (bot)	#033
009_03	3	2000	#034
009_03	4	1500	#035
009_03	4	1500	#036
009_03	9	500	#037
009_03	11	300	#038

Station PS133/1_	Niskin bottle	Depth [m]	$\delta^{18}O$ Bottle ID
009_03	13	200	#039
009_03	15	120	#040
009_03	16	100	#041
009_03	19	40	#042
009_03	23	20	#043
010_03	1	1000	#044
010_03	5	500	#045
010_03	6	300	#046
010_03	8	200	#047
010_03	10	150	#048
010_03	14	100	#049
010_03	18	60	#050
010_03	21	20	#051
010_03	24	10	#052

Lowered ADCP

Two 300 kHz RDI Workhorse ADCPs were mounted on the rosette to act as lowered ADCPs (LADCP). The LADCP consists of the two 300 kHz ADCPs and a battery container. Communication was established to a computer in the winch room via two cables (for master and slave). The wall-installed cables COM1 and COM3 were used as the wall plug of COM2 appears to have sustained damage in the room where the CTD is stored. The ADCPs were operated using the GUI of the LADCP tool V1.7 from GEOMAR. The LADCP computer time was synchronized with the ships NTP server directly.

During the entire cruise, the settings documented in Table. 3.7 and 3.8 were used. Specifically, they use a bin size of 10 m, a maximum range of 200 m, beam coordinates, no blanking after transmission, narrow band processing, and a timing of the master and slave such that the acoustic energy of the master is separated by 0.55 seconds from the acoustic energy of the slave.

The Master (downward looking device) and slave (upward looking device) data file names consist of the station number (three digits), an abbreviation indicating the viewing direction (UP for upward and DN for downward) and a running number with three digits beginning with 000, representing the file number, in case there are multiple files (e.g., 001DN000.000 and 001UP000.000). These files were stored in a folder named according to the station number. Also log files documenting all actions conducted as starting (with configurations), stopping and downloading were kept.

The LADCP cable (at its connection to the wall) went into the water without dummy plugs on one occasion. It was thoroughly cleaned and greased afterwards and no permanent issues seem to have occurred as a result. Serial communication between the computer and the LADCPs was stable and without problems throughout the cruise.

Table. 3.9 shows the matching between CTD file names and file names of the LADCPs. The data was not processed on board.

Tab. 3.7: Start protocol of the Master LADCP used during PS133/1

For further information see the end of the Chapter.

Tab. 3.8: Start protocol of the Slave LADCP used during PS133/1

For further information see the end of the Chapter.

Tab. 3.9: LADCP profile no. with corresponding CTD cast no.

Station no.	LADCP no.
002_02	004
005_02	005
006_04	006
007_01	007
008_03	008
009_03	009
010_03	010
014_04	011
015_03	012
016_03	013
017_03	014

Thermosalinograph

The thermosalinograph was continuously operated in international waters and territorial areas where authorization had been granted (i.e., outside of the 12 nm territorial waters). Standard settings were used. The data was screened in near real time during the cruise and no remarkable problems were identified.

Vessel mounted ADCP

The vessel-mounted Acoustic Doppler Current Profiler (VMADCP) was in operation from 03 October 2022 08:15 UTC until entering the 12 nm territorial waters of the Falkland Islands on 27 October 2022 17:44; and again, from 29 October 2022 17:35 until entering the 12 nm territorial waters of Argentina at the end of the cruise. The RDI Ocean Surveyor instrument (150 kHz) was mounted at an angle of 45 degrees in the 'Kastenkiel' (box kiel) of *Polarstern* and provides continuous (underway) profiles of ocean current velocity in the upper 300 m of the water column. The instrument was configured in narrowband mode and set up to use a 4 m bin size (configuration file cmd_OS150NB_trigger_off.txt as shown in Table 3.10), covering a range from 15 m to around 200 – 300 m depth depending on sea state, ship speed and the presence of back-scatterers in the water column.

Overall, the system functioned without any issues and all data were collected entirely in the data files (file format: PS133_1[three digit deployment number]_000[three digit file number]. ENX, *.ENR, *.ENS, *.N1R, *.N2R, *.NMS, *.STA, *.LTA, *.VMO, *.LOG), as we did not apply any changes to the instrument configuration. Navigational input was used from the vessel's GPS system.

The software VmDas (Teledyne RD Instruments) was used to set the ADCP's operating parameters and to record the data. Finally, the data conversion was done using Matlab routines of the Ocean Surveyor Sputum Interpreter (OSSI) version 1.9 (osheader.m, osdatasip.m, osrefine.m, osbottom.m). Hereby the VMADCP data was corrected by using a misalignment angle of 0.8686° and an amplitude factor of 1.016912 (Fig. 3.3 and Fig. 3.4).

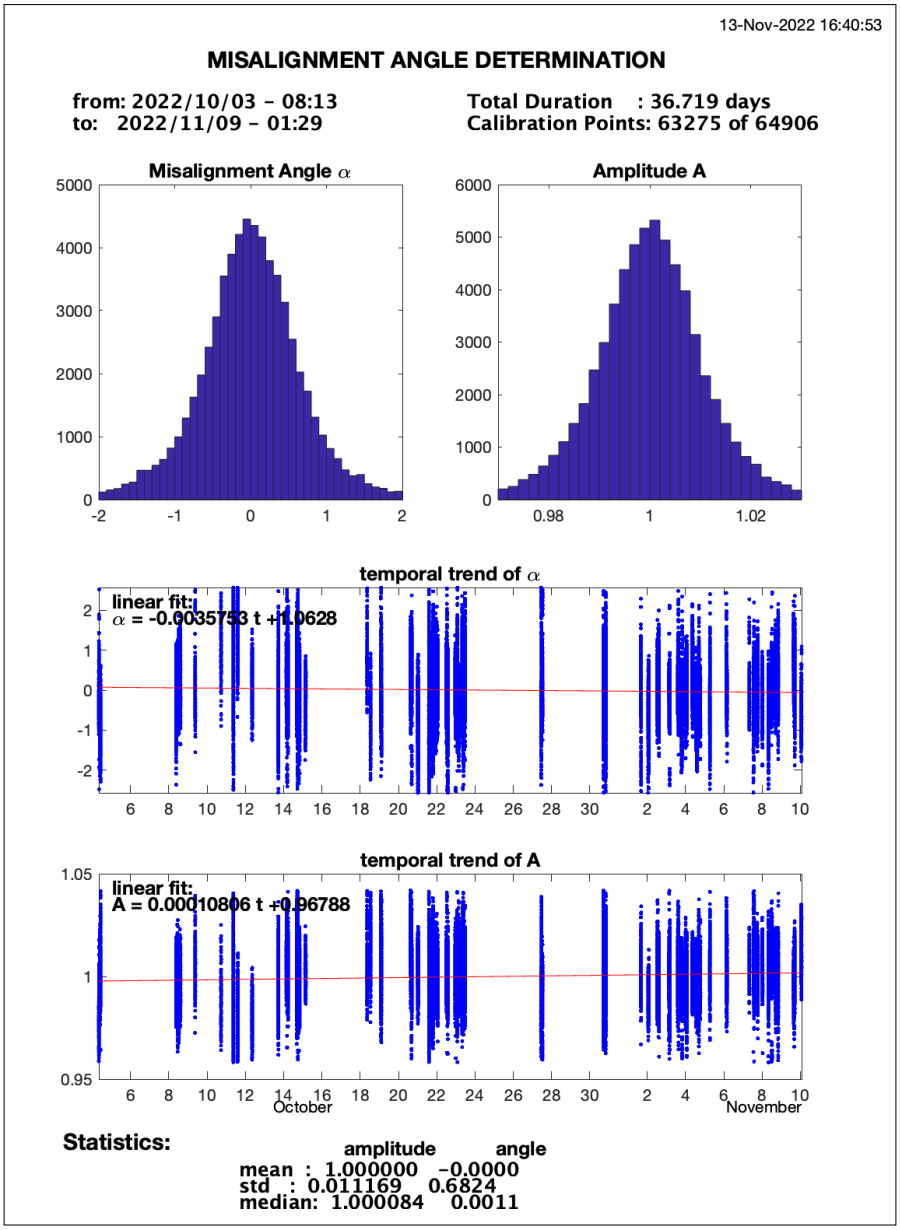

Fig. 3.3: Misalignment determination of the OSSI software

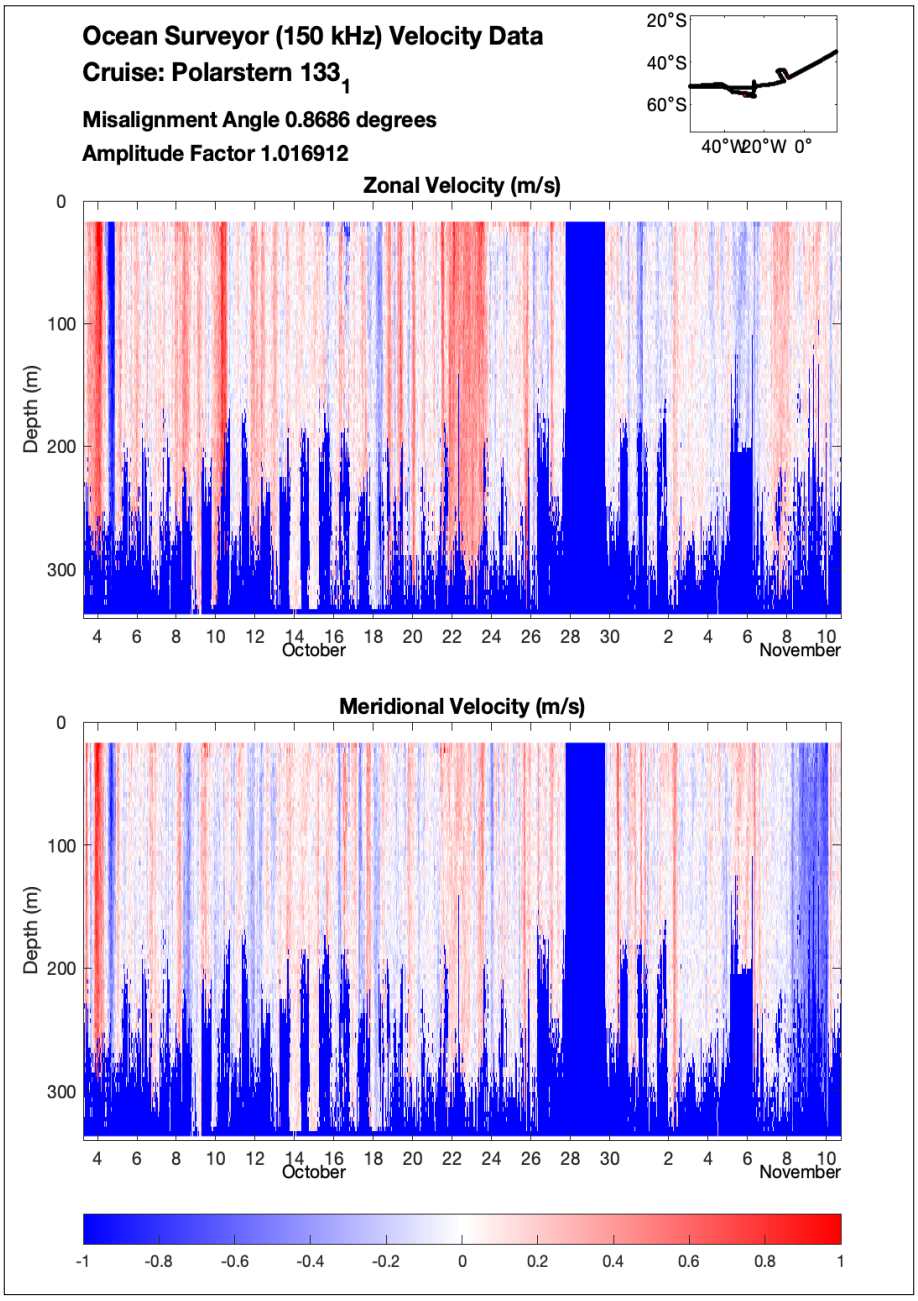

Fig. 3.4: Resulting ocean velocities [m s^{-1}] during PS133/1

Tab. 3.10: VMADCP command file cmd_OS150NB_trigger_off.txt
For further information see the end of the Chapter.

Triaxus towed ocean profiler of the AWI (topAWI)

The remotely operated towed profiler topAWI/Triaxus from MacArtney serves as a platform for multiple instruments and allows to gather a high-resolution dataset. The system is towed behind the ship either in a saw-tooth pattern or at a constant depth. The main aim of the Triaxus work on PS133/1 was to gather a horizontally highly resolved section prior to subsequently planned lower resolution station work. Table 3.11 provides an overview of the Triaxus transects during PS133/1.

An example of the Triaxus data obtained is shown in Fig. 3.5.

Chronological timeline of deployments

11.10.2022:

Test Deployment of the system, aiming for a general check of the system, as well as the launch and recovery and tension behaviour at high seas up to 4 meters.

During this first test, we learned a few relevant items for a successful dive, such as:

The launch and recovery of the system at high sea states is only possible with 3 engines, a higher deployment velocity from 4 meter and with at least 4 crew members on deck to manoeuvre the system.

The tension on the cable due to the waves was between 3000 and 7000 N. This results in an earlier reaction of the automatic overload function of the Triaxus software, which reduced the diving depths of the system.

18.10.-20.10.2022:

Deployment of the system for a 58 hour transect over several fronts of the polar region, at high seas up to 5 meters.

During the deployment as approximately 200 m cable had been spooled out, a 5 m wave pulled the Triaxus out of the water and caused a tension peak of around 15 000 N. This resulted in an overload stop of the winch. After a short analysis of the problem, the winch could be restarted and the deployment could be continued.

During the 58 hours in the water the system ran with only small issues caused by the changing tension from the waves. All activated sensors collected data over the whole time period.

During the recovery process, a 5 m high wave smashed the Triaxus system against the stern of the ship, which caused a structural damage of the system. Only because of the good reaction of all participants, the system could be recovered successfully. A detailed analysis of the system afterwards showed that the system could not be used as repair at sea was not possible.

Tab. 3.11: Overview of the topAWI/Triaxus transects during PS133/1.
For further information see the end of the Chapter.

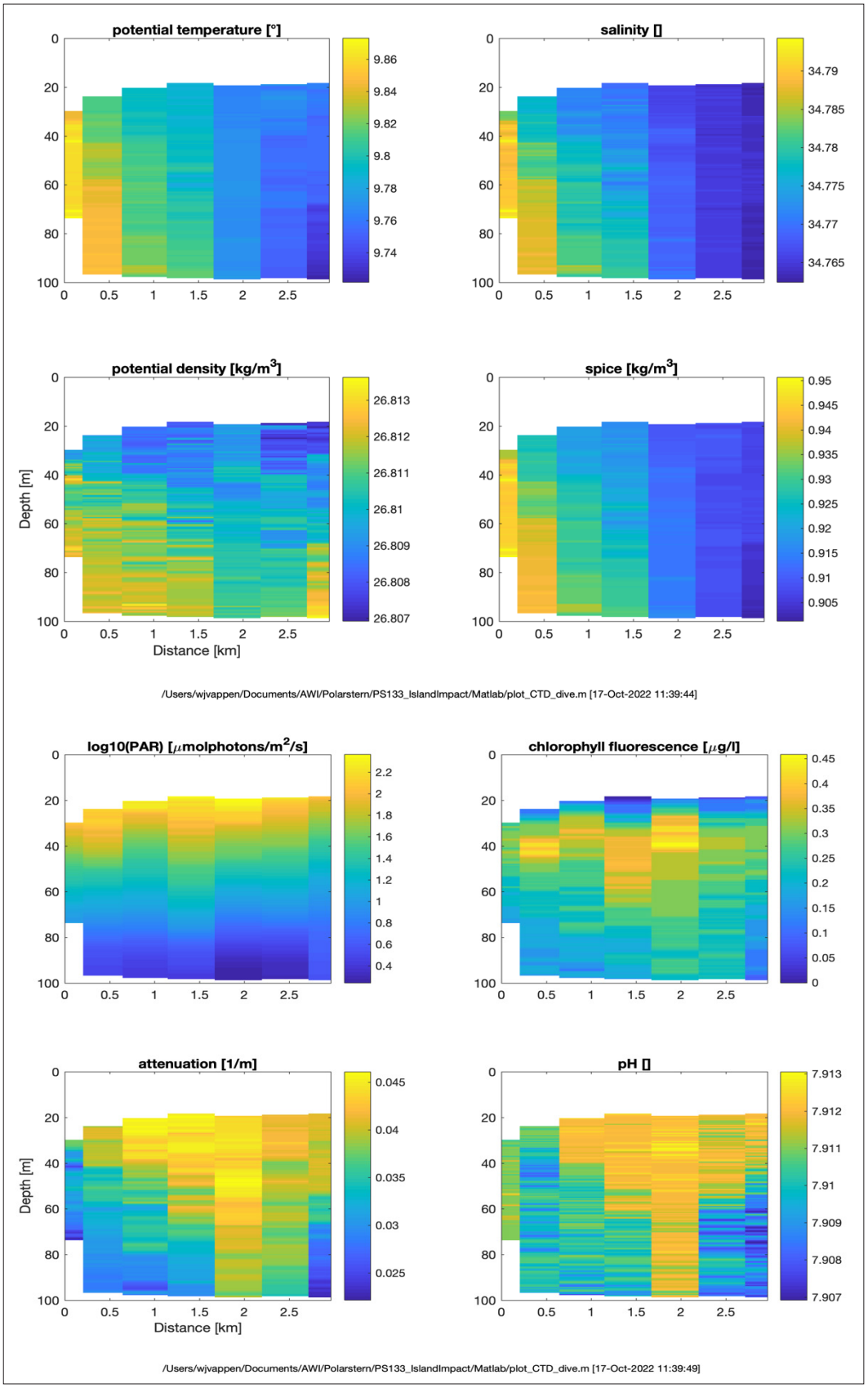

Fig. 3.5: Data from the first Triaxus dive ("test_dive"; PS133/1_1-3) of PS133/1; the following parameters are plotted versus distance and depth: potential temperature, salinity, potential density, spice, log10 of the photosynthetically available radiation, chlorophyll fluorescence, attenuation, and pH.

Underway CTD

The Teledyne Underway CTD (UCTD) was operated at times when the Triaxus ought to have been used scientifically, but was not operational, because it had been damaged (see Triaxus subsection). Table 3.12 provides an overview of the UCTD transects during PS133.1 ("GB" refers to "Georgia Basin transect").

The UCTD was operated in tow-yo mode: the winch brake is disengaged and the probe is in approximate free-fall at 4 m/s to 1 m/s vertical speed collecting data for a cast. Then the brake is engaged and the probe is hauled in until it is within 10 m horizontal distance behind the vessel at the sea surface. The winch is then disengaged and the next cast starts. We checked the condition of the loop splice that attaches the probe every ~30 minutes. Every probe was used for approximately ~60 minutes. Then it was recovered and the section was continued with another probe. The just recovered probe was then brought inside for data download and battery charging.

At all times when the UCTD was operated, two scientists were on deck: An operator of the winch and a person taking notes and counting the free-fall and haul-in times. Four different probes were used during PS133/1: serial numbers 347, 350, 351, and 352. Probe 352 was lost to the sea at the end of the first section (test_section; PS133/1_2-1), at which point the test_section was also stopped.

The operation in tow-yo mode entails a trade-off between horizontal resolution, vertical profile depth, and time taken for a section. This was achieved by adapting the ship speed and the time between the start of consecutive profiles. We operated at a ship speed of 8 knots (approximately 4 m/s) and total time between consecutive down casts of 7 to 9 minutes. An example of the underway CTD data obtained is shown in Fig. 3.6.

Tab. 3.12: Overview of the underway CTD transects during PS133/1

For further information see the end of the Chapter.

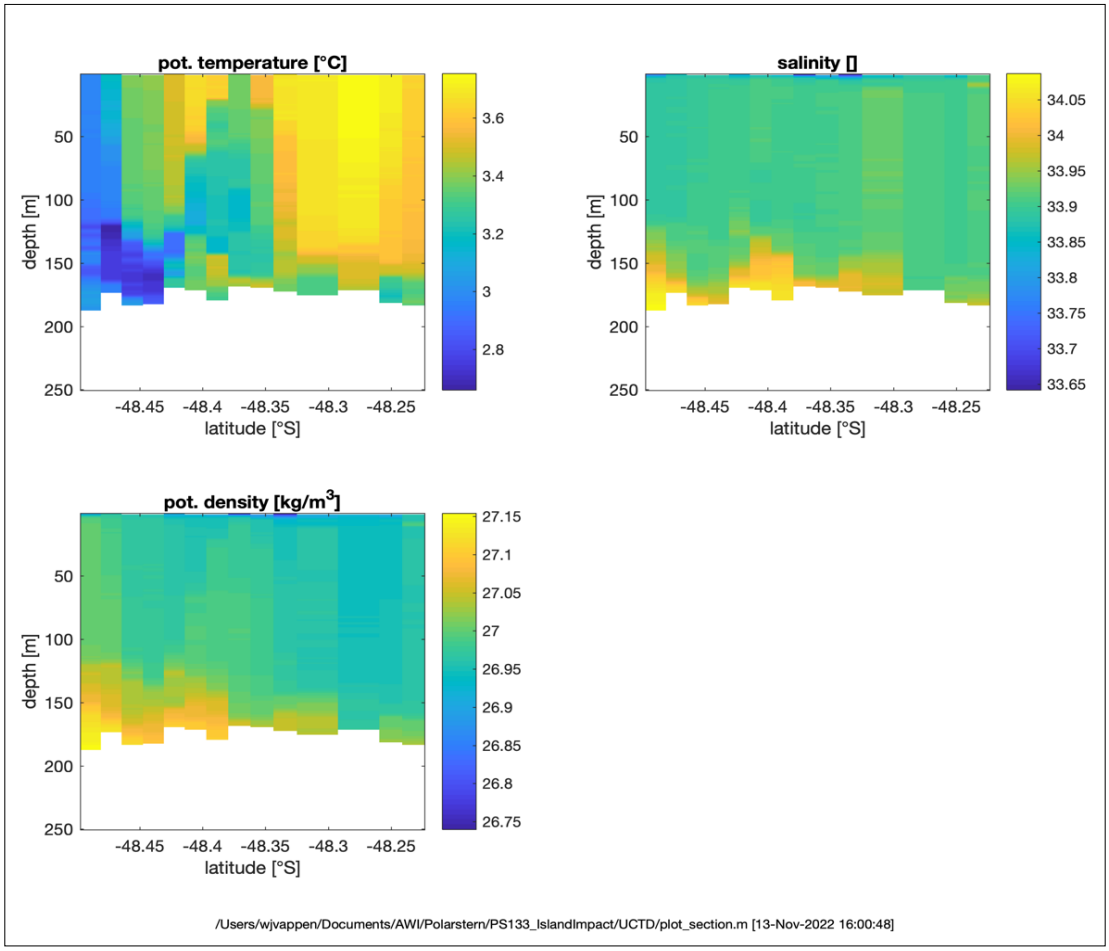

Fig. 3.6: Data from the first underway CTD dive ("test_section") of PS133/1; the following parameters are plotted versus latitude and depth: potential temperature, salinity, and potential density.

GPS Drifters

6 Southtek Iridium GPS drifters of type Offshore NOMAD-T V3 and 6 MetOcean Iridium GPS drifters of type SVP were deployed during PS133/1. All of the drifters had water temperature sensors. The 6 Southtek and 2 MetOcean drifters were deployed upon the departure from the 25°W section. 4 MetOcean drifters were deployed during the UCTD transect in the Georgia Basin. Unfortunately, 1 Southek (ID 627) and 4 MetOcean drifters (ID 1010, 2010, 3010 and 4000) did not survive their deployments from the ship even though the approved deployment procedure was followed. The Southtek drifters mostly failed after a few weeks in the water with only 1 Southtek (ID 594) and 2 MetOcean drifters (ID 8020 and 8480) alive as of November 13, 2022. Tables 3.13 and 3.14 provide the deployment details of the 12 drifters and Fig. 3.7 shows the drifters' trajectories until November 13, 2022.

Tab. 3.13: Overview of Southtek Nomad deployments

For further information see the end of the Chapter.

Tab. 3.14: Overview of MetOcean iSVP deployments

For further information see the end of the Chapter.

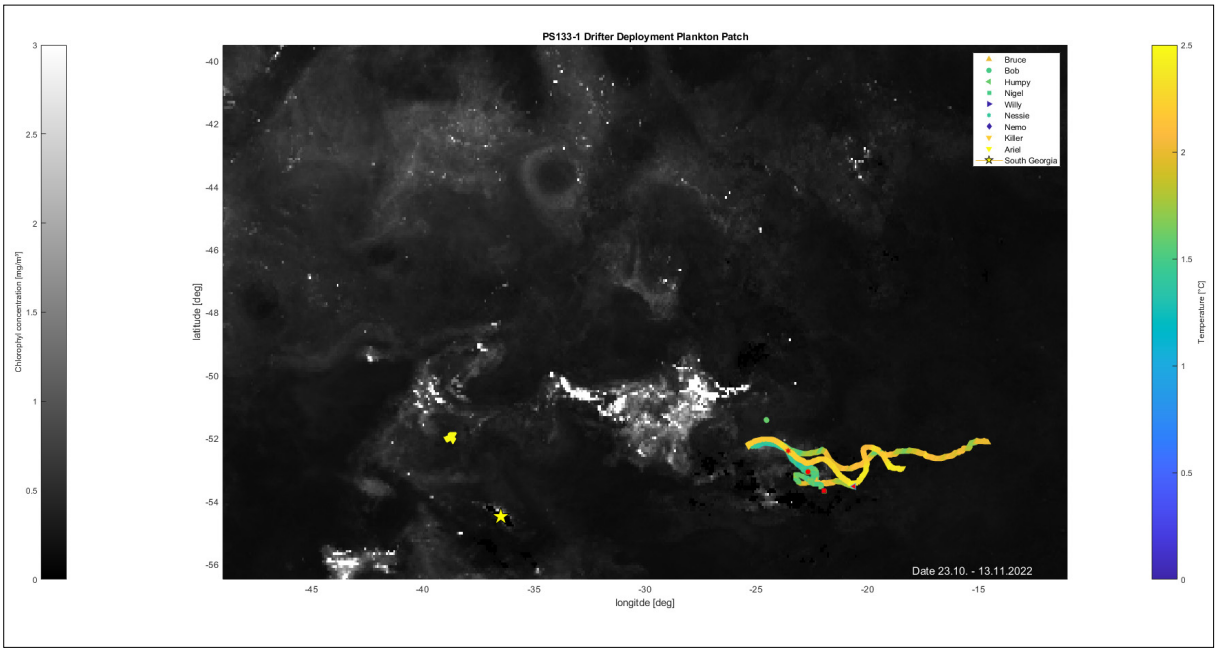

Fig. 3.7: Deployment locations and drift trajectories of Southtek Nomad-T V3 and MetOcean SVP drifting buoys between their deployment and 13 November 2022. The colour scale indicates surface water temperature measured by the drifters and the background indicates average chlorophyll concentration between 23 October and 13 November.

Preliminary (expected) results

Preliminary example plots of the data have been shown above for e.g. the CTD, VMADCP, UCTD, and Triaxus transects.

Data management

Environmental data will be archived, published and disseminated according to international standards by the World Data Center PANGAEA Data Publisher for Earth & Environmental Science (https://www.pangaea.de) within two years after the end of the cruise at the latest. By default, the CC-BY license will be applied.

Southtek Nomad data are transmitted via the iridium satellite network using the short burst data (sbd) protocol, and are decoded and stored on dedicated servers at the Southtek IT infrastructure in Spain for several years. After all buoys of this deployment will have ceased transmitting, the entire raw dataset will be uploaded to www.pangaea.de. After processing and quality-control, the data will also be made publicly available on www.pangaea.de.

MetOcean iSVP data are also transmitted via the iridium satellite network using the short burst data (sbd) protocol, and are decoded and stored on dedicated servers at MeteoFrance for several years. Additionally, the data are fed into the GTS in near-real time, from where they are immediately available to the public. After the last buoy of this deployment will have ceased transmitting, the dataset will be made publicly available on www.pangaea.de.

This expedition was supported by the Helmholtz Research Programme “Changing Earth – Sustaining our Future” Topic 6, Subtopic 3 and Topic 2, Subtopic 1.

In all publications based on this expedition, the **Grant No. AWI_PS133/1_02** will be quoted and the following publication will be cited:

Alfred-Wegener-Institut Helmholtz-Zentrum für Polar- und Meeresforschung (2017) Polar Research and Supply Vessel POLARSTERN Operated by the Alfred-Wegener-Institute. Journal of large-scale research facilities, 3, A119. http://dx.doi.org/10.17815/jlsrf-3-163.

Tab. 3.7: Start protocol of the Master LADCP used during PS133/1

```
[BREAK Wakeup A]
WorkHorse Broadband ADCP Version 50.40
Teledyne RD Instruments (c) 1996-2010
All Rights Reserved.
SB0  Writing Channel B Break State [DISABLED].

CR1
[Parameters set to FACTORY defaults]
SB0  Writing Channel B Break State [DISABLED].

TS yy/mm/dd,hh:MM:ss
WM15                        ; LADCP water ping mode 15
WV250                       ; ambiguity velocity
WN20                        ; 20 bins
WS1000                      ; 10 m bins
WF0                         ; no blank after transmit
WB1                         ; narrow band
EZ0111101                   ; fixed speed of sound
EX00111      ; beam coordinates, use pitch/roll, 3 beam solution, bin mapping
CF11101                     ; allow serial output
WP1                         ; single ping data
TP 00:00.00                 ; ping length of <0.00 seconds
TE 00:00:01.20              ; ensemble length of 1.2 seconds
SM1                         ; Master
SI0     ; sync pulse on every ping, n/a for Slave, but needs ST0200
SA011                       ; sync pulse before every ensemble
SW5500                      ; wait 0.55 seconds, n/a for Slave
CQ255                               ;
RN (three-digit cast no.)DN    ; file name
CK
[Parameters saved as USER defaults]
SA = 011      ---------- Synch Before/After Ping/Ensemble Bottom/Water/Both
SI = 00000    ---------- Synch Interval (0-65535)
SM = 1        ---------- Mode Select (0=OFF,1=MASTER,2=SLAVE,3=NEMO)
SS = 0        ---------- RDS3 Sleep Mode (0=No Sleep)
ST = 00000    ---------- Slave Timeout (seconds,0=indefinite)
SW = 05500    ---------- Synch Delay (1/10 msec)
T?
Available Commands:

TB 00:00:00.00              ---------- Time per Burst (hrs:min:sec.sec/100)
TC 00000                    ---------- Ensembles Per Burst (0-65535)
TE 00:00:01.20              ---------- Time per Ensemble (hrs:min:sec.sec/100)
```

```
TF **/**/**,**:**:**          ---------- Time of First Ping (yr/mon/day,hour:min:sec)
TG ****/**/**,**:**:**       ---------- Time of First Ping (CCYY/MM/DD,hh:mm:ss)
TP 00:00.00                  ---------- Time per Ping (min:sec.sec/100)
TS yy/mm/dd,hh:MM:ss         ---------- Time Set (yr/mon/day,hour:min:sec)
TT yyyy/mm/dd,hh:MM:ss       ---------- Time Set (CCYY/MM/DD,hh:mm:ss)
TX 00:00:00                  ---------- Buffer Output Period: (hh:mm:ss)
T?                           ---------- Display Time Help

W?
Available Commands:

WD 111100000      ---------- Data Out (Vel;Cor;Amp  PG;St;P0  P1;P2;P3)
WF 0000           ---------- Blank After Transmit (cm)
WG 000            ---------- Percent Good Minimum (1-100%)
WN 020            ---------- Number of depth cells (1-255)
WP 00001          ---------- Pings per Ensemble (0-16384)
WS 1000           ---------- Depth Cell Size (cm)
WV 250            ---------- Mode 1 Ambiguity Vel (cm/s radial)
WZ 010            ---------- Mode 5 Ambiguity Velocity (cm/s radial)
W?                ---------- Display Water-Profile Help

E?
EA = +00000             ---------- Heading Alignment (1/100 deg)
EB = +00000             ---------- Heading Bias (1/100 deg)
ED = 00000        ---------- Transducer Depth (0 - 65535 dm)
ES = 35           ---------- Salinity (0-40 pp thousand)
EX = 00111        ---------- Coord Transform (Xform:Type; Tilts; 3Bm; Map)
EZ = 0111101      ---------- Sensor Source (C;D;H;P;R;S;T)
CS                ; start pinging
```

Tab. 3.8: Start protocol of the Slave LADCP used during PS133/1

```
TS yy/mm/dd,hh:MM:ss
WM15                        ; LADCP water ping mode 15
WV250                ; ambiguity velocity
WN20                        ; 20 bins
WS1000                      ; 10 m bins
WF0                         ; no blank after transmit
WB1                         ; narrow band
EZ0111101                   ; fixed speed of sound
EX00111      ; beam coordinates, use pitch/roll, 3 beam solution, bin mapping
CF11101                     ; allow serial output
WP1                         ; single ping data
TP 00:00.00                 ; ping length of <0.00 seconds
TE 00:00:01.20              ; ensemble length of 1.2 seconds
SM2                         ; Slave
SA011                       ; sync pulse before every ensemble
ST200                       ; slave timout 200 seconds, n/a for Master, but needs SI0
CQ255                       ;
RN (three-digit cast no.)UP ; file name
CK
[Parameters saved as USER defaults]
S?
SA = 011      ---------- Synch Before/After Ping/Ensemble Bottom/Water/Both
SI = 00000    ---------- Synch Interval (0-65535)
SM = 2        ---------- Mode Select (0=OFF,1=MASTER,2=SLAVE,3=NEMO)
SS = 0 ---------- RDS3 Sleep Mode (0=No Sleep)
ST = 00200    ---------- Slave Timeout (seconds,0=indefinite)
SW = 00000    ---------- Synch Delay (1/10 msec)
T?
Available Commands:

TB 00:00:00.00              ---------- Time per Burst (hrs:min:sec.sec/100)
TC 00000                    ---------- Ensembles Per Burst (0-65535)
TE 00:00:01.20              ---------- Time per Ensemble (hrs:min:sec.sec/100)
TF **/**/**,**:**:**        ---------- Time of First Ping (yr/mon/day,hour:min:sec)
TG ****/**/**,**:**:**      ---------- Time of First Ping (CCYY/MM/DD,hh:mm:ss)
TP 00:00.00                 ---------- Time per Ping (min:sec.sec/100)
TS yy/mm/dd,hh:MM:ss        ---------- Time Set (yr/mon/day,hour:min:sec)
TT yyyy/mm/dd,hh:MM:ss      ---------- Time Set (CCYY/MM/DD,hh:mm:ss)
TX 00:00:00                 ---------- Buffer Output Period: (hh:mm:ss)
T?                          ---------- Display Time Help
```

W?

Available Commands:

WD 111100000 ---------- Data Out (Vel;Cor;Amp PG;St;P0 P1;P2;P3)
WF 0000 ---------- Blank After Transmit (cm)
WG 000 ---------- Percent Good Minimum (1-100%)
WN 020 ---------- Number of depth cells (1-255)
WP 00001 ---------- Pings per Ensemble (0-16384)
WS 1000 ---------- Depth Cell Size (cm)
WV 250 ---------- Mode 1 Ambiguity Vel (cm/s radial)
WZ 010 ---------- Mode 5 Ambiguity Velocity (cm/s radial)
W? ---------- Display Water-Profile Help

E?
EA = +00000 ---------- Heading Alignment (1/100 deg)
EB = +00000 ---------- Heading Bias (1/100 deg)
ED = 00000 ---------- Transducer Depth (0 - 65535 dm)
ES = 35 ---------- Salinity (0-40 pp thousand)
EX = 00111 ---------- Coord Transform (Xform:Type; Tilts; 3Bm; Map)
EZ = 0111101 ---------- Sensor Source (C;D;H;P;R;S;T)
CS

Tab. 3.10: VMADCP command file cmd_OS150NB_trigger_off.txt

```
;-------------------------------------------------------------------------\
; ADCP Command File for use with VmDas software.
;
; ADCP type:     150 Khz Ocean Surveyor
; Setup name:    for Polarstern in 6/2014
; Setup type:    Low resolution, long range profile (Narrowband)
;
; NOTE:  Any line beginning with a semicolon in the first
;        column is treated as a comment and is ignored by
;        the VmDas software.
;
; NOTE:  This file is best viewed with a fixed-point font (e.g. courier).
; Modified Last: 12Jun2014
;-------------------------------------------------------------------------/
; Restore factory default settings in the ADCP
cr1
; set the data collection baud rate to 9600 bps,
; no parity, one stop bit, 8 data bits
; NOTE:  VmDas sends baud rate change command after all other commands in
; this file, so that it is not made permanent by a CK command.
cb411
; Set for narrowband single-ping profile mode (NP), 100 (NN) 4 meter bins (NS),
; 2 meter blanking distance (NF), 390 cm/s ambiguity vel (WV)
WP000
NP001
NN080
NS0400
NF0400
;WV390
; Disable single-ping bottom track (BP),
; Set maximum bottom search depth to 1200 meters (BX)
BP000
;BX12000
; output velocity, correlation, echo intensity, percent good
ND111100000
; Ping as fast as possible
TP000000
; Since VmDas uses manual pinging, TE is ignored by the ADCP
; and should not be set.
;TE0000000
; Set to calculate speed-of-sound, no depth sensor, external synchro heading
; sensor,  pitch or roll being used, no salinity sensor, use internal transducer
```

```
; temperature sensor

EZ1011101
; Output beam data (rotations are done in software)
EX00000
; Set transducer misalignment (hundredths of degrees).
; Ignored here but set in VmDAS options.
;EA00000
; Set transducer depth (decimeters)
ED00110
; Set Salinity (ppt)
ES35
;set external triggering and output trigger; no trigger
CX0,0
;set external triggering and output trigger
;CX1,3
; save this setup to non-volatile memory in the ADCP
CK
```

Tab. 3.11: Overview of the topAWI/Triaxus transects during PS133/1

number	dive	section	name	Syear	Smonth	Sday	Shour	Sminute	Ssecond	Eyear	Emonth	Eday	Ehour	Eminute	Esecond	Sx	Ex	xyar	cable	minz	maxz	station	comment
1	1	1	test_ dive	2022	10	11	15	8	0	2022	10	11	15	24	27	-11.715	-11.755	lon	500	20	100	001_02	
1	2	2	225W_ part1	2022	10	18	14	44	46	2022	10	19	2	14	41	-50.849	-49.475	lat	2000	15	300	004_01	turn from NW-ward to N-ward at 50.5°S
3	2	2	25W_ part2	2022	10	19	2	55	45	2022	10	20	15	5	29	-49.464	-53.995	lat	1820	15	300	004_01	structurally damaged during recovery

Tab. 3.12: Ovwerview of the underway CTD transects during PS133/1

number	name	SNs	Syear	Smonth	Sday	Shour	Sminute	Ssecond	Eyear	Emonth	Eday	Ehour	Eminute	Esecond	station	comment
1	test_ section	352, 351, 352	2022	10	13	11	46	0	2022	10	13	14	56	0	002_01	SN352 was lost in water
2	GB_part1	350, 347, 350, 347, 350, 347, 350, 347, 350, 347	2022	11	2	2	13	0	2022	11	2	12	17	0	008_09	
3	GB_part2	347, 350, 347, 351, 350	2022	11	3	19	43	0	2022	11	3	23	55	0	009_24	
4	GB_part3	351, 347, 350, 351	2022	11	4	9	5	0	2022	11	4	13	3	0	010_10	
5	GB_part4	347, 350	2022	11	4	14	54	0	2022	11	4	16	32	0	011_02	

Tab. 3.13: Overview of Southtek Nomad deployments

ID	Alias	AWI ID	IMEI	Type	Date	Latitude	Longitude	Location
594	Bruce	2022p10003	300534062075100	Nomad T V3	20221123T11:45	52° 16.831’ S	025° 02.914’ W	25 W Section
604	Bob	2022p10011	300534062177020	Nomad T V3	20221123T12:25	52° 16.281’ S	025° 12.178’ W	25 W Section
612	Humpy	2022p10019	300534062175050	Nomad T V3	20221123T12:04	52° 16.393’ S	025° 07.530’ W	25 W Section
615	Nigel	2022p10022	300534062171030	Nomad T V3	20221123T12:45	52° 16.287’ S	025° 16.950’ S	25 W Section
627	Willy	2022p10034	300534062175230	Nomad T V3	20221123T13:27	52° 16.286’ S	025° 26.925’ S	25 W Section
631	Nessie	2022p10038	300534062076090	Nomad T V3	20221123T13:05	52° 16.286’ S	025° 21.821’ S	25 W Section

Tab. 3.14: Overview of MetOcean iSVP deployments

ID	Alias	AWI ID	IMEI	Type	Datetime	Latitude	Longitude	Location
8020	Killer	2022p253	300534063038020	MetOcean SVP	20221123T11:43	52° 16.284’ S	025° 27.071’ W	25 W Section
2010	Nemo	2022p255	300534063032010	MetOcean SVP	20221123T13:27	52° 16.867’ S	025° 02.395’ W	25 W Section
1010	Jacques	2022p254	300534063031010	MetOcean SVP	20221103T19:43	51° 18.428’ S	039° 54.887’ W	GB Transect
3010	Ursula	2022p257	300534063033010	MetOcean SVP	20221103T20:07	51° 20.333’ S	039° 50.662’ W	GB Transect
4000	Flounder	2022p256	300534063034000	MetOcean SVP	20221104T14:54	52° 03.964’ S	038° 40.979’ W	GB Transect
8480	Ariel	2022p258	300534063928480	MetOcean SVP	20221104T15:12	52° 05.377’ S	038° 38.073’ W	GB Transect

4. ISLAND IMPACT-NUTRIENTS & DOC

Kai-Uwe Ludwichowski[1], Matthias Woll[1] [1]DE.AWI
Not on board: Martin Graeve[1], Boris Koch[1]

Grant-No. AWI_PS133/1_03

Objectives

The determination of nutrients and biogeochemical parameters is closely connected to the physical and planktological investigations. The development of phytoplankton blooms is especially dependent on the available nutrients. Nutrients are also well suited as tracers for the identification of water masses. Our interests on this expedition are focused to shed light on the sources and transport pathways of Fe and on nutrient distribution in the upper water layer. During the CTD-transects, all inorganic nutrients (nitrate, nitrite, ammonium, silicate and phosphate) will be measured in the samples drawn from the rosette bottle system. In addition, dissolved organic matter (DOM) samples will be taken for bulk determinations (DOC/DON).

Work at sea

From water samples collected with the CTD-rosette samplers at various depths as well as underway from the ship's moonpool, phosphate (Murphy & Riley, 1962), silicate (Strickland & Parsons, 1968), nitrite and nitrate (Grasshoff et al., 1983), and ammonium (Kerouel & Aminot, 1997) were determined immediately on board using a Continuous Flow Seal 500 auto-analyser system according to standard methods. For DOC samples, 40 mL of the seawater sample was filtered through annealed glass fibre filters (Whatman, 450° C, 5 h, 0.7 µm nominal pore size) with a maximum pressure < 200 mbar.

DOC samples were stored at -20°C in pre-cleaned high-density polyethylene (HDPE) bottles for analysis back in the home laboratory.

Preliminary (expected) results

During this cruise we measured 440 nutrient-samples from the trace-metal clean CTD (CTD-Clean), the oceanographic CTD (CTD-OZE) and underway-samples from the moonpool of *Polarstern*. 185 nutrient-samples from onboard experiments were also analyzed. We filtered also 270 samples for DOC measurements at the AWI in Bremerhaven. This work will investigate the oceanographic coupling between South Georgia and the Antarctic Circumpolar Current ACC and the sources and biogeochemical processes controlling the transport and transformation of ferrous components along the flow path of the ACC. Nutrient data, which will be available about two days after sampling, will allow us to get an overview of water masses, biological activity, and the operation of our sampling system. Later, the nutrient data will be used for many cruise-related studies to reveal a variety of physical and biological processes.

Data management

We plan that the full data set will be available at least half a year after the cruise. Most of the samples, which will not be analyzed immediately, will be stored at AWI and will be available to other colleagues. The data will be archived, published and disseminated according to international standards by the World Data Center PANGAEA Data Publisher for Earth & Environmental Science (https://www.pangaea.de) within two years after the end of the cruise at the latest. By default, the CC-BY license will be applied.

This expedition was supported by the Helmholtz Research Programme “Changing Earth – Sustaining our Future” Topic 6, Subtopic 3 and Topic 2, Subtopic 1.

In all publications based on this expedition, the **Grant No. AWI_PS133/1_03** will be quoted and the following publication will be cited:

Alfred-Wegener-Institut Helmholtz-Zentrum für Polar- und Meeresforschung (2017) Polar Research and Supply Vessel POLARSTERN Operated by the Alfred-Wegener-Institute. Journal of large-scale research facilities, 3, A119. http://dx.doi.org/10.17815/jlsrf-3-163.

References

Grasshoff K et al., (1983) Methods of seawater analysis. Verlag Chemie GmbH, Weinheim, 419 pp.

Murphy J & Riley JP (1962) A modified single solution method for the determination of phosphate in natural waters. Analytica Chim. Acta, 27:31–36.

Kerouel R & Aminot A (1997) Fluorometric determination of ammonia in sea and estuarine waters by direct segmented flow analysis. Marine Chemistry, 57:265–275.

Strickland JDH and Parsons TR (1968) A practical handbook of seawater analysis. first edition, Fisheries Research Board of Canada, Bulletin, 167:65.

5. TRACE METAL DISTRIBUTION AND BIOGEOCHEMISTRY IN THE OPEN WATERS DOWNSTREAM OF SOUTH GEORGIA

Scarlett Trimborn[1], Frederik Bußmann[2], Berenice Ebner[1], Joshua Hübner[1], Jeff McQuaid[3], Marta Pérez-Rodriguez[4], Ingrid Stimac[1], Jasmin Stimpfle[1], Anja Terbrüggen[1], Christian Völkner[1];
not on board: Andrew Allen[3], Harald Biester[4], Susann Henkel[1], Florian Koch[1], Mak Saito[5], Michael Staubwasser[6]

[1]DE.AWI
[2]DE.GEOMAR
[3]US.UCSD
[4]DE.TU_Braunschweig
[5]US.WHO
[6]DE.Uni_Köln

Grant-No. AWI_PS133/1_04

Objectives

Extensive open water phytoplankton blooms occur along the flow of the southern Antarctic Circumpolar Current downstream of the island South Georgia. The sources and magnitude of iron (Fe) inputs fueling productivity in these land-remote areas are poorly known. These substantial algal blooms require significant Fe inputs, but the actual Fe supply mechanisms and their relative importance for primary production and biogeochemical processes along the flow of the southern Antarctic Circumpolar Current (S-ACC) remain largely unconstrained. Current hypotheses for the main Fe sources fuelling the large blooms along the S-ACC downstream of South Georgia are: i) Entrainment into the mixed layer of Fe-enriched deep waters originating around South Georgia through winter mixing and deep sources east of the large S-ACC bloom. ii) External sources such as atmospheric dust and icebergs and iii) lateral advection and recycling of particle associated Fe (living matter and detritus), potentially mediated by zooplankton feeding activity. Currently, we lack observational data on the relative importance of each of these different Fe supply mechanisms. We, therefore, first aim to quantify the main Fe pools in several surveys across the main flow of the S-ACC from the potential source in South Georgia (38°W) to the eastern boundary of the high productivity plume around 0°E. The second important aim will be to investigate how bioavailable the Fe in different pools is to SO phytoplankton. Thirdly, changes in the ocean's primary productivity affect the distribution of trace metals. The uptake or scavenging of mercury (Hg) by algae is suggested as a critical vector of the biomagnification of Hg in the marine food chain. We will investigate the relation between Hg algae scavenging and Methyl-Hg formation in the water column with the bioaccumulation in the trophic web and the final accumulation in the sediments.

As part of the overall goal of PS133/1 we aimed to:

- characterize the Fe distribution patterns, stocks and origin along the water column
- determine Fe isotope fractionation between dissolved and suspended Fe to identify potential mineral Fe sources and internal Fe cycling
- measure primary and bacterial production rates in the euphotic zone
- determine pico- and nanoplankton composition at 20 m depth

- assess Fe uptake rates, trace metal quotas, photo-physiological status and *in-situ* diatom species-specific growth rate at 20 m depth
- use transcriptomics to identify temporal and spatial difference in taxa-specific iron acquisition strategies among phytoplankton taxonomic groups (20 – 300 µm)
- use proteomics to quantify the contribution of dissolved proteins, particularly ferritins, to the cycling and transport of iron in the euphotic zone
- quantify transcriptional abundance to link Fe uptake rates and Fe acquisition strategies to specific phytoplankton taxonomic groups (at 20 m depth)
- determine the Fe bioavailability of different Fe sources (deep water, hydrothermal influenced seawater, grazing products from copepods) through several 24 h incubation experiments
- characterize the mercury (Hg) and Methyl-Hg distribution patterns (in sinking particular material, phyto- and zooplankton and water) along the water column as well as along productivity gradients
- determine the role of sinking particles on the Methyl-Hg distribution on the water column and how changes in the primary production can affect them

Work at sea

At 10 stations (3, 5, 6, 8, 9, 10, 11, 13, 14, 17, Fig. 4.1), seawater was collected with the AWI's new, state of the art, trace metal clean sampling infrastructure including a Teflon CTD (CTD-Clean) equipped with Ocean Test Equipment (OTE) bottles (12 L/bottle capacity) and winch.

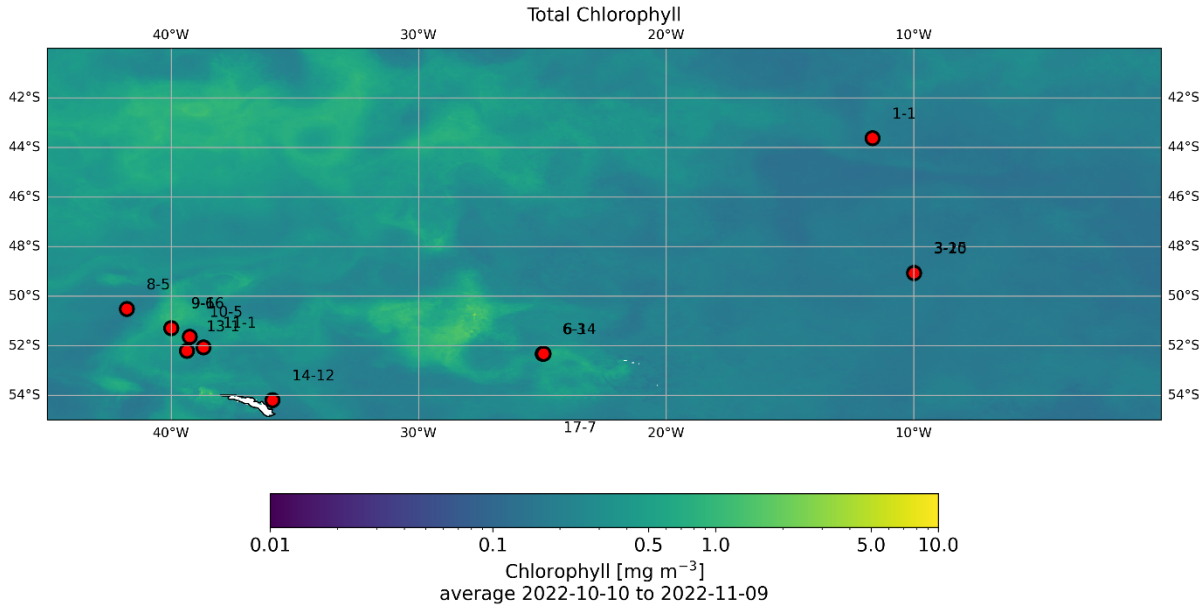

Fig. 4.1: Map of the 9 clean CTD stations (3, 5, 6, 8, 9, 10, 11, 13, 14) and the total chlorophyll concentrations determined from satellite imaging and averaged over the sampling period (10.10.22 to 9.11.22); the map was produced by Astrid Bracher.

In order to characterize trace metal chemistry (dissolved and particulate Fe, dissolved and particulate Fe isotopes, Fe chemical speciation, concentrations of ligands and humic acid-like substances, mercury) seawater was sampled as follows:

- At each station, we collected seawater to determine concentrations of dissolved trace metals (Fe, Mn, Zn, Co and Cu) from each depth where bottles were closed.
- At each station, we sampled for particulate Fe and Fe chemical speciation at 6 depths (20, 60, 100, 150, 300, 500 m).
- At each station, we collected seawater for the determination of the concentrations of humic acid-like substances at 5 depths (20, 60, 100, 150, 300 m).
- At 5 stations (3, 6, 9, 11, 17) we sampled seawater to estimate ligand concentrations at 5 depths (20, 60, 100, 150, 300 m).
- At 4 stations (station numbers 3, 6, 9,14) we collected particulate Fe isotope samples and at 8 stations (station numbers 3, 6, 8, 9, 11, 13, 14, 17) we collected dissolved Fe isotope samples from 8 depths (20, 60, 100, 150, 200, 300, 500 and 1,000 m).
- At 8 stations (station numbers 3, 5, 6, 8, 9, 13, 14 and 17), we collected seawater to determine the total concentration of Hg and MeHg. At stations 3, 6 and 9 samples were taken from each depth. At stations (3, 5, 8, 13 and 14) samples were taken at 7 depths (20, 60, 100, 150, 300, 500 and 1,000 m). At Station 17, samples were taken from 10 depths (20, 60, 100, 150, 500, 1,000, 4,000, 5,000, 6,000 and 7,000 m).
- Except for station 11, at each station samples were taken to determine the intracellular content of the trace metals Fe, Mn, Zn, Co and Cu of phytoplankton.

Additional samples were collected to investigate the transfer of mercury in pelagic and benthic foodwebs.

- At 7 stations (station number 3, 6, 9, 14, 15, 16 and 17), we collected particulate suspended matter using *in-situ* pumps from 6 different depths. For this, we deployed two types of *in-situ* pumps (McLane and Challenger Oceanic) equipped with two different filter types i.e., QMA filters with a nominal pore size of ~1 µm and a polyester pre-filter of 51 µm. Target depths were 25, 50, 75, 100, 150, 350 m. Due to the malfunction of some of the pumps, there is no single profile in which all the desired depths were collected.
- At 3 stations (station number 6, 9 and 14) subsamples from a vertically towed net (20 µm mesh size; see below) were collected to determine Hg and Methyl-Hg and carbon and nitrogen concentrations.
- At 6 stations (station number 3, 6, 8, 9, 10 and 14), zooplankton (meso- and macrozooplankton) samples were collected. Mesozooplankton samples were collected at 3 stations (3, 6 and 14) using a WP2 net. By filtration two different zooplankton size classes (50 µm and 150 µm) were separated. Macroozooplankton samples were collected at 4 stations using a RMT net (stations 6, 8 and 9) and a IKMT net (station 10).
- At 4 stations (station number 9, 15, 16 and 17), bottom sediment cores were collected using a multicorer (MUC). Each core was sampled at 1 cm resolution in the upper 10 cm; 2.5 cm resolution from 10 to 20 cm and 5 cm resolution below 20 cm.

All samples will be analyzed for total Hg, Methyl-Hg and carbon and nitrogen concentrations back in the home laboratory.

•

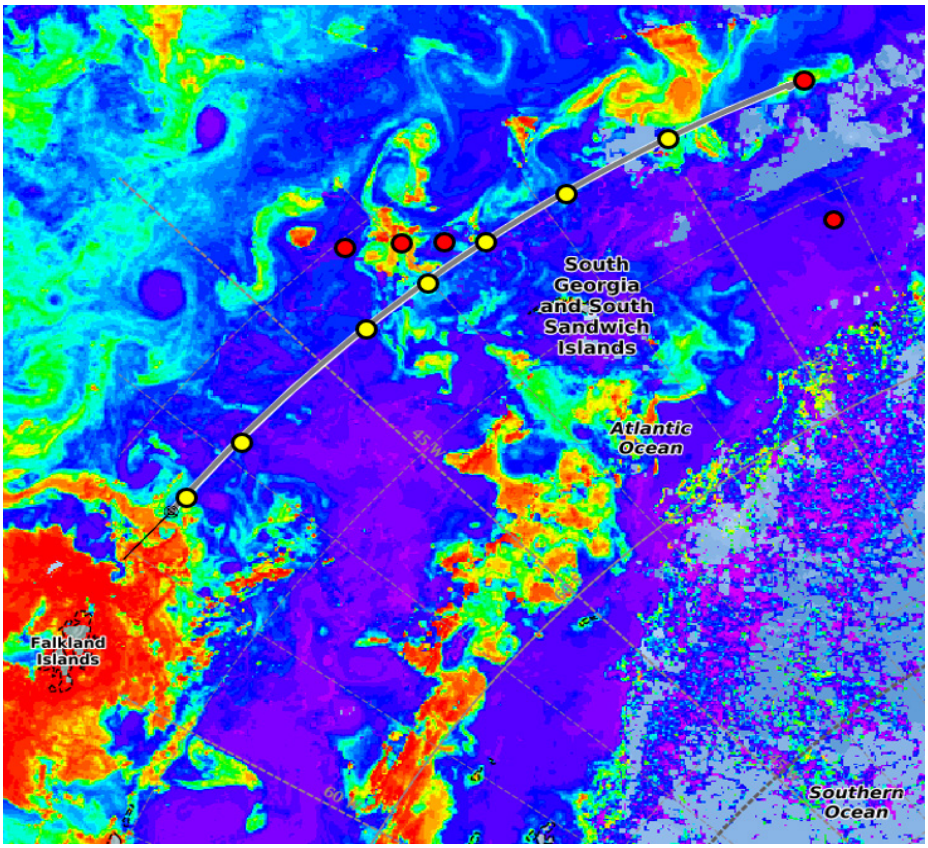

Fig. 4.2: Map of the sampling locations for coupled transcriptomic and proteomic sampling during PS 133/1

Coupled transcriptomic and proteomic samples were taken at 12 locations (Fig. 4.2). Stations indicated in red are collocated with trace metal CTD casts; stations in yellow were sampled underway from the ship's moon pool collocated with nutrient and chlorophyll sampling (see Chapters 4 and 8). In addition, at each station, RNA was sampled by concentrating 4 L of seawater onto a 0.22 µm sterivex capsule filter and snap-freezing at -80° C for subsequent extraction. Seawater proteins were concentrated by sequentially passing 50 L of seawater though two 3.0 and 0.2 µm high surface area capsule filters, followed by concentration using a 30 kD tangential flow filtration (TFF) membrane system. Final volume of the protein concentrate was 0.5 – 1.0 L. At two stations, water was available from the CTD, and sampled at 20 m; all other stations were sampled from the specially-installed sipper tube extending 11 m to the bottom of the *Polarstern's* moon pool.

At the 3 process stations (station number 6, 9 and 14), we took two 20 m deep net tows (20 µm) determine concentrations of plankton toxins. Samples were preserved for later analysis back in the home laboratory. Additionally, we used Solid Phase Absorption Toxin Tracking (SPATT-) bags as a sensitive *in situ* monitoring method to examine biotoxins due passive adsorption onto porous synthetic resin.

Bacterial production rates using ^{3}H-leucine as well as size-fractionated (0.2-2, 2-20 and >20 µm), primary production and Fe uptake rates using ^{14}C-bicarbonate and ^{55}Fe, respectively were estimated at 20 m depth at all stations. At the three process stations (3, 6, 9), size-fractionated (0.2-2, 2-20 and >20 µm) uptake rates of B_{12} were also determined using ^{57}Co-B_{12}. We further collected seawater from 20 m depth to determine B_1, B_7 and B_{12} vitamin concentrations using C18-bondisil-resin columns. We also assessed the photo-physiological status of the sampled phytoplankton community at 20 m depth from each station by means of a fast repetition rate fluorometer. At the three process stations (station numbers 3, 6, 9), PDMPO incubations were conducted over 48 h to estimate *in-situ* diatom species-specific growth rates.

FeMn addition experiments with natural phytoplankton communities sampled from 20 m depth at stations 8, 9, 13 and 14 were conducted to identify whether Mn is limiting or a co-limiting factor together with Fe. Experiments were carried out in triplicate 2.5 L polycarbonate bottles. The treatments consisted of either 0.5 nm inorganic Fe, 1 nm Mn while a combination of Fe with Mn together was also added to investigate potential co-limitation. All incubations were grown in a temperature-controlled growth chamber (2° C) at 30 µmol photons m^{-2} s^{-1} daylight irradiance under a light-dark cycle of 14,5 : 9,5 h. Macronutrient concentrations (nitrate, phosphate, silicate and ammonium) were measured at latest every second day over the course of the experiments. Similarly, the physiological state of the cells was determined via fast repetition rate fluorometry (FRRf, Chelsea) onboard. Samples for RNA analysis were collected during the light phase after at least 72 h after the onset of the first light phase. Moreover, at the beginning and end of the experiments, samples for taxonomic species composition, cell density and chemical parameters were taken as follows: To determine taxonomic composition aliquots of 100 mL unfiltered seawater were preserved with lugol at a final concentration of 1 %. Preserved samples were stored at 4° C in the dark until further analysis by light and epifluorescence microscopy back at the AWI. For bacterial and picoplankton composition via flow cytometry, seawater was transferred into cryovials and stored at -80°C for analysis at the home laboratory. Seawater pH was measured onboard using a calibrated pH/ion meter (Metrohm, three-point calibration). Information on the efficiency of photochemistry in PSII after dark acclimation for 1 h and during varying light exposure was obtained using FRRf by exposure to increasing irradiance (from 11 up to 600 µmol photons m^{-2} s^{-1}). Moreover, pigment samples were collected, filtered and stored at -80°C for high performance liquid chromatography (HPLC) analysis at the University of Bremen. Samples for particulate organic (POC) were filtered onto pre-combusted (500°C; 12 h) GFF filters and stored in pre-combusted petri dishes (500°C; 12 h) at -20°C. Samples for the determination of biogenic silicate were taken, filtered and stored at -20°C until further analysis. To test aggregation capacity and carbon export potential of all communities (Control, +Mn, +Fe, and +FeMn), 900 mL aliquots were taken from each triplicate bottle at the end of the incubation experiment and combined in a roller tank to induce aggregation via differential settling, the tanks were rotated at 1 rotation per minute (rpm) over 48 h at a constant temperature of 2°C in the dark. After 48 h, all tanks were filmed with a Canon EOS 650 to record aggregate formation, size/volume, and sinking velocity. At the end of the roller tank incubation, aggregated material was collected for POC content determination.

Unfortunately, due to bad weather conditions and time constraints, no experiments could be conducted to characterize the Fe bioavailability of different Fe sources (deep water, volcanically influenced seawater, grazing products from copepods) through 24 h incubation experiments.

Preliminary (expected) results

The expected data set will characterize the trace metal distribution and biogeochemistry in the open waters downstream of South Georgia. Our study will provide vertical profiles of trace metals in this biologically active area and elucidate their vertical distribution and possible sources. Rate measurements of primary and secondary production, coupled to uptake and

recycling rates of Fe and vitamins will shed light on the cycling and dynamics between these essential trace nutrients and the pelagic plankton community. Environmental transcriptomic and proteomic analyses will reveal the identities and metabolic strategies of plankton and enable the identification of dissolved extracellular proteins.

Data management

Environmental data will be archived, published and disseminated according to international standards by the World Data Center PANGAEA Data Publisher for Earth & Environmental Science (www.pangaea.de) within two years after the end of the cruise at the latest. By default the CC-BY license will be applied.

Molecular data (DNA and RNA data) will be archived, published and disseminated within one of the repositories of the International Nucleotide Sequence Data Collaboration (INSDC, www.insdc.org) comprising of EMBL-EBI/ENA, GenBank and DDBJ). Environmental proteome data will be deposited in the publicly accessible Ocean Protein Portal (https://proteinportal.whoi.edu).

Any other data will be submitted to an appropriate long-term archive that provides unique and stable identifiers for the datasets and allows open online access to the data.

In all publications based on this expedition, the **Grant-No. AWI_PS133/1_04** will be quoted and the following publication will be cited:

Alfred-Wegener-Institut Helmholtz-Zentrum für Polar- und Meeresforschung (2017) Polar Research and Supply Vessel POLARSTERN Operated by the Alfred-Wegener-Institute. Journal of large-scale research facilities, 3, A119. http://dx.doi.org/10.17815/jlsrf-3-163.

6. CARBON CHEMISTRY

Leticia Cotrim da Cunha[1], Lorenz Eckardt[2], [1]BR.UERJ
Raquel A. dos Santos[1], Sebastian Rokitta[2], [2]DE.AWI
Iole Orselli[3] [3]BR.FURG
Not on board: Rodrigo Kerr[3]

Grant-No. AWI_PS133/1_05

Objectives

In order to improve carbon budget estimates during the growth season in the Atlantic sector of the S-ACC downstream of South Georgia and understand the effect of biological processes in the regional ocean carbon uptake, it is critical to increase spatial and depth coverage of ocean carbon essential ocean variables (EOVs). Here we sampled and measured these variables along the cruise path and at stations, including the short time-scale variability and response during the process stations (24-hour monitoring).

Work at sea

During the cruise, the analyses of the carbon chemistry in seawater were carried out using 3 different approaches (Table 6.1):

- Water samples at all possible discrete depths were collected from the oceanographic CTD (CTD-OZE) and Trace Metal Clean CTD (CTD-Clean) casts for analysis of total CO_2 and alkalinity (here referred as DIC and TA, respectively)
- Surface “underway” discrete water samples were collected from a tubing and peristaltic pump system installed in the ship’s moon pool (~11 m depth) for analysis of DIC and TA
- Surface "underway” continuous measurements of seawater and atmosphere CO_2 content were carried out with the General Oceanics system installed onboard with an infrared analyser (LiCOR), both for seawater using a water-air equilibrator and for the atmosphere, the air being pumped from the crow’s nest

All CTD-rosette and underway samples were collected using acid-washed glass bottles (250 mL borosilicate) that were thoroughly rinsed with the sampled water.

On board, water samples were analyzed for TA (in µmol/kg) and DIC (µmol/kg) with a VINDTA 3C Marianda system (Fig. 6.1); sampling as well as analyses (TA, DIC), were carried out following the standard methods described in Dickson et al. (2007). Measurements were calibrated with three types of certified reference materials: Dickson/Scripps/USA, ICOS/Geomar/Germany, and Tris/AWI/Germany.

Tab. 6.1: List of analyzed discrete samples and their types

Sample type	Number of samples	Parameters
CTD–OZE	185	TA and DIC
CTD-Clean	29	TA and DIC
Hadal sites	6	TA and DIC
Underway (moon pool)	270	TA and DIC

Total alkalinity (open cell):

From a calibrated pipette, a known amount of sea water was placed in an open cell at controlled temperature (~25°C) where it was titrated with a solution of 0.1 M hydrochloric acid in a two-stage titration continued until a pH of about 3.0 has been reached. The progress of the titration was monitored using a thermometer and pH glass electrode/reference electrode cell. The final TA value is calculated from the amount of titrant (acid) used and the potential measurements in mV using a non-linear least-squares approach that corrects for the reactions with sulfate and fluoride ions.

DIC (coulometry):

From a calibrated pipette, a known amount of sea water was dispensed into a stripping chamber where it is acidified with H_3PO_4 and purged with an inert gas (N_2). At this stage, all forms of dissolved inorganic carbon become gaseous CO_2, and the resulting gas stream were determined by trapping the CO_2 in a coulometric cell, containing an absorbent solution (ethanolamine) and titrating coulometrically the hydroxyethylcarbamic acid that is formed.

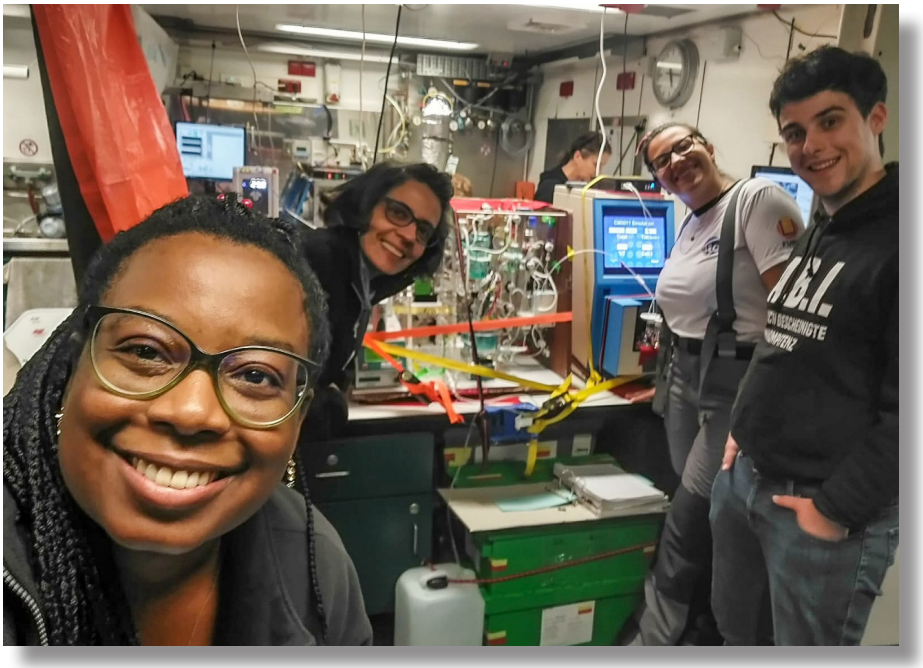

Fig. 6.1: The Carbon chemistry group on board the lab of Polarstern; from left to right: Raquel Avelina, Leticia Cotrim, Iole Orselli and Lorenz Eckardt, and at the back the VINDTA Marianda system for the simultaneous determination of AT and DIC in discrete seawater samples; photo credit: Raquel Avelina

Preliminary results

Most of the discrete samples (CTD-rosette and underway) analyses were performed on board (Figs. 6.2 and 6.3). A total of 30 preserved samples will be further analyzed at the home laboratory in Bremerhaven by April/May 2023.

The underway, continuous ocean surface CO_2 measurements were downloaded every day to help assess the biological activity, one of the tools used to decide the location of the process stations. All along the ship's track, and with help of the discrete samples, it was possible to estimate if the CO_2 molar fraction on the surface ocean was smaller than the theoretical value, calculated using TA and DIC values. Atmospheric CO_2 values were stable around circa 409 ppm. During the process stations, the continuous measurements of surface seawater CO_2 could also be used to estimate the role of biological carbon uptake (Fig. 6.4).

The DIC, total alkalinity and pCO_2 data will be processed and quality checked after the cruise in the home laboratory.

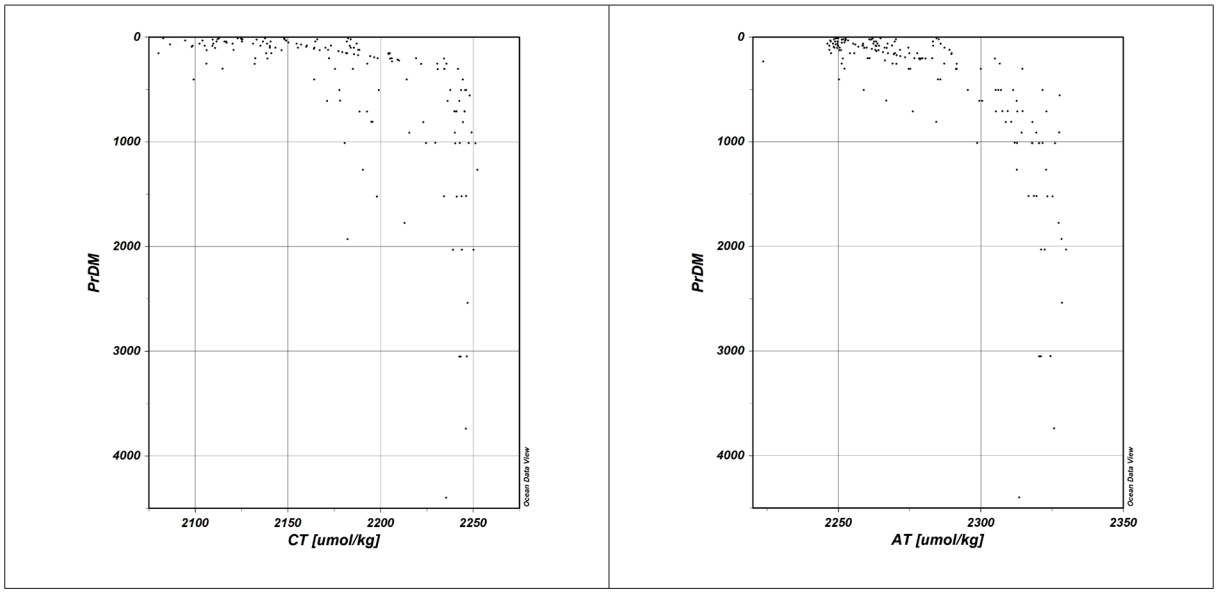

Fig. 6.2: Vertical profiles of DIC (left panel, in µmol/kg) and total alkalinity (right panel, in µmol/kg) from the Niskin bottles (CTD-OZE samples) and OTE bottles (CTD-Clean)

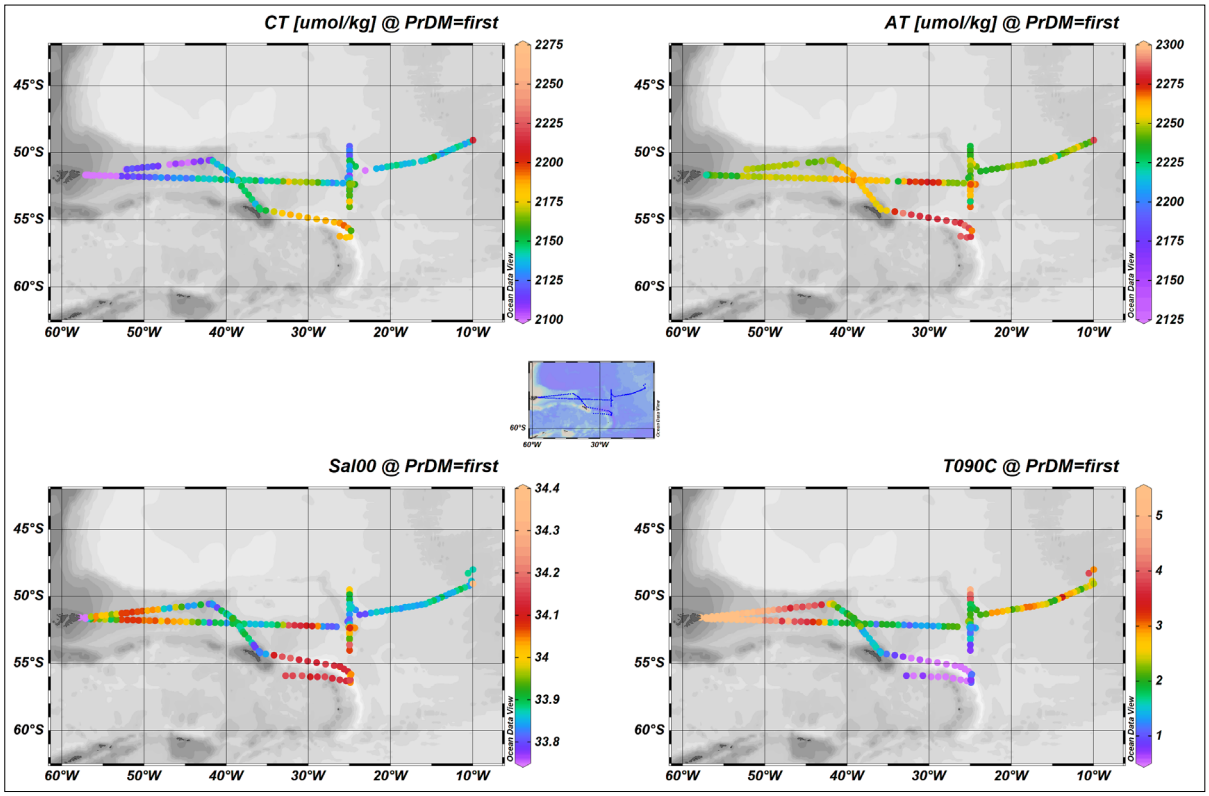

Fig. 6.3: Map of the underway discrete samples (from the ship's moon pool) during the Island Impact expedition (PS133/1), with the preliminary results obtained onboard; Upper left panel: DIC (µmol/kg); upper right panel: TA (µmol/kg); lower left panel: sea surface salinity (from the ship's thermosalinograph); lower right panel: sea surface temperature (from the ship's thermosalinograph)

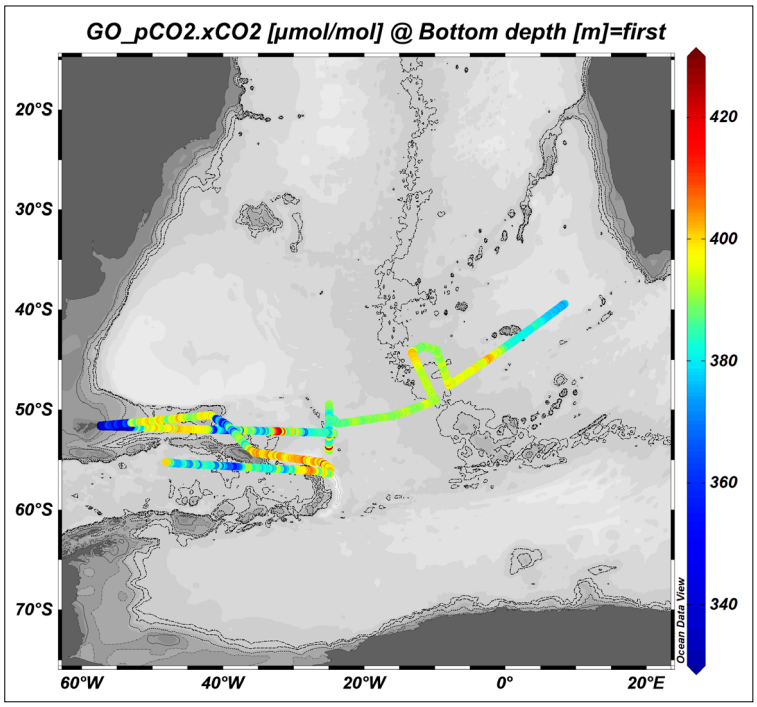

Fig. 6.4: Underway continuous measurements of surface ocean molar fraction of CO_2 (xCO_2, in µmol/mol) during the Island Impact expedition (PS133/1)

Data management

Environmental data will be archived, published and disseminated according to international standards by the World Data Center PANGAEA Data Publisher for Earth & Environmental Science (https://www.pangaea.de) within two years after the end of the cruise at the latest. By default, the CC-BY license will be applied.

Any other data will be submitted to an appropriate long-term archive that provides unique and stable identifiers for the datasets and allows open online access to the data.

This expedition was supported by the Helmholtz Research Programme “Changing Earth – Sustaining our Future” Topic 6, Subtopic 3, Topic 2, Subtopic 1.

In all publications based on this expedition, the **Grant No. AWI_PS133/1_05** will be quoted and the following publication will be cited:

Alfred-Wegener-Institut Helmholtz-Zentrum für Polar- und Meeresforschung (2017) Polar Research and Supply Vessel POLARSTERN Operated by the Alfred-Wegener-Institute. Journal of large-scale research facilities, 3, A119. http://dx.doi.org/10.17815/jlsrf-3-163.

References

Dickson A, Sabine CL, and Christian J R (Eds.) (2007) Guide to best practices for ocean CO_2 measurements, 191 pp.

7. NET COMMUNITY PRODUCTION

Sebastian Rokitta[1] [1]DE.AWI
Not on board:
Klaus-Uwe Richter[1], Björn Rost[1]

Grant-No. AWI_PS133/1_05

Outline

One of the major open questions regarding the biogeochemistry of the Atlantic sector of the Southern Ocean is how and to which extent the micronutrient iron from the continental shelf and/or depth waters around Southern Georgia, controls the primary productivity in this region.

The study region regularly exhibits extensive primary production, and also features rapid transfer of carbon to higher trophic levels as well as considerable export fluxes to depth. The magnitude of these biogeochemical fluxes, and the controls on regional patchiness are, however, uncertain.

Over the past 10 years, an extended mobile Membrane-Inlet Mass Spectrometer (MIMS) system has been developed at the Alfred Wegener Institute section *Marine Biogeosciences* that can be deployed onboard research vessels to measure the concentrations of dissolved gases in the ship´s seawater supply or in discrete bottle samples derived from CTD-rosette casts.

Fig. 7.1: The ship-going MIMS system during the MOSAiC drift;
photo credit: Emelia Chamberlain, Scripps Institute for Oceanography

Objectives

To better understand the magnitude as well as the local gradients of primary productivity, we have assessed concentrations of dissolved O_2 and Ar using membrane-inlet mass spectrometry (MIMS) in order to determine net community production of transected water masses (Craig and Hayward, 1987). Data is being combined with other oceanographic data (temperature, salinity, macro-/micronutrients, mixed-layer depths), chemical data (nutrient fluxes, CO_2 concentrations), biological data (phytoplankton abundance, chlorophyll concentrations), and meteorological data (insolation, wind speed) to derive estimates of net community production (Kaiser et al., 2005; Ulfsbo et al., 2014)

Work at sea

This work was conducted continuously, i.e., started on 6 October after leaving the exclusive economic zone of South Africa and ended on 14 November, when we set course for Punta Arenas. During the short stay at the Falkland Islands, no data was recorded. Besides these downtimes, the instrument ran in continuous mode and acquired data over more than 40 days. During these times, the Antarctic Polar Front was crossed several times, and the cruise steamed across regions of low, moderate and exceptionally high phytoplankton biomass. Similarly, a Fast Repetition Rate Fluorometer (FRRF) (Chelsea Technology Group) was used in a flow-through system to provide continuous surface measurement of phytoplankton photosynthetic performance (photosynthetic efficiency Fv/Fm), an indicator for iron limitation, during the entire cruise**.**

Preliminary results

We have recorded a high-resolution dataset of O_2:Ar ratios in surface water that was combined with the output from the ship´s thermosalinograph to derive biologically mediated O_2 concentrations (Fig. 7.2). As expected, in regions with high chlorophyll, also productivity was high, causing strong excursions in surface O_2 concentrations. We will further use published methods (Kaiser et al., 2005; Ulfsbo et al., 2014) to estimate net community production from these data. We will compare our findings with budget calculations based on nutrients and dissolved inorganic carbon, and correlate our findings with the results of the other cruise participants.

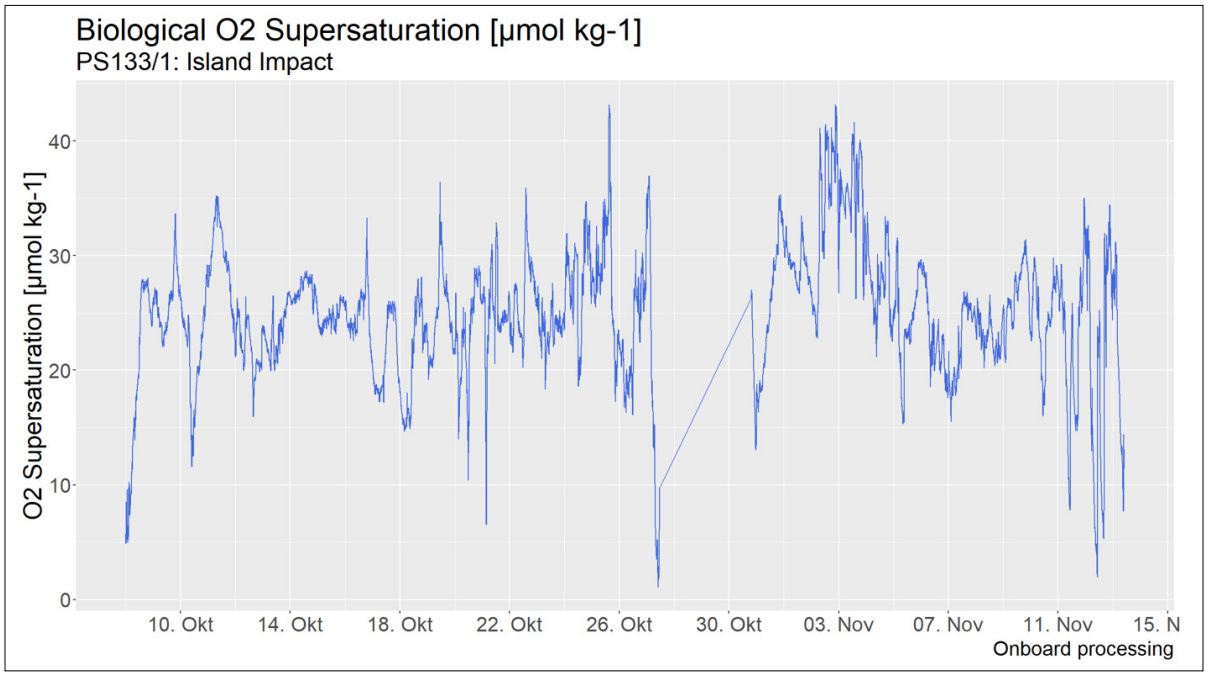

Fig. 7.2: Oxygen saturation throughout PS133/1 (Island Impact)

Data management

Environmental data will be archived, published and disseminated according to international standards by the World Data Center PANGAEA Data Publisher for Earth & Environmental Science (https://www.pangaea.de) within two years after the end of the cruise at the latest. By default, the CC-BY license will be applied.

Any other data will be submitted to an appropriate long-term archive that provides unique and stable identifiers for the datasets and allows open online access to the data.

This expedition project was supported by the Helmholtz Research Programme “Changing Earth – Sustaining our Future” Topic 6, Subtopics 2 and 3.

In all publications based on this expedition, the **Grant No. AWI_PS133/1_05** will be quoted and the following publication will be cited:

Alfred-Wegener-Institut Helmholtz-Zentrum für Polar- und Meeresforschung (2017) Polar Research and Supply Vessel POLARSTERN Operated by the Alfred-Wegener-Institute. Journal of large-scale research facilities, 3, A119. http://dx.doi.org/10.17815/jlsrf-3-163

References

Craig H, Hayward T (1987) Oxygen Supersaturation in the Ocean: Biological Versus Physical Contributions. Science, 235(4785):199–202.

Kaiser J, Reuer MK, Barnett B, Bender ML (2005) Marine productivity estimates from continuous O_2/Ar ratio measurements by membrane inlet mass spectrometry. Geophysical Research Letters, 32(19): L19605.

Ulfsbo A, Cassar N, Korhonen M, van Heuven S, Hoppema M, Kattner G, Anderson LG (2014) Late summer net community production in the central Arctic Ocean using multiple approaches. Global Biogeochemical Cycles, 28(10):1129–1148.

8. UNICELLULAR PLANKTON AND PARTICULATE MATTER

Christine Klaas[1], Clara Iachetti[2], Alexandra Kraberg[1], Larissa Pattison[3], Nadia Soledad Rolandi[4], Leonard Rößler[5], Susanne Spahic[1], Dieter Wolf-Gladrow[1]
Not on board: Rudolf Amann[5], Irene Ruth Schloss[6]

[1]DE.AWI
[2]AR.CADIC
[3]CA.DAL
[4]AR.ARA
[5]DE.MPIMM
[6]AR.IAA

Grant-No. AWI_PS133/1_06

Objectives

Our aim is to determine how different environmental factors influence plankton assemblage composition and dynamics and the resulting impacts on biogeochemical fluxes. During PS133/1, in particular, we will investigate how differences in trace metal inputs (with increasing distance from South Georgia) versus other environmental parameters affect distribution patterns of key diatom and heterotrophic pro- and eukaryotes species, and the consequences for accumulation and export of organic matter and nutrients from the surface mixed layer. The study combines sampling of surface waters for bulk particulate matter standing stocks and composition, microscopy and molecular analysis of plankton communities.

Work at sea

Suspended particulate matter

Water samples were collected from the CTD-rosette deployments at 8-10 discrete depths ranging from 10 to 250 m at all stations. Additional sampling in deeper layers (> 250 m) and underway (from the ship's moon pool, see Table 14.3 for sample position) were collected to expand data coverage and to be used for the calibration of sensors (transmissometer and fluorometer) from the CTD-rosette and towed system (topAWITriaxus). Water samples for chlorophyll a (Chl *a*) analysis were filtered onto 25 mm diameter GF/F filters at pressures not exceeding 200 mbar. Filters were immediately transferred to centrifuge tubes with 6 mL 90 % acetone and 1 ccm of glass beads. The sealed tubes were stored at -20°C for at least 30 min. Chl *a* was extracted by placing the centrifuge tubes in a grinder (Precellys®) for 30 seconds followed by centrifugation at 4,000 rpm and 0°C. The supernatant was poured in quartz tubes and measured for Chl *a* content in a calibrated Turner Trilogy fluorometer following the procedures described in Knap et al. (1996). Seawater (1-2 L and up to 10 L in deeper layers) samples for POC and PON analysis were filtered onto pre-combusted 25 mm diameter GF/F filters and stored in pre-combusted glass Petri dishes. Filters were dried overnight at 50°C and stored (-20°C) for further analysis on land. Seawater (1-2 L) samples for BSi analysis were filtered onto polycarbonate filters (0.8 µm pore size), transferred to Eppendorf tubes, dried overnight at 50°C and stored at -20°C for further analysis on land.

Quantitative assessment of phyto- and heterotrophic assemblages

Duplicate water samples for microscopic analysis of protist assemblages were preserved with hexamine-buffered formalin solution (200 mL) and with Lugol's iodine (100 mL), respectively, at a final concentration of 2 %. Fixed samples were stored at 4°C in the dark for transfer back to the home laboratory. Hand net samples (20 µm mesh size) from the upper 20 m of the water column were also used to collect plankton cells for more detailed taxonomic studies.

Further, samples for molecular analysis of the microbial communities were collected to characterize assemblage diversity and composition of protists and procaryotes (metagenomics, transcriptomics and fluorescent *in-situ* hybridisation) that cannot be identified using light microscopy. Samples for procaryotic diversity analyses and metabolism were collected from the surface mixed layer (20 m depth), filtered (size fractionated in pico 0.2-3 µm, nano: 3-10 µm and microplankton: >10 µm) and stored at -80°C for later metagenomics and tag-sequencing analyses. Samples for fluorescence *in situ* hybridization (FISH) and total cell counts (TCC) were taken from three discrete depths (Tab. 8.1). Upon fixation in 1 % formaldehyde, the samples were filtered directly on 0.2 µm polycarbonate filters, which were stored at -20 °C until processing. In some cases the fraction 0.02-0.2 was also filtered for fluorescence *in situ* hybridization analysis of viruses.

Tab. 8.1: Sampling stations for microbial community

Station_ Cast	Depth [m]	Latitude [°S]	Longitude [°W]	Sample	Quantity	Purpose
3_3	20, 150, 300	49.065	9.993	Filter	7	FISH and TCC
3_3	20, 150, 300	49.065	9.993	Water	3x10 ml	Bioarchive sample in collaboration with Prof. Dr. Jens Harder
3_3	20	49.065	9.993	Filter	3	Genomic Analyses
3_3	20	49.065	9.993	Filter	1	Virus (FISH)
5_1	20, 150, 500	54.000	25.000	Filter	4	FISH and TCC
5_1	20	54.000	25.000	Filter	3	Genomic Analyses
5_1	20	54.000	25.000	Filter	1	Virus Filter
6_3	40, 150, 500	52.330	24.998	Filter	4	FISH and TCC
6_3	40	52.330	24.998	Filter	3	Genomic Analyses
6_3	40	52.330	24.998	Filter	1	Virus Filter
7_1	50, 150, 300	51.232	52.236	Filter	4	FISH and TCC
7_1	50	51.232	52.236	Filter	3	Genomic Analyses
7_1	50	51.232	52.236	Filter	1	Virus Filter
8_3	40, 150, 300	50.519	41.796	Filter	7	FISH and TCC
8_3	40	50.519	41.796	Filter	3	Genomic Analyses
8_3	40	50.519	41.796	Filter	1	Virus Filter
9_3	20, 150, 300	51.288	40.003	Filter	7	FISH and TCC
9_3	20	51.288	40.003	Filter	3	Genomic Analyses
9_3	20	51.288	40.003	Filter	1	Virus Filter
10_3	40, 150, 300	51.636	39.245	Filter	4	FISH and TCC
10_3	40	51.636	39.245	Filter	3	Genomic Analyses
10_3	40	51.636	39.245	Filter	1	Virus Filter
13_1	20, 150, 300	52.214	38.368	Filter	4	FISH and TCC
13_1	20	52.214	38.368	Filter	3	Genomic Analyses

Station_ Cast	Depth [m]	Latitude [°S]	Longitude [°W]	Sample	Quantity	Purpose
13_1	20	52.214	38.368	Filter	1	Virus Filter
14_4	40, 110, 210	54.194	35.910	Filter	4	FISH and TCC
14_4	40	54.194	35.910	Filter	3	Genomic Analyses
14_4	40	54.194	35.910	Filter	1	Virus Filter
15_3	10, 160, 300	55.215	26.163	Filter	4	FISH and TCC
15_3	10	55.215	26.163	Filter	3	Genomic Analyses
15_3	10	55.215	26.163	Filter	1	Virus Filter
16_3	40, 150, 300	55.803	24.839	Filter	4	FISH and TCC
16_3	40	55.803	24.839	Filter	3	Genomic Analyses
16_3	40	55.803	24.839	Filter	1	Virus Filter
Underway	Moonpool	52.266	25.816	Filter	1	FISH and TCC
Underway	Moonpool	52.25	26.603	Filter	1	FISH and TCC
Underway	Moonpool	52.227	27.658	Filter	1	FISH and TCC
Underway	Moonpool	52.206	28.832	Filter	1	FISH and TCC
Underway	Moonpool	52.179	30.206	Filter	1	FISH and TCC
Underway	Moonpool	52.15	31.63	Filter	1	FISH and TCC
Underway	Moonpool	52.122	33.063	Filter	2	FISH and TCC
Underway	Moonpool	52.122	33.063	Filter	1	Genomic Analyses
Underway	Moonpool	52.011	34.501	Filter	1	FISH and TCC
Underway	Moonpool	52.068	35.775	Filter	1	FISH and TCC
Underway	Moonpool	52.041	37.158	Filter	2	FISH and TCC
Underway	Moonpool	52.041	37.158	Filter	1	Genomic Analyses
Underway	Moonpool	52.014	38.508	Filter	1	FISH and TCC
Underway	Moonpool	51.976	39.983	Filter	1	FISH and TCC
Underway	Moonpool	51.957	41.365	Filter	1	FISH and TCC
Underway	Moonpool	51.929	42.743	Filter	2	FISH and TCC
Underway	Moonpool	51.929	42.743	Filter	1	Genomic Analyses
Underway	Moonpool	51.884	45.000	Filter	2	FISH and TCC
Underway	Moonpool	51.884	45.000	Filter	1	Genomic Analyses
Underway	Moonpool	50.767	45.749	Filter	2	FISH and TCC
Underway	Moonpool	50.767	45.749	Filter	1	Genomic Analyses

In addition, for the analysis of eukaryotic diversity, surface water samples were collected with an automated sampler (AUTOFIM), stored at –20°C for later metabarcoding analysis.

Preliminary (expected) results

The samples and results from the suspended matter analysis will provide basic information to understand the drivers and dynamics of the carbon and silicon cycles at large and small spatial and temporal scales. This information is complemented by the analysis of plankton abundances, composition combined with data from other working groups on board, to understand factors driving phytoplankton species dynamics and processes (biological, chemical and physical) and biogeochemical export fluxes in the open waters downstream of South Georgia. Finally, we will contribute to the study of how physical processes affect biogeochemical processes from the regional to the sub-mesoscale.

Results from the underway and surface station samples for Chl *a* (Fig. 8.1) show sizeable and patchy development of phytoplankton biomass (> 0.5 µg L^{-1}) in October over most of the Southern ACC. Further, both North-South and East-West gradients can be seen (Fig. 8.1) with hotspots of high Chl *a* found close to the Polar Front at 10°W (see also Fig. 8.2), while at 25°W, higher concentrations were located in the vicinity of the Southern ACC Front. Highest phytoplankton biomass was also found towards the east in the Northern Georgia Basin with values exceeding 4 µg Chl *a* L^{-1} over a 100 m deep surface mixed layer (Fig. 8.1 and 8.2). These are, to the best of our knowledge, the highest Chl *a* stocks (379 mg m^{-2}) ever recorded in oceanic waters. Surprisingly, despite the early season, these values were similar to peak concentrations in coastal areas of the Southern Ocean (Moline et al., 1997; Smith et al., 2000) and higher than Chl *a* concentrations in the shelf of South Georgia, were higher productivity due to shallower mixing and higher iron concentrations would be expected.

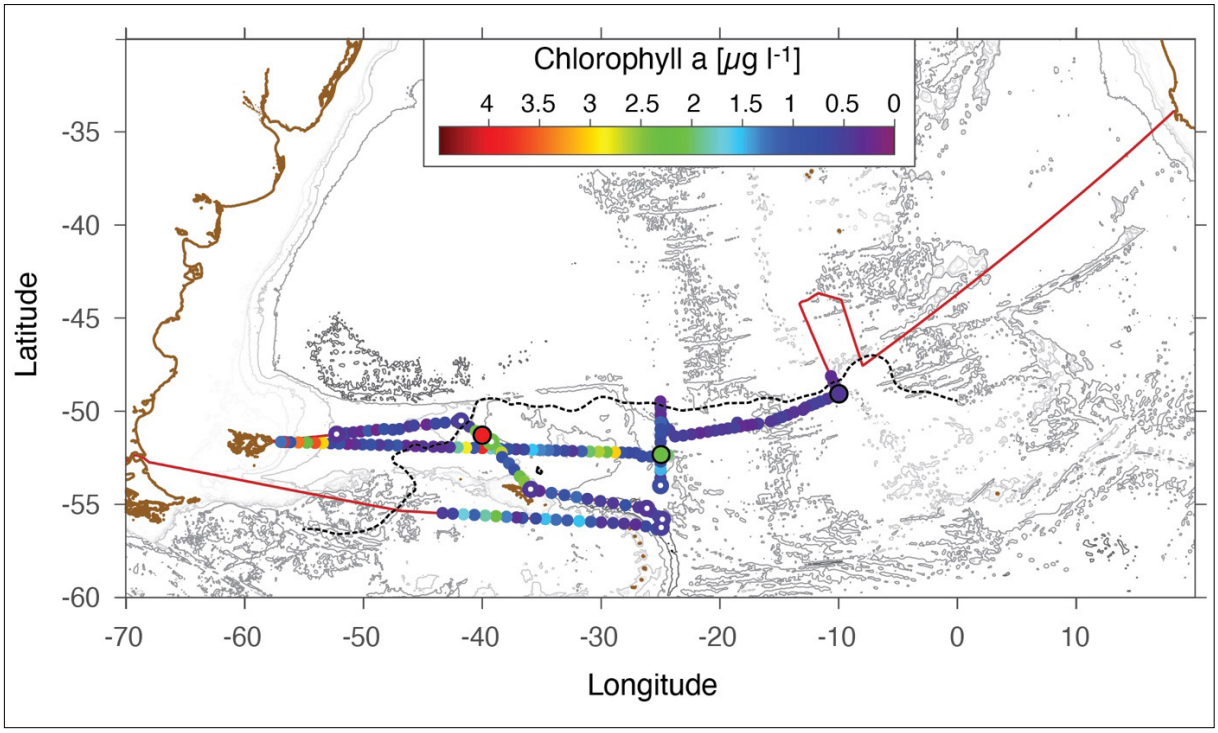

Fig. 8.1: Cruise track (red line) and underway and surface Chl a distribution (coloured circles) during PS133/1; process station are indicated by the black circles, other stations are indicated by the small white dots. Dotted line marks the climatological position of the Polar Front based on Sea Surface Height.

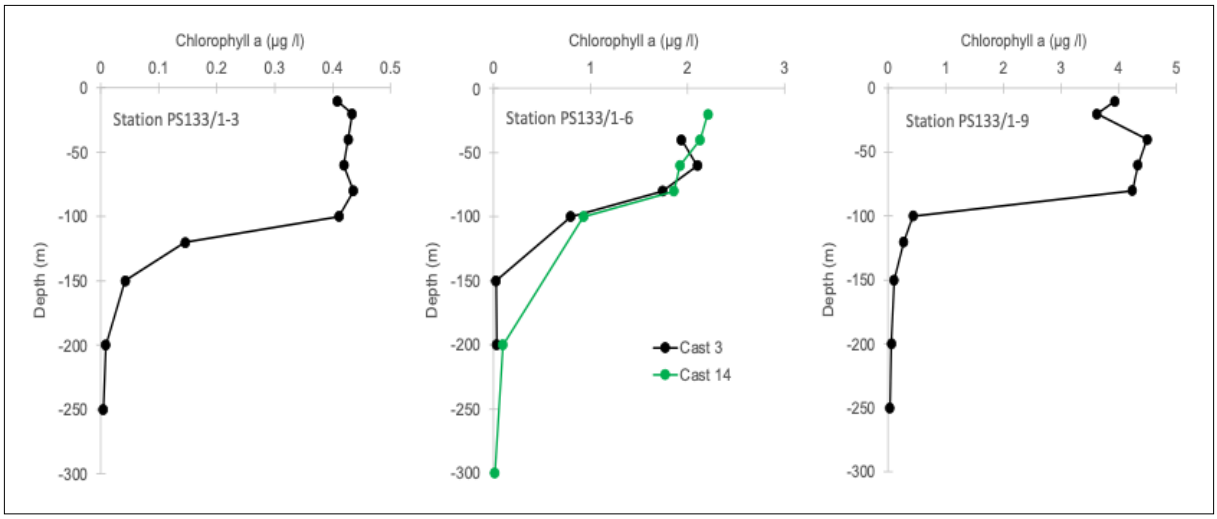

Fig. 8.2: Vertical Chl a distribution at the three process stations (PS133/1-3, PS133/1-6 and PS133/1-9)

Data management

Environmental data will be archived, published and disseminated according to international standards by the World Data Center PANGAEA Data Publisher for Earth & Environmental Science (https://www.pangaea.de) within two years after the end of the cruise at the latest. By default, the CC-BY license will be applied.

Molecular data (DNA and RNA data) will be archived, published and disseminated within one of the repositories of the International Nucleotide Sequence Data Collaboration (INSDC, www.insdc.org) comprising of EMBL-EBI/ENA, GenBank and DDBJ).

Any other data will be submitted to an appropriate long-term archive that provides unique and stable identifiers for the datasets and allows open online access to the data.

This expedition is supported by the Helmholtz Research Programme “Changing Earth – Sustaining our Future” Topic 6, Subtopic 3 and Topic 2, Subtopic 1.

In all publications based on this expedition, the **Grant No. AWI_PS133/1_06** will be quoted and the following publication will be cited:

Alfred-Wegener-Institut Helmholtz-Zentrum für Polar- und Meeresforschung (2017) Polar Research and Supply Vessel POLARSTERN Operated by the Alfred-Wegener-Institute. Journal of large-scale research facilities, 3, A119. http://dx.doi.org/10.17815/jlsrf-3-163.

References

Knap A, Michaels A, Close A, Ducklow H and A. Dickson (eds.). 1996. Protocols for the Joint Global Ocean Flux Study (JGOFS) Core Measurements. JGOFS Report Nr. 19, vi+170 pp. Reprint of the IOC Manuals and Guides No. 29, UNESCO 1994.

Moline, Mark A, Prezelin BB, Schofield O (1997) Palmer LTER: Stable interannual successional patterns of phytoplankton communities in the coastal waters off Palmer Station, Antarctica. Antarctic Journal of the United States, 32(5):151.

Smith Jr, Walker O, et al. (2000) The seasonal cycle of phytoplankton biomass and primary productivity in the Ross Sea, Antarctica. Deep Sea Research Part II: Topical Studies in Oceanography, 47(15-16:3119-3140.

9. MESOZOOPLANKTON

Jörg Dutz[1], Delove Asiedu[2], Jonas Bolduan[2] [1]DE.IOW
Not on board: Marja Koski[2] [2]DK.DTU

Grant-No. AWI_PS133_07

Outline

The zooplankton community structure and the species-specific ecophysiology and behaviour can significantly affect the efficiency of the biological carbon pump. In principle, this can be related to the activity and stock size of large and small zooplankton, which have an antagonistic effect. Large copepods contribute to the vertical transport of organic material into the ocean interior by the production of fast sinking faecal pellets during grazing and the respiration of ingested material at depth during intense vertical migrations (Steinberg and Landry, 2017). Small copepods, in contrast, may play a contrasting role and reduce the vertical flux by feeding on sinking pellets and aggregates (Koski et al., 2020). Recent research demonstrates that they might be far more abundant than previously thought and could dominate the zooplankton community in many polar areas (Dubischar et al., 2002; Arendt et al., 2013). The community structure of the zooplankton in the Atlantic sector of the Antarctic Circumpolar Current (ACC) is largely understudied with regard to the size composition and the contribution of small copepods to the stock, which is due to the general use of nets with mesh size larger than 200 µm which show the dominance of *Calanoides acutus*, *Rhincalanus gigas* or *Metridia gerlachei* among the large zooplankton (e.g., Voronina 1998; Pakhomov et al. 2000, Ward et al 2012). In addition, only few studies have been conducted during the early spring when the spring bloom is initiated.

Objectives

In contrast to other areas in the world ocean, a negative correlation between primary production and export flux in the Southern Ocean (Le Moigne et al., 2016) suggests that despite a high primary production not much organic material leaves the euphotic zone. We hypothesize that a balance between stocks of large flux-producing copepods (e.g., *Rhincalanus gigas*) and small flux attenuators (e.g., *Oncaea* spp.) may explain this pattern. We aimed to test this along the productivity gradient from South Georgia and downstream along the flow of the ACC. Within the scope of expedition PS133/1, our key objectives were to:

- Investigate the change in community composition of the mesozooplankton along a latitudinal gradient with regard to size structure and functional types.
- Estimate the importance of large vs. small copepods to export production, by comparing their stock sizes and faecal pellet production and degradation (feeding) of sinking particles.
- Understand the effect of environmental conditions (temperature, food availability) on the production of key players in both size groups.

Work at sea

The community composition, abundance, vertical distribution, population structure and vertical migration of small (< 1 mm) and large mesozooplankton (> 1 mm) was studied by vertical tows of a MultiNets equipped with 55 and 200 µm mesh size, respectively. A total of eight stations were sampled during the cruise (Table 9.1). They followed generally the expected productivity gradient with high chlorophyll stocks at station PS133/1_9 north of South Georgia and decreasing concentrations downstream the ACC (stations PS133/1_3, PS133/1_5, and PS133/1_6). In the high productivity area north of South Georgia a transect across the main flow of the ACC was conducted with the stations PS133/1_8 to PS133/1_14. Finally, one neritic station located northeast on the shelf of South Georgia and one deep station located in the South Sandwich Trench system were sampled. The sampling resulted in a total of 22 profiles with 111 samples for both net types, including: four day/night profiles to study the diel migration of zooplankton. The vertical tows were generally done at depth intervals of 0 to 50 m, 50 to 100 m, 100 to 200 m, 200 to 400 m and 400 to 600 m. However, the shallower neritic station was sampled at narrower intervals of 0 to 25 m, 25 to 80 m, 80 to 140 m, 140 to 200 m and 200 to 225 m that were chosen on basis of the vertical CTD profile. All samples were conserved in 4 % seawater-formalin solution stored at 4°C in the dark for later analysis of species composition, abundance, and biomass. Estimates of the egg production rates of small copepods (*Oithona* spp., *Microsetella* spp., *Oncaea* spp.) will be carried out based on the egg ratio method using the 55 µm MultiNet casts.

Tab. 9.1: Location and timing of the vertical net tows conducted with the Multinet equipped with 55 µm and 200 µm mesh size nets and the number of samples obtained

Station	Date	Day	Mesh size	Sample Number	Latitude	Longitude
PS133/1_3-5	13.10.2022	23:15	55 µm	4	49° 03,983’ S	009° 59,564’ W
PS133/1_3-6	14.10.2022	00:40	200 µm	5	49° 04,026’ S	009° 59,431’ W
PS133/1_3-17	14.10.2022	14:46	55 µm	5	49° 03,418’ S	009° 58,763’ W
PS133/1_3-18	14.10.2022	16:09	200 µm	5	49° 03,356’ S	009° 58,714’ W
PS133/1_5-4	20.10.2022	22:30	55 µm	5	54° 00,127’ S	024° 59,549’ W
PS133/1_6-6	22.10.2022	06:58	55 µm	5	52° 19,761’ S	024° 59,646’ W
PS133/1_6-7	22.10.2022	08:22	200 µm	5	52° 19,659’ S	024° 59,314’ W
PS133/1_6-16	22.10.2022	18:58	55 µm	5	52° 19,648’ S	024° 52,859’ W
PS133/1_6-17	22.10.2022	20:18	200 µm	5	52° 19,530’ S	024° 51,586’ W
PS133/1_8-6	01.11.2022	21:30	55 µm	5	50° 31,223’ S	041° 47,631’ W
PS133/1_8-7	01.11.2022	23:01	200 µm	5	50° 31,174’ S	041° 47,672’ W
PS133/1_9-9	02.11.2022	23:19	55 µm	4	51° 17,334’ S	039° 59,950’ W
PS133/1_9-10	03.11.2022	00:32	200 µm	5	51° 17,492’ S	039° 59,707’ W
PS133/1_9-19	03.11.2022	12:26	55 µm	4	51° 17,447’ S	039° 59,957’ W
PS133/1_9-20	03.11.2022	13:34	200 µm	5	51° 17,462’ S	039° 59,975’ W
PS133/1_10-7	04.11.2022	06:04	55 µm	5	51° 38,164’ S	039° 14,719’ W
PS133/1_10-8	04.11.2022	07:32	200 µm	5	51° 38,248’ S	039° 14,583’ W
PS133/1_14-6	05.11.2022	16:51	55 µm	5	54° 11,629’ S	035° 54,613’ W

Station	Date	Day	Mesh size	Sample Number	Latitude	Longitude
PS133/1_14-7	05.11.2022	17:30	200 µm	5	54° 11,635’ S	035° 54,599’ W
PS133/1_14-14	06.11.2022	00:24	55 µm	5	54° 11,608’ S	035° 54,698’ W
PS133/1_14-15	06.11.2022	01:04	200 µm	5	54° 11,618’ S	035° 54,832’ W
PS133/1_17-9	10.11.2022	22:52	55 µm	5	56° 20,306’ S	024° 55,225’ W

In addition to the MultiNet sampling, nine vertical hauls from 100 m depth to the surface were conducted with Working Party 2 Nets (WP-2) equipped with 100 and 400 µm mesh size, respectively, and closed cod ends in order to obtain intact zooplankton for gut fluorescence measurements and experiments on copepod egg production and faecal pellet production rates of key species (Table 9.2). Casts with the 100 µm WP-2 were divided into two fractions. One split was used to obtain samples for gut fluorescence of copepods by size fractionation through 100 and 200 µm sieves. The samples were immediately frozen with freeze spray and stored at -80°C. Incubation experiments on egg production and faecal pellet production were conducted (in incubation experiments over 24 h) with the respective dominant key species at the stations isolated from the other fraction of the WP-2 100 µm catch or the WP-2 400 µm net catch. The species included the large copepods *Rhincalanus gigas*, *Calanoides acutus*, *Calanus propinquus*, *Calanus simillimus* and *Metridia gerlachei* as well as smaller specimen from the Ctenocalanus/Clausocalanus group. Except for the latter, which were incubated in groups of 10 individuals, incubations were done with single specimens in order to obtain additional information about spawning frequency and the egg production of the individuals that produced these. The rest of the samples was frozen at -80°C for later mercury analyses by partners in the cruise (see Chapter 5).

Tab. 9.2: Vertical hauls conducted with the Working Party-2 nets for experiments (WP-2, 400 µm) and gut fluorescence (WP-2, 100 µm). Samples were taken from tows between 100 m depth and the surface.

Station	Date	Mesh size	Latitude	Longitude
PS133/1_3-8	14.10.2022	400 µm	49° 03,973’ S	009° 59,392’ W
PS133/1_3-9	14.10.2022	100 µm	49° 04,015’ S	009° 59,357’ W
PS133/1_6-9	22.10.2022	400 µm	52° 19,722’ S	024° 58,594’ W
PS133/1_6-10	22.10.2022	100 µm	52° 19,649’ S	024° 58,548’ W
PS133/1_9-11	03.11.2022	400 µm	51° 17,502’ S	039° 59,700’ W
PS133/1_9-12	03.11.2022	100 µm	51° 17,524’ S	039° 59,731’ W
PS133/1_10-6	03.11.2022	400 µm	51° 38,145’ S	039° 14,674’ W
PS133/1_14-13	06.11.2022	100 µm	54° 11,648’ S	035° 54,596’ W
PS133/1_14-13	06.11.2022	400 µm	54° 11,612’ S	035° 54,674’ W

In total, six samples for gut fluorescence of copepods in size fractions and 11 experiments were conducted.

Preliminary (expected) results

The MultiNet samples for the investigation of the community composition, abundance, vertical distribution, population structure and vertical migration of small (< 1 mm) and large mesozooplankton (> 1 mm) will be analyzed back in the home laboratory; the detailed description of the results is pending. The first characterization of the zooplankton community composition is, therefore, based on the onboard analysis of the life catches performed with the WP-2 nets taken for experimental purposes.

Typically for the zooplankton of the Antarctic Circumpolar Current (ACC), copepods dominated the mesozooplankton during the cruise. In accordance with the early stage in the seasonal development of the ecosystem, adult individuals were most abundant with only a few nauplii and copepodite stages present. An outstanding exception, however, were the dominance of juvenile stages at the neritic station on the South Georgia shelf. Apart from the copepods, ostracods, pteropods and Copelata were regularly observed in the samples; amphipods and euphausiid larvae were only occasionally found.

The copepod community showed a gradual change in the composition along the Antarctic Circumpolar Current. At station PS133/1_3, in the easternmost location of the investigation area, *Metridia gerlachei* and *Calanus cf. propinquus* were dominating. *Rhincalanus gigas*, in contrast, was rather rare as well as smaller species such as *Ctenocalanus* or *Clausocalanus*. *Oithona* spp. exclusively dominated the smaller size fraction, only a few other species such as *Microsetella norvegiga* were observed. With the westward progression of sampling, *Rhincalanus gigas* dominated the community, while *Oithona* spp. was increasingly replaced by *Oncaea* spp. This appears to be related to the increasing productivity upstream the ACC. At station PS133/1_9 characterized by very high chlorophyll standing stocks, the community consistent entirely of *Rhincalanus gigas* and *Oncaea* spp. Outside the patch (PS133/1_8 and PS133/1_10), other species such as *Calanoides acutus, Metridia gerlachei/Metridia longa* and smaller *Ctenocalanus*/*Clasusocalanus* were more abundant. The Calanidae showed some variability. While *Calanus* cf. *propinquus* were primarily observed north of South Georgia and at the eastmost station, *Calanoides acutus* dominated the station in-between. In summary, the zooplankton showed a gradual change from a *Rhincalanus gigas/ Oncaea* dominated community at the productivity maximum to a more diverse community downstream in which *Metridia gerlachei* and *Oithona* spp played a major role. An exception in community composition was the neritic shelf station. Adult stages were rare and mostly consisted of females of *Calanus* cf. *simillimus* and young stages of *Rhincalanus gigas* and *Metridia* spp. dominated. *Metridia gerlachaei* showed intense vertical migration below the mixed water layer. During day catches, the species was not observed in the top 100 m of the water column.

Egg production and faecal pellet production experiments across the process stations were done with *Rhincalanus gigas*, *Metridia gerlachaei* and three species of the Calanidae (*Calanoides acutus*, *Calanus* cf. *propinquus*, *Calanus* cf. *simillimus*). Values are presented with their standard deviations in the following, based on sample size of approximately 30 individuals. In accordance with the early stage of the seasonal development, production of eggs was generally low with the exception of the Calanidae at station 6 (Fig. 9.1).

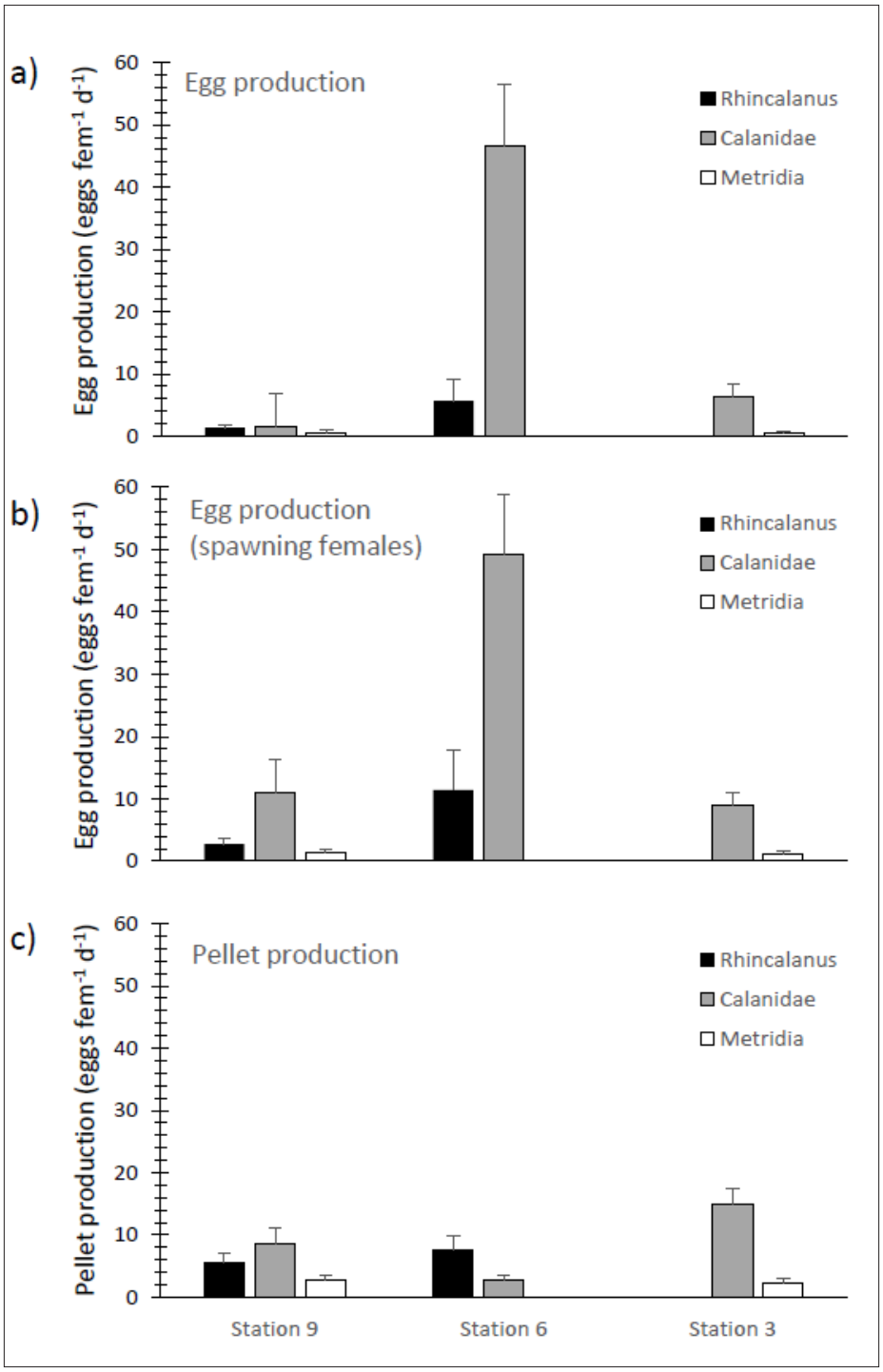

Fig.9.1: Egg production (a), spawning female egg production (b) and faecal pellet production (c) of three key species at the process stations during the cruise PS133/1; error bars correspond to the standard deviation (n~30).

Sufficient specimens of *Rhincalanus gigas* for conducting experiments were only found at station PS133/1_6 and PS133/1_9. For *R. gigas*, the egg production varied on average between 1.4 ± 0.5 and 5.7 ± 3.4 eggs female^{-1} d^{-1} (Fig. 9.1 a). Since the lowest rates were observed at the site with highest chlorophyll a concentrations (station PS133/1_9), apparently no relationship to the productivity in the area in this period exists. The spawning frequency (percentage of females spawning) was 50 % and, thus, spawning female egg production rates

were slightly higher than the population production (2.7 ± 0.9 and 11.4 ± 6.5 eggs fem^{-1} d^{-1}, Fig 9.1 b). The individual egg production rates varied between 1.0 and 67 eggs fem^{-1} d^{-1}. The pellet production rate of the species ranged from 5.5 ± 1.6 to 7.6 ± 2.2 eggs fem^{-1} d^{-1}, again with a large range in the individual rates (0 – 34 pellets fem^{-1} d^{-1}, Fig 9.1 c). Although very active *Metridia gerlachei* were observed (e.g. high swimming and searching speed), egg production and faecal pellet production rates were low: rates varied from 0.4 ± 0.2 to 0.5 ± 0.2 eggs fem^{-1} d^{-1} and 2.3 ± 0.6 to 2.8 ± 0.8 pellets fem^{-1} d^{-1}, respectively (Fig. 9.1 a). Individual rates were also low and ranged from 1 – 4 eggs 1 – 8 pellets fem^{-1} d^{-1}. The highest rates were observed among the Calanidae (Fig. 9.1), but some variability was observed due to difference in species that were encountered at the different stations. *Calanoides acutus* was primarily observed at station PS133/1_6. The species showed very high egg production rates of 46.8 ± 9.6 eggs fem^{-1} d^{-1} with individual rates ranging from 1 to 168 eggs fem^{-1} d^{-1}. The specimen showed large amounts of lipid storage and produced only very few faecal pellets (2.9 ± 0.6 pellets fem^{-1} d^{-1}) indicating that reproduction was based on internal reserves. In contrast, comparatively high pellet production rates were observed by *Calanus* cf. *propinquus*, which produced on average 8.6 ± 2.6 to 15.0 ± 2.3 pellets fem^{-1} d^{-1} with a range of 3 – 44 pellets fem^{-1} d^{-1}. Despite this, egg production was low and indicated that feeding conditions were sub-optimal. On average females produced between 1.7 ± 1.1 and 6.3 ± 1.7 eggs fem^{-1} d^{-1} (Fig. 9.1 a). The spawning frequency varied considerably and ranged from 10 to 70 % resulting in spawning female egg production rates of 11.0 ± 5.3 and 9.0 ± 2.1 eggs fem^{-1} d^{-1}.

A different, smaller *Calanus* species was found on the shelf of South Georgia, presumably *Calanus simillimus*. Similar to *Calanus* cf. *propinquus*, faecal pellet production rates of 10.5 ± 1.6 pellets fem^{-1} d^{-1} (individual range 1 – 26 pellets d^{-1}) indicate that the species was actively feeding (Fig. 9.2). The egg production rates of 16.1 ± 2.9 eggs fem^{-1} d^{-1}, in contrast, were considerably higher and indicate that the species had better feeding conditions (Fig. 9.2). The spawning frequency was 70 % and, thus the rates of spawning female egg production were only slightly higher than the population average (23.0 ± 2.3 eggs fem^{-1} d^{-1}, Fig. 9.2).

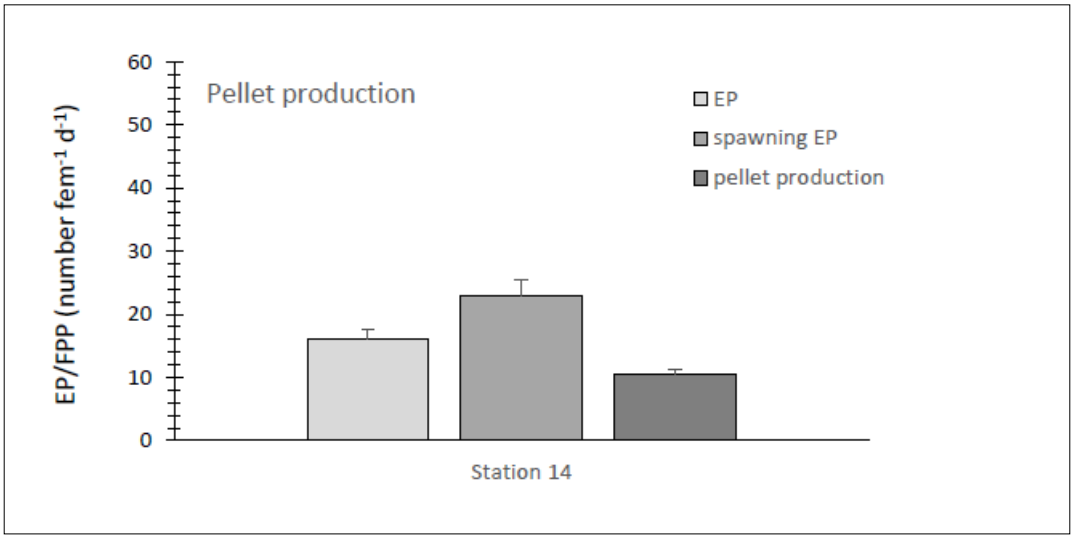

Fig. 9.2: Egg production (EP), spawning female egg production and faecal pellet production of Calanus cf. simillimus at the neritic station on the South Georgia shelf during the cruise PS133/1. Error bars correspond to the standard deviation (n~30).

Data management

Environmental data will be archived, published and disseminated according to international standards by the World Data Center PANGAEA Data Publisher for Earth & Environmental Science (https://www.pangaea.de) within two years after the end of the cruise at the latest. By default, the CC-BY license will be applied.

Molecular data (DNA and RNA data) will be archived, published and disseminated within one of the repositories of the International Nucleotide Sequence Data Collaboration (INSDC, www.insdc.org) comprising of EMBL-EBI/ENA, GenBank and DDBJ).

Any other data will be submitted to an appropriate long-term archive that provides unique and stable identifiers for the datasets and allows open online access to the data.

In all publications based on this expedition, the **Grant No. AWI_PS133_07** will be quoted and the following publication will be cited:

Alfred-Wegener-Institut Helmholtz-Zentrum für Polar- und Meeresforschung (2017) Polar Research and Supply Vessel POLARSTERN Operated by the Alfred-Wegener-Institute.

References

Arendt KE, Juul-Pedersen TA, Mortensen J, Blicher M, Rysgaard S (2013) A five years study of seasonal patterns in mesozooplankton community structure in a sub-arctic fjord reveals dominance of Microsetella norvegica (Crustacea, Copepoda). J. Plankton Res., 35:105–120. https://doi.org/10.1093/plankt/fbs087.

Dubischar CD, Lopez RM, Bathmann UV (2002) High summer abundances of small pelagic copepods at the Antarctic Polar Front—implications for ecosystem dynamics. Deep-Sea Research II, 49:3871–3887. https://doi.org/10.1016/S0967-0645(02)00115-7.

Koski M, Valencia B, Newstead R, Thiele C (2020) The missing piece of the upper mesopelagic carbon budget? Biomass, vertical distribution and feeding of aggregate-associated copepods at the PAP site. Prog. Oceanogr., 181:102243. https://doi.org/10.1016/j.pocean.2019.102243.

Le Moigne FAC., Henson SA, Cavan E, Georges C, Pabortsava K, Achterberg EP, Ceballos-Romero E, Zubkov M, Sanders RJ (2016) What causes the inverse relationship between primary production and export efficiency in the Southern Ocean? Geophys. Res. Lett., 43:4457–4466. https://doi.org/10.1002/2016GL068480.

Pakhomov EA, Perissinotto R, McQuaid CD, Froneman PW (2000) Zooplankton structure and grazing in the Atlantic sector of the Southern Ocean in late austral summer 1993. Part 1. Ecological zonation. Deep-Sea Res. I, 47:1663–1686. https://doi.org/10.1016/S0967-0637(99)00122-3.

Steinberg DK, Landry MR (2017) Zooplnakton and the ocean carbon cycle. Annu. Rev. Mar. Sci., 9:413–44. https://doi.org/10.1146/annurev-marine-010814-015924.

Voronina NM (1998) Comparative abundance and distribution of major filter-feeders in the Antarctic pelagic zone. J. Mar. Sys., 17:375–390. https://doi.org/10.1016/S0924-7963(98)00050-5.

Ward P, Atkinson A, Tarling G (2012) Mesozooplankton community structure and variability in the Scotia Sea: A seasonal comparison. Deep-Sea Res. II, 59-60:78–92. https://doi.org/10.1016/j.dsr2.2011.07.004.

10. MACROZOOPLANTON AND MICRONEKTON DISTRIBUTION AND BIOMASS DURING EARLY AUSTRAL SPRING IN THE ATLANTIC SECTOR OF THE SOUTHERN OCEAN

Evgeny A. Pakhomov[1], Alexis A. Bahl[1], [1]CA.UBC
Florian Lüskow[1], Larysa G. Pakhomova[1]

Grant-No. AWI_PS133/1_08

Objectives

Large zooplankton and micronekton are a cornerstone of the biological pump occupying an important intermediate position between primary producers and secondary consumers (Kwong and Pakhomov, 2017). Their role in the ocean is multifaceted as zooplankton and micronekton acts as a “gatekeeper” for the carbon leaving the euphotic zone into the mesopelagic realm. Aggregation of particles, grazing, active vertical migrations, nutrient and iron release during feeding are all critically important in the dynamics of the organic matter vertical flux in the ocean (Volk and Hoffert, 1985; Steinberg et al., 2000). In order to understand factors controlling the transformation of organic matter in the ocean, it is critical to characterize the composition and assess the standing stock of the macrozooplankton and micronekton. Winter and spring seasons are traditionally poorly sampled in the Southern Ocean. The “Island Impact” cruise provided a unique opportunity to study the zooplankton dynamics, with a particular emphasis to macrozooplankton and micronekton, across various oceanographic regimes. With this in mind, the main objectives of the voyage were:

- to study the composition, size structure, abundance, and biomass of macrozooplankton and micronekton in the upper 600 m and mixed layer depths;
- to assess the contribution of selected taxonomic groups to passive and active carbon transport;
- to obtain material for stoichiometric and genetic work for gelatinous (jellyfish, ctenophores, and tunicates) zooplankton.

Work at sea

During the expedition, seven RMT-8 (rectangular midwater trawl, mouth area 8 m^2, mesh size 4.5 mm) and seven IKMT (Isaacs-Kidd midwater trawl, mouth area 2.5 m^2, mesh size 0.5 mm) trawls were carried out (Fig. 10.1). Double oblique tows were undertaken either in the upper layer (~ 0-150 m depth, IKMT) or in the upper 600 m of the water column (RMT-8) during day- and nighttime. Samples were directly processed onboard. All animals were identified to the lowest possible taxonomic level (mostly to species and genus levels), counted, and individually measured (either in the whole sample or a quantitative subsample) to obtain abundance data. After removing large and rare species (that were counted and measured), IKMT samples were size fractionated using 0.5, 1-, 2-, and 4-mm sieves and all species, except copepods, were

identified to species level, counted, and measured. Copepods were counted and identified to the genus level only. Using the length-weight relationships (Mizdalski, 1988), all abundance data were converted into dry biomass. Volume filtered was estimated using HYDRO-BIOS flowmeters. Specimens for stoichiometric analyses were measured and frozen at -80°C either individually or in small groups (up to 7 specimens). For large jellyfish, tissues (gametogenic tissue, stomach, umbrella/tentacles) were separated before freezing.

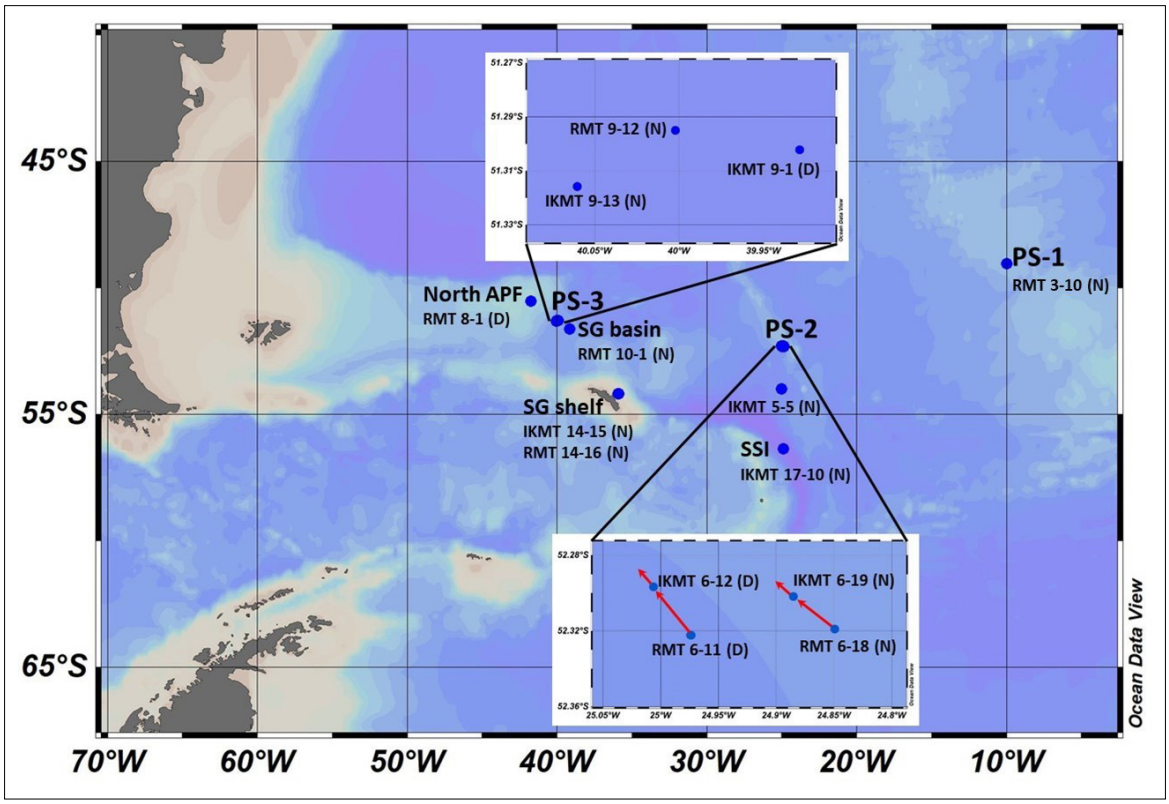

Fig. 10.1: Sampling station positions of RMT and IKMT tow during the PS 133/1 voyage. PS refers to the 3 process stations (with sediment trap deployments). Smaller numbers correspond to the station-cast numbers. (N) indicates night trawls, (D) day trawls.

Preliminary results

RMT-8 estimated abundance values ranged from 0.02 to 0.1 ind.m^{-3}, with lowest values recorded at Stn. PS133/1_8-1 (North of the APF; Fig. 10.2A). Euphausiids numerically dominated samples accounting generally for > 50 % (up to 70 %) of total macrozooplankton and micronekton (MM) abundance (Fig. 10.2A). Chaetognaths were the second dominant group followed by tunicates, amphipods, and cnidarians (Fig. 10.2A). Total MM biomass generally was around 1 mg DW m^{-3}, except for Stn. PS133/1_3 (PS-1 in Fig. 10.1) where it reached 4 mg DW m^{-3} and Stns. PS133/1_8 (North of the APF) and PS133/1_14 (shelf of South Georgia) where it was the lowest (< 0.3 mg DW m^{-3}) (Fig. 10.2B). Unlike abundance, total MM biomass was generally dominated by Osteichthyes and euphausiids with occasional high contribution of cnidarians and ctenophores (Fig. 10.2B lower panel).

IKMT estimates of abundance and biomass ranged from 7 to 70 ind.m^{-3} and from 5 to 29 mg DW m^{-3}, respectively (Figs. 10.3A and 10.3B). Numerically, copepods always accounted for > 50 % (generally > 70 %) of total abundance (Fig. 10.3A lower panel). Euphausiids were the second most abundant group of zooplankton, but their contribution normally did not exceed 35 % and generally ranged from 10 to 20 % of total abundance (Fig. 10.3A lower panel). In

terms of biomass, copepods and euphausiids interchangeably dominated samples (Fig. 10.3B lower panel). Ctenophores were the third most important group in terms of biomass. This group was particularly dominant during the surface IKMT Stn. PS133/1_14 at the South Georgia shelf, where two of almost intact specimens of *Bathocyroe* sp. were collected (Fig. 10.3B).

Overall, both RMT-8 and IKMT catches were on the lower range end of values previously reported in the region investigated during the austral summer 2012 (Pakhomov and Hunt, 2017). They were, however, comparable to limited estimates obtained with similar gear types during springs of 1980s (Nast, 1986; Lancraft et al., 1989, 1991). It appears that the composition and standing stock of MM estimates during the PS133/1 expedition reflected the early developing season in the Southern Ocean.

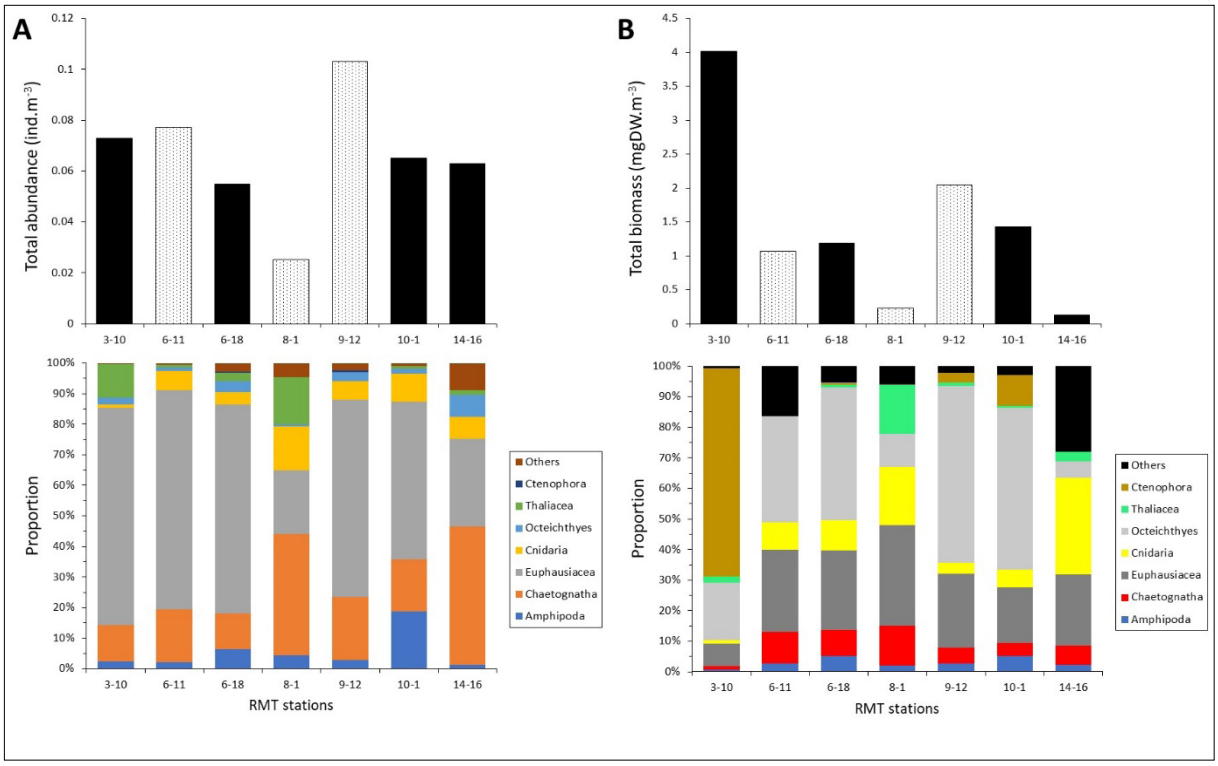

Fig. 10.2: Total abundance (A) and biomass (B) as well as corresponding abundance and biomass of major taxonomic group (lower panels) of macrozooplankton/micronekton sampled with RMT-8 trawls during the PS133/1 expedition; grey bars in the upper panels indicate daytime catches, black bars nighttime catches.

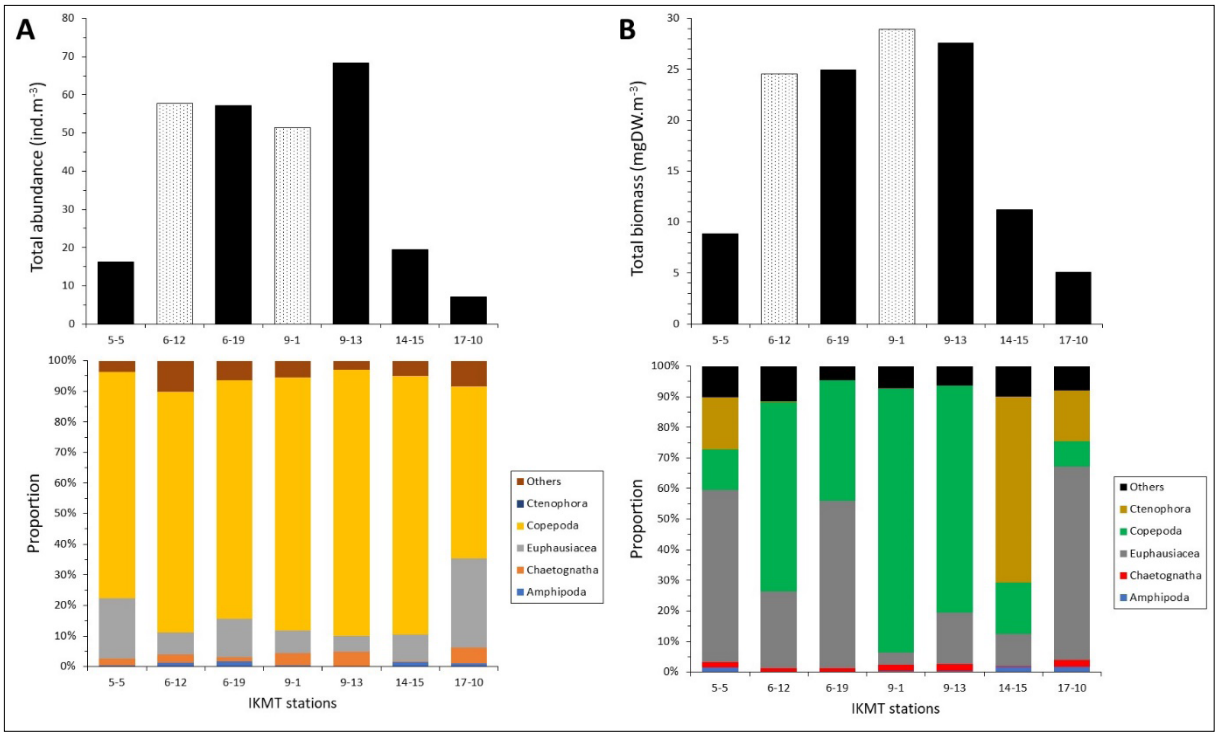

Fig. 10.3: Total abundance (A) and biomass (B) as well as corresponding abundance and biomass of major taxonomic group (lower panels) of macrozooplankton/micronekton sampled with IKMT trawls during the PS 133/1 expedition. Grey bars in the upper panels indicate daytime catches, black bars nighttime catches.

Daytime/nighttime comparison of taxa biomass was possible at the second process station (PS-2 in Fig 10.1). IKMT total catches were not significantly different in terms of biomass between day- and nighttime (Fig. 10.3B). Copepods had higher abundance during the daytime, while euphausiids dramatically increased in number during the nighttime (Fig. 10.4A). Like IKMT samples, total RMT-8 catch biomass were similar during day- and nighttime (Fig. 10.2A). Nevertheless, several taxonomic groups, e.g., medusae, thaliaceans, euphausiids, amphipods, and Osteichthyes, showed higher nighttime biomass (Fig. 10.4B). For the latter group, the increase was the most prominent (Fig. 10.4B).

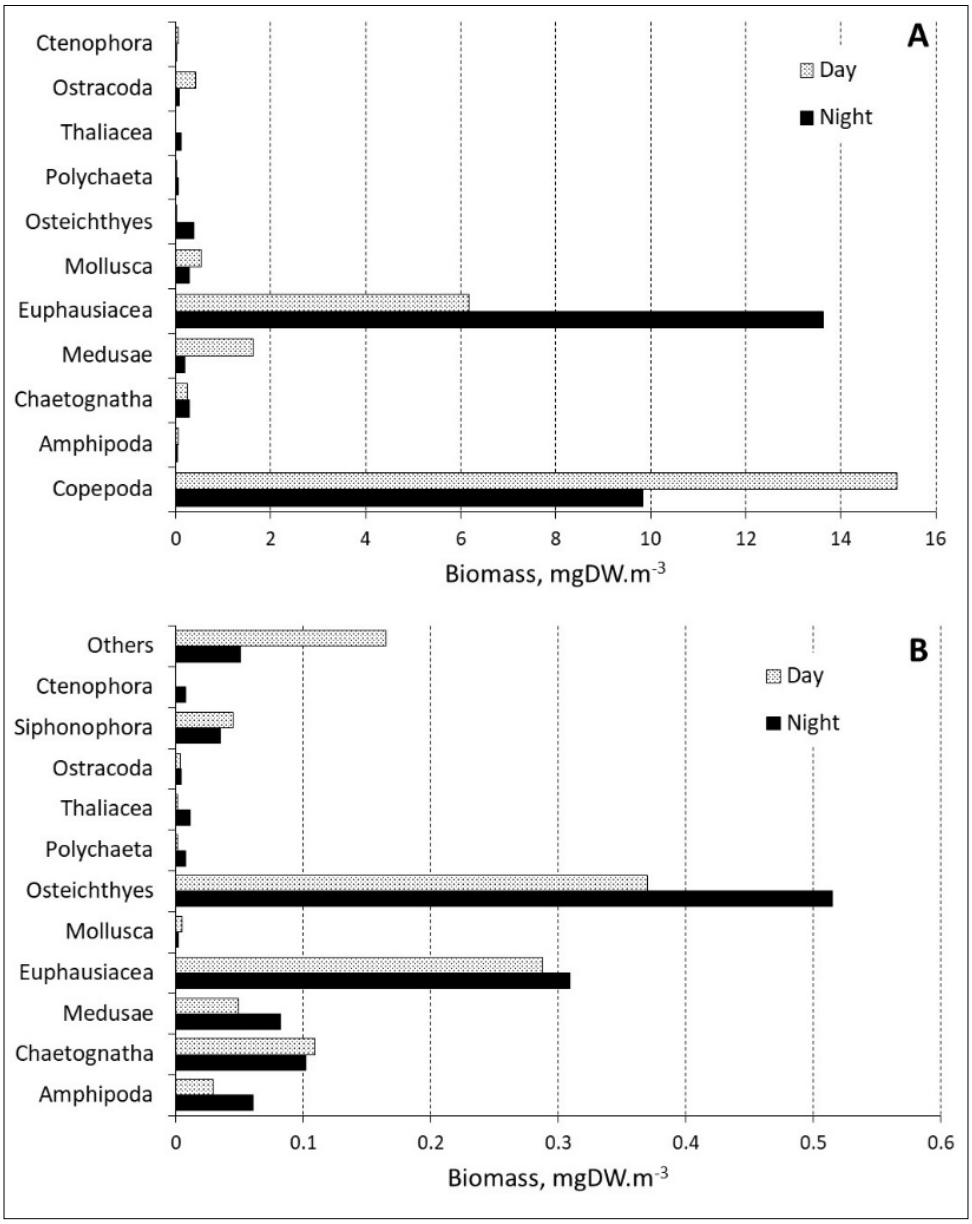

Fig. 10.4: Daytime and nighttime biomass composition in the IKMT (A) and RMT-8 (B) catches during the PS133/1 expedition

Daytime and nighttime comparison of size groups sampled at the second process station (PS 133/1_6) revealed that IKMT sampled larger-sized MM during nighttime, strongly suggesting their active diel vertical migration to the mixed layer (Fig. 10.5A). While there were minor taxonomic differences that could be attributed to MM patchiness, RMT-8 catches showed almost identical MM size distribution in day- and nighttime samples (Fig. 10.5B) suggesting that in the top 600 m water layer we sampled adequately the entire range of the MM independent of their migration range.

Fifty-six tissue samples (either entire animals or specific tissues) were sampled across the PS133/1 expedition. These include ctenophores and cnidarians (i.e., scyphomedusae, siphonophores, and hydromedusae). For transcriptomics, about sixty thaliaceans (*Salpa thompsoni*) were collected. Analysis of these samples will take place in the home laboratory.

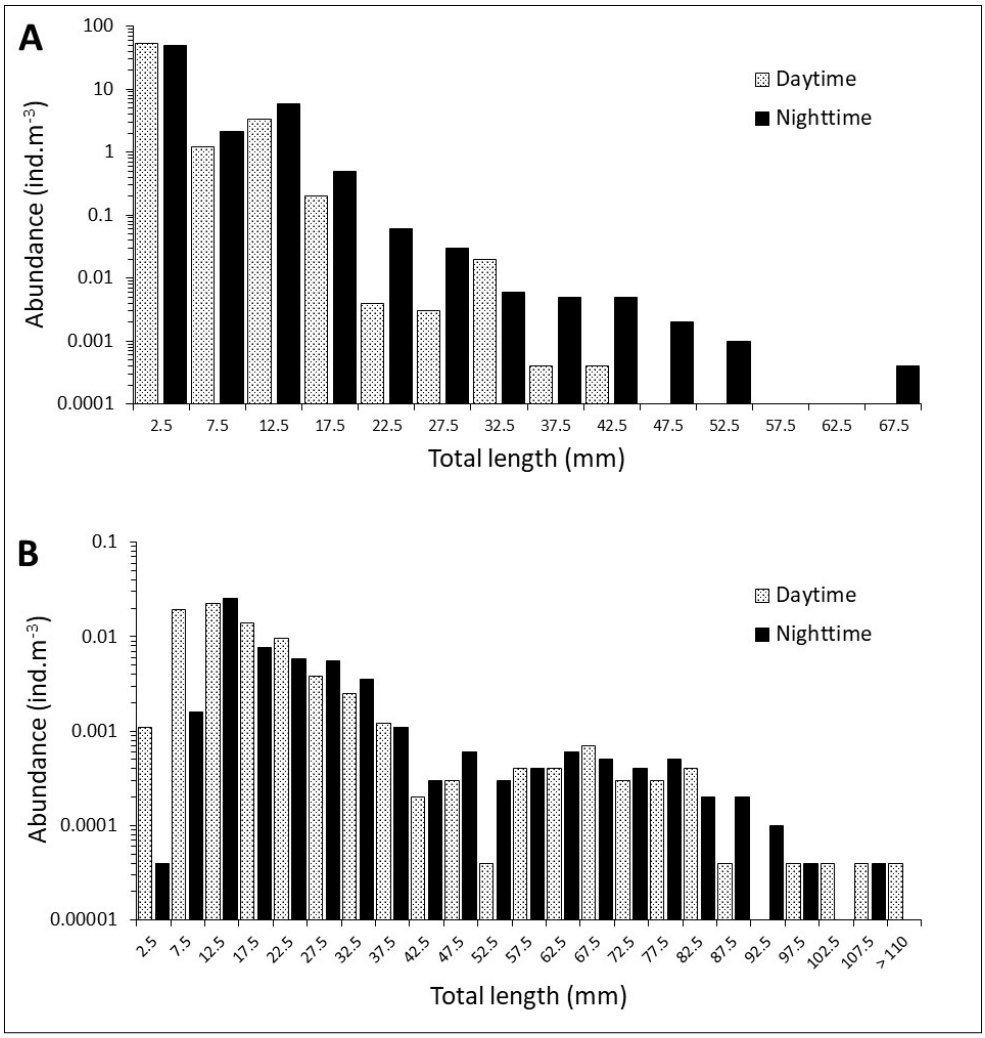

Fig. 10.5: Daytime and nighttime comparison of the MM size distribution collected by IKMT (A) and RMT-8 (B) in the mixed layer and 0-600 m, respectively.

Data management

Faunal assemblage composition and distribution data together with environmental co-variables will be archived, published, and disseminated according to international standards by the World Data Center PANGAEA Data Publisher for Earth & Environmental Science (https://www.pangaea.de) within two years after the end of the cruise at the latest. By default, the CC-BY license will be applied.

Molecular data (DNA and RNA data) will be archived, published and disseminated within one of the repositories of the International Nucleotide Sequence Data Collaboration (INSDC, www.insdc.org) comprising of EMBL-EBI/ENA, GenBank and DDBJ).

Any other data will be submitted to an appropriate long-term archive that provides unique and stable identifiers for the datasets and allows open online access to the data.

In all publications based on this expedition, the **Grant No. AWI_PS131/1_08** will be quoted and the following publication will be cited:

Alfred-Wegener-Institut Helmholtz-Zentrum für Polar- und Meeresforschung (2012) Polar Research and Supply Vessel POLARSTERN Operated by the Alfred-Wegener-Institute. Journal of large-scale research facilities, 3, A119. http://dx.doi.org/10.17815/jlsrf-3-163.

References

Kwong LE, Pakhomov EA (2017) Assessment of active vertical carbon transport: new methodology. Proceedings of Kazan University Natural Sciences Series, 159(3):492–509.

Lancraft TM, Torres JJ, Hopkins TL (1989) Micronekton and macrozooplankton in the open waters near Antarctic ice edge zones (AMERIEZ 1983 and 1986). Pol Biol, 9:225–233.

Lancraft TM, Hopkins TL, Torres JJ, Donnelly J (1991) Oceanic micronektonic/macrozooplanktonic community structure and feeding in ice covered Antarctic waters during the winter (AMERIEZ 1988). Pol Biol, 11:157–167.

Mizdalski E (1988) Weight and length data of zooplankton in the Weddell Sea in austral spring 1986 (ANT V/3). Ber Polarforsch, 55:1–72.

Nast F (1986) Changes in krill abundance and in other zooplankton relative to the Weddell–Scotia Confluence around Elephant Island in November 1983, November 1984 and March 1985. Arch Fischereiwiss, 37:73–94.

Pakhomov EA, Hunt BPV (2017) Trans-Atlantic variability in ecology of the pelagic tunicate Salpa thompsoni near the Antarctic Polar Front. Deep-Sea Res I,I 138:126–140.

Steinberg DK, Carlson CA, Bates NR, Goldthwait SA, Madin LP, Michaels AF (2000) Zooplankton vertical migration and the active transport of dissolved organic and inorganic carbon in the Sargasso Sea. Deep Sea Res I, 47:137–158. https://doi.org/10.1016/S0967-0637(99)00052-7.

Volk T, Hoffert MI (1985) Ocean carbon pumps: Analysis of relative strengths and efficiencies in ocean-drive atmospheric CO2 changes. Geophys Monogr Ser, 32:99–110.

11. WHAT WE SEE IS NOT WHAT WE CATCH: A COMPARISON BETWEEN THE NET AND OPTICAL SAMPLING

Florian Lüskow[1], Alexis Bahl[1], Christian Konrad[2], Hannah Marchant[3], Larysa G. Pakhomova[1], Morten H. Iversen[2], Evgeny A. Pakhomov[1]

[1]CA.UBC
[2]DE.AWI
[3]DE.MARUM

Grant-No. AWI_PS133/1_08

Objectives

Gelatinous and soft-bodied zooplankton (GZ; e.g., medusae, siphonophores, ctenophores, salps) have historically been deemed an unimportant component of marine ecosystems (thought as 'trophic dead-ends') due to their high water content compared to crustacean zooplankton (Hansson and Norman, 1995). Given their fragile body structure, traditional net tows, such as mid-water trawls and plankton nets, severely undersample GZ, further contributing to the perception that GZ has low diversity, abundance, and ecological influence in the open oceans. However, with newly developed optical, acoustic, and analytical techniques, it has become apparent that our limited knowledge of GZ is highly dependent on the sampling strategies employed (e.g., Choy et al., 2017; Chi et al. 2021). Comparative studies on net-collected faunal assemblages versus those recorded with underwater camera systems (e.g., Hoving et al., 2019; Hetherington et al., 2022) found strong evidence of the highly abundant, yet vastly under-sampled soft-bodied GZ community. This gave support to the 'jelly web' concept introduced by Robison (2004) that describes the highly diverse interconnectedness of GZ on ocean ecosystems, especially in the mesopelagic realm (about 200 to 1,000 m depth). Plankton communities in the Atlantic Sector of the Southern Ocean are typically numerically dominated by copepods, but GZ such as *Salpa thompsoni*, a major metazoan grazer in the region, were found to be dominant in terms of biomass (e.g., Pakhomov et al., 2002). This contribution (and diversity), however, is likely vastly underestimated and deserves more research. Biological processes important for understanding the population dynamics of salps requires traditional net tows for ontogenetic description, while photographic evidence with deep-sea camera systems can shed light on salp migratory behaviour. Combining these approaches, as well as acoustics can provide species-level identification (nets), large-scale distribution (acoustics), and fine-scale distribution (optics) to improve our knowledge of *S. thompsoni* in the Southern Ocean (Lüskow et al., to be submitted). The objective of this project was to compare the abundance and species composition of macrozooplankton and micronekton in the Atlantic Sector of the Southern Ocean (and north of the Antarctic Polar Front) using integrative RMT-8 tows and JellyCam footage down to 600 m. The goal of this project is to quantitatively contrast the contribution of GZ with a strong focus on salps, to the faunal community, by using nets and an *in-situ* state-of-the-art visual techniques to infer biological processes (i.e., reproduction).

Work at sea

Details about the RMT-8 (rectangular mid-water trawl with *circa* 8 m^2 mouth opening and 4.5 mm mesh size) and JellyCam (mounted on the ROSINA) deployments are described in the Table 11.1. In total, seven RMT-8 and eight JellyCam deployments were made during the PS133/1 expedition. The original goal was to sample day and night communities with RMT-8 within a 24-hour window (further termed as a "pair") accompanied by JellyCam casts to analyze

vertical distributions as well as infer diel vertical migration behaviour. However, due to logistical challenges this plan was amended. Ultimately, four potential pairs (defined by a deployment time differences of less than three hours) were conducted – one during the nighttime/twilight of 14 October, and three during the nighttime of 3, 4, and 6 November (Table 11.1). Other RMT-8 deployments and JellyCam casts are incomparable because they occurred outside the ideal time window. This data, however, is still valuable for faunal assemblage characterization and distribution.

RMT-8 catches were analyzed for species composition immediately after retrieval, whereas footage of the JellyCam was analyzed quantitatively only once (for station PS133/1_3-12) due to time limitations during the cruise. Examples of JellyCam footage and the sorted RMT-8 catch are shown in Figure 11.1.

Tab. 11.1: Deployment details for the RMT-8 and JellyCam. Potential pairs are indicated based on a maximum time difference (Time diff.) between deployments of less than three hours. N = night, T = twilight

Date	Station-cast ID PS133/1_	Gear	Start [UTC]	Depth [m]	Latitude [S]	Longitude [W]	Pot. pair	Time diff. [h]
14-Oct-22	3-10	RMT-8	03:10	603	49°03.150’	09°59.529’	1 (N)	02:35
14-Oct-22	3-12	JellyCam	05:45	600	49°03.080’	09°59.161’	1 (T)	
22-Oct-22	6-11	RMT-8	10:51	620	52°19.307’	24°58.479’		
22-Oct-22	6-18	RMT-8	22:04	611	52°19.100’	24°51.046’		
23-Oct-22	6-21	JellyCam	03:25	-	52°20.609’	24°21.330’		
01-Nov-22	8-1	RMT-8	16:22	611	50°32.032’	41°44.086’		
02-Nov-22	8-8	JellyCam	00:19	600	50°31.072’	41°47.598’		
03-Nov-22	9-12	RMT-8	02:21	555	51°17.700’	40°00.136’	2 (N)	02:16
03-Nov-22	9-15	JellyCam	04:37	600	51°18.564’	40°02.572’	2 (N)	
03-Nov-22	9-18	JellyCam	11:03	600	51°17.355’	39°59.970’		
03-Nov-22	10-1	RMT-8	00:19	560	51°37.875’	39°08.665’	3 (N)	01:35
04-Nov-22	10-2	JellyCam	01:54	600	51°38.162’	39°14.705’	3 (N)	
05-Nov-22	14-9	JellyCam	21:08	-	54°11.702’	35°54.749’		
06-Nov-22	14-16	RMT-8	02:10	140	54°10.960’	35°53.577’	4 (N)	00:41
06-Nov-22	14-18	JellyCam	02:51	220	54°10.915’	35°53.698’	4 (N)	

Preliminary (expected) results

As shown in previous studies in other regions of the world’s oceans, the plankton community sampled by nets (RMT-8) and/or camera systems (JellyCam) differed considerably. While the RMT-8 catches were numerically dominated by euphausiids, chaetognaths, and thaliaceans (i.e., salps) (Figs. 11.2A and 11.3), JellyCam footage was dominated by siphonophores, euphausiids, and chaetognaths (Figs. 11.2B and 11.3). The total group abundance values differed vastly between the two gears, e.g., euphausiids had five times higher abundance when sampled with the RMT-8 than with the JellyCam (Fig. 11.3). This was, however, the only taxon oversampled by the RMT-8. All other groups (chaetognaths, ctenophores, medusae, polychaetes, siphonophores, thaliaceans) occurred in higher abundance based on the JellyCam footage (Fig. 11.3). In this preliminary analysis, we should not overstate the importance of JellyCam-derived abundance data, as they will likely change in subsequent analyses. While not all taxa were encountered (e.g., fish, amphipods) in this first attempt, the data clearly suggest that with traditional net tows, GZ are heavily undersampled. Thus, the paradigm of a crustacean-

dominated community in epi- and mesopelagic of the Southern Ocean requires revision. The RMT-8 does not quantitatively sample the mesozooplankton fraction (0.2–20 mm), which is also not satisfyingly captured from the JellyCam. Thus, the comparison should be restricted to macrozooplankton and micronekton. An additional finding from this preliminary analysis is that large ctenophores are almost entirely destroyed in mid-water trawls but can be recorded using visual techniques. The high number of observed siphonophores, medusae, and chaetognaths provide a strong support to the open ocean mesopelagic jelly web presence.

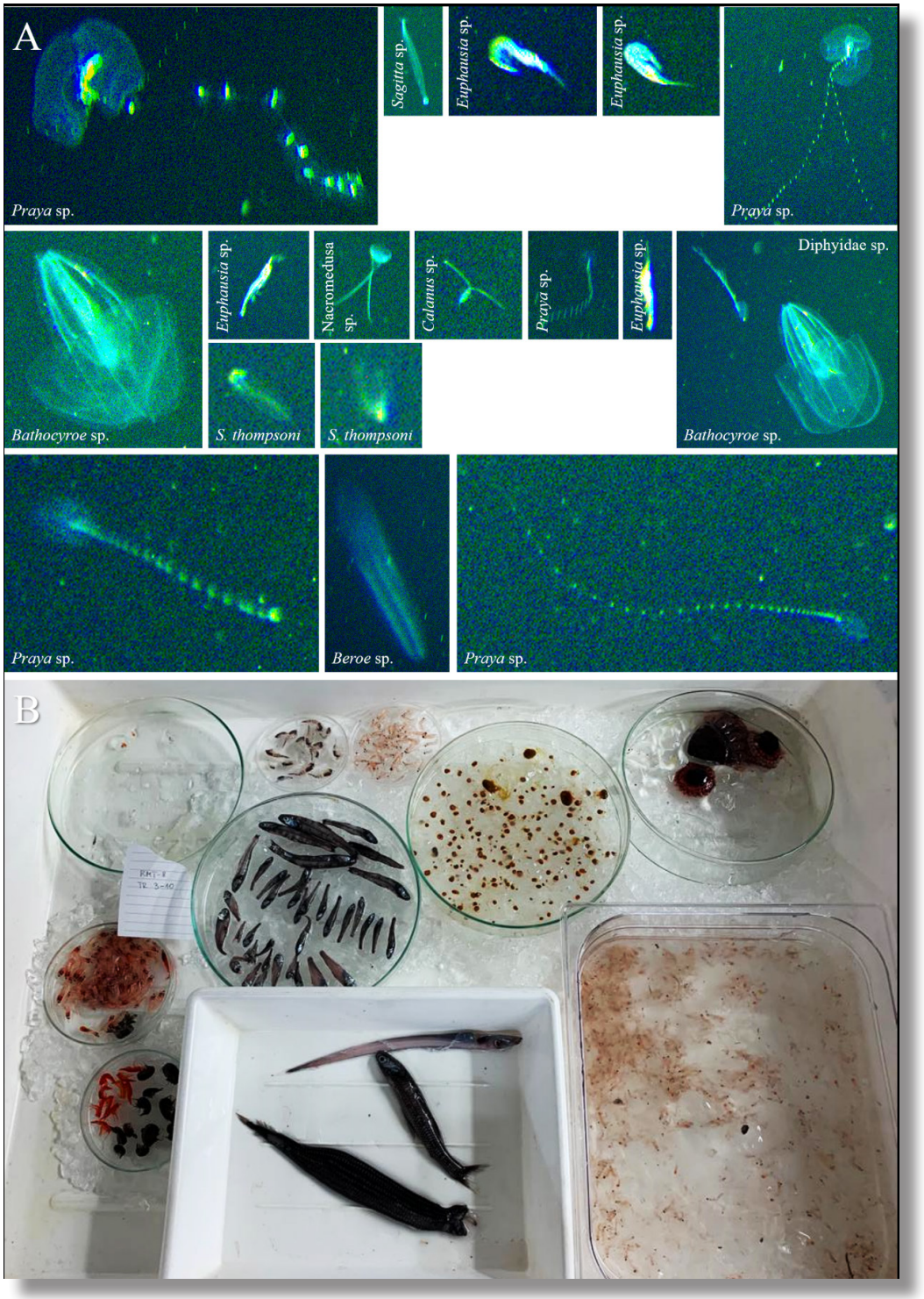

Fig. 11.1: Example footage of A) the JellyCam cast (station 3-12) and B) the sorted RMT-8 net catch (station 3-10) – both collected on 14 October 2022

The total abundance of macrozooplankton and micronekton organisms picked at the 100-150 m depth (about 22 ind. 1,000 m^{-3}), and 300 - 400 m depth (about 37 ind. 1,000 m^{-3}) strata (Fig. 11.2B). In the deepest sampled layer (550 - 600 m), the total abundance slowly decreased to ~7 ind. 1000 m^{-3}. Siphonophores numerically dominated the faunal assemblage between 40 and 350 m but were not found outside this depth interval. Large copepods were predominantly observed below 350 m, suggesting a predator-prey relationship in which copepods were avoiding siphonophores. Chaetognaths occurred throughout the sampled depth layer of 600 m, but primarily occurred below 350 m, similar to that of large copepods and euphausiids. Other groups, such as polychaetes, ctenophores, medusae, and thaliaceans occurred sporadically over the sampled depth range. As suggested by the total group abundance data, the mid-waters (40 to 350 m) were GZ-dominated. Why this changed below 350 m, whether this was the same case at other sampled locations, and what drives these faunal composition changes have not yet been investigated.

Footage obtained by the JellyCam is of high enough quality to look into intraspecific patterns, of *Salpa thompsoni*, such as life cycle stages, reproduction events, and vertical distribution. At station 133/1_3 (cast 12) on 14 October 2022, only two salp specimens were recorded, making size-distribution and life cycle stage composition analyses impractical. This, however, may be different at the other sampling locations. At the time of all RMT-8 and JellyCam deployments, acoustic data were collected with in-ship sensors. This source of information will be utilized in future work in an effort to quantify biomass peaks occurring in the sampled depth range and infer temporal high-resolution diel vertical migration behaviour. Additionally, environmental co-variables collected on accompanied CTD casts have yet to be analysed, but will be included in future studies to discern any environmental influence.

Data generated by robust integrative gears such as the RMT-8 are not able to depict depth-stratified patterns in species distribution. An animal could have been caught near the surface, in the mid-water, or at the lower end of the sampling interval (in case of the 14 October 2022 deployment, 603 m). Thus, the deployment of an optical sampling strategy, preferably augmented by acoustic data, such as the JellyCam contributed highly important information on GZ total abundance and composition data that could not have been done with net sampling alone.

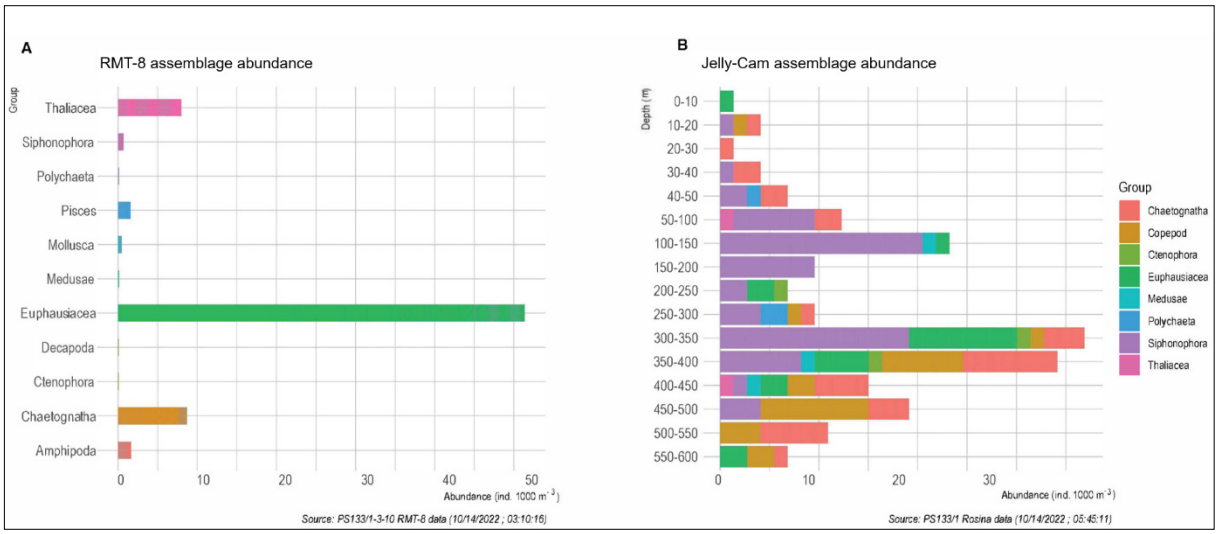

Fig. 11.2: Assemblage composition obtained with A) RMT-8 (station PS133/1_3 cast 10) and B) JellyCam (station PS133/1_3 cast 12) on 14 October 2022; the RMT-8 data are averaged for the top 603 m of the water column, whereas the JellyCam footage observations were binned in 10 or 50 m depth intervals.

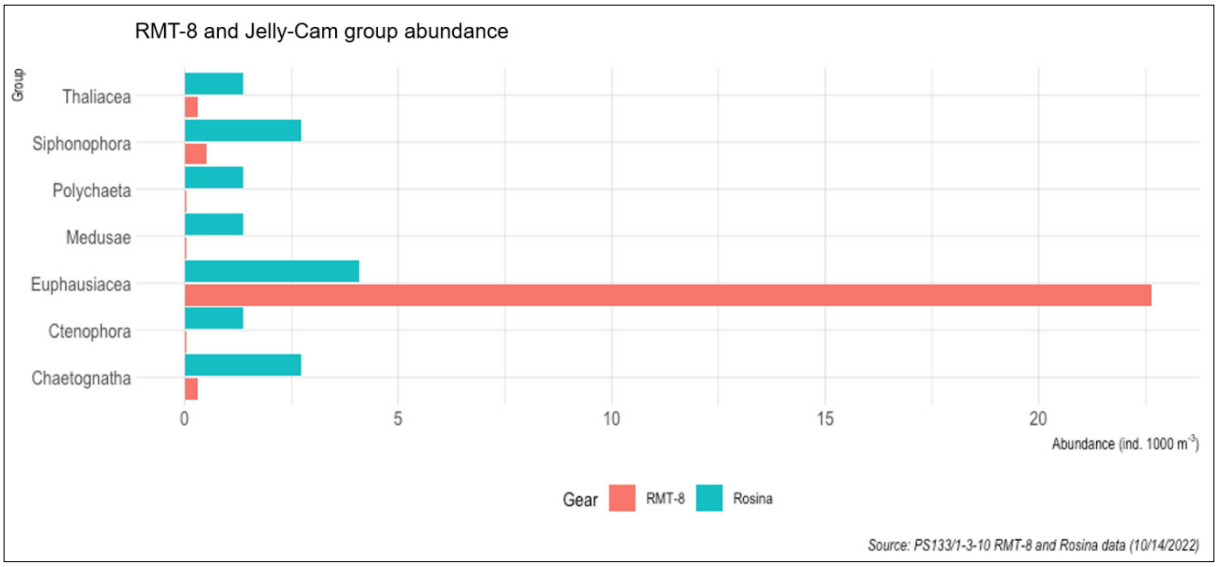

Fig. 11.3: Comparison of abundances obtained by RMT-8 deployment and JellyCam cast for the top 600 m of the water column by group on 14 October 2022

Data management

Faunal assemblage composition and distribution data together with environmental co-variables will be archived, published, and disseminated according to international standards by the World Data Center PANGAEA Data Publisher for Earth & Environmental Science (https://www.pangaea.de) within two years after the end of the cruise at the latest. By default, the CC-BY license will be applied. Any other data will be submitted to an appropriate long-term archive that provides unique and stable identifiers for the datasets and allows open online access to the data.

In all publications based on this expedition, the **Grant No. AWI_PS131/1_08** will be quoted and the following publication will be cited:

Alfred-Wegener-Institut Helmholtz-Zentrum für Polar- und Meeresforschung (2012) Polar Research and Supply Vessel POLARSTERN Operated by the Alfred-Wegener-Institute. Journal of large-scale research facilities, 3, A119. http://dx.doi.org/10.17815/jlsrf-3-163.

References

Chi X, Dierking J, Hoving HJT, Lüskow F, Denda A, Christiansen B, Sommer U, Hansen T, Javidpour J (2021) Tackling the jelly web: Trophic ecology of gelatinous zooplankton in oceanic food webs of the eastern tropical Atlantic assessed by stable isotope analysis. Limnol Oceanogr, 66:289−305.

Choy CA, Haddock SHD, Robison BH (2017) Deep pelagic food web structure as revealed by *in situ* feeding observations. Proc R Soc B, 284:20172116.

Hansson LJ, Norman B (1995) Release of dissolved organic carbon (DOC) by the scyphozoan jellyfish *Aurelia aurita* and its potential influence on the production of planktic bacteria. Mar Biol, 121:52–532.

Hetherington ED, Choy CA, Thuesen EV, Haddock SHD (2022) Three distinct views of deep pelagic community composition based on complementary sampling approaches. Front Mar Sci, 9:864004.

Hoving H-JT, Christiansen S, Fabrizius E, Hauss H, Kiko R, Linke P, Neitzel P, Piatkowski U, Körtzinger A (2019) The Pelagic *In situ* Observation System (PELAGIOS) to reveal biodiversity, behavior, and ecology of elusive oceanic fauna. Ocean Sci, 15:1327–1340.

Lüskow F, Bahl AA, Décima M, Steinberg DK, Pakhomov EA (to be submitted) Size- and stage-specific diel vertical migration patterns of two cold-water salp species.

Pakhomov EA, Froneman PW, Perissinotto R (2002) Salp/krill interactions in the Southern Ocean: spatial segregation and implications for the carbon flux. Deep-Sea Res II, 49(9-10):1881–1907.

Robison BH (2004) Deep pelagic biology. J Exp Mar Biol Ecol, 300:253–272.

12. *SALPA THOMPSONI* POPULATION DYNAMICS DURING EARLY AUSTRAL SPRING IN THE ATLANTIC SECTOR OF THE SOUTHERN OCEAN

Evgeny A. Pakhomov[1], Alexis A. Bahl[1], [1]CA.UBC
Florian Lüskow[1], Larysa G. Pakhomova[1]

Grant-No. AWI_PS133/1_08

Objectives

Pelagic tunicates, namely *Salpa thompsoni*, are conspicuous in the Southern Ocean and often account for a large portion of the zooplankton and micronekton catches (e.g., Pakhomov and Hunt, 2017). They are considered one of the major re-packagers of the phytoplankton and microzooplankton, and contribute significantly to the biochemical, including iron, cycling and the vertical carbon flux (Pakhomov et al. 2002; Iversen et al. 2017, Pauli et al. 2022). During the PS 133/1 expedition, *S. thompsoni* was among the target species for the collection of distribution and population dynamics data during the poorly sampled austral spring. This species is known to be influential in shaping plankton communities and has shifted its distribution southward invading traditionally Antarctic krill-dominated habitats (Pakhomov et al., 2002; Atkinson et al., 2004). It is also envisaged that with climate change, *S. thompsoni* interactions with Antarctic krill will increase and, as a consequence, their contribution to carbon flux may be altered. Winter and spring seasons are traditionally seldom sampled for salp biology and currently there is no data on the salp population development during the austral spring in the Atlantic sector of the Southern Ocean.

Therefore, the main objectives of the expedition were:

- to study the pelagic tunicate, S. thompsoni, horizontal and vertical distribution, density, developmental composition, population biology, and feeding ecophysiology;
- to collect form-, stage- and size-specific data on the vertical distribution of *S. thompsoni*;
- to assess the contribution of salps to passive and active carbon transport;
- to collect material for subsequent stoichiometric and genetic (transcriptomics) work on S. thompsoni.

Work at sea

Salps were collected during the RMT-8 and IKMT trawls described in chapter 10 (Pakhomov et al. this issue). All salps were immediately picked from the entire sample, counted, separated into solitary and aggregate forms, stage of development recorded, and measured for oral-atrial length (OAL). When possible, shortly after the sampling, salps were blast frozen in liquid nitrogen and stored in a -80°C freezer for transcriptomic analyses. Remaining salps were used to assess their feeding activity by placing entire salps (if small) or their stomach (if large) into plastic tubes with 8 mL of 90 % acetone. Chlorophyll-a and phaeopigments were subsequently measured before and after acidification using Turner Design *Trilogy* fluorometer. The salp density was assessed using volume filtered and depth sampled and expressed as individuals

per m^{-2} (Tab. 12.1). Unfortunately, the total number of salps collected did not allow for the stoichiometric analysis sampling, as other analyses were prioritized.

Preliminary results

Salpa thompsoni abundances were very low ranging from < 0.1 to 4.8 ind.m^{-2} (Tab. 12.1). It appeared similar to the previous limited spring estimates varying between 0.1 and 34 ind.m^{-2} (Nast, 1986; Lancraft et al., 1991). These estimates were, however, at least one order of magnitude lower than summer-fall values reported in the literature that normally range on average between 10 s and 100 s ind.m^{-2} and may reach up to 6,000 ind.m^{-2} (Pakhomov et al., 2002).

Biologically, the *S. thompsoni* population was at the most advanced stages of development of aggregates at the first process station (PS133/1_3). The length-frequency distribution was bimodal, salps with 9-11 and 17-21 mm OAL dominated (Fig. 12.1). The developmental stage consisting of aggregates suggested that salps had already at least two chain-release events and had the most diverse stage composition (Fig. 12.2). This was in line with the solitary form development, as only large (>70 mm) and mature solitary specimens were encountered (Figs. 12.3 and 12.4).

The North APF station (Tab. 12.1) had very similar solitary and aggregate stage and size compositions as PS-1, but aggregates were smaller in both size cohorts (Figs. 12.1-12.4). The population also had a high proportion of aggregates that were not fertilized, signalling low overall abundance, of males in particular (Fig. 12.2).

Tab. 12.1: *Salpa thompsoni* density values. PS: process station (see Fig. 10.1); A/S: aggregate to solitary ratio; D/N: daytime or nighttime; SG: South Georgia; APF: Antarctic Polar Front; SSI: South Sandwich Islands.

Station	Station ID	Cast	Gear	Day [D] Night [N]	Depth [m]	Abundance [Ind. m^{-2}]	A/S
PS1	PS133/1_3	10	RMT-8	N	0-603	4.8	52
5-5	PS133/1_5	5	IKMT	N	0-184	0.1	Only S
PS2	PS133/1_6	11	RMT-8	D	0-620	0.5	16
	PS133/1_6	18	RMT-8	N	0-611	0.9	6
	PS133/1_6	19	IKMT	N	0-160	3.7	27
North APF	PS133/1_8	1	RMT-8	D	0-611	2.3	31
PS3	PS133/1_9	1	IKMT	D	0-125	0.1	Only S
	PS133/1_9	13	RMT-8	N	0-555	0.2	Only S
	PS133/1_9	14	IKMT	N	0-149	0.7	4
SG-Basin	PS133/1_10	1	RMT-8	N	0-560	0.3	7
SG-Shelf	PS133/1_14	16	IKMT	N	0-50	2.5	Only A
	PS133/1_14	17	RMT-8	N	0-140	0.03	4
SSI	PS133/1_17	10	IKMT	N	0-222	0.04	Only S

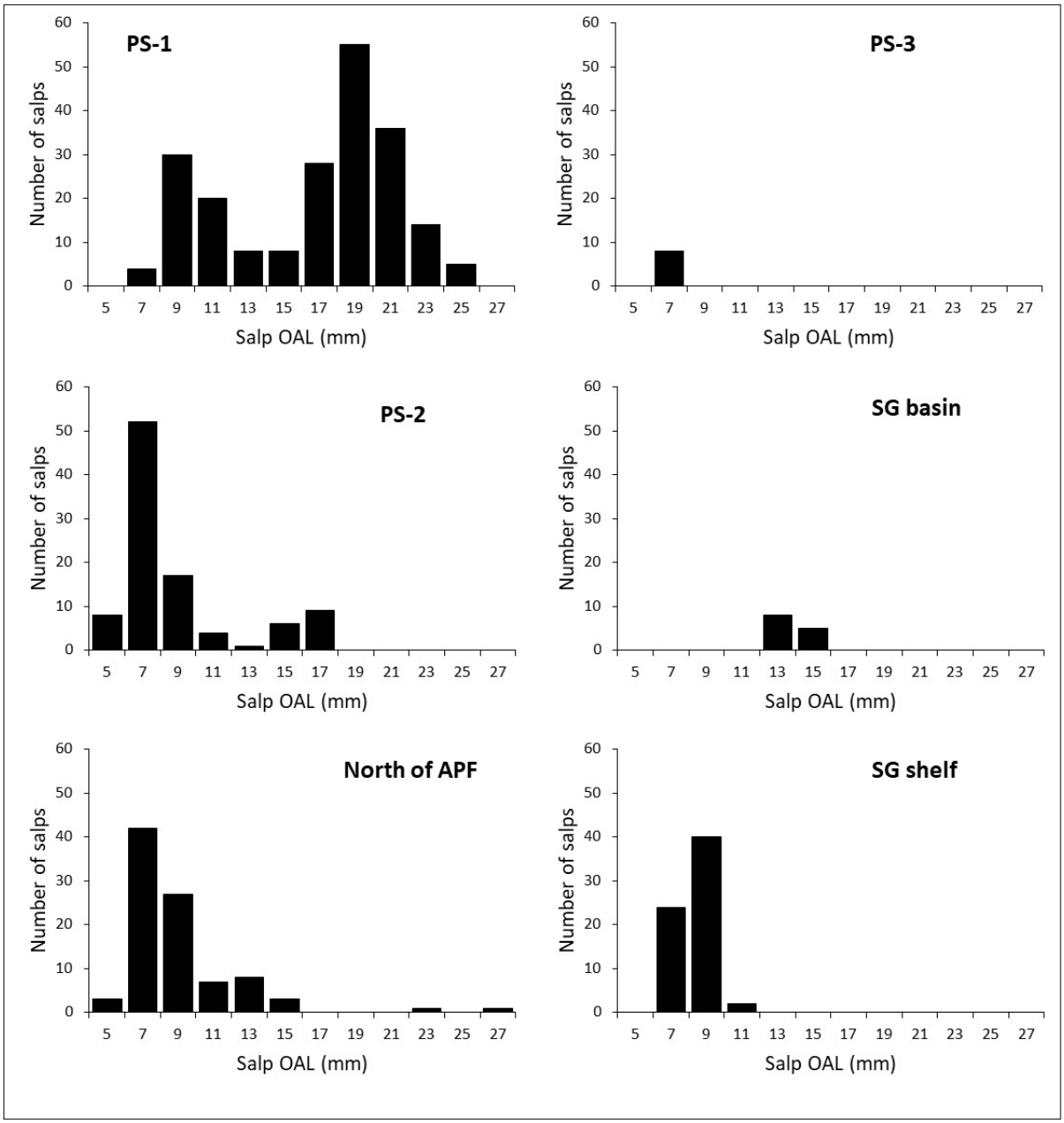

Fig. 12.1: Length frequency distribution of Salpa thompsoni aggregates during the PS133/1 expedition, austral spring 2022. Stations ID and positions are given in Fig. 10.1.

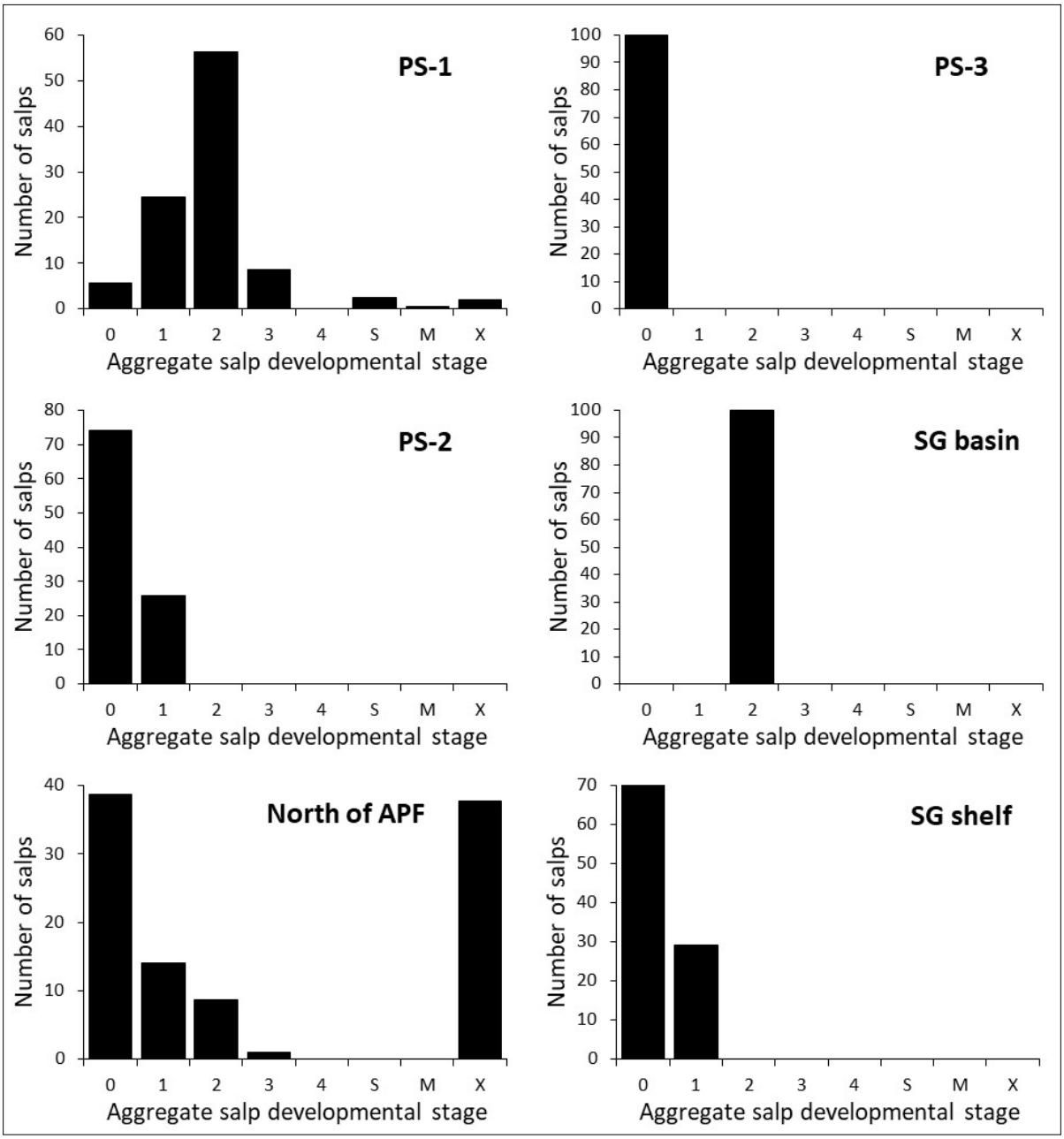

Fig. 12.2: Developmental stage composition of Salpa thompsoni aggregates during the PS 133/1 expedition, austral spring 2022; stations ID and positions are given in Fig. 10.1.

Aggregates at station PS-2 showed intermediate size composition between PS-1 and the North APF sampling locations (Fig. 12.1). However, their aggregate (Fig. 12.2) and solitary stage (Fig.12. 4) composition showed early developing population, e.g. solitaries dominated by salps < 40 mm mostly at earlier developmental stages 1-3 (Figs. 12.3 and 12.4).

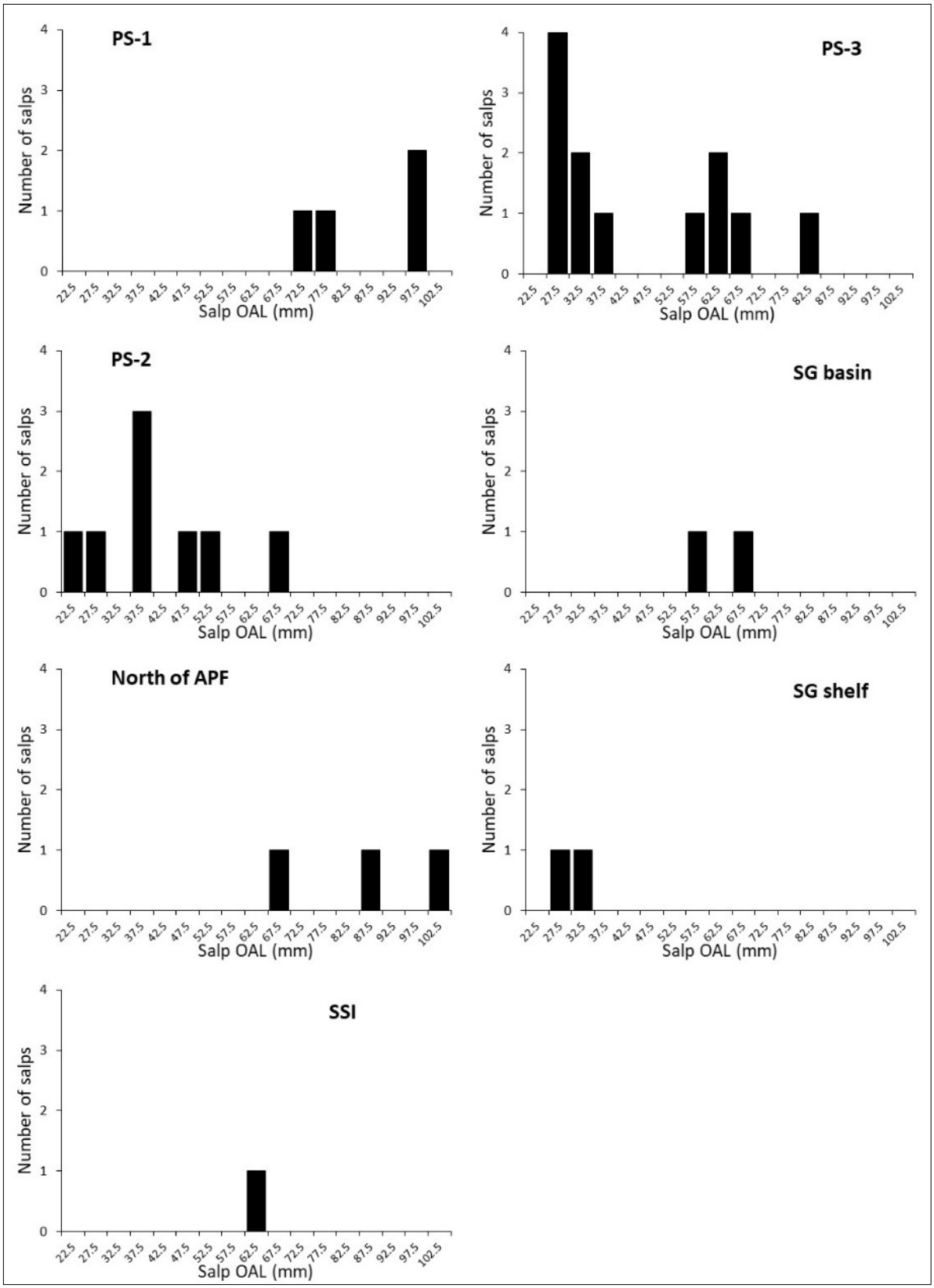

Fig. 12.3: Length frequency distribution of Salpa thompsoni solitaries during the PS 133/1 expedition, austral spring 2022.Stations ID and positions are given in Fig. 10.1.

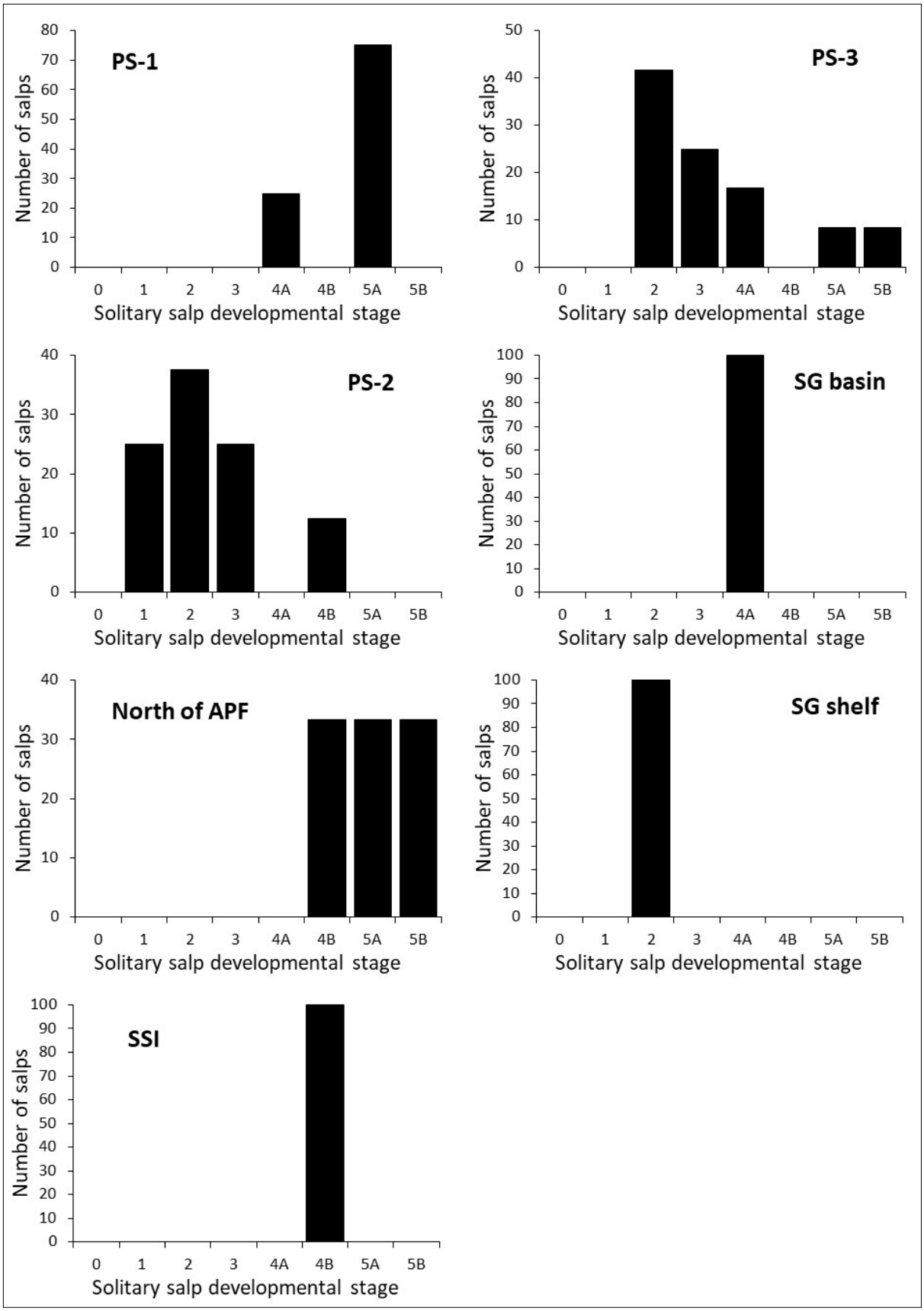

Fig. 12.4: Developmental stage composition of Salpa thompsoni solitaries during the PS 133/1 expedition, austral spring 2022; stations ID and positions are given in Fig. 10.1.

Finally, stations in waters south of the APF (SP-3, SG basin, SG shelf, Stn. PS133/1_5 and SSI) showed even earlier developmental status and were composed by young and first maturing solitaries (often the only salps in the catch, Tab. 12.1) and young and undeveloped aggregates (Figs. 12.1-12.4). It appears that while moving westward during the PS 133/1 expedition, we encountered 'younger' salp populations and it seems that the oceanographic setting, and partially productivity, defined the salp demographic development. Stations that were mostly influenced by Antarctic waters had a *S. thompsoni* population at their spring development, e.g., population only initiating its development, which is defined by the presence of young, not matured solitaries in the water column and a few that already reached their maturity releasing first chains (i.e., many very small aggregates). Moving towards the APF with higher Chl a standing stock, salps were at more advanced stages of development and more numerous. This is also confirmed by the increase in the aggregate to solitary ratios from single digits to > 50, a clear indication of the start of active aggregate chain-release (Tab. 12.1).

While the oceanographic setting had a high explanatory power, salp response to the overall productivity was complex. The gut pigment content at the stations PS-2 and SG shelf were generally in line with the summer gut pigment values (Fig. 12.5). However, the SG basin station had the lowest gut pigment values that were only comparable to the summer 'Salpastan' station, where Chl*a* values were <0.1 mg.m^{-3} (Pakhomov and Hunt 2017). Salps at the SG station were hardly feeding and their embryos, while being at more advanced stages than at SG shelf, showed signs of degradation and maldevelopment.

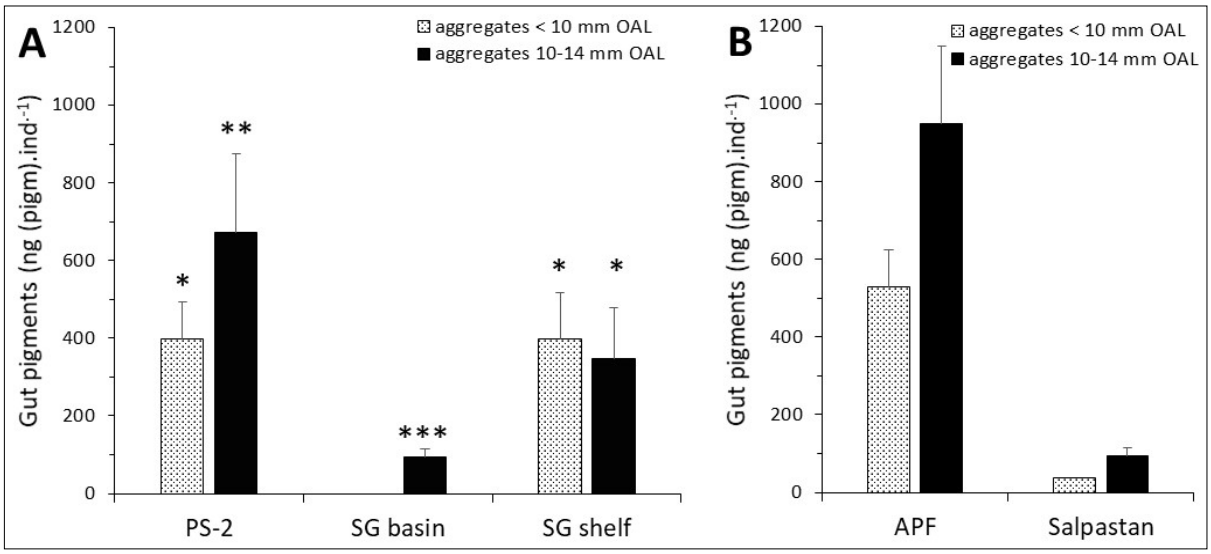

Fig. 12.5: Gut pigment content of Salpa thompsoni aggregates during spring 2022 (A) and summer 2012 (B); stations ID and positions during spring 2022 are given in Fig. 10.

During the expedition, a total of 64 *Salpa thompsoni* were frozen at -80°C for the transcriptomic analyses at the AWI.

Data management

Faunal assemblage composition and distribution data together with environmental co-variables will be archived, published, and disseminated according to international standards by the World Data Center PANGAEA Data Publisher for Earth & Environmental Science (https://www.pangaea.de) within two years after the end of the cruise at the latest. By default, the CC-BY license will be applied.

Molecular data (DNA and RNA data) will be archived, published and disseminated within one of the repositories of the International Nucleotide Sequence Data Collaboration (INSDC, www.insdc.org) comprising of EMBL-EBI/ENA, GenBank and DDBJ).

Any other data will be submitted to an appropriate long-term archive that provides unique and stable identifiers for the datasets and allows open online access to the data.

In all publications based on this expedition, the **Grant No. AWI_PS131/1_08** will be quoted and the following publication will be cited:

Alfred-Wegener-Institut Helmholtz-Zentrum für Polar- und Meeresforschung (2012) Polar Research and Supply Vessel POLARSTERN Operated by the Alfred-Wegener-Institute. Journal of large-scale research facilities, 3, A119. http://dx.doi.org/10.17815/jlsrf-3-163.

References

Atkinson A, Siegel V, Pakhomov EA, Rothery P (2004) Long-term decline in krill stock and increase in salps within the Southern Ocean. Nature, 432:100–103.

Iversen MH, Pakhomov EA, Hunt BPV, van der Jagt H, Wolf-Gladrow D, Klaas C (2017) Sinkers or floaters? Contribution from salp pellets to the export flux during a large bloom event in the Southern Ocean. Deep-Sea Res II, 138:116–125.

Lancraft TM, Hopkins TL, Torres JJ, Donnelly J (1991) Oceanic micronektonic/macrozooplanktonic community structure and feeding in ice covered Antarctic waters during the winter (AMERIEZ 1988). Pol Biol, 11:157–167.

Nast F (1986) Changes in krill abundance and in other zooplankton relative to the Weddell–Scotia Confluence around Elephant Island in November 1983, November 1984 and March 1985. Arch Fischereiwiss, 37:73–94.

Pakhomov EA, Hunt BPV (2017) Trans_Atlantic variability in ecology of the pelagic tunicate *Salpa thompsoni* near the Antarctic Polar Front. Deep-Sea Res II, 138:126–140.

Pakhomov EA, Froneman PW, Perissinotto R (2002) Salp/krill interactions in the Southern Ocean: spatial segregation and implications for the carbon flux. Deep-Sea Res II, 49(9-10):1881–1907.

Pauli N-C, Flintrop CM, Konrad C, Pakhomov EA, Swoboda S, Koch F, Wang X-L, Zhang J-C, Brierley AS, Bernasconi M, Meyer B, Iversen MH (2021) Krill and salp faecal pellets contribute equally to the carbon flux at the Antarctic Peninsula. Nature Comm, 12:7168.

13. MARINE PARTICLES AND SINKING FLUXES

Morten Iversen[1], Hannah Marchant[2], Susanne Spahic[1], Larissa Pattison[3], Christian Konrad[1]
Not on board: Anya Waite[4]

[1]DE.AWI
[2]DE.MARUM
[3]CA.DAL
[4]CA.OFI

Grant-No. AWI_PS133/1_09

Objectives

In the oceans, a suite of complex processes produces and transports organic carbon from the surface to depth via setting organic aggregates, i.e., marine snow (phytoplankton aggregates) and zooplankton fecal pellets. Taken together these processes are referred to as the Biological Carbon Pump (BCP). It is essential to understand how carbon is removed from the surface ocean by the BCP in order to determine the role that the oceans play in mitigating carbon dioxide emissions. At the same time, we also need to understand the biological processes that attenuate and transform organic matter as it sinks through the water and determine how biologically driven attenuation processes impact nutrient recycling (i.e., nitrogen and iron) and, as a result, support ongoing production in the upper, sunlit water column.

The main objectives of our working group were to understand the dynamics and export of marine particles in the different productivity regimes and differences in iron availability along the cruise track of PS133/1 “Island Impact”. During this voyage we focused on:

- Measuring particle (plankton and aggregates) distribution and composition in the water column.
- Measuring export fluxes below the upper mixed layer depth and the permanent thermocline.
- Determining the stoichiometric and lipid composition of the sinking matter.
- Determining how particles influence nutrient recycling.
- Determining the processes that influence particle dynamics and sinking fluxes.

Work at sea

Particle characteristic (size, shape, type, and abundance) were determined through the deployment of a UVP5 underwater video profiling system attached to the CTD-rosette sampler. At the longer “process study” stations we deployed an underwater camera platform (ROSINA) with an integrated CTD to image and quantify a wider size spectrum: from phytoplankton through to aggregates (ROSINA) and larger macrozooplankton (JellyCam) (Table 13.1).

During the process stations, export fluxes were collected using a free drifting array (DF) equipped with three sediment trap stations positioned at 135 m, 235 m and 435 m depth including a camera system designed to measure *in-situ* particle settling rates at 185 m depth. Each trap consisted of four cylindrical sinking matter collectors. Material from two collectors at each depth were fixed with mercury chloride and one collector was frozen for later biogeochemical

analyses (among others particulate organic matter composition), molecular and microscopic analysis of planktonic organisms. The fourth collector at each depth was filled with a viscous gel to preserve size and shape of sinking particles. These were digitally analyzed on board (Table 13.1).

At the process stations, two Marine Snow Catchers (MSC), were used to collect *in situ* formed marine snow and other particles. The MSC consisted of a 100 L cylindrical water sampler with a particle collection tray at the bottom deployed with a winch to the target depth and closed via a release mechanism. The closed MSC was placed on deck for a few hours to allow the collected particles to sink into the collection tray. After gently draining the water from the 100 L cylinder, aggregates were collected from the tray and their size-specific sinking velocities, composition, and respiration rates were determined. Aggregate size, sinking velocities, and microbial respiration were measured on board in a vertical flow chamber at *in situ* temperatures. Individual aggregates were placed in the flow chamber, and the upward flow was increased until the aggregate remained suspended. The sinking velocity of each aggregate was then determined from the flow rate divided by the cross-sectional area of the flow chamber. Microbial respiration was determined from the oxygen gradients through the aggregate-water interface measured using a Clark-type oxygen microelectrode mounted in a micromanipulator and calibrated at air-saturation and at anoxic conditions. Subsequently, aggregates were frozen for later determination of POC and PON contents (Table 13.1).

Tab. 13.1: List of instruments deployed at stations during PS133/1

Station No	Gear	Date	Start Time	Profile depth (m)
PS133/1_3-1	DF1 deployment	2022-10-13	18:05:00	135, 185, 235, 435
PS133/1_3-12	Rosina - P01	2022-10-14	05:45:07	600
PS133/1_3-13	MSC 1-1	2022-10-14	07:33:00	100
PS133/1_3-13	MSC 1-2	2022-10-14	07:58:00	100
PS133/1_3-9	DF1 recovery	2022-10-14	18:10:00	135, 185, 235, 435
PS133/1_6-21	DF2 deployment	2022-10-22	00:56:00	135, 185, 235, 435
PS133/1_6-21	Rosina-P02	2022-10-23	03:25:30	---
PS133/1_6-20	DF2 recovery	2022-10-23	02:25:00	135, 185, 235, 435
PS133/1_8-8	Rosina -P03	2022-11-02	00:19:30	600
PS133/1_9-5	DF3 deployment	2022-11-02	18:46:00	135, 185, 235, 435
PS133/1_9-8	MSC 2-1	2022-11-02	22:46:00	50
PS133/1_9-8	MSC 2-2	2022-11-02	23:00:00	70
PS133/1_9-15	Rosina - P04	2022-11-03	04:37:02	600
PS133/1_9-18	Rosina - P05	2022-11-03	11:03:45	600
PS133/1_9-21	DF3 recovery	2022-11-03	15:34:00	135, 185, 235, 435
PS133/1_10-2	Rosina - P06	2022-11-04	01:54:35	600
PS133/1_14-9	Rosina - P07	2022-11-05	21:08:05	220
PS133/1_14-10	MSC 3-1	2022-11-05	21:58:00	75
PS133/1_14-10	MSC 3-2	2022-11-05	22:16:00	80
PS133/1_14-18	Rosina -P08	2022-11-06	02:51:50	220

In order to investigate how aggregate formation and sinking can impact nutrient release and recycling over diel cycles, we collected water from the ship inlet every four hours at the process study stations. Around 2 L of water each was filtered onto 3 pre-combusted glass fiber filters (GFF, Whatman) which were frozen at either -20°C or -80°C and will be analyzed for POC/PON, POP and lipid characteristics, respectively. Furthermore, at the 3 process stations and station PS133/1_8, water was collected from the CTD-rosette and the moon pool, distributed into 256 mL glass serum bottles to determine ammonia oxidation and nitrite oxidation rates (using ^{15}N-ammonium and ^{15}N-nitrite stable isotope tracers) in the presence and absence of particles (Table 13.2). These rates will be compared to *in situ* particle abundances determined by both the UVP5 and ROSINA systems. To assess the microbial communities involved in the nitrogen recycling, a further 2 L of water was filtered onto a 0.22 µm Sterivex filter for later DNA extraction and sequencing and 50 mL of water was fixed with formaldehyde and filtered for microscopic analysis. To gain further insights into ammonia oxidation rates directly associated with the particles, water was collected from the ship inlet at process station PS133/1_9 and transferred to roller tanks. After 48 h, particles were harvested from the tanks and their oxygen consumption rates, size and sinking velocities were determined, after which they were incubated for 24 h in sterile filtered water containing ^{15}N-ammonium.

Tab. 13.2: Depths sampled for nitrification incubations

Station No	Gear	Date	Bottle number	Profile depth (m)
PS133/1_3-2	CTD-OZE	2022-10-13	8, 10, 11	600, 400, 300
PS133/1_3	Moon pool	2022-10-13	N/A	11
PS133/1_6-14	CTD- Clean	2022-10-22	N/A	100, 300
PS133/1_6	Moon pool	2022-10-22	N/A	11
PS133/1_8-3	CTD-OZE	2022-11-02	7, 10, 13	600, 300, 150
PS133/1_8	Moon pool	2022-11-02	N/A	11
PS133/1_9-3	CTD-OZE	2022-11-02	8, 11, 14	600, 300, 150
PS133/1_9	Moon pool	2022-11-02	N/A	11

Preliminary (expected) results

Vertical particle size-distribution and abundance (ROSINA)

We made eight vertical profiles with the camera platform ROSINA down to 220 and 600 m depth, depending on station (Table 13.1). However, due to communication issues via the winch cable we had to abort two deployments with the ROSINA and we only obtained six full profiles. Lowering speed of ROSINA was 0.3 m s^{-1}, during the downcast ROSINA captured images with a backlight illumination to allow accurate size measurements of the particles (Fig. 13.1 and 13.2). During the upcast, ROSINA was illuminated by reflective light to obtain colour information for the particles in the water column. The JellyCam was operated with front light and illuminated a large water volume to determine the vertical distribution of meso- and microzooplankton (see JellyCam and RMT section).

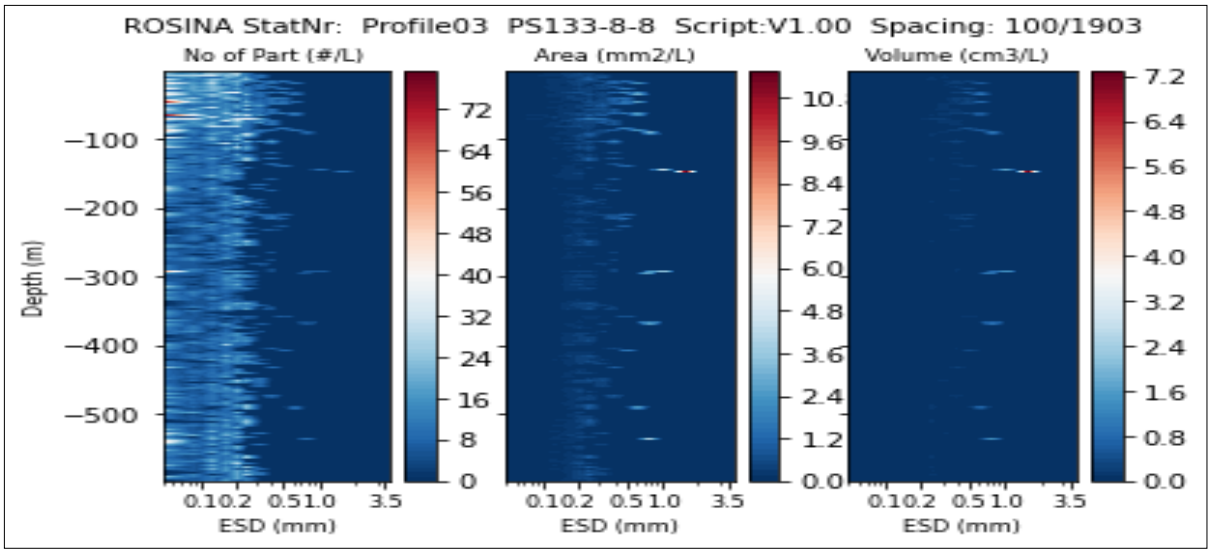

Fig. 13.1: Vertical abundance, area, and volume of particles at Station PS133/1_8 cast 8

Drifting sediment traps:

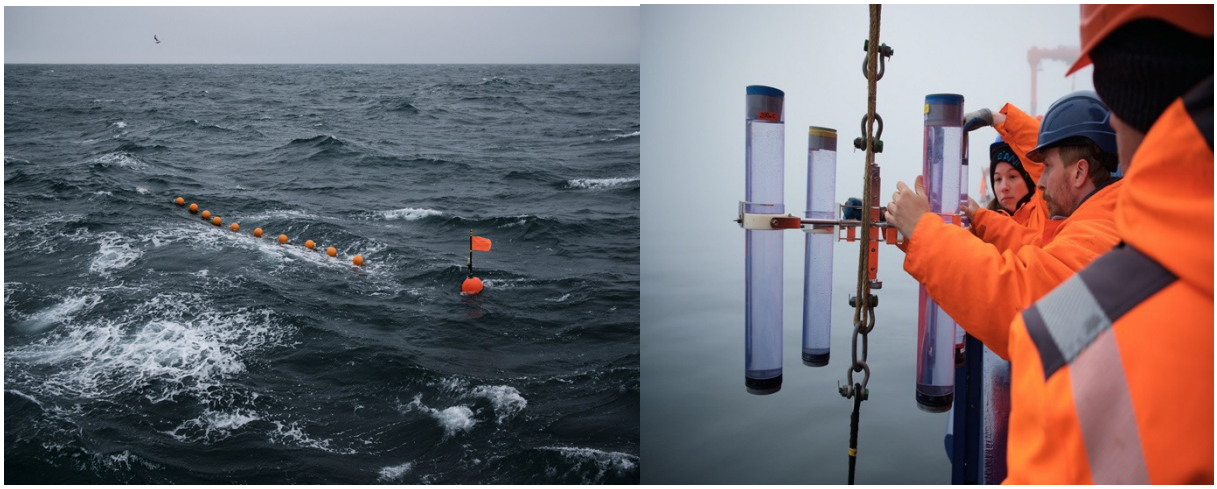

We deployed the drifting trap array three times during the cruise. The drifting array (Fig. 13.2) consisted of a surface buoy equipped with an Iridium satellite unit that provided trap positions every 10 minutes with a temporal resolution of two minutes. Since the drifting trap was further used to deploy the *In-situ* Camera, we used four benthos floats for buoyancy and 16 small buoyancy balls placed between the surface buoy and the four benthos floats to act as wave breakers, thereby reducing the hydrodynamic effects on the sediment traps. The trap cylinders were mounted to a sediment station with gimbal mounts ensuring that they maintained a vertical position in the water column. Each cylinder was 1 m tall and had a diameter 10.4 cm, which resulted in a collection area of 84.95 cm^2.

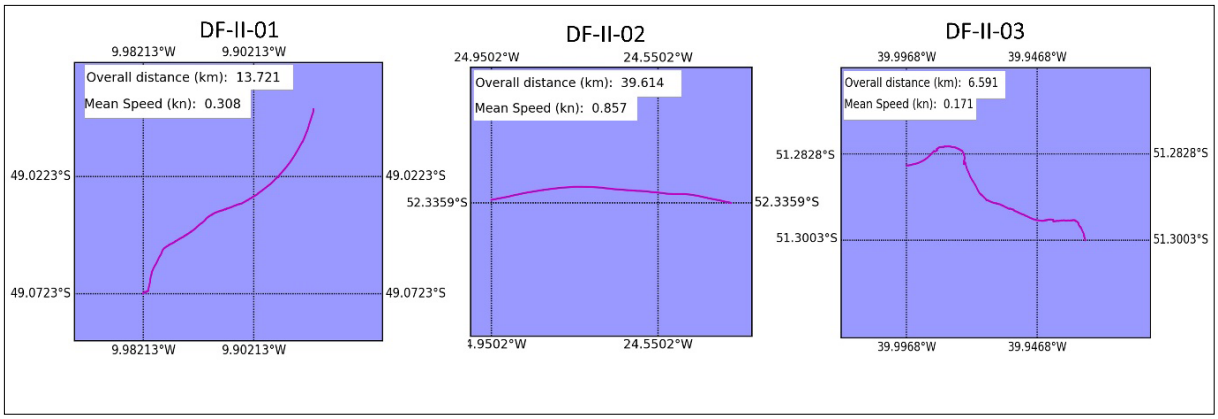

Fig. 13.2: Images of the drifting sediment trap during deployment (upper left): One of the trap stations with the four sediment trap cylinders (upper right). The drifting track for each of the three deployments are shown below, from left to right: process stations PS133/1_3; PS133/1_6 and PS133/1_9, respectively.

The gel traps from the sediment trap at the third process station (PS133/1_9) showed that there was a high flux of faecal pellets to 135 m. However, those faecal pellets did not sink to 235 or 435 m and we only observed few faecal pellets in the traps deployed below 135 m (Fig. 13.3).

Considering that the faecal pellets had sinking velocities ranging between 40 to 360 m d^{-1} (Fig. 13.4), it was surprising that the faecal pellets seemed to be degraded before they reached 235 m. We measured the microbial degradation of the faecal pellets using the oxygen sensor in the flow chamber and estimated that only around 1% of the particulate organic carbon within the faecal pellets were degraded per day. Hence, it is clear that other organisms than microbes are responsible for the flux attenuation of the faecal pellets. To identify the degradation mechanisms of the settling aggregates, we will collaborate with the meso- and macrozooplankton groups as well as looking into the different imaging system deployed during the cruise.

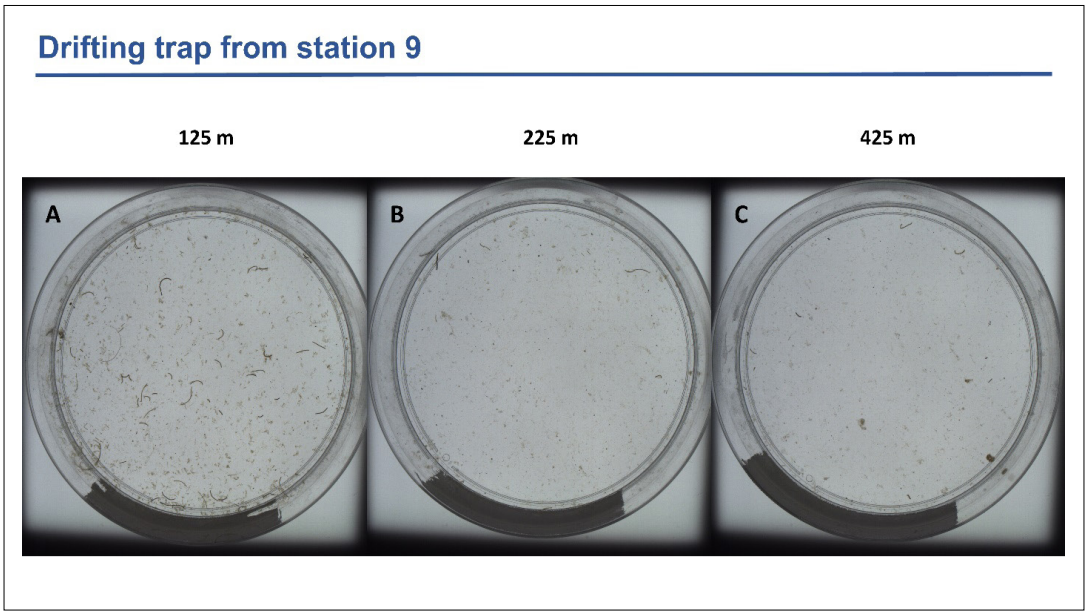

Fig. 13.3: Overview of gel traps from the sediment trap deployment at station PS133/1_9: A) 135 m gel trap, B) 235 m gel trap, and C) 435 m gel trap.

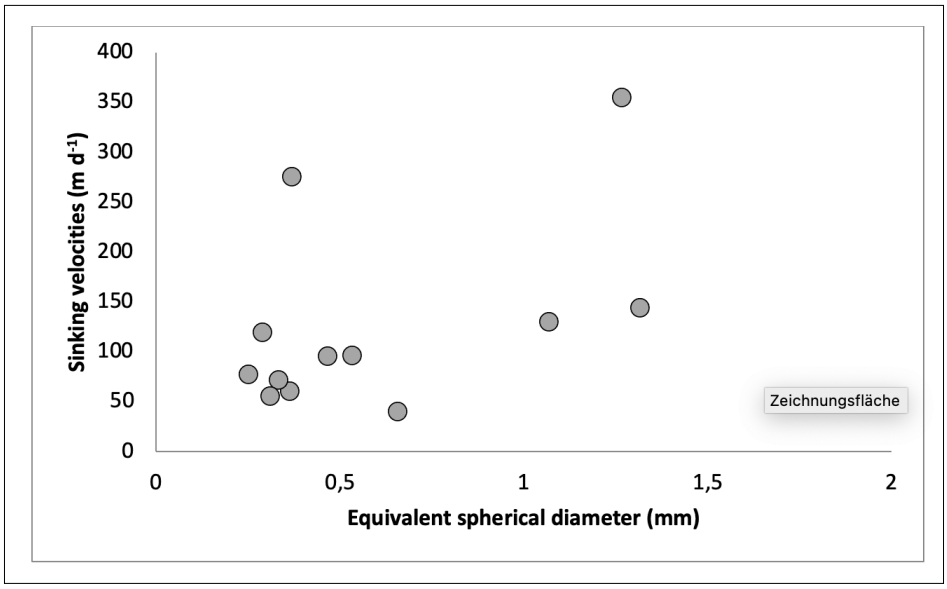

Fig. 13.4: Size vs. settling velocity of faecal pellets collected using the marine snow catchers during the first process station (Ps133/1_3)

Data management

Environmental data will be archived, published and disseminated according to international standards by the World Data Center PANGAEA Data Publisher for Earth & Environmental Science (https://www.pangaea.de) within two years after the end of the cruise at the latest. By default, the CC-BY license will be applied.

Molecular data (DNA and RNA data) will be archived, published and disseminated within one of the repositories of the International Nucleotide Sequence Data Collaboration (INSDC, www.insdc.org) comprising of EMBL-EBI/ENA, GenBank and DDBJ).

Any other data will be submitted to an appropriate long-term archive that provides unique and stable identifiers for the datasets and allows open online access to the data.

This expedition was supported by the Helmholtz Research Programme “Changing Earth – Sustaining our Future” Topic 6, Subtopic 6.3.

In all publications based on this expedition, the **Grant No. AWI_PS133/1_09** will be quoted and the following publication will be cited:

Alfred-Wegener-Institut Helmholtz-Zentrum für Polar- und Meeresforschung (2017) Polar Research and Supply Vessel POLARSTERN Operated by the Alfred-Wegener-Institute. Journal of large-scale research facilities, 3, A119. http://dx.doi.org/10.17815/jlsrf-3-163.

14. PHYTOOPTICS

Astrid Bracher[1], Moritz Zeising[1]; [1]DE.AWI
not on board: Ehsan Mehdipour[1], Hongyan Xi[1],
Sonja Wiegmann[1]

Grant-No. AWI_PS133/1_11

Objectives

Marine phytoplankton constitutes the basis of the marine food web and also a main component of biogeochemical fluxes, thus, an important source of dissolved and particulate organic substances, including volatile organic substances (i.e., DMS, isoprene, halocarbons). The contribution of the Phytooptics group during PS133/1 was the measurements of bio-optical properties and pigment composition. During this expedition we focused on increasing the sampling resolution of information on phytoplankton, particulate and chromophoric dissolved organic matter (CDOM) abundance and composition through continuous and profiles measurements to obtain inherent and apparent optical properties (IOPs, and AOPs, respectively). The specific objectives of our group on the PS131 were to:

- collect high spatially and temporally resolved data on phytoplankton pigments and their degradation products at the surface and for the full euphotic zone using continuous optical observations during the cruise and from ocean colour remote sensing calibrated with discrete water sample measurements.
- develop and validate (global and regional) algorithms and associated radiative transfer models in accordance to the previous objective by using discrete water samples for pigment analysis and absorption measurement.
- obtain a big data set for ground-truthing ocean colour satellite data, specifically from the new Sentinel-3 (A and B) OLCI and the Sentinel-5-Precursor TROPOMI sensors,
- support the optical data collection by the topAWI/Triaxus via instrument calibration, monitoring and comparisons to our underway and station optical data collection,
- obtain a spectral characterization of the underwater light field and its interplay with optical constituents, such as phytoplankton and CDOM abundance and composition.

Work at sea

The contribution of the Phytooptics group was the acquisition of high resolved information on the amount and composition of phytoplankton and its pigments, coloured dissolved organic matter (CDOM) and particles along the cruise. These data collection enables, together with satellite and previous field data acquisition, the analysis of long-term trends of these parameters in the South Atlantic region (Bracher, 1999; Bracher et al., 1999; Soppa et al., 2013; Soppa et al., 2014; Soppa et al., 2016; Cheah et al., 2017; Bracher et al., 2020; Xi et al. under revision). In addition to that, these *in-situ* data are important for the validation of the group's own satellite products (e.g., Oelker et al., 2022; Xi et al., 2021; Bracher et al.,

2009) on phytoplankton composition and its distribution. The continuous surface and profile bio-optical data were regularly calibrated with measurements from discrete water samples determining the phytoplankton pigment composition using HPLC and the optical properties using spectrophotometric instrumentation. Further, these data will help validation of satellite products (The Phytooptics groups is within the Sentinel-3 Validation Team.) through collocation with ocean colour sensors OLCI data (launched in February 2016 and April 2018, respectively, on Sentinel-3A and -3B).

Active and passive bio-optical measurements for underwater light field, specific light attenuation, particle and phytoplankton composition and distribution were carried out continuously in the surface water but also at high vertical and horizontal resolution during the topAWI/Triaxus operation, and at nine (only eight valid data sets) light profiler stations where also CTD casts took place. In particular the following work was carried out:

a) Continuous measurements of inherent optical properties (IOPs) with a hyperspectral spectrophotometer: For the continuous underway surface sampling an *in-situ* spectrophotometer (ACS; Wetlabs) was operated in flow-through mode from 3 October 7:00 UTC to 27 October 18:00 UTC and from 29 October UTC 18:20 to 15 November 13:00 UTC (outside the 12 nautical mile zone of the Falkland Islands) to obtain total and particulate matter attenuation and absorption of surface water. The instrument was mounted to a seawater supply (pumped from the box keel via the membrane pump) in order to deliver living phytoplankton cells. A flow-control with a time-programmed filter was mounted to the ACS to allow alternating measurements of the total and CDOM inherent optical properties of the sea water. Flow-control and a de-bubbler system ensured water flow through the instrument with no air bubbles. The instrument was calibrated daily by measurements with MilliQ water. The system measured continuously except for the daily calibrations (with MilliQ) and during a few occasions due to strong ship movements. Mostly these created data gaps of only a few minutes (during 12 October and 1 November data gaps were, however, larger).

b) A second ACS instrument was mounted on a steel frame together with a depth sensor and a set of hyperspectral radiometers (RAMSES sensors from TRIOS) and operated during 9 stations (see Fig. 14.1, Tab. 14.1) during daylight and out of the ship's shadow. The frame was lowered at 0.1 m/s down to 100 to 150 m depth with stops at 5, 10, 15, 20, 25 and 40, 60, 80, 100 m depth during daylight hours to allow a better collection of radiometric data. The Apparent Optical Properties of water (AOPs: surface reflectance and light attenuation through the water column) were calculated based on downwelling and upwelling irradiance measurements in the profiles (down to the 0.1 % light depth) from the radiometers calibrated for the incident sunlight with measurements of a radiometer on deck. The ACS measured the inherent optical properties (IOPs: total attenuation, scattering and absorption) in the water profiles.

Tab. 14.1: Station positions and depth of profiles for hyperspectral upwelling and downwelling radiation in the water with the RAMSES radiometers and for hyperspectral total absorption and attenuation with the ACS spectrophotometer

	Date	Time	Latitude	Longitude	Max depth [m]
PS133/1_3-16	2022-10-14	14:11:30	-49.058	-9.978	110.00
PS133/1_6-13	2022-10-22	13:08:18	-52.330	-24.993	130.00
PS133/1_8-2	2022-11-01	17:38:09	-50.520	-41.798	100.00*
PS133/1_9-2	2022-11-02	13:08:18	-52.330	-24.993	100.00
PS133/1_10-9	2022-11-04	08:31:02	-51.637	-39.244	100.00
PS133/1_14-1	2022-11-05	10:53:00	-54.193	-35.908	130.00

	Date	Time	Latitude	Longitude	Max depth [m]
PS133/1_14-2	2022-11-05	12:58:00	-54.190	-35.917	150.00
PS133/1_14-3	2022-11-05	15:46:00	-54.193	-35.910	150.00
PS133/1_17-6	2022-11-09	15:22:54	-56.332	-24.862	130.00

*At this station the data logger turned off in water and no data were recorded.

c) Discrete measurements of IOPs (absorption) at water samples were performed i) for 83 samples at five to eight different depths sampled from the CTD-rosettes during 13 clean CTD or CTD-OZE casts within the top 100 to 200 m of the water column (Fig. 14.2 and Tab. 14.2). ii) for 306 underway surface water samples (as for the ACS flow-through system from the ship's sea water pump) at an interval of 3 hours from 3 October ~7:00 UTC to 27 October ~18:00 UTC and 30 October 18:00 UTC until 15 November 12:00 UTC (Tab. 14.3). Water samples for CDOM absorption analysis were filtered through 0.2 µm filters and analyzed onboard with a 2.5-m path length liquid waveguide capillary cell system (LWCC, WPI) following Levering et al. 2017 (further detailed for our setup in Alvarez et al. 2022). Particulate and phytoplankton absorption coefficients were determined with the quantitative filter techniques using sample filtered onto glass-fiber filters QFT-ICAM and measuring them in a portable QFT integrating cavity setup (Röttgers et al. 2016).

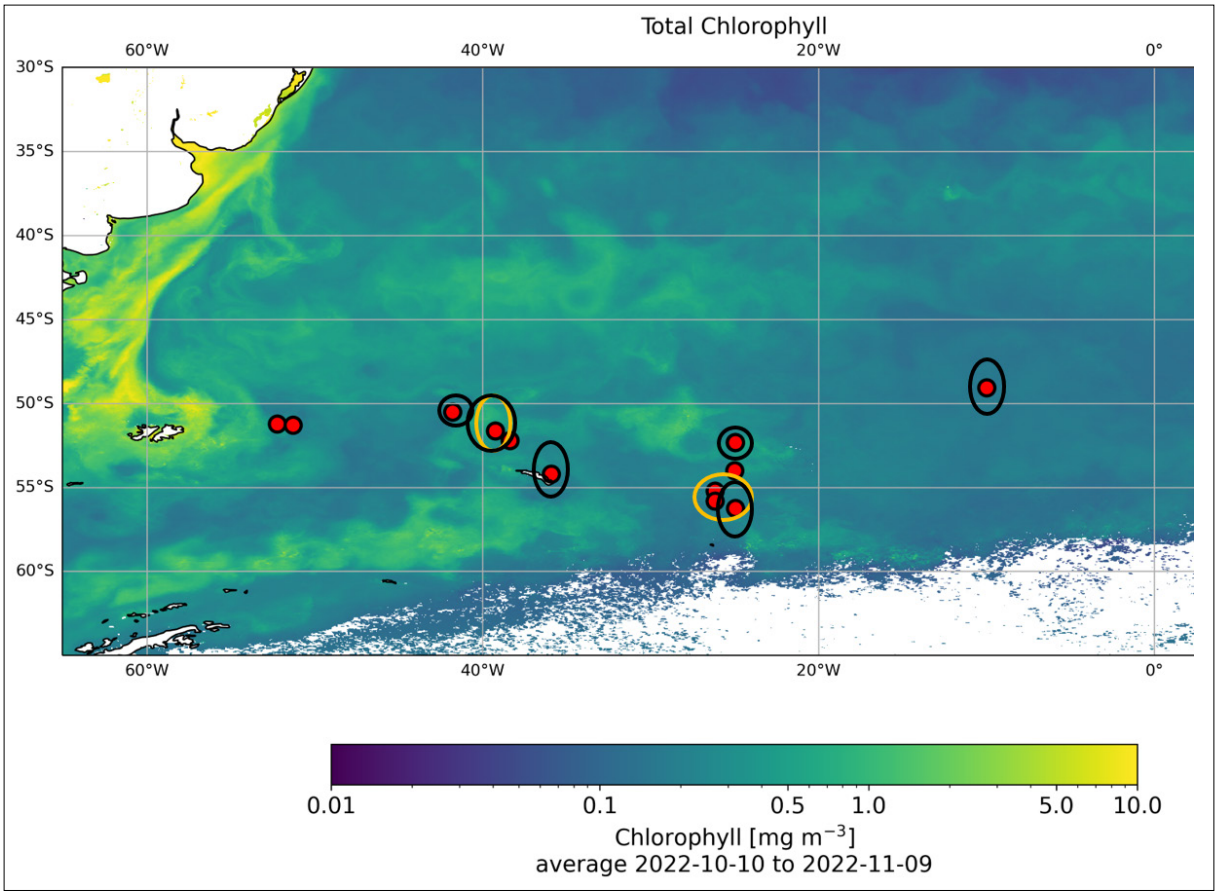

Fig. 14.1: Position of CTD stations sampled for phytoplankton pigment and absorption measurements (red dots), for sediments (yellow circles) and for light profiles (black circles) during PS133-1: Background colour corresponds to the average CMEMS satellite product chl-a conc. (chlorophyll a concentration) for the month when station work was carried out (10 October to 9 November 2022).

Tab. 14.2: List of water sample collected from the CTD-rosettes for the analysis of phytoplankton pigments (HPLC), CDOM (analyzed with LWCC on board), particulate and phytoplankton absorption (analyzed with QFT-ICAM on board) during stations. (*) Sample collected from the ship's seawater intake; (**) sample collected for HPLC analysis only.

Station	Date	Time	Latitude	Longitude	Depth [m]
PS133/1_3-3	2022-10-13	22:30:00	-49.075	-9.988	10,20,40,60,100,120
PS133/1_5-1	2022-10-20	17:34:12	-53.999	-24.996	9*,20,40,80**,100
PS133/1_6-3	2022-10-22	02:16:36	-52.331	-24.976	9*,40,60,80,100,150,200**
PS133/1_6-14	2022-10-22	15:00:45	-52.331	-24.982	9*,20,40,60**,80,100,200
PS133/1_7-1	2022-10-30	18:52:30	-52.328	-24.945	10,20,30,40,50,60,80,100
PS133/1_8-3	2022-11-01	18:57:28	-51.232	-52.236	10,20,40,60,80,100
PS133/1_9-3	2022-11-02	20:44:41	-50.519	-41.794	10,20,40,60,80,100
PS133/1_10-3	2022-11-04	03:59:00	-51.288	-51.288	10,20,40,60,80,100
PS133/1_13-1	2022-11-04	17:19:09	-51.636	-39.245	9*,20,40,60,80,100
PS133/1_14-4	2022-11-05	16:09:27	-52.214	-38.368	10,20,40,60,100,150
PS133/1_15-3	2022-11-07	17:28:54	-54.194	-35.919	10,20,40,60,80,100,150
PS133/1_16-3	2022-11-08	16:18:18	-55.215	-26.163	10,20,40,60,79,100,120
PS133/1_17-3	2022-11-09	19:31:50	-55.803	-26.163	10,20,40,60,80,100,120

Tab. 14.3: Positions of collected underway discrete water sample used to determine the absorption of particulate matter (also differentiated as non-algal and phytoplankton) and of CDOM.

Label	Date and time [UTC]	Latitude	Longitude
UW1	03/10/2022 07:07	-35.107	16.2382
UW2	03/10/2022 09:03	-35.2973	15.9577
UW3	03/10/2022 11:58	-35.5115	15.4373
UW4	03/10/2022 14:59	-35.8021	14.9331
UW5	03/10/2022 17:55	-36.0864	14.4273
UW6	03/10/2022 20:51	-36.3658	13.9249
UW7	04/10/2022 23:56	-38.6799	9.69208
UW8	04/10/2022 02:52	-36.8679	13.0176
UW9	04/10/2022 06:03	-37.1363	12.5304
UW10	04/10/2022 08:57	-37.3574	12.1188
UW11	04/10/2022 11:56	-37.5017	11.8638
UW12	04/10/2022 14:55	-37.8029	11.3122
UW13	04/10/2022 17:58	-38.1031	10.7601
UW14	04/10/2022 20:48	-38.3751	10.257
UW15	04/10/2022 23:55	-38.6784	9.69505
UW16	05/10/2022 02:54	-38.9418	9.20452
UW17	05/10/2022 06:00	-39.1959	8.72973
UW18	05/10/2022 08:57	-39.4398	8.27237
UW19	05/10/2022 11:55	-39.6834	7.81394
UW20	05/10/2022 15:00	-39.9332	7.34213
UW21	05/10/2022 18:42	-40.2403	6.75981
UW22	05/10/2022 21:00	-40.4297	6.3995
UW23	05/10/2022 23:55	-40.6459	5.9864

Label	Date and time [UTC]	Latitude	Longitude
UW24	06/10/2022 02:53	-40.8555	5.58532
UW25	06/10/2022 05:56	-41.0771	5.15917
UW26	06/10/2022 08:55	-41.2961	4.73693
UW27	06/10/2022 11:54	-41.5338	4.27695
UW28	06/10/2022 14:43	-41.7874	3.78412
UW29	06/10/2022 18:00	-42.101	3.17276
UW30	06/10/2022 20:56	-42.3731	2.63914
UW31	06/10/2022 23:55	-42.6477	2.09832
UW32	07/10/2022 02:57	-42.9304	1.53927
UW33	07/10/2022 05:58	-43.2092	0.98537
UW34	07/10/2022 08:56	-43.4889	0.42705
UW35	07/10/2022 11:57	-43.7826	-0.16234
UW36	07/10/2022 15:34	-44.1284	-0.8592
UW37	07/10/2022 18:23	-44.3793	-1.36767
UW38	07/10/2022 20:59	-44.6152	-1.84783
UW39	07/10/2022 23:45	-44.8836	-2.39648
UW40	08/10/2022 02:57	-45.1862	-3.01813
UW41	08/10/2022 06:01	-45.4787	-3.62219
UW42	08/10/2022 08:55	-45.7565	-4.19875
UW43	08/10/2022 12:03	-45.8626	-4.41994
UW44	08/10/2022 14:53	-45.9547	-4.57708
UW45	08/10/2022 18:04	-46.2041	-5.13402
UW46	08/10/2022 21:26	-46.4941	-5.74415
UW47	08/10/2022 23:53	-46.7153	-6.21142
UW48	09/10/2022 03:07	-47.0041	-6.82492
UW49	09/10/2022 06:00	-47.2564	-7.36356
UW50	09/10/2022 09:02	-47.5238	-7.93696
UW51	09/10/2022 11:50	-47.1879	-8.15301
UW52	09/10/2022 14:54	-46.8627	-8.32354
UW53	09/10/2022 17:41	-46.6417	-8.43548
UW54	09/10/2022 20:55	-46.342	-8.58933
UW55	09/10/2022 23:51	-46.0314	-8.74779
UW56	10/10/2022 02:54	-45.7093	-8.91108
UW57	10/10/2022 05:56	-45.4054	-9.06456
UW58	10/10/2022 08:53	-45.0849	-9.22554
UW59	10/10/2022 11:56	-44.7207	-9.41261
UW60	10/10/2022 14:51	-44.3258	-9.60938
UW61	10/10/2022 17:41	-43.9914	-9.77936
UW62	10/10/2022 20:52	-43.9145	-10.2019
UW63	10/10/2022 23:55	-43.8466	-10.5762
UW64	11/10/2022 02:55	-43.7956	-10.857
UW65	11/10/2022 05:58	-43.7436	-11.1395
UW66	11/10/2022 08:53	-43.6607	-11.5979
UW67	11/10/2022 13:25	-43.6294	-11.6649
UW68	11/10/2022 15:02	-43.6512	-11.7059
UW69	11/10/2022 17:55	-43.7488	-12.0004
UW70	11/10/2022 21:02	-43.8566	-12.2554

Label	Date and time [UTC]	Latitude	Longitude
UW71	12/10/2022 00:01	-43.9689	-12.5138
UW72	12/10/2022 02:56	-44.0585	-12.8341
UW73	12/10/2022 05:57	-44.0964	-13.0851
UW74	12/10/2022 09:01	-44.2497	-13.2637
UW75	12/10/2022 11:56	-44.6783	-12.9871
UW76	12/10/2022 14:54	-45.1155	-12.6982
UW77	12/10/2022 17:52	-45.5737	-12.3921
UW78	12/10/2022 21:04	-46.0505	-12.0705
UW79	12/10/2022 23:45	-46.4548	-11.7956
UW80	13/10/2022 02:55	-46.925	-11.4808
UW81	13/10/2022 05:58	-47.3706	-11.1794
UW82	13/10/2022 08:55	-47.8092	-10.8659
UW83	13/10/2022 12:05	-48.2795	-10.543
UW84	13/10/2022 14:45	-48.6762	-10.2692
UW85	13/10/2022 17:52	-49.0744	-9.98132
UW86	14/10/2022 13:40	-49.0581	-9.97853
UW87	14/10/2022 19:24	-49.0046	-9.87246
UW88	15/10/2022 06:00	-49.1908	-10.4382
UW89	15/10/2022 09:02	-49.344	-11.0006
UW90	15/10/2022 11:41	-49.4625	-11.475
UW91	15/10/2022 14:53	-49.5888	-11.9687
UW92	15/10/2022 17:53	-49.6811	-12.3511
UW93	15/10/2022 20:59	-49.8078	-12.8249
UW94	15/10/2022 23:58	-49.9293	-13.284
UW95	16/10/2022 02:58	-50.0567	-13.786
UW96	16/10/2022 05:51	-50.1969	-14.2669
UW97	16/10/2022 08:58	-50.3112	-14.7641
UW98	16/10/2022 11:56	-50.4266	-15.2393
UW99	16/10/2022 14:52	-50.5511	-15.7211
UW100	16/10/2022 17:55	-50.6159	-16.2594
UW101	16/10/2022 20:57	-50.6654	-16.7854
UW102	17/10/2022 00:05	-50.7138	-17.2651
UW103	17/10/2022 02:55	-50.7639	-17.7268
UW104	17/10/2022 05:56	-50.8149	-18.2528
UW105	17/10/2022 09:00	-50.8772	-18.7816
UW106	17/10/2022 12:02	-50.9266	-19.3225
UW107	17/10/2022 14:58	-50.9825	-19.8753
UW108	17/10/2022 18:01	-51.0427	-20.468
UW109	17/10/2022 21:00	-51.1052	-21.0747
UW110	17/10/2022 23:57	-51.1674	-21.6978
UW111	18/10/2022 02:57	-51.2363	-22.3816
UW112	18/10/2022 05:53	-51.3068	-23.0733
UW113	18/10/2022 08:57	-51.3582	-23.7647
UW114	18/10/2022 11:57	-51.0203	-24.2488
UW115	18/10/2022 14:59	-50.8112	-24.715
UW116	18/10/2022 16:04	-50.6849	-24.7855
UW117	18/10/2022 16:57	-50.588	-24.8568

Label	Date and time [UTC]	Latitude	Longitude
UW118	18/10/2022 17:57	-50.4891	-24.9472
UW119	18/10/2022 20:59	-50.1087	-24.9877
UW120	18/10/2022 23:56	-49.7419	-24.9954
UW121	19/10/2022 02:55	-49.4774	-25.0112
UW122	19/10/2022 05:55	-49.8505	-24.9823
UW123	19/10/2022 08:59	-50.2229	-24.9954
UW124	19/10/2022 11:57	-50.5894	-24.9977
UW125	19/10/2022 15:00	-50.9827	-24.9968
UW126	19/10/2022 17:57	-51.3426	-24.9959
UW127	19/10/2022 20:59	-51.6858	-24.9951
UW128	20/10/2022 00:05	-52.0719	-24.9945
UW129	20/10/2022 02:57	-52.4223	-24.9937
UW130	20/10/2022 05:54	-52.7934	-24.9999
UW131	20/10/2022 08:59	-53.2011	-25
UW132	20/10/2022 11:51	-53.5857	-25.0003
UW133	20/10/2022 15:01	-54.0006	-25
UW134	20/10/2022 22:39	-54.0022	-24.993
UW135	20/10/2022 23:53	-54.0016	-25
UW136	21/10/2022 02:53	-53.6435	-25.0037
UW137	21/10/2022 05:55	-53.1309	-24.9869
UW138	21/10/2022 08:56	-52.6957	-24.9788
UW139	21/10/2022 11:54	-52.2748	-24.9814
UW140	21/10/2022 15:03	-51.918	-25.0201
UW141	21/10/2022 17:59	-51.8753	-25.2043
UW142	21/10/2022 21:01	-52.0793	-24.9979
UW143	21/10/2022 23:49	-52.2902	-25.0276
UW144	22/10/2022 06:48	-52.3311	-24.9765
UW145	22/10/2022 11:02	-52.3186	-24.981
UW146	22/10/2022 12:01	-52.296	-25.007
UW147	22/10/2022 13:07	-52.3313	-24.994
UW148	22/10/2022 15:23	-52.3284	-24.9438
UW149	22/10/2022 17:53	-52.3276	-24.8947
UW150	22/10/2022 20:48	-52.3232	-24.8523
UW151	23/10/2022 00:03	-52.2881	-24.8318
UW152	23/10/2022 02:55	-52.3398	-24.3625
UW153	23/10/2022 05:51	-52.3167	-24.6759
UW154	23/10/2022 08:59	-52.2799	-25.0374
UW155	23/10/2022 11:59	-52.2757	-25.1002
UW156	23/10/2022 14:59	-52.2658	-25.8158
UW157	23/10/2022 17:49	-52.2513	-26.5351
UW158	23/10/2022 19:55	-52.2401	-27.095
UW159	23/10/2022 21:58	-52.2271	-27.671
UW160	23/10/2022 23:49	-52.218	-28.2181
UW161	24/10/2022 02:06	-52.2046	-28.8976
UW162	24/10/2022 03:53	-52.1925	-29.5021
UW163	24/10/2022 05:55	-52.1786	-30.2109
UW164	24/10/2022 08:01	-52.1638	-30.9536

Label	Date and time [UTC]	Latitude	Longitude
UW165	24/10/2022 10:00	-52.1495	-31.6773
UW166	24/10/2022 11:58	-52.1354	-32.3881
UW167	24/10/2022 13:57	-52.1214	-33.0919
UW168	24/10/2022 15:54	-52.108	-33.7701
UW169	24/10/2022 17:56	-52.0945	-34.4468
UW170	24/10/2022 19:54	-52.0816	-35.0993
UW171	24/10/2022 21:58	-52.0678	-35.7869
UW172	24/10/2022 23:55	-52.0549	-36.4377
UW173	25/10/2022 01:54	-52.0413	-37.1219
UW174	25/10/2022 03:53	-52.0278	-37.8014
UW175	25/10/2022 05:54	-52.0138	-38.5043
UW176	25/10/2022 08:00	-51.9986	-39.2514
UW177	25/10/2022 09:56	-51.9786	-39.9362
UW178	25/10/2022 12:01	-51.9705	-40.6722
UW179	25/10/2022 13:58	-51.9569	-41.3555
UW180	25/10/2022 15:58	-51.943	-42.0499
UW181	25/10/2022 18:03	-51.9285	-42.7758
UW182	25/10/2022 19:59	-51.9152	-43.4473
UW183	25/10/2022 22:37	-51.8967	-44.3741
UW184	26/10/2022 00:00	-51.8864	-44.8894
UW185	26/10/2022 01:57	-51.8716	-45.6258
UW186	26/10/2022 03:55	-51.8566	-46.3788
UW187	26/10/2022 05:57	-51.8409	-47.1638
UW188	26/10/2022 07:56	-51.8256	-47.9107
UW189	26/10/2022 10:04	-51.81	-48.6826
UW190	26/10/2022 11:57	-51.7967	-49.3357
UW191	26/10/2022 13:57	-51.7831	-50.0084
UW192	26/10/2022 15:58	-51.7692	-50.6861
UW193	26/10/2022 17:57	-51.7557	-51.3583
UW194	26/10/2022 19:53	-51.7421	-52.0202
UW195	26/10/2022 21:54	-51.7271	-52.7154
UW196	26/10/2022 23:51	-51.7162	-53.3607
UW197	27/10/2022 01:52	-51.7037	-54.021
UW198	27/10/2022 03:57	-51.6898	-54.7474
UW199	27/10/2022 05:57	-51.6767	-55.4369
UW200	27/10/2022 07:56	-51.6645	-56.0791
UW201	27/10/2022 10:01	-51.6574	-56.5266
UW202	27/10/2022 11:58	-51.6486	-56.7183
UW203	27/10/2022 14:09	-51.6482	-56.9369
UW204	27/10/2022 16:06	-51.644	-57.1522
UW205	27/10/2022 17:54	-51.6402	-57.3569
UW206	30/10/2022 16:38	-51.2391	-52.3868
UW207	30/10/2022 18:07	-51.2314	-52.236
UW208	30/10/2022 20:57	-51.2187	-52.0867
UW209	30/10/2022 23:58	-51.1768	-51.4649
UW210	31/10/2022 02:56	-51.1348	-50.8401
UW211	31/10/2022 05:55	-51.0929	-50.2227

Label	Date and time [UTC]	Latitude	Longitude
UW212	31/10/2022 09:00	-51.0505	-49.5953
UW213	31/10/2022 11:54	-51.0086	-48.9763
UW214	31/10/2022 15:03	-50.9624	-48.2968
UW215	31/10/2022 17:52	-50.9173	-47.6302
UW216	31/10/2022 21:04	-50.8679	-46.8799
UW217	31/10/2022 23:59	-50.8179	-46.1671
UW218	01/11/2022 02:58	-50.7676	-45.428
UW219	01/11/2022 05:55	-50.7167	-44.6807
UW220	01/11/2022 09:03	-50.6638	-43.9049
UW221	01/11/2022 12:00	-50.6091	-43.1039
UW222	01/11/2022 15:00	-50.5426	-42.13
UW223	01/11/2022 17:45	-50.5195	-41.7977
UW224	02/11/2022 02:56	-50.5964	-41.6229
UW225	02/11/2022 05:55	-50.8173	-41.1076
UW226	02/11/2022 09:02	-51.0477	-40.571
UW227	02/11/2022 11:55	-51.2444	-40.062
UW228	02/11/2022 13:43	-51.3034	-39.9697
UW229	02/11/2022 23:53	-51.2907	-39.9967
UW230	03/11/2022 11:57	-51.2904	-39.9998
UW231	03/11/2022 15:23	-51.3014	-39.9255
UW232	03/11/2022 19:58	-51.3263	-39.8725
UW233	03/11/2022 21:56	-51.4848	-39.5422
UW234	03/11/2022 23:58	-51.6166	-39.1725
UW235	04/11/2022 08:37	-51.6365	-39.245
UW236	04/11/2022 10:59	-51.8309	-38.9932
UW237	04/11/2022 13:07	-52.0431	-38.7005
UW238	04/11/2022 17:23	-52.214	-38.3684
UW239	04/11/2022 19:55	-52.4531	-38.1914
UW240	04/11/2022 21:58	-52.7965	-37.7485
UW241	04/11/2022 23:48	-53.0989	-37.3551
UW242	05/11/2022 01:59	-53.4574	-36.8857
UW243	05/11/2022 03:58	-53.7805	-36.4591
UW244	05/11/2022 05:55	-54.0938	-36.0423
UW245	05/11/2022 11:06	-54.1933	-35.9077
UW246	05/11/2022 13:01	-54.1899	-35.9136
UW247	05/11/2022 15:07	-54.1927	-35.9098
UW248	06/11/2022 05:55	-54.2729	-35.2197
UW249	06/11/2022 09:02	-54.3825	-34.1951
UW250	06/11/2022 12:07	-54.4922	-33.1658
UW251	06/11/2022 14:57	-54.5925	-32.222
UW252	06/11/2022 18:02	-54.7073	-31.1416
UW253	06/11/2022 21:03	-54.8216	-30.0599
UW254	06/11/2022 23:57	-54.9312	-29.0214
UW255	07/11/2022 02:57	-55.0439	-27.9502
UW256	07/11/2022 05:56	-55.1566	-26.8766
UW257	07/11/2022 08:56	-55.2316	-26.17
UW258	08/11/2022 02:58	-55.4093	-25.7558

Label	Date and time [UTC]	Latitude	Longitude
UW259	08/11/2022 05:54	-55.6323	-25.2343
UW260	08/11/2022 10:49	-55.8005	-24.8391
UW261	08/11/2022 17:53	-55.897	-24.8632
UW262	09/11/2022 15:25	-56.3322	-24.862
UW263	10/11/2022 02:56	-56.3223	-25.3375
UW264	10/11/2022 05:54	-56.1843	-26.2026
UW265	10/11/2022 09:02	-56.0826	-27.1165
UW266	10/11/2022 11:56	-56.0372	-27.9846
UW267	10/11/2022 14:57	-56.0047	-28.8706
UW268	10/11/2022 17:57	-55.9697	-29.8192
UW269	10/11/2022 21:03	-55.931	-30.8664
UW270	10/11/2022 23:58	-55.8951	-31.8414
UW271	11/11/2022 02:56	-55.859	-32.8186
UW272	11/11/2022 05:55	-55.8241	-33.7626
UW273	11/11/2022 09:00	-55.7915	-34.6427
UW274	11/11/2022 11:53	-55.7618	-35.4481
UW275	11/11/2022 15:02	-55.73	-36.304
UW276	11/11/2022 18:03	-55.7002	-37.1065
UW277	11/11/2022 20:57	-55.669	-37.9464
UW278	11/11/2022 23:58	-55.636	-38.8374
UW279	12/11/2022 02:58	-55.6023	-39.7376
UW280	12/11/2022 05:53	-55.5695	-40.6225
UW281	12/11/2022 09:02	-55.5337	-41.5868
UW282	12/11/2022 12:02	-55.5002	-42.4843
UW283	12/11/2022 14:57	-55.4688	-43.3249
UW284	12/11/2022 18:00	-55.4351	-44.2254
UW285	12/11/2022 20:54	-55.4027	-45.0963
UW286	13/11/2022 00:00	-55.3727	-45.8981
UW287	13/11/2022 02:55	-55.3464	-46.5983
UW288	13/11/2022 05:56	-55.2846	-47.3005
UW289	13/11/2022 09:59	-55.1647	-48.3081
UW290	13/11/2022 11:57	-55.1313	-48.5885
UW291	13/11/2022 14:54	-55.0429	-49.3274
UW292	13/11/2022 18:04	-54.958	-50.0353
UW293	13/11/2022 21:03	-54.8773	-50.7085
UW294	13/11/2022 23:56	-54.7981	-51.3669
UW295	14/11/2022 02:59	-54.717	-52.0405
UW296	14/11/2022 05:39	-54.6479	-52.6124
UW297	14/11/2022 09:00	-54.5613	-53.328
UW298	14/11/2022 12:08	-54.4734	-54.0539
UW299	14/11/2022 15:00	-54.3889	-54.7354
UW300	14/11/2022 17:44	-54.3101	-55.3695
UW301	14/11/2022 21:06	-54.2059	-56.2052
UW302	15/11/2022 00:02	-54.1132	-56.9466
UW303	15/11/2022 02:59	-54.0191	-57.6976
UW304	15/11/2022 05:58	-53.9219	-58.4703
UW305	15/11/2022 08:58	-53.827	-59.2249
UW306	15/11/2022 11:59	-53.737	-59.9388

d) Samples for determination of phytoplankton pigment concentrations and composition were taken underway and from the CTD deployments similar to the other optical parameters (Tab. 14.2 and 14.3). These water samples were filtered on board immediately after sampling, filters were thermally shocked in liquid nitrogen and stored at -80°C for analysis by High Performance Liquid Chromatography Technique (HPLC) in the home laboratory following Taylor et al. (2011) adapted to our new instrumentation as described in Alvarez et al. (2022). Additionally, sediment samples collected by multicorer (Tab. 14.4, Fig. 14.1) were taken at 4 stations from 0 to 10 cm depth in 1 cm intervals. Pigments will be determined following the method outlined in Cedhagen et al. (2014).

Tab. 14.4: List of sediment samples for phytoplankton pigments analysis.

Station	Date time (UTC)	Latitude	Longitude
PS133/1_9-22	03/11/2022 17:46	-50.519	-41.794
PS133/1_15-5	07/11/2022 21:22	-54.194	-35.919
PS133/1_16-1	08/11/2022 10:15	-55.215	-26.163
PS133/1_17-1	08/11/2022 23:13	-55.803	-26.163

e) Further, during the topAWI/Triaxus survey (18-20 October 2022; Tab. 3.11) approximately 300 up- and downcast profiles (each at about 1 m/s profiling speed) were measured for hyperspectrally resolved apparent (surface reflectance, diffuse attenuation, water leaving radiance) and inherent (absorption, scattering) optical properties. The acquisition of optical data (hyperspectral AOPs from one downwelling RAMSES sensors, hyperspectral IOPs from the same ACS instrument as used on the light profiler, Chlorophyll and backscatter at 550 nm from a WETLabs triplet sensor, and overall visible light from a PAR sensor) during the Triaxus survey is supported by our team with output data control, instrument calibration and later analysis of the data.

Preliminary (expected) results

On board we were already able to analyze the RAMSES station and topAWI/Triaxus, and the QFT particulate (phytoplankton and non-algal) absorption data. Further, we processed part of the ACS flowthrough data and LWCC CDOM absorption data. Preliminary results which later will be further quality controlled are presented here.

From the measurements of the QFT-ICAM we calculated the total particulate, phytoplankton and non-algal absorption and the absorption line height at 676 nm (aLH). From the later we obtained a proxy for the chlorophyll-a concentrations (chl-a), following Roesler and Barnard (2013) via calibration (chl-a proxy = 181.1 * (aLH^1.11)) with the chl-a measured on board by Klaas et al. (Chapter 8; this issue). Figure 14.2 shows the resulting underway derived chl-a concentrations. Maximum chl-a values were measured close to the Falkland Island and around several areas south of the Polar Front as also indicated by the satellite data (Fig. 14.1). Similarly, filtered water samples measured for CDOM absorption with LWCC can provide insights on the magnitude, but also the source (e.g., terrigenous vs. marine) of dissolved optical active components. Processing shall be completed shortly after expedition (within 3 months). These discrete water hyperspectral absorption data set will then later be used to validate the continuous ACS-derived absorption spectra in order determine their uncertainties.

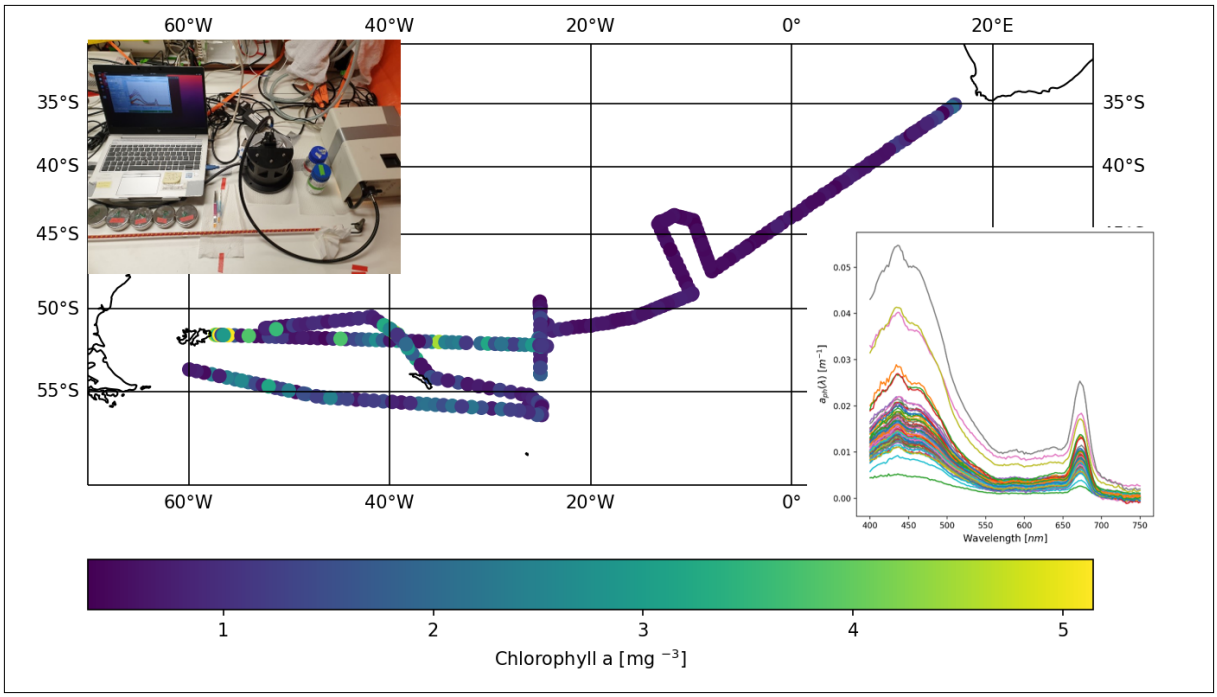

Fig. 14.2: Chlorophyll a along the cruise track estimated from particulate absorption, measured with the QFT-ICAM technique, used to determine the absorption line height at 676 nm following Roesler and Barnard (2013); examples from measurements of absorption spectra of particulate matter obtained during the cruise are shown on the insert: The upper left photograph shows the set-up of QFT-ICAM measurements during the cruise.

Most of the continuous ACS flowthrough data (4 to 23 October, 1-6 November 2022) were processed to total and particulate absorption data. Figure 14.3 shows the directly obtained raw ACS sensor data, their processing to phytoplankton absorption for 4 Nov 2022 measurements and the setup of the instrumentation. Similar to the discrete water QFT particulate absorption data, the aLH and the chl-a conc. were also calculated (using calibration data from the former transatlantic expedition PS113).

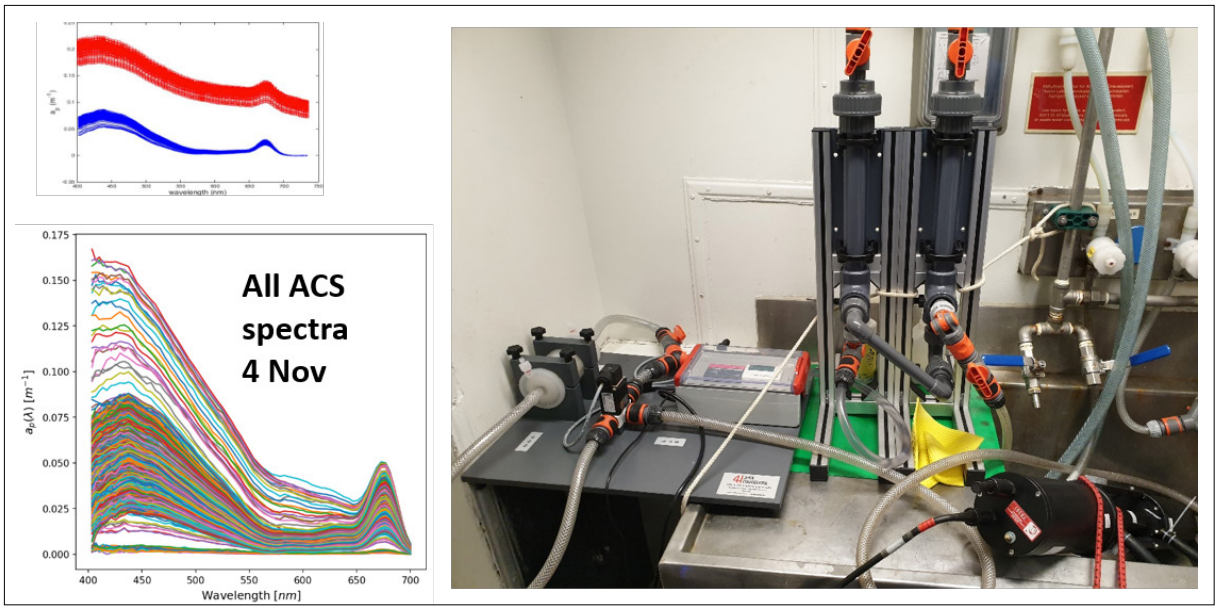

Fig. 14.3: Right panel: Setup of ACS-flowthrough system including de-bubbler, valve, tubing and filter to separate total from CDOM +water absorption measurements. Left panel: Raw data of hyperspectral attenuation (red) and absorption (blue) and further processed to particulate absorption for 4 November 2022.

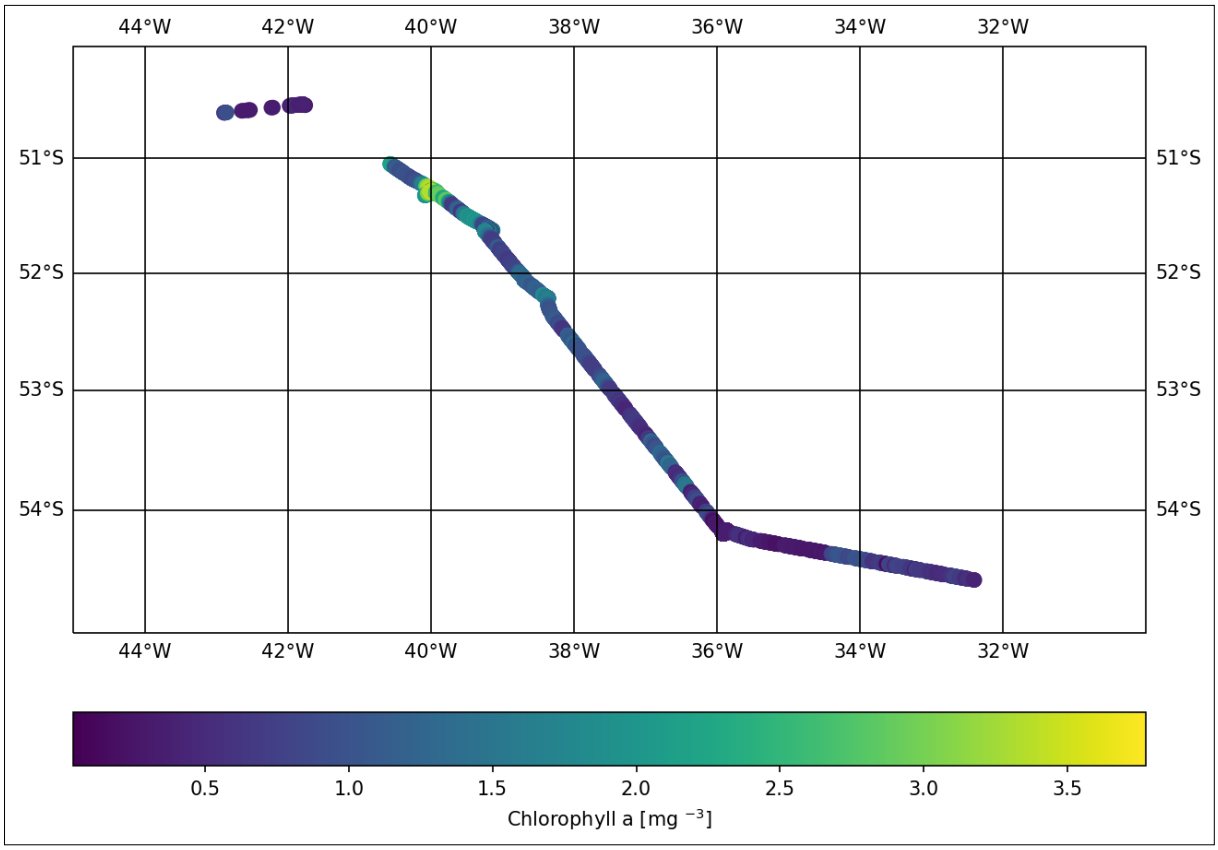

Fig. 14.4: Chl-a concentrations along the cruise track from 1 to 6 November 2022 derived from particulate absorption measured with the ACS-flowthrough setup shown in Fig. 14.3, used to determine the absorption line height at 676 nm following Roesler and Barnard (2013).

Results of chl-a determined from the ACS flowthrough setup for the Georgia Basin and around South Georgia (1-6 November 2022) are shown in Figure 14.4, and in Figure 14.5, as function of time with the Ferrybox chl-a fluorimeter sensor data. They clearly show the peak in chl-a at the third PS133/1 process station (PS133/1-9). While the Ferrybox data provides a qualitative indication of chl-a patterns, it requires further calibration and corrections as the signal is significantly affected by photosynthetic activity and non-photochemical quenching during daylight hours. The ACS-flowthrough data will be processed for the entire cruise data set, including calibration with the HPLC data and further quality controlled to provide reliable particulate absorption data for all surface waters crossed during PS133/1. Finally, the PFT (Phytoplankton Functional Types) algorithm by Bracher et al. (2015) further updated in Xi et al. (2020) will be used to derive the contributions of different phytoplankton group to total chl-a for these measurements based on the diagnostic pigment (HPLC) data for the major phytoplankton groups (PFTs). Pigment analysis from the sediments will be used to estimate the contribution of PFTs to sedimentation at the hadal stations in the South Sandwich Trench (> 8,000 m, station PS133-1_15-2 and PS133-1_17-1).

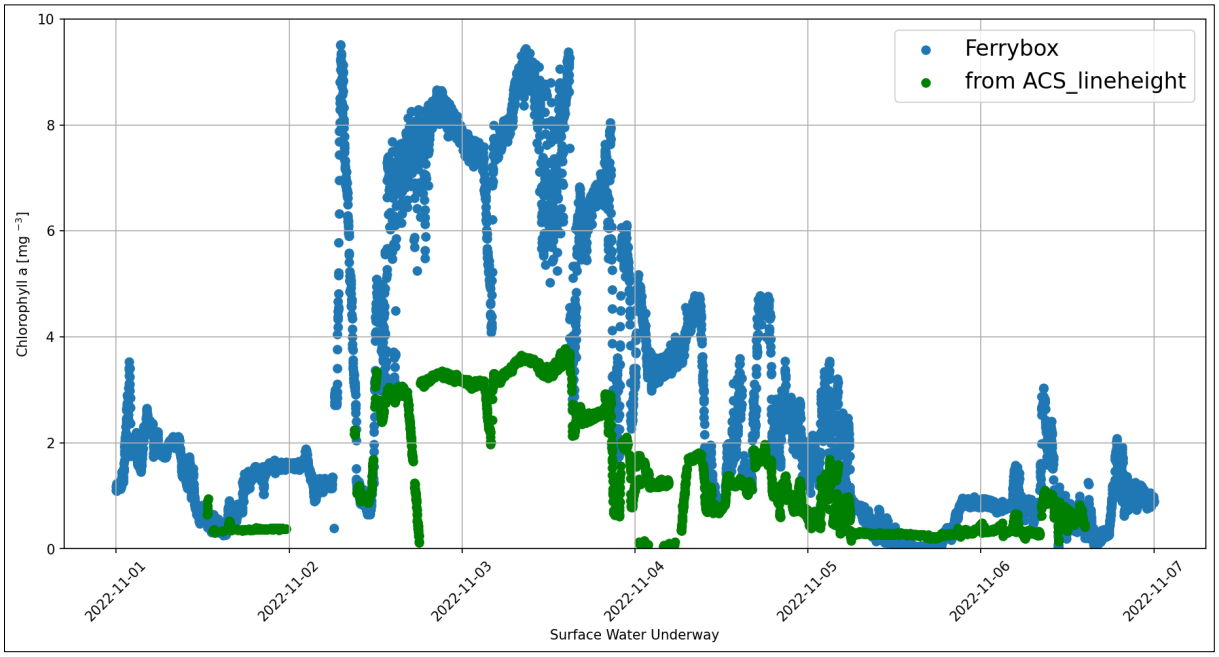

Fig. 14.5: Chl-a concentrations from 1 to 6 Nov 2022 derived from particulate absorption, measured with the ACS-flowthrough setup shown in Fig. 14.3 (green dots), used to determine the absorption line height at 676 nm following Roesler and Barnard (2013), and from the ship's Ferrybox chl-a fluorometer (blue dots).

During the 52-hour topAWI/Triaxus cast from 18 to 20 October 2022, we obtained approximately 300 up- and downcast profiles of underwater hyperspectral irradiance (at about 1 m/s profiling speed) from the RAMSES radiometers. These data were then processed to hyperspectral underwater diffuse attenuation and transmission coefficients and the euphotic depth (deeper layer where net photosynthesis/growth occurs). Figure 14.6 shows the setup of the RAMSES and ACS on the topAWI/Triaxus towing platform, the hyperspectral downwelling irradiance for one representative downcast profile and the euphotic depth for all quality controlled downcast and upcast profiles (note that up- and downcast are not yet corrected for varying rope lengths which causes the observed offset between the two casts in Fig. 14.6).

All radiometric hyperspectral downwelling irradiance and upwelling radiance data obtained during the stations (Tab. 14.1) have been processed following Taylor et al. (2011), Tilstone et al. (2020) and Bracher et al. (2022) to obtain AOPs. Remote Sensing Reflectance (RRS) data will be used for validating Satellite L2 RRS data products (The three casts at station PS133/1-14 are perfect matchups with Sentinel-3 Sensor OLCI-A). Further, all hyperspectral diffuse attenuation and transmission data (from stations and topAWI/Triaxus) together with the particulate absorption data measured by the second ACS will be used as input data for predicting the chl-a of all and the major PFTs (as shown for PS113 in Bracher et al., 2020) along the different transects. Finally, as one of the main objectives of the MARDATA PhD thesis, these data sets are planned to be combined via data fusion with CMEMS PFT products (also developed within our group, Xi et al. 2020 & 2021) in order to provide high resolution information in space and time on the major groups of phytoplankton during PS133/1.

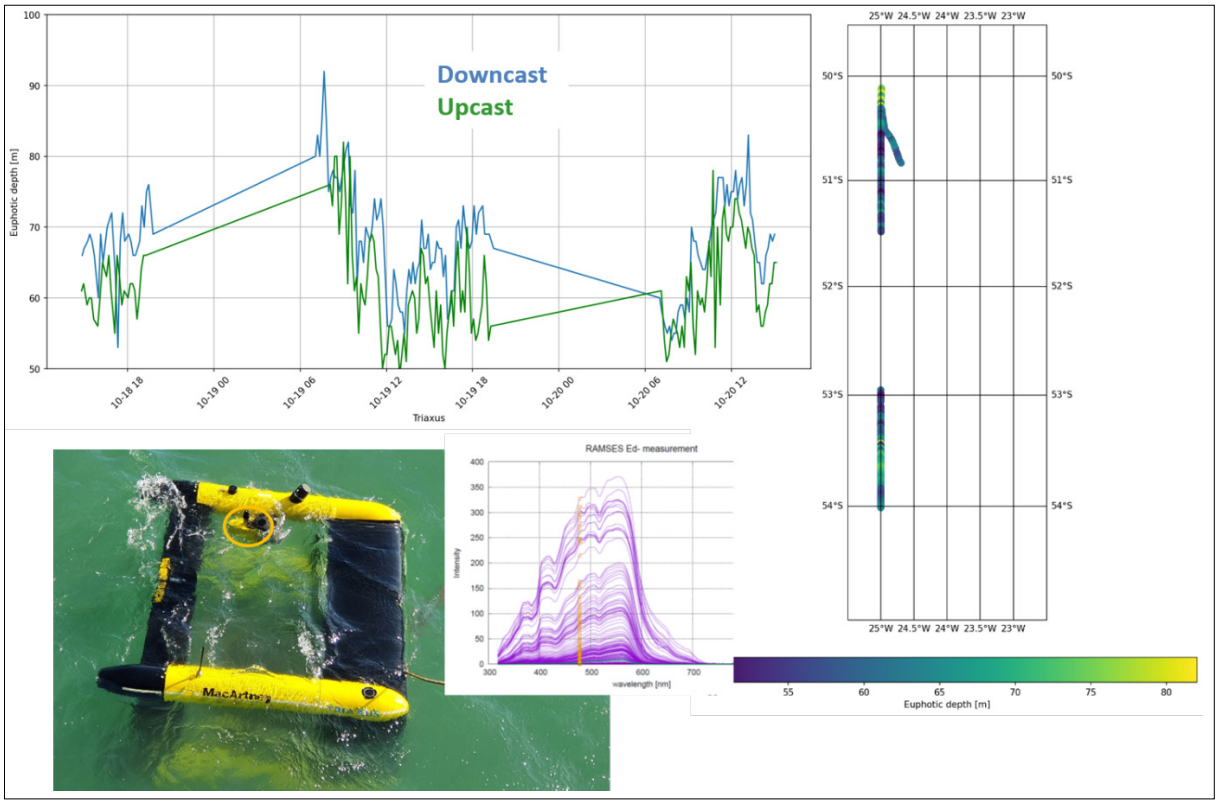

Fig. 14.6: Upper left panel: Euphotic depths along the topAWI/Triaxus towed transect between 18 and 20 Oct 2022 from RAMSES irradiance measurements during down- and upcast. Colour map of euphotic depths based on the upcasts only. Lower left panel shows the setup of the RAMSES and ACS on the topAWI/Triaxus towing platform. Middle insert shows an example of the hyperspectral downwelling irradiance for one representative downcast profile.

Data management

The quality controlled optical and pigment sampled during this expedition and further processed to geophysical quantities will be archived, published and disseminated according to international standards by the World Data Center PANGAEA Data Publisher for Earth & Environmental Science (https://www.pangaea.de) within two years after the end of the cruise at the latest. By default, the CC-BY license will be applied.

This expedition was supported by the Helmholtz Research Programme “Changing Earth – Sustaining our Future” Topic 6, Subtopic 3 and additional funding by HGF/MARDATA to project “4D Phyto”.

In all publications based on this expedition, the **Grant-No. AWI_PS133/1_11** will be quoted and the following publication will be cited:

Alfred-Wegener-Institut Helmholtz-Zentrum für Polar- und Meeresforschung (2017) Polar Research and Supply Vessel POLARSTERN Operated by the Alfred-Wegener-Institute. Journal of large-scale research facilities, 3, A119. http://dx.doi.org/10.17815/jlsrf-3-163.

References

Álvarez E, Losa S, Bracher A, Thoms S, Völker C (2022) Phytoplankton Light Absorption Impacted by Photoprotective Carotenoids in a Global Ocean Spectrally-Resolved Biogeochemistry Model. Journal of Advances in Modeling Earth Systems, 14(11):e2022MS003126.

Bracher A (1999) Photoacclimation of phytoplankton in different biogeochemical provinces of the Southern Ocean and its significance for estimating primary production. Reports on Polar Research, 341:90p (Dissertation).

Bracher AU, Kroon BMA, Lucas MI (1999) Primary production, physiological state and composition of phytoplankton in the Atlantic sector of the Southern Ocean. Marine Ecology Progress Series, 190:1-16.

Bracher A, Vountas M, Dinter T, Burrows JP, Röttgers R, Peeken I (2009) Quantitative observation of cyanobacteria and diatoms from space using PhytoDOAS on SCIAMACHY data. Biogeosciences 6:751-764, https://doi.org/10.5194/bg-6-751-2009.

Bracher A, Xi H, Dinter T, Mangin A, Strass VH, von Appen W-J, Wiegmann S (2020) High resolution water column phytoplankton composition across the Atlantic Ocean from ship-towed vertical undulating radiometry. Frontiers in Marine Science, 7:235, https://doi.org/10.3389/fmars.2020.00235.

Cheah W, Soppa M A, Wiegmann S, Ossebaar S, Laglera L M, Strass V, Santos-Echeandia J, Hoppema M, Wolf-Gladrow D, Bracher A (2017) Importance of deep mixing and silicic acid in regulating phytoplankton biomass and community in the iron-limited Antarctic Polar Front region in summer. Deep Sea Research II, 138:74-85, http://dx.doi.org/10.1016/j.dsr2.2016.05.019.

Lefering I, Röttgers R, Utschig, McKee D (2017) Uncertainty budgets for liquid waveguide CDOM absorption measurements. Applied Optics, 56(22):6357, https://doi.org/10.1364/AO.56.006357.

Oelker J, Losa SN, Richter A, Bracher A (2022) TROPOMI-retrieved underwater light attenuation in three spectral regions in the ultraviolet to blue. Frontiers in Marine Science, 9:787992, https://doi.org/10.3389/fmars.2022.787992.

Roesler S, Barnard AH (2013) Optical proxy for phytoplankton biomass in the absence of photophysiology: Rethinking the absorption line height, Methods in Oceanography, 7:79-94.

Röttgers R, Doxaran D, Dupouy C (2016) Quantitative filter technique measurements of spectral light absorption by aquatic particles using a portable integrating cavity absorption meter (QFT-ICAM). Opt. Express, 24(2):A1-A20.

Soppa M, Dinter T, Taylor B, Bracher A (2013) Satellite derived euphotic depth in the Southern Ocean: Implications for primary production modeling. Remote Sensing of Environment, 137:198-211, https://doi.org/10.1016/j.rse.2013.06.017.

Soppa M A, Hirata T, Silva B, Dinter T, Peeken I, Wiegmann S, Bracher A (2014) Global retrieval of diatoms abundance based on phytoplankton pigments and satellite. Remote Sensing, 6:10089-10106.

Soppa MA, Völker C, Bracher A (2016) Diatom Phenology in the Southern Ocean: Mean Patterns, Trends and the Role of Climate Oscillations. Remote Sensing, 8: 420, https://doi.org/10.3390/rs8050420.

Taylor BB, Torrecilla E, Bernhardt A, Taylor MH, Peeken I, Röttgers R, Piera J, Bracher A (2011) Bio-optical provinces in the eastern Atlantic Ocean. Biogeosciences 8:3609-3629. https://doi.org/10.5194/bg-8-3609-2011.

Tilstone G, Dall'Olmo G, Hieronymi M, Ruddick K, Beck M, Ligi M, Costa M, D'Alimonte D, Vellucci V, Vansteenwegen D, Bracher A, Wiegmann S, Kuusk J, Vabson V, Ansko I, Vendt R, Donlon C, Casal T (2020) Field intercomparison of radiometer measurements for ocean colour validation. Remote Sensing, 12(10):1587, https://doi.org/10.3390/rs12101587.

Xi H, Losa SN, Mangin A, Garnesson P, Bretagnon M, Demaria J, Soppa MA, d'Andon OHF, Bracher A (2021) Global chlorophyll a concentrations of phytoplankton functional types with detailed uncertainty assessment using multi-sensor ocean color and sea surface temperature satellite products. Journal Geoph. Res.-Oceans, 126 e2020JC017127, .

Xi H, Bretagnon M, Losa S, Brotas V, Gomes M, Peeken I, Mangin A, Bracher A (submitted 31 Jul 2022, under revision) Two-decade satellite monitoring of surface phytoplankton functional types in the Atlantic Ocean. Report: 7th edition of the Copernicus Marine Service Ocean State Report (OSR 7). State of the Planet. SP-2022-6.

15. SEDIMENT BIOGEOCHEMISTRY

Ronnie N. Glud[1], Anni Glud[1], Axel Nordhausen[2];
Frank Wenzhöfer[1, 3]

[1]DK.SDU
[2]DE.MPIMM
[3]DE.AWI

Grant-No. AWI_PS133/1_10

Outline

The amount of organic material that escapes mineralization and is retained in the sediment record is the single most important factor determining the long-term O_2 levels of the global ocean. Today we generally have a relatively good understanding of the processes that contribute to the mineralization of organic material and factors regulating the burial efficiency of organic material of most oceanic environments. However, hadal trenches are largely unexplored but appear to be quantitatively important depocenters with unique deposition dynamics. Their biogeochemical function cannot be understood by extrapolating findings from shallower settings. The Atlantic sector of the Southern Ocean, including the South Sandwich Trench, encompasses some of the most productive marine regions and is characterized by an efficient biological pump carrying large quantities of organic carbon to deep-sea sediments. We hypothesize that the trench system acts as a regionally important site for deposition and sequestration of organic carbon but might at the same time host unique benthic microbial communities flourishing under these extreme hydrostatic pressure and low temperature. We thus want to quantify the carbon mineralization efficiency of bathyal, abyssal and hadal sediments in the Southern Ocean, identify the key players for the processing and compare rates and communities with other deep-sea and trench ecosystems around the world.

Objectives

The proposed work targeted stations with variable surface production covering a depth range from 2.0 to 8.2 km in the Southern Polar Ocean and South Sandwich Trench system. The specific research aims included:

1. Quantification of the pelagic export and benthic mineralization of organic carbon: Using state-of-the-art lander technology, we will measure the *in-situ* benthic oxygen consumption rates within and around the South Sandwich Trench. The data will provide a unique assessment of the regional benthic carbon mineralization rate and fill data gaps in the current global data base. The involved diagenetic pathways will be quantified from onboard i) porewater profiles of nutrients and Dissolved Inorganic Carbon (DIC), ii) the distribution of solid-state iron and manganese and iii) measurements of denitrification, anammox and sulphate reduction. The site-specific turn-over rates will be linked to the pelagic productivity as derived from remote sensing and to sedimentation rates as derived from the distribution of natural radio nuclides (Wenzhöfer and Glud 2002; Glud et al., 2021; Oguri et al., 2022; Jørgensen et al., 2022). Thereby we will assess the quantitative link between surface production and underlying benthic activity, and evaluate the potential importance of horizontal transport of organic material in the complex benthic seascape of the region.

2. Characterization of the quantity and quality of deposited organic material: Recovered sediment cores will be used to assess the source, quantity and quality of organic material deposited at the respective sites. Beside basic quantification of total organic carbon (TOC), the analyses will include detailed pyrolysis for assessing lability, stable isotopes ($\delta^{13}C$, ^{15}N signatures), phytodetrital pigments and specific biomarker investigations using procedures that we previously have applied in other marine and hadal settings.

3. Explore benthic communities (from viruses to the meiofaunal communities) in relation to ocean depth, food supply, and biogeochemical function – we will analyze the benthic community structures through next-generation sequencing (metagenomics and amplicom sequencing). Organisms will be extracted from recovered cores applying well-established procedures used in other deep sea and hadal settings (e.g., Thamdrup et al., 2021; Schauberger et al., 2021). The resolved community structures will be linked to the zonation of the respective diagenetic pathways to explore succession and evolution of key players involved in benthic mineralization at the respective site.

4. Generic understanding of the biogeochemical function and community composition in hadal settings: The proposed study is essential for understanding carbon cycling, pelagic-benthic coupling, and benthic community structures in this very important region of the Southern Ocean. However, the work should also be seen in the context of a wider ambition of exploring life and biogeochemical function of the global hadal realm. The proposed work in the productive region of the South Sandwich Trench system will complement previous and ongoing investigations in other hadal systems. The combined data will provide generic insights on the biogeochemical function and life in hadal trench systems underlying different productivity regimes (e.g., Glud et al., 2021). The analysis on community structures will explore the extent by which trench systems act as isolated biogeographic habitats dominated by unique co-evolving communities adapted to the extreme environments or if they are interconnected.

Work at sea

We addressed ecosystem functions such as benthic respiration, remineralization and matter transport, microbial and meiofauna biodiversity in the South Sandwich Trench and adjacent abyssal and bathyal sediments of the Southern Ocean. During the cruise, we investigated 2 trench sites (> 6,000 m) and 3 sites at a depth ranging from 6,000 to 3,000 m. The main focus was on *in-situ* benthic flux rate measurements and sediment sampling. Measurements will add to the existing scarce data base of deep sea and hadal data. We planned to perform *in-situ* measurements using a new Hadal-benthic Flux Lander (11,000 m) to study benthic oxygen uptake and fluxes of other solutes at the sediment water interface (Wenzhöfer & Glud, 2002; Glud et al., 2013). The Lander was equipped with two benthic chambers and a 2-axis microprofiler. The benthic chambers are used to measure total exchange rates of the sediment integrating all relevant solute transport processes (diffusion, advection and fauna-mediated transport) and an area of 400 cm^2. During the deployment an oxygen optode measures changes in the oxygen concentration of the enclosed overlying water (total oxygen uptake, TOU) and 7 syringes take water samples at pre-programmed time intervals for analyses of DIC and nutrients. In addition, a novel Lab-on-a-Chip (LOC) system was used to continuously follow DIC exchange rates during chamber incubations. Furthermore, the enclosed sediments are retrieved and sampled on board for additional analysis and the abundance of macrofauna. The X-Y microprofiler was used to perform multiple vertical oxygen profiles across the sediment-water interface. It is equipped with up to 9 O_2 electrodes, 1 conductivity sensor and 1 temperature sensor capable to perform multiple vertical sets of concentration profiles along a horizontal distance of 50 cm.

Measurements across the water-sediment interface and within the upper sediment layer are performed with a vertical resolution of 100 µm and extending over a total length of 15-25 cm. The X-Y microprofiler will be used to quantify the diffusive oxygen uptake (DOU), which is generally assigned to microbial respiration.

A multiple corer (MUC) was used to retrieve intact sediment cores. The sediments were sectioned (1 cm slices to 10 cm, then in 2.5 cm slices to the bottom of the core), and the respective sediment horizons preserved for analyses in the home laboratory. Onboard measurements included laboratory based (micro-)profiles of O_2 and ammonia as well as process rates of anammox, denitrification and sulphate reduction. The list of analyses is provided below.

- Vertical abundance of microbes and viruses
- Vertical community structures of Nematodes, Microbes and Virus
- Porewater profiles of NH_4^+, NO_3^-, Fe, Mn, SO_4^{2}+, DIC
- Solid state profiles of Fe and Mn
- Sediment porosity, density and grain size
- Sediment accumulation – natural ^{210}Pb
- Amount and quality of deposited organic carbon
- Trace metals, pigments, biomarkers and stable C & N isotopes
- Persistent Organic Pollutants (POP) and nano plastics
- Anammox and denitrification rates by ^{15}N slurry experiments
- Sulphate reduction rates

Preliminary results

In situ work:

After several attempts, because of a medical emergency requiring an urgent transfer to the Falkland Islands, we had to abort the recovery of our lander system at station PS133/1-6 (Table 15.1). Therefore, no *in-situ* data could be collected during this expedition. We hope that the instrument is still positioned at the seabed where it could be recovered during a later visit to the site.

Tab. 15.1: Lander deployments

Station No	Station	Event Time	Latitude	Longitude	Depth (m)
PS133/1_6-1	Process	21.10.22 23:33	52° 16,693‘ S	025° 02,290‘ W	3,814

Laboratory work:

The visit to Falklands Islands and bad weather during the beginning of the voyage markedly reduced the number of benthic stations that could be sampled. However, sediment was recovered from 5 sites: 3 abyssal and 2 hadal stations (Table 15.3). The targeted sites are underlying areas with large differences in surface production regimes. This was evident from basic geochemical observation and onboard measurements of oxygen and ammonia profiles. Sites underlying productive provinces exhibited high benthic mineralization rates, while sediment recovered from oligotrophic settings were characterized by deep O_2 penetration and low ammonia concentrations. The hadal sediment was of particular interest and especially site PS133/1_17**,** exhibited massive retention of organic material and intense anaerobic mineralization at a water depth of almost 8 km. The site exhibited much higher benthic activity than the shallower abyssal sites. These preliminary observations support our original hypothesis that

the trench is a regionally important depocenter for organic material (and potentially for trace metals and pollutants). A depocenter characterized by extremely high carbon sequestration rates but also by high benthic mineralization rates that presumably is mediated by specialized microbial communities adapted to the extreme conditions at the trench bottom.

Tab. 15.2: MUC deployments

Station No.	Station	Event Time	Latitude	Longitude	Depth (m)
PS133/1_3-21	Process	15.10.22 01:45	49° 04,416' S	009° 59,165' W	3421
PS133/1_9-22	Process	03.11.22 17:46	51° 18,070' S	039° 55,520' W	3795
PS133/1_15-1	Meteor Deep	07.11.22 10:56	55° 13,874' S	026° 10,264' W	8200
PS133/1_15-5	Meteor Deep	07.11.22 21:22	55° 13,793' S	026° 11,089' W	8200
PS133/1_16-1	Reference	08.11.22 10:15	55° 48,050' S	024° 50,343' W	5700
PS133/1_17-1	Site 1b	08.11.22 23:13	56° 14,379' S	024° 56,740' W	7800
PS133/1_17-2	Site 1b	09.11.22 04:52	56° 14,434' S	024° 56,680' W	7800

Data management

Environmental data will be archived, published and disseminated according to international standards by the World Data Center PANGAEA Data Publisher for Earth & Environmental Science (https://www.pangaea.de) within two years after the end of the cruise at the latest. By default, the CC-BY license will be applied.

Molecular data (DNA and RNA data) will be archived, published and disseminated within one of the repositories of the International Nucleotide Sequence Data Collaboration (INSDC, www.insdc.org) comprising of EMBL-EBI/ENA, GenBank and DDBJ).

Any other data will be submitted to an appropriate long-term archive that provides unique and stable identifiers for the datasets and allows open online access to the data.

This expedition was supported by the Helmholtz Research Programme "Changing Earth – Sustaining our Future" Topic 6, Subtopic 3 and the Center of Excellence; "Danish Center for Hadal Research – HADAL".

In all publications based on this expedition, the **Grant No. AWI_PS133/1_10** will be quoted and the following publication will be cited:

Alfred-Wegener-Institut Helmholtz-Zentrum für Polar- und Meeresforschung (2017) Polar Research and Supply Vessel POLARSTERN Operated by the Alfred-Wegener-Institute. Journal of large-scale research facilities, 3, A119. http://dx.doi.org/10.17815/jlsrf-3-163.

References

Glud RN, Berg P, Thamdrup B, Larsen M, Stewart HA, Jamieson AJ, Glud A, Oguri K, Sanei H, Rowden AA, Wenzhöfer F (2021) Hadal trenches are dynamic hotspots for early diagenesis in the deep-sea. Commun Earth Environ, 2:21; https://doi.org/10.1038/s43247-020-00087-2.

Glud RN, Wenzhöfer F, Middelboe M, Oguri K Turnewitsch R, Canfield DE, Kitazato H (2013) High rates of benthic microbial activity at 10.900 meters depth: Results from the Challenger Deep (Mariana Trench), Nature Geoscience, 6:284–288, https://doi.org/10.1038/NGEO1773.

Jørgensen BB, Wenzhöfer F, Egger M, Glud RN (2022) Sediment oxygen consumption: Role in the global marine carbon cycle. Earth-Science Reviews, 228:103987 https://doi.org/10.1016/j.

earscirev.2022.103987.

Oguri K, Masque P, Zabel M, Stewart HA, McKinnon G, Rowden AA, Wenzhöfer F, Glud RN (2022) Sediment accumulation and carbon burial in four hadal Trench systems. Journal of Geophysical Research: Biogeosciences, 127:e2022JG006814. https://doi.org/10.1029/2022JG006814

Thamdrup B, Schauberger C, Larsen M, Trouche B, Maignien L, Arnaud-Haond S, Wenzhöfer F, Glud RN (2021) Anammox bacteria drive fixed nitrogen loss in hadal trench sediments. PNAS, 118:e2104529118.

Schauberger C, Glud RN, Hausmann B, Trouche B, Maignien L, Poulain J, Winker P, Arnoud-Haond S, Wenzhöfer F, Thamdrup B (2021) Microbial community structure in hadal sediments: High similarity along trench axes and strong changes along redox gradients. ISME Journal, 15:3455–3467

Wenzhöfer F, Glud RN (2002) Benthic carbon mineralization in the Atlantic: A synthesis based on *in situ* data from the last decade. Deep-Sea Research I, 49(7):1255–1279

Wenzhöfer F, Oguri K, Middelboe M, Turnewitsch R, Toyofuku T, Kitazato H, Glud RN (2016) Benthic carbon mineralization in hadal trenches: Assessment by *in situ* O2 microprofile measurements. Deep Sea Res I, 116:276–286

APPENDIX

A.1 TEILNEHMENDE INSTITUTE / PARTICIPATING INSTITUTES

A.2 FAHRTTEILNEHMER:INNEN / CRUISE PARTICIPANTS

A.3 SCHIFFSBESATZUNG / SHIP'S CREW

A.4 STATIONSLISTE / STATION LIST

A.1 TEILNEHMENDE INSTITUTE / PARTICIPATING INSTITUTES

Affiliation	Address
AR.ARA	Armada Argentina Comodoro Py 2055 1104 Buenos Aires Argentina
AR.IAA	Instituto Antártico Argentino 25 de Mayo 1143 San Martín Provincia de Buenos Aires Argentina
AR.CADIC	Centro Austral de Investigaciones Cientificas Bernardo Houssay 200 9410 Ushuaia Argentina
BR.UERJ	Universidade do Estado do Rio de Janeiro R. São Francisco Xavier 524 – Campus Maracanã sala 4008 bloco E 20550-900 Rio de Janeiro Brazil
BR.UFRG	Universidade Federal do Rio Grande Av. Itália, Km 8 LEOC 96203900 Rio Grande Brazil
CA.DAL	Dalhousie University 1355 Oxford Street PO Box 15000 B3H 4R2 Halifax Canada
CA.OFI	Ocean Frontier Institute Steele Ocean Sciences Building 1355 Oxford Street Halifax, NS B3H 3Z1 Canada

Affiliation	Address
CA.UBC	University of British Columbia 2020 – 2207 Main Mall V6T 1Z4 Vancouver Canada
DE.AWI	Alfred-Wegener-Institut Helmholtz-Zentrum für Polar- und Meeresforschung Postfach 120161 27515 Bremerhaven Germany
DE.DWD	Deutscher Wetterdienst Seewetteramt Bernhard Nocht Str. 76 20359 Hamburg Germany
DE.GEOMAR	GEOMAR Helmholtz-Zentrum für Ozeanforschung Wischhofstraße 1-3 24148 Kiel Germany
DE.IOW	Leibnitz-Institut für Ostseeforschung Seestraße 15 18119 Rostock-Warnemünde Germany
DE.MARUM	MARUM - Zentrum für Marine Umweltwissenschaften der Universität Bremen Leobener Str. 8 28359 Bremen Germany
DE.MPIMM	Max Planck Institute for Marine Microbiology Celsiusstraße 1 28359 Bremen Germany
DE.NHC	Northern HeliCopter GmbH Gorch-Fock-Straße 103 26721 Emden Germany
DE.TU_Braunschweig	Technische Universität Braunschweig Langer Kamp 19 C Raum 303 C 38106 Braunschweig Germany
DE.Uni_Hamburg	Universität Hamburg Mittelweg 177 20148 Hamburg Germany

Affiliation	Address
DE.Uni_Köln	Universität Köln Zülpicher Strasse 49 b 50764 Köln Germany
DK.SDU	University of Southern Denmark Campusvej 55 5230 Odense Denmark
DK.DTU	Technical University of Denmark National Institute of Aquatic Resources Kemitorvet Building 202 2800 Kgs. Lyngby Denmark
US.Caltech	California Institute of Technology 1200 East California Boulevard 91125 Pasadena CA United States
US.ODU	Old Dominion University 4600 Hampton Boulevard OCNPS 423 VA 23529 Norfolk United States
US.Princeton	Atmospheric and Oceanic Sciences Program Princeton University 300 Forrestal Road, Sayre Hall Princeton, NJ 08540 United States
US.UCD	University of California San Diego Scripps Institution of Oceanography 9500 Gilman Drive 92093 La Jolla CA United States
US.WHO	Woods Hole Oceanographic Institution 266 Woods Hole Road Woods Hole MA 02543-1050 USA

A.2 FAHRTTEILNEHMER:INNEN / CRUISE PARTICIPANTS

Name/ Last name	Vorname/ First name	Institut/ Institute	Beruf/ Profession	Fachrichtung/ Discipline
Asiedu	Delove	DK.DTU	PhD student	Oceanography
Avelina	Raquel	BR.UERJ	PhD student	Oceanography
Bahl	Alexis	CA.UBC	PhD student	Oceanography
Becker	Hauke	DE.AWI	Engineer	Oceanography
Bolduan	Jonas	DK.DTU	Master student	Oceanography
Bracher	Astrid	DE.AWI	Scientist	Oceanography
Bussmann	Frederik	DE.GEOMAR	Student	Chemistry
Cotrim da Cunha	Leticia	BR.UERJ	Scientist	Chemistry
Dutz	Jörg	DE.IOW	Scientist	Biology
Ebner	Berenice	DE.AWI	PhD student	Geology
Eckardt	Lorenz	DE.AWI	Technician	Biology
Gischler	Michael	DE.NHC	Pilot	Helicopter service
Glud	Anni	DK.SDU	Technician	Biology
Glud	Ronnie	DK.SDU	Scientist	Oceanography
Hölemann	Anna	DE.Uni_Hamburg	Student	Oceanography
Hölemann	Jens	DE.AWI	Scientist	Oceanography
Hübner	Joshua	DE.AWI	Student	Chemistry
Iachetti	Clara	AR.CADIC	Scientist	Biology
Iversen	Morten	DE.AWI	Scientist	Biology
Klaas	Christine	DE.AWI	Scientist	Biology
Konrad	Christian	DE.AWI	Engineer	Biology
Kraberg	Alexandra	DE.AWI	Scientist	Biology
Ludwichowski	Kai-Uwe	DE.AWI	Engineer	Chemistry
Lüskow	Florian	CA.UBC	PhD student	Biology
Marchant	Hannah	DE.MARUM	Scientist	Biogeochemistry
Marques Orselli	Iole Beatriz	BR.UFRG	Scientist	Oceanography
McQuaid	Jeff	US.UCSD	Scientist	Biology
Mole	Ryan	DE.AWI	PhD student	Oceanography

Name/ Last name	Vorname/ First name	Institut/ Institute	Beruf/ Profession	Fachrichtung/ Discipline
Nordhausen	Axel	DE.MPIMM	Technician	Engineering
Oetjens	Annika	DE.Uni_Heidelberg	Student	Physics
Otte	Frank	DE.DWD	Scientist	Meteorology
Pakhomov	Evgeny	CA.UBC	Scientist	Biology
Pakhomova	Larysa	CA.UBC	Technician	Oceanography
Panter	Gabriel	DE.DRF	Technician	Helicopter service
Pattison	Larissa	CA.DAL	Technician	Biology
Perez-Rodriguez	Marta	DE.TU_Braunschweig	Scientist	Geochemistry
Rokitta	Sebastian	DE.AWI	Scientist	Biology
Rolandi	Nadia	AR.ARA	Public outreach	Armada Argentina
Rössler	Leonard	DE.MPIMM	Student	Biology
Schaubensteiner	Stefan	DE.NHC	Pilot	Helicopter service
Spahic	Susanne	DE.AWI	Technician	Biology
Stimac	Ingrid	DE.AWI	Technician	Chemistry
Stimpfle	Jasmin	DE.AWI	PhD student	Biology
Stöckle	Sonja	DE.DWD	Scientist	Meteorology
Terbrüggen	Anja	DE.AWI	Engineer	Biology
Trimborn	Scarlett	DE.AWI	Scientist	Biology
Völkner	Christian	DE.AWI	Engineer	Biology
von Appen	Wilken-Jon	DE.AWI	Scientist	Oceanography
Wenzhöffer	Frank	DE.AWI	Scientist	Biology
Wolf-Gladrow	Dieter	DE.AWI	Scientist	Physics
Woll	Matthias	DE.AWI	Engineer	Chemistry
Zeising	Moritz	DE.AWI	PhD student	Oceanography

A.3 SCHIFFSBESATZUNG / SHIP'S CREW

No.	Nachname	Name	Position
1	Schwarze	Stefan	Master
2	Kentges	Felix	Chief Mate
3	Grafe	Jens	Chief
4	Falk	Stefan	2nd Mate
5	Hering	Igor	2nd Mate
6	Lange	Felix	3rd Mate
7	Müller	Andreas	Comm Offc.
8	Gößmann-Lange	Petra	Ships doc
9	Beyer	Mario	2nd Eng.
10	Brose	Thomas Christian	2nd Eng.
11	Haack	Michael Detlev	2nd Eng.
12	Redmer	Jens Dirk	E-Eng
13	Hüttebräucker	Olaf	ELO
14	Jäger	Vladimir	ELO
15	Kliemann	Olaf	ELO
16	Nasis	Ilias	ELO
17	Sedlak	Andreas Enrico	Bosun
18	Neisner	Winfried	Carpent.
19	Denzer	Florian	MP Rat.
20	Frerichs	Nils	MP Rat.
21	Grünberg	Niklas	MP Rat.
22	Jassmann	Marvin	MP Rat.
23	Klee	Philip	MP Rat.
24	Meier	Jan	MP Rat.
25	Bäcker	Andreas	AB
26	Burzan	Gerd-Ekkehard	AB
27	Wende	Uwe	AB
28	Preußner	Jörg	Storek
30	Claasen	Thies	MP Rat.
30	Hänert	Ove	MP Rat.
31	Klinger	Dana Maria	MP Rat.
32	Rhau	Lars-Peter	MP Rat.
33	Schwarz	Uwe	MP Rat.
34	Matter	Sebastian	Cook

No.	Nachname	Name	Position
35	Hammelsmann	Louisa	Cooksm.
36	Silinski	Frank	Cooksm.
37	Pieper	Daniel	Chief Stew.
38	Prummer	Leon	Nurse
39	Arendt	René	2nd. Stew.
40	Chen	Dansheng	2nd. Stew.
41	Krause	Tomasz	2nd. Stew.
42	Silinski	Carmen	2nd. Stew.
43	Sun	Yong Shen	Laundrym.

A.4 STATIONSLISTE / STATION LIST PS133/1

Station list of expedition PS133/1 from Bremerhaven to Cape Town;
the list details the action log for all stations along the cruise track.

See https://www.pangaea.de/expeditions/events/PS133/1 to display the station (event) list for expedition PS133/1.
This version contains Uniform Resource Identifiers for all sensors listed under https://sensor.awi.de. See https://www.awi.de/en/about-us/service/computing-centre/data-flow-framework.html for further information about AWI's data flow framework from sensor observations to

Event label	Optional label	Date/Time	Latitude	Longitude	Depth [m]	Gear	Action	Comment
PS133/1-track		2022-10-02T00:00:00	-33.90680	18.43370		CT	Station start	Cape Town – Punta Arenas
PS133/1-track		2022-11-17T00:00:00	-53.14470	-70.90910		CT	Station end	Cape Town – Punta Arenas
PS133/1_0_Underway-28		2022-10-02T13:50:13	-33.90963	18.43567		SWEAS	Station start	
PS133/1_0_Underway-28		2022-11-16T11:31:51	-52.88668	-66.75408		SWEAS	Station end	
PS133/1_0_ Underway-24_1		2022-10-03T08:52:33	-35.21783	15.94484	4445.6	TSG	Station start	TSK2, PS133/1_0_ Underway-24
PS133/1_0_ Underway-24_1		2022-10-27T17:46:04	-51.64053	-57.34016	168.0	TSG	Station end	TSK2, PS133/1_0_ Underway-24
PS133/1_0_ Underway-23_1		2022-10-03T09:55:22	-35.31870	15.77040	4540.3	TSG	Station start	TSK1, PS133/1_0_ Underway-23
PS133/1_0_ Underway-23_1		2022-10-27T17:45:32	-51.64054	-57.33908	169.0	TSG	Station end	TSK1, PS133/1_0_ Underway-23
PS133/1_0_ Underway-22_1		2022-10-03T13:59:21	-35.70582	15.10018	4725.4	SNDVELPR	Station start	PS133/1_0_Underway-22
PS133/1_0_ Underway-22_1		2022-10-27T17:45:23	-51.64054	-57.33873	170.0	SNDVELPR	Station end	PS133/1_0_Underway-22
PS133/1_0_ Underway-1_1		2022-10-04T06:46:01	-37.19820	12.41767	3097.6	ADCP	Station start	PS133/1_0_Underway-1

** Comments are limited to 130 characters. See https://www.pangaea.de/expeditions/events/PS133/1 to show full comments in conjunction with the station (event) list for expedition PS133/1*

Event label	Optional label	Date/Time	Latitude	Longitude	Depth [m]	Gear	Action	Comment
PS133/1_0_ Underway-1_1		2022-10-27T17:45:13	-51.64054	-57.33841	170.0	ADCP	Station end	PS133/1_0_Underway-1
PS133/1_0_ Underway-14_1		2022-10-04T07:48:24	-37.29257	12.24550	4970.0	NEUMON	Station start	PS133/1_0_Underway-14
PS133/1_0_ Underway-14_1		2022-10-27T17:45:03	-51.64054	-57.33806	170.0	NEUMON	Station end	PS133/1_0_Underway-14
PS133/1_0_ Underway-6_1		2022-10-04T07:51:36	-37.29732	12.23685	4985.1	MYON	Station start	PS133/1_0_Underway-6
PS133/1_0_ Underway-6_1		2022-10-27T17:44:51	-51.64055	-57.33765	170.0	MYON	Station end	PS133/1_0_Underway-6
PS133/1_0_Underway-29		2022-10-04T09:30:10	-37.35716	12.11872	3712.8	CTD-RO	Station start	Deployment depth: 2000 m
PS133/1_0_Underway-29		2022-10-04T10:18:55	-37.35727	12.12012	5015.7	CTD-RO	Station end	Deployment depth: 2000 m
PS133/1_0_ Underway-17_1		2022-10-05T08:03:04	-39.36921	8.40455	5324.6	pCO2	Station start	PS133/1_0_Underway-17
PS133/1_0_ Underway-17_1		2022-10-27T17:44:05	-51.64059	-57.33604	169.0	pCO2	Station end	PS133/1_0_Underway-17
PS133/1_0_ Underway-7_1		2022-10-05T08:03:48	-39.37031	8.40268	5319.7	FBOX	Station start	PS133/1_0_Underway-7
PS133/1_0_ Underway-7_1		2022-10-27T17:43:51	-51.64060	-57.33552	169.0	FBOX	Station end	PS133/1_0_Underway-7
PS133/1_0_ Underway-18_1		2022-10-05T08:06:33	-39.37421	8.39543	5291.0	pCO2	Station start	PS133/1_0_Underway-18
PS133/1_0_ Underway-18_1		2022-10-27T17:43:29	-51.64062	-57.33476	170.0	pCO2	Station end	PS133/1_0_Underway-18
PS133/1_0_clean_2_ Test1		2022-10-08T10:05:00	-45.80840	-4.29740	3762.2	CTD-TM	Station start	Deployment depth: 50 m
PS133/1_0_clean_2_ Test1		2022-10-08T11:18:18	-45.81132	-4.29429	3745.2	CTD-TM	Station end	Deployment depth: 50 m
PS133/1_0_clean_2_ Test2		2022-10-08T13:48:00	-45.93680	-4.55570	3745.2	CTD-TM	Station start	Deployment depth: 1000 m

Event label	Optional label	Date/Time	Latitude	Longitude	Depth [m]	Gear	Action	Comment
PS133/1_0_clean_2_Test2		2022-10-08T14:39:40	-45.94249	-4.54152	3518.3	CTD-TM	Station end	Deployment depth: 1000 m
PS133/1_1-2		2022-10-11T13:18:09	-43.62963	-11.66491	4583.9	HN	Station start	Deployment depth: 20 m
PS133/1_1-2		2022-10-11T13:34:27	-43.62963	-11.66482		HN	Station end	Deployment depth: 20 m
PS133/1_1-1		2022-10-11T13:40:42	-43.63001	-11.66500	5887.9	CTD-TM	Station start	Deployment depth: 52 m
PS133/1_1-1		2022-10-11T14:07:29	-43.63186	-11.66436	4053.3	CTD-TM	Station end	Deployment depth: 52 m
PS133/1_1-3		2022-10-11T14:19:27	-43.63288	-11.66412	4052.7	TOPR	Station start	Deployment depth: 300 m
PS133/1_1-3		2022-10-11T15:50:19	-43.68464	-11.81587	4119.2	TOPR	Station end	Deployment depth: 300 m
PS133/1_2-1		2022-10-13T11:45:45	-48.23083	-10.57756	2546.3	CTD-UW	Station start	CTD-UW lost, deployment depth: 200 m
PS133/1_2-1		2022-10-13T15:10:48	-48.73953	-10.22451	2476.2	CTD-UW	Station end	CTD-UW lost, deployment depth: 200 m
PS133/1_3-1		2022-10-13T17:37:33	-49.07653	-9.98339	3439.1	DF	Station start	Deployment, deployment depth: 435 m
PS133/1_3-1		2022-10-13T18:49:47	-49.07139	-9.97872	3307.4	DF	Station end	Deployment, deployment depth: 435 m
PS133/1_3-2		2022-10-13T18:53:48	-49.07124	-9.97732			Station start	Deployment cancelled
PS133/1_3-2		2022-10-13T19:50:34	-49.06450	-9.99277	3278.0		Station end	Deployment cancelled
PS133/1_3-4		2022-10-13T20:23:48	-49.06439	-9.99405	3275.6	HN	Station start	Deployment depth: 20 m
PS133/1_3-4		2022-10-13T20:31:22	-49.06454	-9.99413	3273.4	HN	Station end	Deployment depth: 20 m
PS133/1_3-3		2022-10-13T21:33:29	-49.06475	-9.99203	3280.3	CTD-RO	Station start	Deployment depth: 3240 m
PS133/1_3-3		2022-10-13T23:03:03	-49.06610	-49.06610	3280.3	CTD-RO	Station end	Deployment depth: 3240 m
PS133/1_3-5		2022-10-13T23:15:50	-49.06639	-9.99273	3271.5	MSN	Station start	MN55, deployment depth: 600 m
PS133/1_3-5		2022-10-14T00:38:27	-49.06740	-9.99093	3279.9	MSN	Station end	MN55, deployment depth: 600 m
PS133/1_3-6		2022-10-14T00:40:18	-49.06710	-9.99052	3281.6	MSN	Station start	MN200, deployment depth: 600 m

Event label	Optional label	Date/Time	Latitude	Longitude	Depth [m]	Gear	Action	Comment
PS133/1_3-6		2022-10-14T01:35:45	-49.06640	-9.98988	3286.2	MSN	Station end	MN200, deployment depth: 600 m
PS133/1_3-7		2022-10-14T01:39:54	-49.06650	-9.98977	3286.7	RN	Station start	Deployment depth: 20 m
PS133/1_3-7		2022-10-14T02:04:04	-49.06624	-9.98991	3287.3	RN	Station end	Deployment depth: 20 m
PS133/1_3-8		2022-10-14T02:08:27	-49.06622	-9.98987	3285.7	WP2	Station start	Deployment depth: 100 m
PS133/1_3-8		2022-10-14T02:23:49	-49.06670	-9.98934	3281.7	WP2	Station end	Deployment depth: 100 m
PS133/1_3-9		2022-10-14T02:26:30	-49.06692	-9.98928	3288.6	WP2	Station start	Deployment depth: 100 m
PS133/1_3-9		2022-10-14T02:38:34	-49.06727	-9.98894	3288.9	WP2	Station end	Deployment depth: 100 m
PS133/1_3-10		2022-10-14T02:45:00	-49.06752	-9.98880	3291.3	RMT	Station start	Deployment depth: 603 m
PS133/1_3-10		2022-10-14T04:17:49	-49.01856	-9.99262	3337.0	RMT	Station end	Deployment depth: 603 m
PS133/1_3-11		2022-10-14T04:30:47	-49.03442	-9.99058	3292.6	IKMT	Station start	Net broken, deployment depth: 200 m
PS133/1_3-11		2022-10-14T05:09:16	-49.00910	-9.98853	2911.7	IKMT	Station end	Net broken, deployment depth: 200 m
PS133/1_3-12		2022-10-14T05:41:25	-49.05091	-9.98635	3030.0	ROSINA	Station start	Deployment depth: 600 m
PS133/1_3-12		2022-10-14T07:05:14	-49.05162	-9.98624	3531.2	ROSINA	Station end	Deployment depth: 600 m
PS133/1_3-13		2022-10-14T07:38:14	-49.05814	-9.98150	3474.2	MSC	Station start	Deployment depth: 100 m
PS133/1_3-13		2022-10-14T08:06:23	-49.05825	-9.98065	3459.1	MSC	Station end	Deployment depth: 100 m
PS133/1_3-14		2022-10-14T08:18:30	-49.05880	-9.97945	3448.5	INSIPU	Station start	Deployment depth: 460 m
PS133/1_3-14		2022-10-14T12:17:54	-49.06028	-9.97900	3453.5	INSIPU	Station end	Deployment depth: 460 m
PS133/1_3-15		2022-10-14T13:28:17	-49.05790	-9.97903	3480.6	CTD-TM	Station start	Deployment depth: 300 m
PS133/1_3-15		2022-10-14T13:56:54	-49.05776	-9.97776	3480.6	CTD-TM	Station end	Deployment depth: 300 m
PS133/1_3-16		2022-10-14T14:08:36	-49.05821	-9.97764	3384.2	ACS-RAM	Station start	Deployment depth: 130 m
PS133/1_3-16		2022-10-14T14:45:27	-49.05705	-9.97930	3490.4	ACS-RAM	Station end	Deployment depth: 130 m
PS133/1_3-17		2022-10-14T14:46:18	-49.05697	-9.97938	3488.4	MSN	Station start	MN55, deployment depth: 600 m
PS133/1_3-17		2022-10-14T15:59:01	-49.05577	-9.97882	3495.6	MSN	Station end	MN55, deployment depth: 600 m

Event label	Optional label	Date/Time	Latitude	Longitude	Depth [m]	Gear	Action	Comment
PS133/1_3-18		2022-10-14T16:09:06	-49.05594	-9.97857	3490.9	MSN	Station start	MN200, deployment depth: 600 m
PS133/1_3-18		2022-10-14T17:00:44	-49.05633	-9.97883	3492.6	MSN	Station end	MN200, deployment depth: 600 m
PS133/1_3-19		2022-10-14T18:00:54	-48.99534	-9.85817	2948.4	DF	Station start	Recovery, deployment depth: 435 m
PS133/1_3-19		2022-10-14T19:02:51	-48.99441	-9.86069	2981.9	DF	Station end	Recovery, deployment depth: 435 m
PS133/1_3-20		2022-10-14T21:29:50	-49.07475	-9.98827	3289.4	CTD-TM	Station start	Deployment depth: 2500 m
PS133/1_3-20		2022-10-14T23:26:15	-49.07392	-9.98751	3384.4	CTD-TM	Station end	Deployment depth: 2500 m
PS133/1_3-21		2022-10-15T01:45:33	-49.07360	-9.98609	3420.5	TVMUC	Station start	Deployment depth: Bottom m
PS133/1_3-21		2022-10-15T03:40:20	-49.07309	-9.98076	3420.5	TVMUC	Station end	Deployment depth: Bottom m
PS133/1_4-1		2022-10-18T13:00:13	-50.90986	-24.41243	4684.6	TOPR	Station start	Deployment depth: 300 m
PS133/1_4-1		2022-10-20T16:31:48	-53.99826	-25.06852	4704.6	TOPR	Station end	Deployment depth: 300 m
PS133/1_5-1		2022-10-20T17:34:12	-53.99993	-24.99676	4702.5	CTD-TM	Station start	Deployment depth: 1000 m
PS133/1_5-1		2022-10-20T18:27:36	-53.99983	-24.99507	4703.0	CTD-TM	Station end	Deployment depth: 1000 m
PS133/1_5-3		2022-10-20T19:06:58	-54.00107	-24.99488	4702.7	HN	Station start	Deployment depth: 20 m
PS133/1_5-3		2022-10-20T19:13:36	-54.00095	-24.99505	4703.5	HN	Station end	Deployment depth: 20 m
PS133/1_5-2		2022-10-20T20:32:29	-54.00098	-24.99367	4703.3	CTD-RO	Station start	Aborted Station while hoisting at 800m depth, because of proplems with the CTD, water samples cannot be used., deployment depth: 4…

Event label	Optional label	Date/Time	Latitude	Longitude	Depth [m]	Gear	Action	Comment
PS133/1_5-2		2022-10-20T22:23:30	-54.00180	-24.99287	4700.5	CTD-RO	Station end	Aborted Station while hoisting at 800m depth, because of proplems with the CTD, water samples cannot be used., deployment depth: 4…
PS133/1_5-4		2022-10-20T22:30:23	-54.00212	-24.99249	4700.1	MSN	Station start	Deployment depth: 600 m
PS133/1_5-4		2022-10-20T23:40:12	-54.00316	-24.99301	4690.3	MSN	Station end	Deployment depth: 600 m
PS133/1_5-5		2022-10-20T23:41:08	-54.00317	-24.99298	4699.8	IKMT	Station start	Deployment depth: 200 m
PS133/1_5-5		2022-10-21T00:46:18	-53.99538	-25.03033	4704.6	IKMT	Station end	Deployment depth: 200 m
PS133/1_6-1		2022-10-21T23:33:16	-52.27822	-25.03816	3813.0	B_LANDER	Station start	Deployment, deployment depth: Bottom
PS133/1_6-1		2022-10-21T22:42:16	-52.27808	-25.03686	3813.5	B_LANDER	Station end	Deployment, deployment depth: Bottom
PS133/1_6-2		2022-10-22T00:12:36	-52.33100	-24.96773	4354.5	DF	Station start	Deployment, deployment depth: 435 m
PS133/1_6-2		2022-10-22T00:57:00	-52.33333	-24.95874	4038.3	DF	Station end	Deployment, deployment depth: 435 m
PS133/1_6-3		2022-10-22T02:01:02	-52.33047	-24.99119	4325.9	CTD-TM	Station start	Deployment depth: 1000 m
PS133/1_6-3		2022-10-22T02:50:18	-52.33036	-24.99520	4325.9	CTD-TM	Station end	Deployment depth: 1000 m
PS133/1_6-5		2022-10-22T03:00:58	-52.33067	-24.99503	3812.5	HN	Station start	Deployment depth: 20 m
PS133/1_6-5		2022-10-22T03:05:06	-52.33076	-24.99351	2968.9	HN	Station end	Deployment depth: 20 m
PS133/1_6-4		2022-10-22T04:35:46	-52.33144	-24.97884	4361.5	CTD-RO	Station start	Deployment depth: 4312 m
PS133/1_6-4		2022-10-22T06:42:36	-52.33215	-24.96773	4345.2	CTD-RO	Station end	Deployment depth: 4312 m
PS133/1_6-6		2022-10-22T06:58:50	-52.32935	-24.99411	4323.1	MSN	Station start	MN55, deployment depth: 600 m
PS133/1_6-6		2022-10-22T08:08:16	-52.32890	-24.98168	4354.2	MSN	Station end	MN55, deployment depth: 600 m
PS133/1_6-7		2022-10-22T08:22:15	-52.32765	-24.98856	4333.5	MSN	Station start	MN200, deployment depth: 600 m

Event label	Optional label	Date/Time	Latitude	Longitude	Depth [m]	Gear	Action	Comment
PS133/1_6-7		2022-10-22T09:24:02	-52.32895	-24.97514	4361.1	MSN	Station end	MN200, deployment depth: 600 m
PS133/1_6-8		2022-10-22T09:29:26	-52.32871	-24.97976	4359.0	RN	Station start	Deployment depth: 20 m
PS133/1_6-8		2022-10-22T09:42:33	-52.32876	-24.97635	4360.7	RN	Station end	Deployment depth: 20 m
PS133/1_6-9		2022-10-22T09:43:14	-52.32870	-24.97657	4361.1	WP2	Station start	WP2-400, deployment depth: 100 m
PS133/1_6-9		2022-10-22T10:12:35	-52.32754	-24.97571	4359.7	WP2	Station end	WP2-400, deployment depth: 100 m
PS133/1_6-10		2022-10-22T10:13:18	-52.32749	-24.97580	4360.5	WP2	Station start	WP2-100, deployment depth: 100 m
PS133/1_6-10		2022-10-22T10:35:39	-52.32626	-24.97182	4358.0	WP2	Station end	WP2-100, deployment depth: 100 m
PS133/1_6-11		2022-10-22T10:43:59	-52.32420	-24.97067	4361.8	RMT	Station start	Deployment depth: 620 m
PS133/1_6-11		2022-10-22T11:48:38	-52.30030	-25.00255	4144.0	RMT	Station end	Deployment depth: 620 m
PS133/1_6-12		2022-10-22T11:49:49	-52.29981	-25.00310	4121.3	IKMT	Station start	Deployment depth: 169 m
PS133/1_6-12		2022-10-22T12:30:54	-52.28813	-25.01596	4162.6	IKMT	Station end	Deployment depth: 169 m
PS133/1_6-13		2022-10-22T13:00:45	-52.33188	-24.99461	4323.5	ACS-RAM	Station start	Deployment depth: 130 m
PS133/1_6-13		2022-10-22T13:35:09	-52.33048	-24.98493	4344.0	ACS-RAM	Station end	Deployment depth: 130 m
PS133/1_6-14		2022-10-22T14:39:36	-52.32912	-24.95599	4317.5	CTD-TM	Station start	Deployment depth: 1000 m
PS133/1_6-14		2022-10-22T15:41:36	-52.32763	-24.93322	4317.5	CTD-TM	Station end	Deployment depth: 1000 m
PS133/1_6-15		2022-10-22T15:51:21	-52.32715	-24.92277	3963.5	INSIPU	Station start	Deployment depth: 410 m
PS133/1_6-15		2022-10-22T18:57:32	-52.32751	-24.88125	4435.5	INSIPU	Station end	Deployment depth: 410 m
PS133/1_6-16		2022-10-22T18:58:54	-52.32746	-24.88097	4460.8	MSN	Station start	MN55, deployment depth: 600 m
PS133/1_6-16		2022-10-22T20:17:34	-52.32552	-24.86006	4623.4	MSN	Station end	MN55, deployment depth: 600 m
PS133/1_6-17		2022-10-22T20:18:48	-52.32550	-24.85976	4623.1	MSN	Station start	MN200, deployment depth: 600 m
PS133/1_6-17		2022-10-22T21:35:27	-52.32349	-24.83986	4612.1	MSN	Station end	MN200, deployment depth: 600 m

Event label	Optional label	Date/Time	Latitude	Longitude	Depth [m]	Gear	Action	Comment
PS133/1_6-18		2022-10-22T21:40:45	-52.32238	-24.84013	4585.0	RMT	Station start	Deployment depth: 611 m
PS133/1_6-18		2022-10-22T23:03:20	-52.30219	-24.88441	4510.7	RMT	Station end	Deployment depth: 611 m
PS133/1_6-19		2022-10-22T23:03:47	-52.30208	-24.88460	4506.9	IKMT	Station start	Deployment depth: 160 m
PS133/1_6-19		2022-10-22T23:40:49	-52.29221	-24.89949	2827.2	IKMT	Station end	Deployment depth: 160 m
PS133/1_6-20		2022-10-23T01:42:00	-52.33609	-24.38257	2974.3	DF	Station start	Recovery, deployment depth: 435 m
PS133/1_6-20		2022-10-23T03:15:00	-52.34312	-24.35642	2968.5	DF	Station end	Recovery, deployment depth: 435 m
PS133/1_6-21		2022-10-23T03:15:51	-52.34317	-24.35638	2968.7	ROSINA	Station start	Cancelled, no communication with device
PS133/1_6-21		2022-10-23T03:48:36	-52.34494	-24.35027	2948.1	ROSINA	Station end	Cancelled, no communication with device
PS133/1_6-22		2022-10-23T08:08:11	-52.28134	-25.03642		B_LANDER	Station start	Recovery (failed), no communication with device, deployment depth: Bottom m
PS133/1_6-22		2022-10-23T11:40:47	-52.27924	-25.03503	3813.5	B_LANDER	Station end	Recovery (failed), no communication with device, deployment depth: Bottom m
PS133/1_6-23		2022-10-23T11:41:23	-52.27978	-25.03555		DRIFT	Station start	8 Drifters released, deployment depth: 0-15 m
PS133/1_6-23		2022-10-23T13:27:54	-52.27141	-25.45074	3879.2	DRIFT	Station end	8 Drifters released, deployment depth: 0-15 m
PS133/1_0_ Underway-18_2		2022-10-29T17:03:11	-51.57498	-57.37952	132.0	pCO2	Station start	PS133/1_0_Underway-18
PS133/1_0_ Underway-18_2		2022-11-16T11:28:25	-52.88892	-66.73605	98.5	pCO2	Station end	PS133/1_0_Underway-18
PS133/1_0_ Underway-7_2		2022-10-29T17:03:29	-51.57478	-57.37825	134.0	FBOX	Station start	PS133/1_0_Underway-7

Event label	Optional label	Date/Time	Latitude	Longitude	Depth [m]	Gear	Action	Comment
PS133/1_0_ Underway-7_2		2022-11-16T11:29:02	-52.88851	-66.73936	98.2	FBOX	Station end	PS133/1_0_Underway-7
PS133/1_0_ Underway-17_2		2022-10-29T17:03:43	-51.57462	-57.37727	134.0	pCO2	Station start	PS133/1_0_Underway-17
PS133/1_0_ Underway-17_2		2022-11-16T11:29:37	-52.88813	-66.74232	98.1	pCO2	Station end	PS133/1_0_Underway-17
PS133/1_0_ Underway-6_2		2022-10-29T17:03:57	-51.57448	-57.37621	134.0	MYON	Station start	PS133/1_0_Underway-6
PS133/1_0_ Underway-6_2		2022-11-16T11:30:07	-52.88779	-66.74501	98.1	MYON	Station end	PS133/1_0_Underway-6
PS133/1_0_ Underway-14_2		2022-10-29T17:04:07	-51.57439	-57.37557	134.0	NEUMON	Station start	PS133/1_0_Underway-14
PS133/1_0_ Underway-14_2		2022-11-16T11:30:16	-52.88769	-66.74580	98.3	NEUMON	Station end	PS133/1_0_Underway-14
PS133/1_0_ Underway-1_2		2022-10-29T17:04:16	-51.57431	-57.37493	135.0	ADCP	Station start	PS133/1_0_Underway-1
PS133/1_0_ Underway-1_2		2022-11-16T11:30:44	-52.88739	-66.74824	98.7	ADCP	Station end	PS133/1_0_Underway-1
PS133/1_0_ Underway-22_2		2022-10-29T17:04:31	-51.57419	-57.37386	134.0	SNDVELPR	Station start	PS133/1_0_Underway-22
PS133/1_0_ Underway-22_2		2022-11-16T11:31:10	-52.88711	-66.75051	98.7	SNDVELPR	Station end	PS133/1_0_Underway-22
PS133/1_0_ Underway-23_2		2022-10-29T17:04:43	-51.57411	-57.37299	134.0	TSG	Station start	TSK1, PS133/1_0_ Underway-23
PS133/1_0_ Underway-23_2		2022-11-16T11:31:29	-52.88691	-66.75217	98.2	TSG	Station end	TSK1, PS133/1_0_ Underway-23
PS133/1_0_ Underway-24_2		2022-10-29T17:04:57	-51.57401	-57.37198	135.0	TSG	Station start	TSK2, PS133/1_0_ Underway-24
PS133/1_0_ Underway-24_2		2022-11-16T11:31:51	-52.88668	-66.75408	98.6	TSG	Station end	TSK2, PS133/1_0_ Underway-24
PS133/1_7-2		2022-10-30T17:40:10	-51.23165	-52.23803	2074.0	HN	Station start	Deployment depth: 20 m

Event label	Optional label	Date/Time	Latitude	Longitude	Depth [m]	Gear	Action	Comment
PS133/1_7-2		2022-10-30T17:45:54	-51.23163	-52.23774	2075.1	HN	Station end	Deployment depth: 20 m
PS133/1_7-1		2022-10-30T18:51:54	-51.23163	-52.23562	2096.5	CTD-RO	Station start	Deployment depth: 2063 m
PS133/1_7-1		2022-10-30T20:12:04	-52.23419	-51.23107	2091.2	CTD-RO	Station end	Deployment depth: 2063 m
PS133/1_8-1		2022-11-01T16:18:45	-50.53406	-41.73291	1764.1	RMT	Station start	Deployment depth: 600 m
PS133/1_8-1		2022-11-01T17:29:45	-50.51989	-41.79933	1721.3	RMT	Station end	Deployment depth: 600 m
PS133/1_8-2		2022-11-01T17:30:45	-50.51979	-41.79918	1720.6	ACS-RAM	Station start	Deployment depth: 100 m
PS133/1_8-2		2022-11-01T18:10:41	-50.51948	-41.79692	1721.0	ACS-RAM	Station end	Deployment depth: 100 m
PS133/1_8-4		2022-11-01T18:22:54	-50.51939	-41.79632	1721.3	HN	Station start	Deployment depth: 20 m
PS133/1_8-4		2022-11-01T18:29:29	-50.51943	-41.79641	1721.3	HN	Station end	Deployment depth: 20 m
PS133/1_8-3		2022-11-01T18:56:34	-50.51913	-41.79635	1720.8	CTD-RO	Station start	Deployment depth: 1679 m
PS133/1_8-3		2022-11-01T12:06:22	-50.51805	-41.79613	1719.0	CTD-RO	Station end	Deployment depth: 1679 m
PS133/1_8-5		2022-11-01T20:44:41	-50.51911	-41.79391	1721.4	CTD-TM	Station start	Deployment depth: 1000 m
PS133/1_8-5		2022-11-01T21:24:12	-50.52017	-41.79384	1722.8	CTD-TM	Station end	Deployment depth: 1000 m
PS133/1_8-6		2022-11-01T21:30:04	-50.52039	-41.79385	1723.6	MSN	Station start	MN55, deployment depth: 600 m
PS133/1_8-6		2022-11-01T22:45:39	-50.51962	-41.79431	1721.8	MSN	Station end	MN55, deployment depth: 600 m
PS133/1_8-7		2022-11-01T22:46:19	-50.51957	-41.79453	1721.9	MSN	Station start	MN200, deployment depth: 600 m
PS133/1_8-7		2022-11-02T00:09:59	-50.51825	-41.79319	1720.2	MSN	Station end	MN200, deployment depth: 600 m
PS133/1_8-8		2022-11-02T00:10:33	-50.51815	-41.79314	1719.9	ROSINA	Station start	Deployment depth: 600 m
PS133/1_8-8		2022-11-02T01:49:23	-50.51811	-41.79194	1720.6	ROSINA	Station end	Deployment depth: 600 m
PS133/1_8-9		2022-11-02T01:52:02	-50.51812	-41.79165	1720.6	CTD-UW	Station start	Deployment depth: 200 m
PS133/1_8-9		2022-11-02T12:27:11	-51.27875	-39.96556	3797.0	CTD-UW	Station end	Deployment depth: 200 m
PS133/1_9-1		2022-11-02T12:52:52	-51.30219	-39.92558	3799.7	IKMT	Station start	Deployment depth: 200 m
PS133/1_9-1		2022-11-02T13:18:58	-51.30270	-39.94617	3728.5	IKMT	Station end	Deployment depth: 200 m
PS133/1_9-2		2022-11-02T13:31:33	-51.30304	-39.97026	3786.1	ACS-RAM	Station start	Deployment depth: 100 m
PS133/1_9-2		2022-11-02T14:11:27	-51.30329	-39.96930	3781.2	ACS-RAM	Station end	Deployment depth: 100 m

Event label	Optional label	Date/Time	Latitude	Longitude	Depth [m]	Gear	Action	Comment
PS133/1_9-4		2022-11-02T14:52:45	-51.28773	-40.00419	3731.9	HN	Station start	Deployment depth: 20 m
PS133/1_9-4		2022-11-02T15:03:00	-51.28789	-40.00317	3785.2	HN	Station end	Deployment depth: 20 m
PS133/1_9-3		2022-11-02T16:21:18	-51.28769	-40.00263	5122.6	CTD-RO	Station start	Deployment depth: 3767 m
PS133/1_9-3		2022-11-02T18:04:49	-51.28753	-40.00200	3792.0	CTD-RO	Station end	Deployment depth: 3767 m
PS133/1_9-5		2022-11-02T18:06:38	-51.28734	-40.00151	3791.6	DF	Station start	Deployment, deployment depth: 435 m
PS133/1_9-5		2022-11-02T18:46:45	-51.28583	-39.99735	3790.7	DF	Station end	Deployment, deployment depth: 435 m
PS133/1_9-6		2022-11-02T20:37:44	-51.28811	-40.00189	3784.9	CTD-TM	Station start	Deployment depth: 3726 m
PS133/1_9-6		2022-11-02T22:20:45	-51.28885	-40.00059	3781.2	CTD-TM	Station end	Deployment depth: 3726 m
PS133/1_9-7		2022-11-02T22:22:43	-51.28874	-40.00063	3789.5	RN	Station start	Deployment depth: 20 m
PS133/1_9-7		2022-11-02T22:35:36	-51.28863	-40.00082	2677.1	RN	Station end	Deployment depth: 20 m
PS133/1_9-8		2022-11-02T22:48:14	-51.28913	-40.00028	3785.9	MSC	Station start	Deployment depth: 100 m
PS133/1_9-8		2022-11-02T23:05:25	-51.28921	-39.99972	3807.6	MSC	Station end	Deployment depth: 100 m
PS133/1_9-9		2022-11-02T23:19:31	-51.28890	-39.99916	3778.6	MSN	Station start	MN55, deployment depth: 600 m
PS133/1_9-9		2022-11-03T00:31:38	-51.29161	-39.99511	3194.9	MSN	Station end	MN55, deployment depth: 600 m
PS133/1_9-10		2022-11-03T00:32:23	-51.29153	-39.99512	3384.6	MSN	Station start	MN200, deployment depth: 600 m
PS133/1_9-10		2022-11-03T01:32:33	-51.29171	-39.99503	3784.2	MSN	Station end	MN200, deployment depth: 600 m
PS133/1_9-11		2022-11-03T01:33:30	-51.29171	-39.99500	3790.6	WP2	Station start	WP2-400, deployment depth: 100 m
PS133/1_9-11		2022-11-03T01:48:41	-51.29201	-39.99546	3790.8	WP2	Station end	WP2-400, deployment depth: 100 m
PS133/1_9-12		2022-11-03T01:49:19	-51.29207	-39.99551	3781.7	WP2	Station start	WP2-100, deployment depth: 100 m
PS133/1_9-12		2022-11-03T02:10:10	-51.29252	-39.99547	3791.4	WP2	Station end	WP2-100, deployment depth: 100 m

Event label	Optional label	Date/Time	Latitude	Longitude	Depth [m]	Gear	Action	Comment
PS133/1_9-13		2022-11-03T02:14:54	-51.29305	-39.99697	3791.1	RMT	Station start	Deployment depth: 555 m
PS133/1_9-13		2022-11-03T03:22:18	-51.31469	-40.05705	3624.7	RMT	Station end	Deployment depth: 555 m
PS133/1_9-14		2022-11-03T03:23:09	-51.31488	-40.05762	3046.0	IKMT	Station start	Deployment depth: 149 m
PS133/1_9-14		2022-11-03T03:54:45	-51.32382	-40.08007	3770.0	IKMT	Station end	Deployment depth: 149 m
PS133/1_9-15		2022-11-03T04:34:34	-51.28979	-39.99892	3780.0	ROSINA	Station start	Deployment depth: 600 m
PS133/1_9-15		2022-11-03T06:10:13	-51.28949	-39.99888	3859.1	ROSINA	Station end	Deployment depth: 600 m
PS133/1_9-16		2022-11-03T06:51:11	-51.28915	-39.99817		CTD-TM	Station start	Deployment depth: 300 m
PS133/1_9-16		2022-11-03T07:16:30	-51.28908	-39.99786	3791.6	CTD-TM	Station end	Deployment depth: 300 m
PS133/1_9-17		2022-11-03T07:17:43	-51.28914	-39.99797	3789.3	INSIPU	Station start	Deployment depth: 400 m
PS133/1_9-17		2022-11-03T10:57:18	-51.28885	-40.00036	3785.1	INSIPU	Station end	Deployment depth: 400 m
PS133/1_9-18		2022-11-03T11:01:52	-51.28923	-40.00061	3790.4	ROSINA	Station start	Deployment depth: 600 m
PS133/1_9-18		2022-11-03T12:35:41	-51.29076	-39.99935	3791.9	ROSINA	Station end	Deployment depth: 600 m
PS133/1_9-19		2022-11-03T12:36:25	-51.29078	-39.99929	3791.1	MSN	Station start	MN55, deployment depth: 600 m
PS133/1_9-19		2022-11-03T13:34:11	-51.29103	-39.99952	3791.6	MSN	Station end	MN55, deployment depth: 600 m
PS133/1_9-20		2022-11-03T13:34:58	-51.29104	-39.99958	3791.9	MSN	Station start	MN200, deployment depth: 600 m
PS133/1_9-20		2022-11-03T14:51:36	-51.29277	-39.99862	3787.3	MSN	Station end	MN200, deployment depth: 600 m
PS133/1_9-21		2022-11-03T14:54:18	-51.29212	-40.00244	3791.1	DF	Station start	Recovery, deployment depth: 435 m
PS133/1_9-21		2022-11-03T16:11:09	-51.30213	-39.92634	3795.5	DF	Station end	Recovery, deployment depth: 435 m
PS133/1_9-22		2022-11-03T17:46:18	-51.30116	-39.92533	3794.8	MUC	Station start	Deployment depth: 3792 m
PS133/1_9-22		2022-11-03T19:14:25	-51.30099	-39.92381	3777.1	MUC	Station end	Deployment depth: 3792 m
PS133/1_9-23		2022-11-03T19:16:50	-51.30099	-39.92371	3687.0	DRIFT	Station start	2 Drifters released, deployment depth: 0-15 m

Event label	Optional label	Date/Time	Latitude	Longitude	Depth [m]	Gear	Action	Comment
PS133/1_9-23		2022-11-03T20:09:29	-51.34095	-39.83973	3792.0	DRIFT	Station end	2 Drifters released, deployment depth: 0-15 m
PS133/1_9-24		2022-11-03T19:19:09	-51.30097	-39.92334	3772.1	CTD-UW	Station start	Deployment depth: 200 m
PS133/1_9-24		2022-11-04T00:06:49	-51.62440	-39.14489	3732.2	CTD-UW	Station end	Deployment depth: 200 m
PS133/1_10-1		2022-11-04T00:07:25	-51.62489	-39.14298	3732.8	RMT	Station start	Deployment depth: 560 m
PS133/1_10-1		2022-11-04T01:40:47	-51.63590	-39.24618	3712.5	RMT	Station end	Deployment depth: 560 m
PS133/1_10-2		2022-11-04T01:41:48	-51.63589	-39.24592	3719.3	ROSINA	Station start	Deployment depth: 600 m
PS133/1_10-2		2022-11-04T03:22:54	-51.63632	-39.24476	3715.9	ROSINA	Station end	Deployment depth: 600 m
PS133/1_10-4		2022-11-04T03:36:24	-51.63636	-39.24474	3710.3	HN	Station start	Deployment depth: 20 m
PS133/1_10-4		2022-11-04T03:38:58	-51.63632	-39.24480	3719.5	HN	Station end	Deployment depth: 20 m
PS133/1_10-3		2022-11-04T03:58:09	-51.63611	-39.24514	3718.5	CTD-RO	Station start	Deployment depth: 1000 m
PS133/1_10-3		2022-11-04T04:40:27	-51.63594	-39.24409	3719.1	CTD-RO	Station end	Deployment depth: 1000 m
PS133/1_10-5		2022-11-04T05:01:45	-51.63598	-39.24428	3720.1	CTD-TM	Station start	Deployment depth: 300 m
PS133/1_10-5		2022-11-04T05:32:45	-51.63570	-39.24455	3719.6	CTD-TM	Station end	Deployment depth: 300 m
PS133/1_10-6		2022-11-04T05:33:33	-51.63575	-39.24457	3717.8	WP2	Station start	WP2-400, deployment depth: 100 m
PS133/1_10-6		2022-11-04T05:58:27	-51.63608	-39.24514	3717.4	WP2	Station end	WP2-400, deployment depth: 100 m
PS133/1_10-7		2022-11-04T06:04:00	-51.63607	-39.24531	3720.3	MSN	Station start	MN55, deployment depth: 600 m
PS133/1_10-7		2022-11-04T07:31:28	-51.63749	-39.24308	3718.4	MSN	Station end	MN55, deployment depth: 600 m
PS133/1_10-8		2022-11-04T07:32:03	-51.63747	-39.24305	3712.6	MSN	Station start	MN200, deployment depth: 600 m
PS133/1_10-8		2022-11-04T08:29:15	-51.63657	-39.24416	3714.6	MSN	Station end	MN200, deployment depth: 600 m
PS133/1_10-9		2022-11-04T08:30:30	-51.63654	-39.24416	3711.4	ACS-RAM	Station start	Deployment depth: 100 m
PS133/1_10-9		2022-11-04T09:01:20	-51.63607	-39.24420	3719.6	ACS-RAM	Station end	Deployment depth: 100 m
PS133/1_10-10		2022-11-04T09:02:19	-51.63588	-39.24354	3720.3	CTD-UW	Station start	Deployment depth: 200 m

Event label	Optional label	Date/Time	Latitude	Longitude	Depth [m]	Gear	Action	Comment
PS133/1_10-10		2022-11-04T13:15:00	-52.05661	-38.68357	3602.2	CTD-UW	Station end	Deployment depth: 200 m
PS133/1_11-1		2022-11-04T13:53:47	-52.06020	-38.69305	3592.6	CTD-TM	Station start	Deployment depth: 1000 m
PS133/1_11-1		2022-11-04T14:46:30	-52.05942	-38.69086	3591.7	CTD-TM	Station end	Deployment depth: 1000 m
PS133/1_12-1		2022-11-04T14:53:36	-52.06523	-38.68460	3590.9	DRIFT	Station start	2 Drifters released, deployment depth: 0-15 m
PS133/1_12-1		2022-11-04T15:13:54	-52.09093	-38.63172	3582.0	DRIFT	Station end	2 Drifters released, deployment depth: 0-15 m
PS133/1_12-2		2022-11-04T14:54:27	-52.06623	-38.68262	3591.0	CTD-UW	Station start	Deployment depth: 200 m
PS133/1_12-2		2022-11-04T16:44:54	-52.21639	-38.37364	3523.6	CTD-UW	Station end	Deployment depth: 200 m
PS133/1_13-1		2022-11-04T17:18:45	-52.21394	-38.36809	3521.5	CTD-TM	Station start	Deployment depth: 1000 m
PS133/1_13-1		2022-11-04T18:24:06	-52.21543	-38.36515	3517.3	CTD-TM	Station end	Deployment depth: 1000 m
PS133/1_14-1		2022-11-05T10:53:19	-54.19388	-35.90740	244.7	ACS-RAM	Station start	Deployment depth: 129 m
PS133/1_14-1		2022-11-05T11:45:48	-54.19251	-35.90667	250.4	ACS-RAM	Station end	Deployment depth: 129 m
PS133/1_14-2		2022-11-05T12:58:02	-54.18995	-35.91317	245.9	ACS-RAM	Station start	Deployment depth: 150 m
PS133/1_14-2		2022-11-05T13:51:36	-54.18969	-35.91788	248.2	ACS-RAM	Station end	Deployment depth: 150 m
PS133/1_14-3		2022-11-05T15:00:00	-54.19288	-35.90964	247.6	ACS-RAM	Station start	Deployment depth: 150 m
PS133/1_14-3		2022-11-05T15:39:09	-54.19399	-35.90943	247.8	ACS-RAM	Station end	Deployment depth: 150 m
PS133/1_14-5		2022-11-05T16:01:47	-54.19393	-35.90983	246.1	HN	Station start	Deployment depth: 20 m
PS133/1_14-5		2022-11-05T16:08:49	-54.19403	-35.91033	246.5	HN	Station end	Deployment depth: 20 m
PS133/1_14-4		2022-11-05T16:09:09	-54.19402	-35.91030	245.8	CTD-RO	Station start	Deployment depth: 228 m
PS133/1_14-4		2022-11-05T16:50:18	-54.19385	-35.91033	244.8	CTD-RO	Station end	Deployment depth: 228 m
PS133/1_14-6		2022-11-05T16:51:18	-54.19382	-35.91022	244.6	MSN	Station start	MN55, deployment depth: 227 m
PS133/1_14-6		2022-11-05T17:27:54	-54.19388	-35.90976	246.3	MSN	Station end	MN55, deployment depth: 227 m
PS133/1_14-7		2022-11-05T17:30:27	-54.19391	-35.90998	245.6	MSN	Station start	MN200, deployment depth: 227 m
PS133/1_14-7		2022-11-05T18:14:08	-54.19437	-35.91162	247.5	MSN	Station end	MN200, deployment depth: 227 m

Event label	Optional label	Date/Time	Latitude	Longitude	Depth [m]	Gear	Action	Comment
PS133/1_14-8		2022-11-05T18:14:44	-54.19433	-35.91163	247.4	INSIPU	Station start	Deployment depth: 210 m
PS133/1_14-8		2022-11-05T21:04:38	-54.19429	-35.91146	247.5	INSIPU	Station end	Deployment depth: 210 m
PS133/1_14-9		2022-11-05T21:05:37	-54.19431	-35.91141	247.5	ROSINA	Station start	Cancelled, no communication with device
PS133/1_14-9		2022-11-05T21:33:20	-54.19557	-35.91099	249.9	ROSINA	Station end	Cancelled, no communication with device
PS133/1_14-10		2022-11-05T21:57:17	-54.19456	-35.90692	248.5	MSC	Station start	Deployment depth: 80 m
PS133/1_14-10		2022-11-05T22:15:29	-54.19463	-35.90760	245.5	MSC	Station end	Deployment depth: 80 m
PS133/1_14-11		2022-11-05T22:27:51	-54.19463	-35.90773	245.0	RN	Station start	Deployment depth: 20 m
PS133/1_14-11		2022-11-05T22:41:14	-54.19457	-35.90878	246.1	RN	Station end	Deployment depth: 20 m
PS133/1_14-12		2022-11-05T23:11:36	-54.19511	-35.90754	243.7	CTD-TM	Station start	Deployment depth: 227 m
PS133/1_14-12		2022-11-05T23:47:50	-54.19417	-35.91025	246.6	CTD-TM	Station end	Deployment depth: 227 m
PS133/1_14-13		2022-11-05T23:51:44	-54.19414	-35.90994	246.7	WP2	Station start	WP2-200 & WP2-400, deployment depth: 100 m
PS133/1_14-13		2022-11-06T00:24:05	-54.19348	-35.91168	242.0	WP2	Station end	WP2-200 & WP2-400, deployment depth: 100 m
PS133/1_14-14		2022-11-06T00:24:46	-54.19347	-35.91163	241.9	MSN	Station start	MN55, deployment depth: 225 m
PS133/1_14-14		2022-11-06T01:04:08	-54.19343	-35.91555	240.8	MSN	Station end	MN55, deployment depth: 225 m
PS133/1_14-15		2022-11-06T01:05:53	-54.19364	-35.91387	239.2	MSN	Station start	MN200, deployment depth: 225 m
PS133/1_14-15		2022-11-06T01:35:34	-54.19437	-35.91450	241.8	MSN	Station end	MN200, deployment depth: 225 m
PS133/1_14-16		2022-11-06T01:42:47	-54.19250	-35.91383	239.5	IKMT	Station start	Deployment depth: 50 m
PS133/1_14-16		2022-11-06T02:05:00	-54.18488	-35.89969	248.7	IKMT	Station end	Deployment depth: 50 m
PS133/1_14-17		2022-11-06T02:06:45	-54.18419	-35.89853	249.2	RMT	Station start	Deployment depth: 140 m
PS133/1_14-17		2022-11-06T02:44:09	-54.16795	-35.87338	243.6	RMT	Station end	Deployment depth: 140 m
PS133/1_14-18		2022-11-06T02:44:45	-54.16785	-35.87321	243.1	ROSINA	Station start	Deployment depth: 220 m
PS133/1_14-18		2022-11-06T03:51:03	-54.16857	-35.86286	245.5	ROSINA	Station end	Deployment depth: 220 m

Event label	Optional label	Date/Time	Latitude	Longitude	Depth [m]	Gear	Action	Comment
PS133/1_15-1		2022-11-07T10:56:25	-55.23124	-26.17107	8106.5	MUC	Station start	Deployment depth: 8081 m
PS133/1_15-1		2022-11-07T13:43:53	-55.23193	-26.17132	7800.0	MUC	Station end	Deployment depth: 8081 m
PS133/1_15-2		2022-11-07T14:01:10	-55.21333	-26.17021	7798.9	INSIPU	Station start	Deployment depth: 400 m
PS133/1_15-2		2022-11-07T16:54:09	-55.21540	-26.16250	7801.0	INSIPU	Station end	Deployment depth: 400 m
PS133/1_15-3		2022-11-07T17:28:09	-55.21535	-26.16303	7800.9	CTD-RO	Station start	Deployment depth: 1000 m
PS133/1_15-3		2022-11-07T18:14:43	-55.21641	-26.15941	8095.0	CTD-RO	Station end	Deployment depth: 1000 m
PS133/1_15-4		2022-11-07T18:15:18	-55.21646	-26.15916	8103.5	HN	Station start	Deployment depth: 20 m
PS133/1_15-4		2022-11-07T18:19:40	-55.21672	-26.15786	7800.8	HN	Station end	Deployment depth: 20 m
PS133/1_15-5		2022-11-07T21:22:55	-55.22989	-26.18481	8066.4	MUC	Station start	Deployment depth: 8236 m
PS133/1_15-5		2022-11-08T00:35:01	-55.23053	-26.18264	7800.8	MUC	Station end	Deployment depth: 8236 m
PS133/1_16-1		2022-11-08T10:15:09	-55.80084	-24.83905	5002.1	MUC	Station start	Deployment depth: 5823 m
PS133/1_16-1		2022-11-08T12:25:56	-55.79921	-24.83882	4043.2	MUC	Station end	Deployment depth: 5823 m
PS133/1_16-2		2022-11-08T12:41:14	-55.78322	-24.84127	4000.9	INSIPU	Station start	Deployment depth: 400 m
PS133/1_16-2		2022-11-08T15:43:36	-55.79933	-24.84011	4857.5	INSIPU	Station end	Deployment depth: 400 m
PS133/1_16-3		2022-11-08T16:17:45	-55.80284	-24.83929	3000.6	CTD-RO	Station start	Deployment depth: 1000 m
PS133/1_16-3		2022-11-08T17:08:54	-55.80978	-24.83970	4181.1	CTD-RO	Station end	Deployment depth: 1000 m
PS133/1_17-1		2022-11-08T23:13:02	-56.23965	-24.94566	7500.4	MUC	Station start	Deployment depth: 7821 m
PS133/1_17-1		2022-11-09T02:09:09	-56.24141	-24.94605	7991.0	MUC	Station end	Deployment depth: 7821 m
PS133/1_17-2		2022-11-09T04:52:09	-56.24056	-24.94467	7595.9	MUC	Station start	Deployment depth: 7921 m
PS133/1_17-2		2022-11-09T07:55:50	-56.23765	-24.94513	7717.4	MUC	Station end	Deployment depth: 7921 m
PS133/1_17-3		2022-11-09T09:30:14	-56.24298	-24.93948	7732.8	CTD-RO	Station start	Deployment depth: 4039 m
PS133/1_17-3		2022-11-09T11:25:43	-56.26644	-24.92513	7816.6	CTD-RO	Station end	Deployment depth: 4039 m
PS133/1_17-4		2022-11-09T11:26:24	-56.26666	-24.92491	7816.6	INSIPU	Station start	Deployment depth: 400 m
PS133/1_17-4		2022-11-09T15:17:18	-56.33041	-24.86257	7724.9	INSIPU	Station end	Deployment depth: 400 m
PS133/1_17-5		2022-11-09T12:12:35	-56.28321	-24.90513	7805.5	HN	Station start	Deployment depth: 20 m
PS133/1_17-5		2022-11-09T12:21:24	-56.28650	-24.90246	7500.8	HN	Station end	Deployment depth: 20 m
PS133/1_17-6		2022-11-09T15:18:09	-56.33062	-24.86246	7500.8	ACS-RAM	Station start	Deployment depth: 130 m

Event label	Optional label	Date/Time	Latitude	Longitude	Depth [m]	Gear	Action	Comment
PS133/1_17-6		2022-11-09T16:07:54	-56.34258	-24.85994	7500.8	ACS-RAM	Station end	Deployment depth: 130 m
PS133/1_17-7		2022-11-09T19:36:26	-56.28945	-24.94616	7300.9	CTD-TM	Station start	Deployment depth: 7000 m
PS133/1_17-7		2022-11-09T22:29:21	-56.32912	-24.92384	7307.4	CTD-TM	Station end	Deployment depth: 7000 m
PS133/1_17-8		2022-11-09T22:43:29	-56.33468	-24.92191	7301.5	CTD-RO	Station start	Deployment depth: 99 m
PS133/1_17-8		2022-11-09T22:51:45	-56.33806	-24.92064	7300.8	CTD-RO	Station end	Deployment depth: 99 m
PS133/1_17-9		2022-11-09T22:52:37	-56.33844	-24.92041	7300.6	MSN	Station start	MN55, deployment depth: 600 m
PS133/1_17-9		2022-11-10T00:23:35	-56.36641	-24.90662	7386.6	MSN	Station end	MN55, deployment depth: 600 m
PS133/1_17-10		2022-11-10T00:31:06	-56.36801	-24.91133	7643.2	IKMT	Station start	Deployment depth: 222 m
PS133/1_17-10		2022-11-10T01:32:46	-56.38048	-24.96138	7779.2	IKMT	Station end	Deployment depth: 222 m

** Comments are limited to 130 characters. See https://www.pangaea.de/expeditions/events/PS133/1 to show full comments in conjunction with the station (event) list for expedition PS133/1*

Abbreviation	Method/Device
ACS-RAM	Spectrophotometer and hyperspectral radiometer (ACS-RAMSES)
ADCP	Acoustic Doppler Current Profiler (VMADCP in text)
B_LANDER	Bottom lander (Hadal-benthic Flux lander)
CT	Underway cruise track measurements
CTD-RO	CTD/Rosette (CTD-OZE in text)
CTD-TM	CTD/Rosette, trace metal clean (CTD-Clean in text)
CTD-UW	CTD, underway (UCTD in text)
DF	Trap, drifting
DRIFT	Drifter
FBOX	FerryBox
HN	Hand net
IKMT	Isaacs-Kidd-Midwater Trawl
INSIPU	In-situ pumps
MSC	Marine snow catcher
MSN	Multiple opening/closing net
MUC	MultiCorer
MYON	DESY Myon Detector
NEUMON	Neutron monitor
RMT	Rectangular midwater trawl
RN	Ring net
ROSINA	Remotely ObServing INsitu camera for Aggregates
SNDVELPR	Sound velocity probe
SWEAS	Ship Weather Station
TOPR	Towed Ocean Profiler (TopAWI/Triaxus)
TSG	Thermosalinograph
TVMUC	Multicorer with television
WP2	WP-2 towed closing plankton net
pCO2	pCO2 sensor (General Oceanics)

Die **Berichte zur Polar- und Meeresforschung** (ISSN 1866-3192) werden beginnend mit dem Band 569 (2008) als Open-Access-Publikation herausgegeben. Ein Verzeichnis aller Bände einschließlich der Druckausgaben (ISSN 1618-3193, Band 377-568, von 2000 bis 2008) sowie der früheren **Berichte zur Polarforschung** (ISSN 0176-5027, Band 1–376, von 1981 bis 2000) befindet sich im electronic Publication Information Center **(ePIC)** des Alfred-Wegener-Instituts, Helmholtz-Zentrum für Polar- und Meeresforschung (AWI); see https://epic.awi.de. Durch Auswahl "Reports on Polar- and Marine Research" (via "browse"/"type") wird eine Liste der Publikationen, sortiert nach Bandnummer, innerhalb der absteigenden chronologischen Reihenfolge der Jahrgänge mit Verweis auf das jeweilige pdf-Symbol zum Herunterladen angezeigt.

The **Reports on Polar and Marine Research** (ISSN 1866-3192) are available as open access publications since 2008. A table of all volumes including the printed issues (ISSN 1618-3193, Vol. 377-568, from 2000 until 2008), as well as the earlier **Reports on Polar Research** (ISSN 0176-5027, Vol. 1–376, from 1981 until 2000) is provided by the electronic Publication Information Center **(ePIC)** of the Alfred Wegener Institute, Helmholtz Centre for Polar and Marine Research (AWI); see URL https://epic.awi.de. To generate a list of all Reports, use the URL http://epic.awi.de and select "browse"/"type" to browse "Reports on Polar and Marine Research". A chronological list in declining order will be presented, and pdf-icons displayed for downloading.

Zuletzt erschienene Ausgaben:

Recently published issues:

774 (2023) The Expedition PS133/1 of the Research Vessel POLARSTERN to the Atlantic Ocean in 2022, edited by Christine Klaas with contributions of the participants

773 (2023) A computational approach of locomotion, energy demand and dispersal of the common comatulid crinoid *Promachocrinus kerguelensis* (Echinodermata) and its circum-Antarctic success, by Nils Owsianowski

772 (2023) Russian-German Cooperation: Expeditions to Siberia in 2021, edited by Anne Morgenstern, Birgit Heim, Luidmila A. Pestryakova, Dmitry Yu. Bolshiyanov, Mikhail N. Grigoriev, Dmitry Ayunov, Antonia Dill, and Iuliia Jünger

771 (2023) The Expedition PS132 of the Research Vessel POLARSTERN to the Atlantic Ocean in 2022, edited by Karen H. Wiltshire and Angelika Dummermuth with contributions of the participants

770 (2023) The Expedition PS131 of the Research Vessel POLARSTERN to the Fram Strait in 2022, edited by Torsten Kanzow with contributions of the participants

769 (2023) The Expedition TRITON2021 of the Hendes Dansk Majestæt Skib TRITON to the Atlantic Ocean in 2021, edited by Rebecca McPherson, Carina Engicht and Torsten Kanzow

768 (2022) Mit Erich von Drygalski in die Ostantarktis – Paul Björvigs Tagebuch von der ersten deutschen Südpolarexpedition 1901-1903. Aus dem Norwegischen übersetzt von Volkert Gazert und herausgegeben von Cornelia Lüdecke

767 (2022) Expeditions to Antarctica: ANT-Land 2021/22 Neumayer Station III, Kohnen Station, Flight Operations and Field Campaigns, edited by Christine Wesche and Julia Regnery with contributions of the participants

766 (2022) The Expedition West-Alaska 2016 of the ERC group PETA-CARB to permafrost regions in western Alaska in 2016, edited by Josefine Lenz, Matthias Fuchs, Ingmar Nitze, Jens Strauss, Guido Grosse

ALFRED-WEGENER-INSTITUT
HELMHOLTZ-ZENTRUM FÜR POLAR-
UND MEERESFORSCHUNG

BREMERHAVEN

Am Handelshafen 12
27570 Bremerhaven
Telefon 0471 4831-0
Telefax 0471 4831-1149
www.awi.de

HELMHOLTZ